UNIVERSITY OF CAMBRIDGE

DEPARTMENT OF CHEMICAL ENGINEERING AND BIOTECHNOLOGY

# Microwave-Assisted Pyrolysis of HDPE using an Activated Carbon Bed

*Author:*
Alan Russell
Clare College

*Supervisor:*
Professor Howard Chase
Magdalene College

September 2012

*This dissertation is submitted for the degree of Doctor of Philosophy*

# Preface

This work was carried out in the Department of Chemical Engineering and Biotechnology, University of Cambridge, from October 2008 to August 2012, and is submitted in fulfilment of the requirements of the degree of Doctor of Philosophy. This dissertation is the result of my own work and includes nothing that is the outcome of work done in collaboration except where specifically indicated in the text. None of the work contained in this dissertation, or any part thereof, has been submitted for any other degree at the University of Cambridge or any other institution. This dissertation does not exceed 65,000 words, and contains fewer than 150 figures.

Alan Russell

20th September 2012

# Summary

Plastics play an enormous role in modern manufacturing, but the extraction and refining of raw materials, followed by the synthesis of plastics themselves, represents an enormous energy investment into a product that is all too often simply “thrown away” into a landfill after a single use. Microwave-assisted pyrolysis is a recycling technique that allows the recovery of chemical value from plastic waste by breaking down polymers into useful smaller hydrocarbons using microwave heat in the absence of oxygen. This dissertation examines the use of a catalytic activated carbon bed in this procedure, using high density polyethylene (HDPE) as a model plastic.

Initial tests with the batch input of HDPE produced a condensed pyrolysis oil comprising 35.5–45.3% aromatics, with the remainder primarily short-chain aliphatics. This oil was approximately three times lighter than that produced in the absence of catalyst, with a narrower range of molecular masses that matched those of the liquid transport fuels petrol and diesel ($C_5$–$C_{21}$). The non-condensable gases that resulted were short-chain aliphatics that could be used as feedstock for the creation of new chemicals (such as virgin HDPE), or fuels such as natural gas and LPG.

The development of apparatus capable of adding sample in a continuous fashion enabled the processing of larger quantities of HDPE, and resulted in condensed products with a significantly higher aromatic content (>80% at 450°C), and which encompassed a somewhat narrower range of molecular masses compared with those produced in the batch mode; this was due to differences in kinetics and residence time that resulted from the different modes of sample introduction. As a result of processing larger quantities of HDPE it became apparent that the activated carbon deactivated over time, with a bed able to process around 3.5 times its mass in HDPE at 450°C before any significant changes in output products occurred.

The decomposition of HDPE proceeds via thermal scission and radical-mediated mechanisms; high energy surface active sites facilitate the transfer of hydrogen and radicals, and this enhances overall cracking and lowers the activation energy for the formation of aromatics. Analysis of material deposited on the surface of the activated carbon confirmed that deactivation occurred through coking, with both cracking and deactivation thought to be enhanced by the formation of microwave-induced microplasmas.

Overall, the microwave-assisted pyrolysis of HDPE using activated carbon produces a much narrower range of more valuable products compared with non-catalytic processing. While the process is not likely to be economic in its current form owing to the relatively rapid deactivation of the activated carbon, future configurations incorporating online reactivation may be able to economically provide a second use cycle for these materials, avoiding expending energy to extract and process increasingly scarce new raw material from the surface of the earth.

# Acknowledgements

I owe a debt of thanks to many people for the support and kindness they have shown me throughout my time in Cambridge. I would like to thank my supervisor, Professor Howard Chase, for his generous provision of tutelage, expertise, and support throughout the production of this work. A further thank you to my colleagues and the department support staff for their extremely skilled time and advice.

I would also like to acknowledge the generous financial support that I have received from the Cambridge Commonwealth Trust, The Higher Education Funding Council for England, Clare College, The Department of Chemical Engineering and Biotechnology, and The Cambridge Philosophical Society, without which my time in Cambridge would not have been possible.

The multitude of amazing people I have met over the last four years have truly made my time at Cambridge special. Thank you to all my friends with whom I have shared the good times and the bad, who have contributed time, thoughts, support, and probably a little too much food, drink, fun, and cupcakes!

My family has always been an incredible source of unwavering encouragement in my life, and antipodean distance has only made me realise and appreciate their love and support all the more. I owe my mother, Anne, an extra special thank you, not least for her willingness to employ her incredible eagle eye in hunting out orthographical errors from this dissertation.

# Contents

# List of Figures

# List of Tables

# Nomenclature

## Roman

| | |
|---|---|
| E | Error from target temperature [°C] |
| k | Constant |
| P | Power [W] |
| T | Temperature [°C] |
| t | Time [s] |
| V | Voltage [V] |
| Z | Electrical Impedance [Ω] |

## Subscripts

| | |
|---|---|
| 0 | Initial |
| D | Derivative |
| I | Integral |
| L | Load |
| P | Proportional |
| S | Source |
| t | time step |

## Abbreviations

| | |
|---|---|
| CN, C$x$ | the number of carbons in a molecule, where $x$ is the number of carbons |
| EDS | Energy-dispersive X-ray spectroscopy |
| FBR | Fluidised bed reactor |
| FCC | Fluid cracking catalyst/catalysis |
| FT-IR | Fourier transform infrared spectroscopy |
| GC/MS | Gas chromatography-Mass spectrometry |
| HDPE | High density polyethylene |
| LDPE | Low density polyethylene |
| MW | Molecular weight [g mol$^{-1}$] |
| PAH | Polyaromatic Hydrocarbon |
| PID | Proportional-Integral-Derivative |
| PMMA | Poly(methylmethacrylate) |
| PP | Polypropylene |
| PS | Polystyrene |
| PTFE | Polytetrafluoroethylene, Teflon |
| PVC | Poly(vinyl chloride) |
| SD | Standard deviation |
| SEM | Scanning electron microscopy |
| wt% | Weight percentage |

# 1

# Introduction

## 1.1 The Problem and Opportunity of Plastic Waste

For a material with a relatively recent genesis, plastics have certainly come to play a dominant role in modern goods and manufacturing. Their low cost, ease of manufacture, and versatility, have led to an enormous growth in their consumption (of roughly 5% a year over the last 20 years), with 265 million tonnes produced worldwide in 2010, of which 57 million tonnes are accounted for by Europe alone [1], and this growth is only expected to continue. This surfeit of plastics presents a significant disposal issue, especially considering the large quantities of single-use items and packaging materials that are fabricated from plastics, and the fact that as highly inert materials, most plastics degrade in the environment only over very long periods of time. Furthermore, the production of plastics represents a significant energy investment, in the extraction and refinement of petrochemical feedstock, and the subsequent synthesis of polymer. As a high-energy material, at the end of a plastic item's useful life, there is significant potential for resource recovery, either to re-use the

plastic itself, or to recover some of the stored energy that has gone into its manufacture. In any case, it is a lamentable waste simply to “throw away” plastic after one use cycle, and with it all the latent energy inherent to the material, as happens all too often in current practice.

## 1.2 Current Plastics Recycling Techniques

The U.K. sees relatively low rates of plastics recycling, with 69% of post-consumer plastic waste generated in 2010 ending up in landfill (compared with 42% across the whole of Europe), with no attempt at recycling or energy recovery made [1]. However, the U.K. government has plans to double the rate of plastic packaging recycling (from the 2007 figure of 24%) by the year 2020 [2], a commitment that will require significant investment in additional recycling capability and techniques.

### 1.2.1 Mechanical Recycling

The simplest and most prevalent form of plastics recycling (comprising 24.3% of plastics disposal in Europe [1]) is achieved by mechanical means: thermoplastics may be melted and moulded into a new form, usually after being shredded or granulated. However, different polymers generally do not mix well, necessitating separating plastic types from one another before processing occurs — a time-consuming and costly process. Indeed, even within a single type of polymer, small differences in composition can cause phase separation when samples are melted together, resulting in structural flaws and a lower quality final product. These issues are only exacerbated by the different additives such as dyes and fillers that each manufacturer uses. Plastics must also be contaminant free in order to be processed in this way, which can necessitate the introduction of a costly washing step, depending on the state of the source material. Polymer degradation over time can also result in inferior product produced using this technique.

### 1.2.2 Energy Recovery

Typical plastics have a calorific value between 40–48 MJ/kg, greater than that of coal [3, 4]; this high energy density makes plastics relatively sought after for energy recovery purposes. Typically this is achieved through incineration, where the polymers are exothermically oxidised in furnaces, and the resulting heat is used to generate

electrical energy. This method can be used with all types of plastics; however, it suffers several drawbacks. The combustion of plastics is essentially equivalent to burning fossil fuels and results in the release of $CO_2$ — a greenhouse gas that contributes to climate change. Furthermore, incineration recovers only thermal energy from plastics, and does not allow for the recovery of any of the chemical value of the polymers. Incineration can also result in the release of toxic compounds (e.g., dioxins and furans) that cause environmental damage and health problems [5, 6], as well as producing hazardous compounds, such as fly ash, which are difficult to dispose of properly [7]. Currently incineration accounts for around 8% of plastics disposal in the U.K., though the rates are much higher in western Europe as a whole, at 33.6% [1].

### 1.2.3 Feedstock Recycling

Feedstock recycling breaks down polymers into smaller molecules that can be used as inputs for the creation of new chemicals and materials. This term incorporates a range of processes such as chemical depolymerisation (yielding the original monomer), thermal decomposition such as pyrolysis, and gasification, where hydrocarbons are broken down into synthesis gas ($H_2$ + CO). This gas can then be used as a fuel directly, or converted into liquid hydrocarbon fuel through the Fischer-Tropsch process [8]. While feedstock recycling is able to deal with a wide variety of plastics, and is generally able to cope with fairly high levels of contamination, it usually requires significant energy and capital intensive plants that only operate economically on large scales [9]. The use of feedstock recycling techniques is not currently widespread, with only 1.6% of plastic waste in Europe recycled using these methods at present [10]. Unfamiliarity and high capital cost barriers to entry are thought to contribute to the current low prevalence of these techniques, though clearly this is a route with the potential to expand in capacity significantly, especially given continuing technological development, and the forecasted continuing rise in the cost of the petrochemicals that these techniques produce, as easily accessible global supplies of raw materials are depleted.

#### 1.2.3.1 Pyrolysis

Pyrolysis is the thermal degradation of a substance in an inert environment (i.e., without the presence of oxygen), and may be used as a plastics feedstock recycling technique where polymers are cracked into shorter hydrocarbons (their constituent monomers, parts or multiples thereof, and more complex species produced when these

products react together) — the final products resulting from this process comprise waxes, oils, gases, and char. It is possible to optimise the process to maximise production of any of these constituents by altering parameters such as process temperature and reactant residence time [11]. For example, a high temperature and residence time promotes gas production; high temperature and low residence time ("flash pyrolysis") maximises the yield of condensates; while a low temperature and heating rate promotes char production [12]. The relatively wide variety of products produced by the pyrolysis of plastics means that they usually have to be separated and purified before use; fortunately this has the potential to be achieved on a commercial scale with existing petrochemical distilleries and refineries.

#### 1.2.3.2 Catalytic Pyrolysis

It is also possible to pyrolyse plastics in the presence of catalysts, which enhance cracking and alter the yields of the pyrolysis products so that lighter products are produced more abundantly. Most studies that have been carried out on catalytically pyrolysing plastics use fluid cracking catalysts (FCCs) such as zeolites and alumino-silicates, which have been developed by the petrochemical industry for the cracking of long-chain hydrocarbons into lighter liquid fuels [13, 14].

## 1.3 Microwave-Assisted Pyrolysis

### 1.3.1 Microwave Heating

"Microwaves" are the portion of the electromagnetic spectrum between 300 MHz and 3 GHz. The practical production and utilisation of this frequency band was first carried out during World War Two in the development of high-definition radar. During this time the cavity magnetron was invented — an inexpensive, highly efficient, high-power microwave source that has allowed the application of microwaves for a range of purposes, heating foremost amongst them, and that has directly enabled the proliferation of the microwave oven so commonplace in households today. The heating of a material by microwaves arises from the resistance of movement by dipoles and charged species to the forces imposed by the alternating electromagnetic microwave field [15].

#### 1.3.1.1 Advantages of Microwave Heating

Microwave heating offers several advantages over conventional techniques such as electrical furnaces:

- As a non-contact form of heating, it is physically gentle, allowing for a diverse range of applications over and above contact surface heating [16–18].
- It is a volumetric heating method, with the diffuse and pervasive nature of the electromagnetic field able to heat many substances evenly and in bulk, without relying on slower and less efficient conductive or convective techniques [19, 20].
- Microwave heating is able to achieve high power densities, allowing rapid heating and the ability to reach high temperatures in short periods of time, which can increase production speeds and reduce costs [21].
- Microwave fields interact only with particular types of materials, giving this form of heating the ability to selectively target areas and substances (and not heat surrounding air or containers). This can dramatically reduce the amount of heating required to achieve a particular end, and with it the associated energy use and costs. By selectively heating only targeted reactants it is possible to achieve a more uniform temperature profile and a higher yield of desired end products [22–24].
- Microwave heating is easily and rapidly initiated and terminated, especially compared with processes that rely on combustion or indirect heating such as steam.
- The electrical origin of microwave heating allows for direct electronic control, providing a higher level of precision, safety, and automation.
- As microwave heating is an electromagnetic means of transmission it is possible to delocalise the energy source from the heating target, with microwaves easily transported over long distances through waveguides. This facilitates modular construction of reactors with easier access and lower maintenance costs [25].
- Magnetrons are available in a wide range of sizes and power outputs, making processes based on this form of heating highly scalable, enabling the same technology used in laboratory-scale experimental reactors to be employed in commercial sized plants, and potentially enabling smaller scale community sized facilities to be constructed with lower initial capital costs.

#### 1.3.1.2 Disadvantages of Microwave Heating

Microwave heating also suffers from some drawbacks in comparison with conventional heating methods:

- Microwave radiation presents an additional hazard over traditional heating methods, although this is easily contained within an appropriate Faraday cage. The non-ionising nature of the radiation also limits risk in the event of exposure, with the radiation having insufficient energy per quantum to create biologically damaging ionised atoms or molecules.
- While the property of microwave heating only to target microwave-receptive materials can be an advantage in some cases, in the event that microwave-transparent materials (such as plastics) require heating, an intermediate microwave receptor must be used.
- With the conversion from electrical energy to electromagnetic radiation to heat, microwave heating is not 100% efficient, though modern equipment is able to achieve over 90% conversion efficiency [26], and this loss is often more than made up for by the ability to selectively target the area to be heated as previously discussed.
- Using microwave heating places limits on the materials that can be used in the construction of a reactor. While metal is essential in an electromagnetic containment role, its use should be minimised within the reactor itself to avoid causing arcing, with sharp metallic corners and small physical gaps between metal surfaces presenting the highest risk of potential arc formation.
- The more complex apparatus required for microwave heating (i.e., magnetron, power supply, waveguides, etc.) means that this form of heating costs more than conventional methods. Furthermore, the cost of microwave heating apparatus scales disproportionally with size, i.e., larger heating installations cost more per watt than smaller ones, though this may be alleviated to some extent by using multiple smaller units in parallel.

### 1.3.2 Microwave-Assisted Pyrolysis of Plastics using a Carbon Bed

Microwave-assisted pyrolysis describes the application of microwave heating to a substance to cause it to undergo pyrolytic breakdown (in the absence of oxygen). It is a relatively new process, first developed by Tech-En Ltd (Essex, U.K.) [27, 28] to combine

the advantages of microwave-mode heating with the commercial and environmental benefits that the pyrolysis of plastics offers. Because of the microwave transparency of plastics, in this application an intermediate receptor is used to absorb the microwave energy and transfer it to the plastic via conduction.

#### 1.3.2.1 Method for Microwave-Assisted Pyrolysis of Plastics Using a Carbon Bed

The microwave-assisted pyrolysis of plastics is performed by heating a reactor bed to a sufficiently high temperature, in the absence of oxygen, that added plastic is cracked into smaller hydrocarbon molecules. The stochastic nature of the pyrolysis process means that products with a wide range of molecular masses are usually produced. These products exit the reactor in the gaseous state and are collected as condensed waxes and oils, and as non-condensable light-chain gases. The cracking, volatilisation, and physical transfer involved in this process also act as a separation mechanism, with many forms of contaminant carbonising and remaining in the reactor, along with any non-volatile species; as a result, microwave-assisted pyrolysis has a relatively robust ability to cope with contaminants without significant impact on the final products [29, 30].

### 1.3.3 Carbon as a Reactor Bed Material

Particulate elemental carbon is the most common material used as a reactor bed in microwave-assisted pyrolysis, owing to its excellent microwave receptivity and low cost. Short transfer distances, the enveloping nature of a particulate bed, and small particle size (with corresponding large surface area) make this a highly efficient method of heat transfer, while by controlling the size of the carbon bed it is possible to localise the heat dispersion within a small area, and maintain the targeted efficiency that microwave heating offers. A further advantage of using carbon as a reaction bed for pyrolysis is the highly reducing environment that it provides, which prevents the formation of undesirable oxidised species, and again enhances the ability of the process to cope with potential contaminants.

#### 1.3.3.1 Coke

The “carbon” used in carbon beds for microwave-assisted pyrolysis is almost always coke (examples of which are discussed in depth in §2.5). Coke is the solid carbonaceous

residue that remains after heating a (primarily) hydrocarbon material to a high temperature in the absence of oxygen (i.e., undergoing pyrolysis of some description itself). It can be produced from a variety of sources, historically deriving from coal, though is now a common by-product of the petroleum industry, produced during the upgrading of heavy oil fractions to lighter hydrocarbons [31]. Owing to its high carbon content, coke may be used as a fuel in its own right, or as a reducing agent in the smelting of iron ore in blast furnaces [32, 33]. Its abundance as a common by-product accounts for its low sourcing cost.

#### 1.3.3.2 Activated Carbon

Activated carbon, the focus of the work presented in this dissertation, is a manufactured form of carbon, with a central characteristic of an extremely high adsorptive capacity that derives from microporous structure and resulting high surface area. It is manufactured from various polymeric carbohydrates and hydrocarbons such as hard woods, coconut shell, fruit stones, coals, and oil bitumen. These are first carbonised (through pyrolysis), and then subjected to a chemical or thermal "activation" process (discussed in depth in §2.3.2) that maximises the material's porous potential, creating and widening micropores on the molecular level, and introducing or enhancing high energy active sites on to the surface.

The very high adsorptive ability of activated carbon has led to its current main industrial use in purification (e.g., water treatment, decolourising). In the chemical context, activated carbon sees high usage as a support material in heterogeneous catalysis (with, e.g., platinum or palladium) to enhance effectiveness and minimise cost [34, 35]. In the recent past, an appreciation has grown for the potential to use activated carbon as a catalyst in its own right, with it being employed commercially in the production of carbonyl chloride from carbon monoxide and chlorine, and it has also been shown to be an effective catalyst for a variety of other reactions involving hydrogen, oxygen, and halogens [36, 37] (a comprehensive account of the applications of activated carbon is given in §2.3.3). More recently, activated carbon has shown promise in the dehydrogenation of hydrocarbons [38, 39], suggesting it may also have the potential to be employed in the catalytic cracking of long-chain polymers such as plastics.

**Table 1.1:** Common hydrocarbon products by carbon number [41, 42].

| Product | Carbon Number |
|---|---|
| Natural Gas | $C_1$ |
| Ethene | $C_2$ |
| Liquid Petroleum Gas (LPG) | $C_3$–$C_4$ |
| Petrol/Gasoline | $C_5$–$C_{12}$ |
| Kerosene/Jet Fuel | $C_8$–$C_{16}$ |
| Diesel | $C_8$–$C_{21}$ |
| Lubricating Oil | $C_{20}$–$C_{40}$ |
| Waxes | $>C_{40}$ |
| HDPE | $C_{\text{hundreds of thousands}}$ |

## 1.4 Petrochemicals and Hydrocarbon Fuels

Petrochemicals and hydrocarbon fuels are central to current human civilisation, with petrochemicals underpinning innumerable products such as plastics, fibres, solvents, pharmaceuticals, and fertilizer, and oil-derived liquid and gas fuels making up 54.3% of total primary energy supply worldwide [40]. That these chemicals have risen to such prominence is a result of several factors, including:

- Historical abundance, with correspondingly cheap (in both monetary and energy terms) extraction and refinement, in comparison with other energy sources.
- Network effects resulting from infrastructure development over time.
- Ease of transport, with the ability to be shipped long distances via pipeline or tanker.
- Availability on a scale that matches societal demand.
- Advantageous physiochemical properties, with liquid transport fuels (e.g., petrol and diesel) exhibiting unparalleled volumetric energy density (excepting nuclear power).

Table 1.1 lists a selected number of common hydrocarbon products by carbon number. The point developed here is that these substances share a common chemical heritage and structure: they are almost always derived from refined crude oil, and are made up of hydrocarbons of various molecular masses, distinguished from one another simply by the number of carbon-hydrogen units present in the molecule. As a result of this underlying similarity of chemistry, it is possible to convert between pure hydrocarbon products by adding units together (e.g., polymerisation and Fischer–Tropsch synthesis) or breaking them apart, achieved through pyrolysis and cracking.

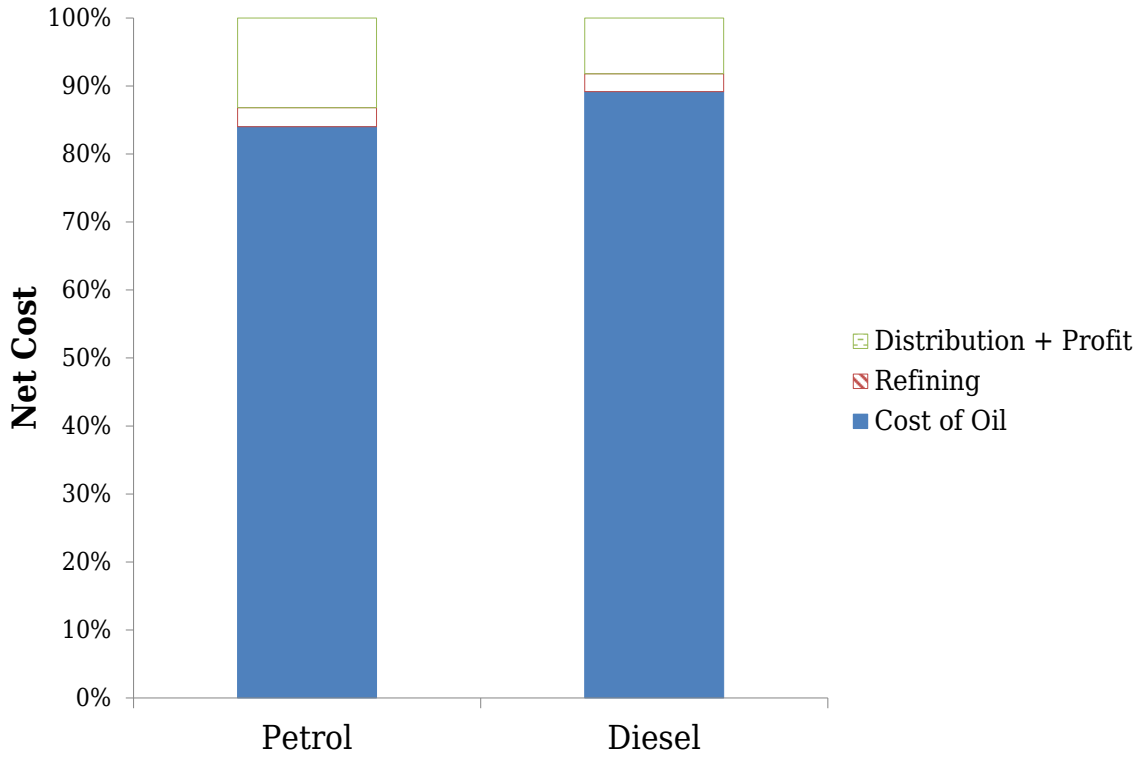


**Figure 1.1:** Cost breakdown of liquid transport fuels in the U.K. *Cost of oil* includes exploration/discovery and extraction/production. *Distribution + Profit* includes retail margin, supply, and distribution. This figure presents net costs and as such excludes duty and VAT, though these contribute significantly to the final cost paid by the consumer. Data adapted from [43].

### 1.4.1 Cost Savings and Efficiency Benefits of Feedstock Recycling

Figure 1.1 gives a breakdown of the net cost of liquid transport fuels in the U.K. By far the greatest proportion of the cost of the final refined product is the cost of the crude oil from which the fuels are made (at 84–89%), which includes exploration/discovery and extraction/production. Refining, distribution, and retail profit make up surprisingly little of the overall costs. By repurposing a waste stream into a raw material from which new products can be fabricated, but one in which the significant discovery and extraction costs *have already been undertaken*, microwave-assisted pyrolysis has enormous potential to make savings in both monetary terms [43] and in terms of the energy required to produce the next cycle of products [44].

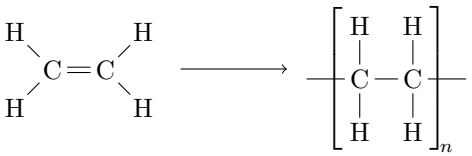


**Figure 1.2:** Ethene monomer and its corresponding polyethylene polymer form.

## 1.5 High Density Polyethylene (HDPE)

While the focus of this introduction thus far has been on plastics generally, this dissertation focuses on high density polyethylene (HDPE) specifically, using it as a model for more general hydrocarbon polymers. Polyethylene is the most common form of plastic, accounting for 29% of total demand in Europe [1]. HDPE is made through chain-growth polymerisation, combining ethene molecules together into chains between 500,000–1,000,000 units long by the application of heat and pressure [14] (see figure 1.2). The "high density" in HDPE describes polyethylene produced with little structural branching, which is ensured by the use of an appropriate catalyst (such as the titanium-based Ziegler–Natta class [45]). This linearity causes HDPE to have a greater proportion of crystalline regions than "low density" polyethylene, and it is as a result harder, and exhibits a higher tensile strength [14]. These properties result in HDPE being employed in a diverse set of applications including bottles and containers, plastic bags, and a wide variety of consumer goods.

HDPE was chosen as a model material for this research because of its abundance and widespread use, the simplicity of its pure hydrocarbon molecular structure (thus avoiding adding complication to the already complex pyrolytic breakdown reaction pathways), and because it is one of the relatively few materials on which microwave pyrolysis research has already been conducted [29, 46], thus offering an external point of comparison and validation to this study.

## 1.6 Potential Benefits from the Microwave-Assisted Pyrolysis of HDPE

In summary, a number of potential benefits arise from the microwave-assisted pyrolysis of HDPE:

- By presenting an alternative disposal route for plastics, microwave-assisted pyrolysis has the potential to divert this waste stream away from incineration

(with its associated toxic emissions and greenhouse gas release) and landfilling (for which space is at a premium in many countries, and which in any case results in extremely long decomposition times).

- With the potential to cope with higher levels of contamination than conventional recycling techniques, microwave-assisted pyrolysis presents a pathway to recycle waste streams that would otherwise be disposed of through less efficient means and/or without resource recovery.
- By creating a valuable end product from a waste stream, microwave-assisted pyrolysis assigns value to that waste, which motivates collection and disposal through this value-added pathway, and potentially disincentivises illegal and inappropriate disposal, which currently causes significant environmental damage [47–49].
- New plastic created from the raw materials produced by the microwave-assisted pyrolysis of waste plastic should be indistinguishable from virgin plastic produced from oil-derived feedstock, avoiding the pitfalls and lower quality inherent to polymer produced through contemporary mechanical recycling techniques.
- While any hydrocarbon fuels produced through the microwave pyrolysis of plastic would contribute equally to greenhouse gas emissions as those produced through conventional means if their combustion alone is considered, given the potential energy savings gained by avoiding the need to discover and extract fresh raw materials for their production (with the $CO_2$ emissions associated with that process), the overall energy use and emissions for fuels produced by microwave-assisted pyrolysis should be less. This makes fuel produced in this manner far preferable, given the fungibility of the international hydrocarbon market, and constant or increasing demand.
- Non-fuel petrochemicals, such as virgin plastic, produced using the products of microwave-assisted pyrolysis as feedstock, should have significantly lower energy and greenhouse gas emissions associated with their manufacture than those derived from conventional sources.

## 1.7 Motivation and Objectives for the Study

It is clear that microwave-assisted pyrolysis has a range of potential environmental, economic, and quality benefits as a plastic recycling technique; however, the stochastic nature of the pyrolytic degradation of hydrocarbon plastics results in the production of a wide range of molecular masses, which necessitates costly processing and separation

of the desirable short-chain hydrocarbons from the less useful long-chain waxes. Catalytic pyrolysis has the potential to narrow the range of molecules produced; microwave pyrolysis requires the use of a carbon bed to transfer microwave energy to microwave-transparent plastics; activated carbon has the potential to combine these two concepts by using the catalyst *as* the microwave-absorbing intermediate.

Generally, the microwave-pyrolysis field is inchoate but burgeoning, as is the use of activated carbon as a catalyst in its own right. While a small body of work exists on the microwave-assisted pyrolysis of HDPE [29, 46], this is the first such application using activated carbon as a catalytic reactor bed. Accordingly, a significant portion of this study is devoted to fundamental work on developing and refining necessary apparatus and demonstrating feasibility. Indeed, a significant motivation behind this work is basic curiosity to "see if it will work".

A second motivation underlying this study is to develop a process that will facilitate an improvement in the efficiency of resource use. Instead of throwing away material that has a large amount of energy invested in it, if the technology exists and is feasible, it makes sense to make the best use of already invested energy by maximising the utility of said material, opening up the possibility of a second use cycle, and avoiding expending energy to extract and process increasingly scarce new raw material from the surface of the earth.

In light of the above, the objectives for this study are as follows:

- To develop suitable apparatus to reliably carry out the microwave-assisted pyrolysis of HDPE, and collect the resulting pyrolysis products.
- To determine whether or not activated carbon is able to act as a catalyst in the microwave-assisted pyrolysis of HDPE.
- To characterise the products produced by the microwave-assisted pyrolysis of HDPE, and evaluate their potential utility.
- If initial results are sufficiently promising and further investigation is warranted, to examine the scale-up of the process with a larger capacity and continuous throughput.
- To understand and characterise the catalytic properties of activated carbon in the context of the pyrolytic breakdown of HDPE.
- To evaluate the potential of microwave-assisted pyrolysis of HDPE for future commercial development on an industrial scale.

## 1.8 Outline of Thesis

Having introduced the foundational concepts and motivations underpinning this study in this chapter, chapter 2 presents a review of previous work in the literature carried out by other researchers relevant to the current study. The development of the microwave-assisted pyrolysis apparatus and the condensation system used for product collection is described in chapter 3. This development allowed an initial feasibility study to be carried out (chapter 4) that investigated the use of an activated carbon bed to conduct microwave-assisted pyrolysis of HDPE, with small quantities of HDPE introduced to the reactor in a batch fashion at a range of reactor temperatures, and an analysis of the products that resulted. On the strength of these results, a rotary feeding mechanism was developed that allowed the processing of larger quantities of plastic with the continuous introduction of material. Chapter 5 assesses the products resulting from the microwave-assisted pyrolysis of HDPE in this reaction mode, and details the changes in the process, products, and reactor bed observed with the processing of larger quantities of material over time. Chapter 6 examines the potential reaction mechanisms that account for the pyrolytic breakdown of HDPE, and the additional pathways that may occur as a result of the activated carbon catalyst. The physical changes in the reactor bed, and in its catalytic ability, as the bed is used to process increasing amounts of material, are also discussed in this section. Finally, chapter 7 provides an overview and candid appraisal of the work carried out in this study, and describes potential avenues of further study that could be carried out to advance this field further.

# 2

# Literature Review

## 2.1 Carbon

Carbon is the fourth most abundant element in the universe [50], and perhaps the most versatile; it is non-metallic, and tetravalent — with four electrons available to form covalent bonds with other atoms in $sp^3$ (tetrahedral), $sp^2$ (ring), and sp (linear) configurations. Its molecular properties and bonding abilities allow carbon to form more compounds than any other element, including the entire gamut of organic compounds, which form the chemical basis of all known life. Carbon also has the ability to form long chains of interconnecting C-C bonds — a property known as catenation, and which is the basis of the element's ability to form macromolecules and polymers such as DNA, proteins, carbohydrates, and lipids, as well as synthetic polymers such as rubbers and plastics — the focus of this study. Carbon is also used in this study as a microwave receptor in the form of coke, and microwave receptor and catalyst in the form of activated carbon, purposes for which it has physical and chemical properties that make it particularly useful, as is developed throughout this review.

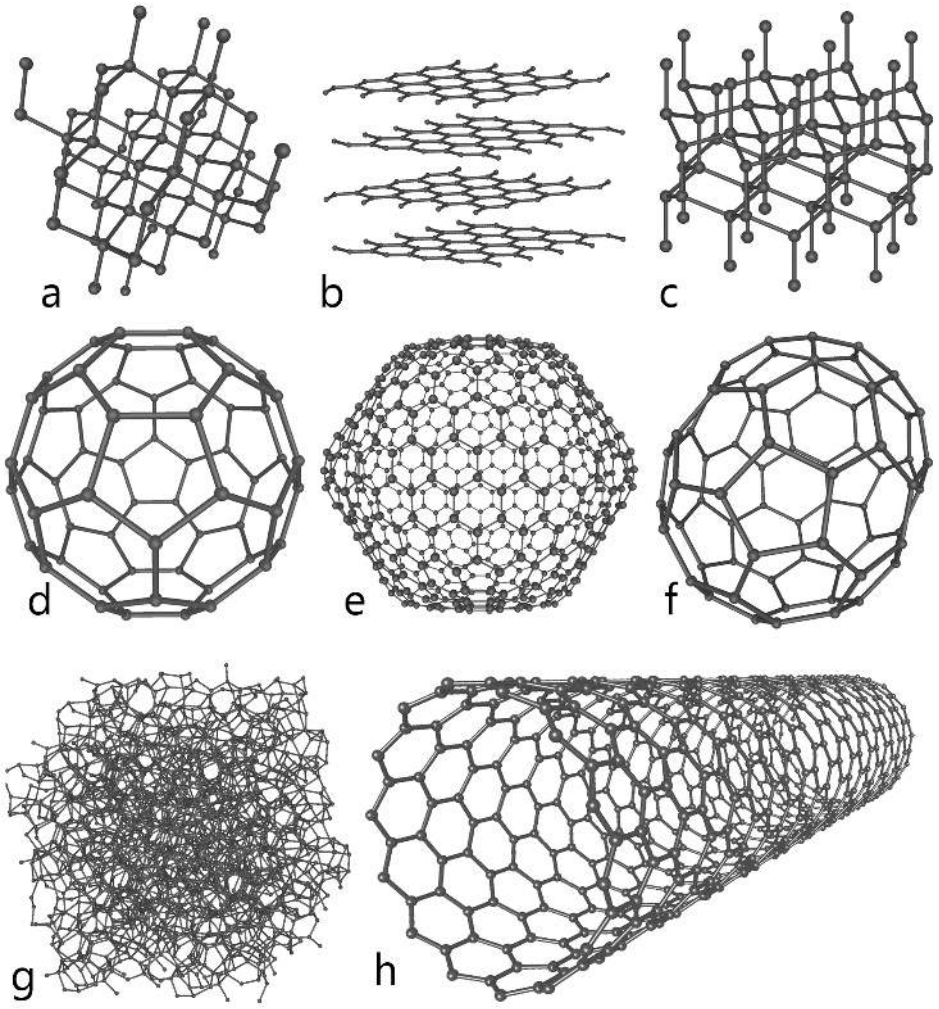


**Figure 2.1:** Some allotropes of carbon: a) diamond, b) graphite, c) lonsdaleite, d–f) fullerenes ($C_{60}$, $C_{540}$, $C_{70}$), g) glass-like carbon, h) carbon nanotubes. Reproduced from [51] under creative commons licensing.

### 2.1.1 Allotropes of Carbon

As a result of its versatile bonding abilities, elemental carbon is able to form a variety of physical molecular forms, or allotropes, the most well known of which include diamond, graphite, and polycrystalline carbon (colloquially, though not technically, “amorphous”) such as coal and soot. Diamond (figure 2.1a) is an extremely hard form of carbon where each carbon atom is bonded to four others in a tetrahedral lattice (its rarer cousin lonsdaleite (figure 2.1c) employs a hexagonal lattice structure but has similar properties).

Graphite (figure 2.1b) is the most thermodynamically stable form of carbon, with a hexagonal lattice structure that forms planar layers; an individual hexagonal plane is known as a *graphene* layer. With each carbon atom bonded to three others, the remaining valence electrons delocalise, which allows graphite to conduct electricity.

Adjacent layers are stacked atop and displaced from one another to form an alternating ABAB sequence; these are held together by van der Waals forces and resonance effects such that the force between layers is approximately one third that of a carbon-carbon double bond [52].

Apart from diamond and lonsdaleite, all known carbon forms are related to the graphite lattice structure, with a continuous spectrum of increasing disorder existing, where layers abandon the ABAB stacking, and become smaller and more defective, until eventually, as in the highly disordered glass-like carbons (figure 2.1g), the existence of identifiable graphene layers is almost lost. The more exotic allotropes of carbon such as fullerene spheres (figure 2.1d–f) and nanotubes (figure 2.1h), while clearly on the more ordered end of this spectrum, lie outside the purview of this study.

The two forms of elemental carbon dealt with in this study are coke, and activated carbon. Coke is the carbonaceous residue that remains after the high temperature pyrolysis of a hydrocarbon material (distinct from ash, which is the residue that remains after a substance is *burned*, and which consists primarily of metal oxides). Activated carbon is described in detail in §2.3.

### 2.1.2 Non-Graphitisable Carbon

Research carried out by Rosalind Franklin (a pioneer in research into the structure of coals and carbons as well as her perhaps more widely known work on DNA) in the 1950s has led to the classification of carbon compounds into *graphitisable* (which are materially anisotropic) and *non-graphitisable* (isotropic) categories, based on their ability to adopt the long-range parallel planar structure (with associated X-ray crystallography patterns) that is characteristic of graphite, when they are heated to over 2000°C [53, 54]. While non-graphitisable carbon exhibits many localised elements of graphene lattice structure (hence its description as *polycrystalline*), it does not exhibit *parallelism* on a *long-range* basis; instead, non-planar elements result in complex three-dimensional structures. The inability of non-graphitisable carbon to change conformation arises from the short range structure of the non-planar units, which are bonded into the overall structure during carbonisation; the activation energy required to simultaneously break so many bonds in order to adopt a graphite structure is prohibitive in all but the most extreme cases [52]. Activated carbon is such a non-graphitisable substance, and it is from this characteristic that its porosity and other useful properties derive.

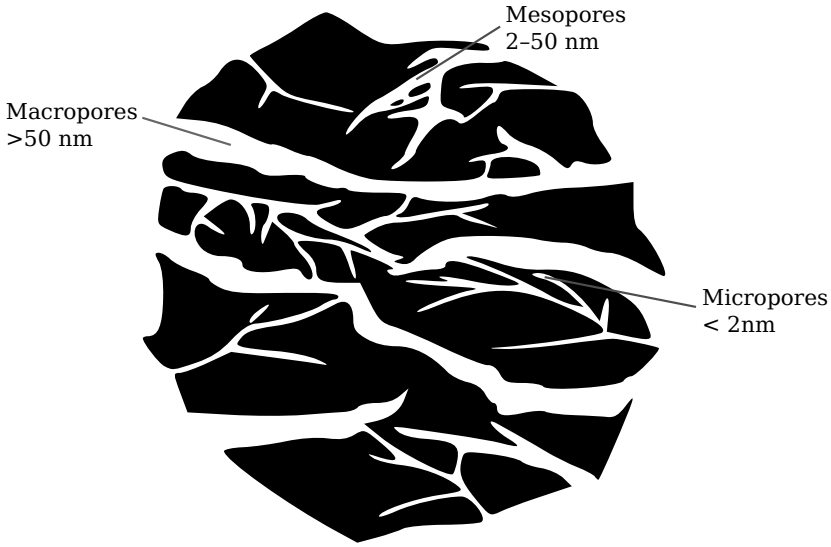


**Figure 2.2:** Schematic representation of pores in an activated carbon particle. Pores are able to extend deep into a substance in three dimensions, significantly increasing its overall surface area.

## 2.2 Porosity

Porosity is quite simply empty space within a structure into which substances of equal or smaller size may adsorb. As illustrated in figure 2.2, porous fissures can extend deep within a substance's structure, significantly enhancing its overall surface area. Porosity is usually categorised into three classes: macropores, with a diameter of >50 nm; mesopores which measure 2.0–50 nm, and micropores with a diameter of <2.0 nm. While small molecule adsorption mostly takes place in micropores (these being of comparable size magnitudes), macro- and mesopores play an important role in providing passage for adsorbate to reach the micropores.

## 2.3 Activated Carbon

Activated carbon is a form of manufactured, non-graphitisable carbon with a very high porosity and absorptive ability, and which shows promising catalytic activity (discussed later in this section) that has made it the subject of this study.

### 2.3.1 Material Origin and Carbonisation

Activated carbon can be manufactured from a wide range of macromolecular carbohydrates and hydrocarbons of natural and synthetic origin, the main requirement of the source material being that it is primarily carbon containing. Activated carbon has

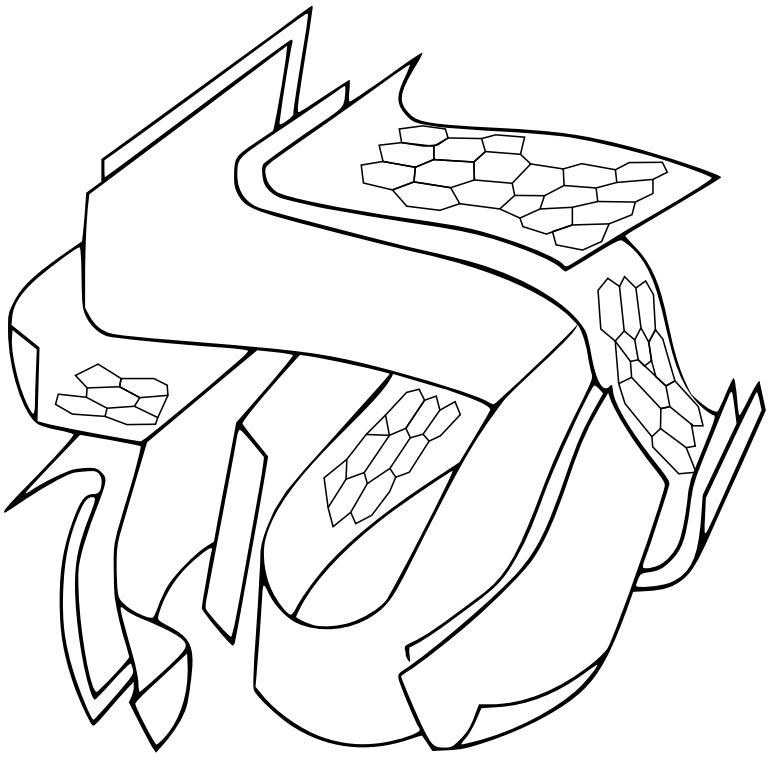

**Figure 2.3:** Schematic structure of activated carbon, showing the folds in the planar structure, and defective graphene lattices, from which the microporous structure of activated carbon derives. Adapted from [71].

been successfully produced from wood [55–57], coconut shell [58–60], fruit stones and nut shells [61–65], coals [66–68], and oil bitumen [68, 69].

These input materials are carbonised/pyrolysed — treated at high temperature in an inert atmosphere, which results in an increase in carbon percentage as volatile gases and liquids are driven off and the number of non-carbon heteroatoms decreases. Research has shown that throughout this process, the macromolecular structure of the material remains mostly intact [70], though carbon atoms rearrange over small distances (probably <1 nm) within the network to positions of greater stability, i.e., closer to the six-membered graphene ring structure [52].

The carbon material remaining at the end of this process will have significant porous structure, with carbon atoms arranged in graphene sheets crosslinked in a random manner. Defects in the graphene lattice cause complex three-dimensional structure including folds and curves in the sheet, and spatial distortions of the sheet itself such as “pinched together” peaks/troughs and discontinuities. An illustrative analogy is the crumpling of a two-dimensional piece of paper resulting in complex three-dimensional structure. The pores in the activated carbon are the interstices in this three-dimensional topology, as depicted in figure 2.3.

### 2.3.2 Activation Process

While material carbonised as described above has porous structure, this is insufficient for commercial applications. In order to make activated carbon, the carbon undergoes a process (eponymously, "activation"), which creates further porosity, widens existing porosity, opens access to previously inaccessible pores, and modifies the surface of the carbon. This is achieved by either thermal or chemical means, or a combination of the two.

#### 2.3.2.1 Thermal Activation

"Thermal" activation involves gasifying the carbon with the oxidising gases, steam, or $CO_2$, at high temperatures (>900°C), according to the following equations:

$$\mathrm{C} + \mathrm{CO_2} = 2\mathrm{CO} \tag{2.1}$$

$$\mathrm{C} + \mathrm{H_2O} = \mathrm{CO} + \mathrm{H_2} \tag{2.2}$$

Oxygen gas is not used as its combination with carbon is highly exothermic, difficult to control, and results in consumption of the carbon (or burning) rather than penetration into, and enhancement of, existing pores. In this way, carbon atoms are *selectively* removed from the molecular surface. The carbonisation pyrolysis process can create tars and other decomposition products that fill or partially block pores; this more disorganised carbon is the first to react with the oxidising gases, creating new accessible porosity by "clearing" the blocked pores [36]. These reactions also widen existing rudimentary porosity of the char, abstracting atoms from the carbon structure, and creating defects in the lattice such as free valencies, which contribute to activated carbon's properties. Furthermore, the reaction of the oxygen-containing gases creates surface oxygen complexes, which themselves have reactivity and contribute to adsorption [52].

#### 2.3.2.2 Chemical Activation

Activation can also proceed via chemical means, where the carbonisation and activation occur simultaneously. This involves impregnating the source material with a chemical agent, heating in an inert atmosphere, and then washing any remaining chemical out. The most commonly used agents for chemical activation are $ZnCl_2$, $H_3PO_4$, and KOH. $ZnCl_2$ (which at high concentrations exhibits Bronsted acidity) and $H_3PO_4$

activation proceed via acid-catalysed dehydration and depolymerisation, promoting bond cleavage and the formation of cross-links (with cyclisation and condensation reactions) [72–74]. KOH activation occurs via a redox reaction where carbon is oxidised to CO or $CO_2$, with the reduction of the potassium to a metal ion that intercalates into the carbon structure and expands the lattice; destructive removal of this ion occurs when the carbon is progressively heated, creating new pores by disrupting the graphene structure as it exits [73, 75]. The different chemical routes produce activated carbon with different porous profiles, but the end result in all cases is a highly porous active carbon.

### 2.3.3 Applications of Activated Carbon

Activated carbon has innumerable applications, though the bulk of these revolve around its superlative ability to physically adsorb chemical species as a result of its highly developed porous structure.

#### 2.3.3.1 Commercial Applications of Activated Carbon

Water treatment is the single largest use of activated carbon worldwide, with the primary focus being the removal of pollutant organic compounds, either to create potable water or to remove toxic and harmful contaminants before discharge to the environment. Specific applications include the removal of volatile organic compounds [76–78], pharmaceuticals [79–81], natural organic matter [82–84], and heavy metals [85–87]. Activated carbon is also used significantly in the food and beverage industries to remove colour or odour from products such as fruit juices [88], sugar [89, 90], and vegetable oil [91]. Activated carbon's excellent adsorptive ability is also used in chemical and pharmaceutical production, especially in fermentation processes where antibiotics, vitamins, and steroids are adsorbed in the activated carbon and then recovered by solvent extraction followed by distillation [52, 92, 93]. The two largest gas-phase applications of activated carbon are solvent vapour recovery [94] and automotive fuel evaporative loss systems [52].

#### 2.3.3.2 Activated Carbon as a Catalyst Support

Activated carbon is widely used as a catalyst substrate, supporting the catalyst and allowing it to be spread over the activated carbon's large surface area, to increase the number of catalytically active atoms exposed to substrate. Activated carbon has

particular utility in this role as it is resistant to acidic and basic media, is stable up to very high temperatures, and allows for the easy recovery of the active phase by simply burning the carbon off [95]. The catalyst is introduced by bringing a solution containing the active phase (or a suitable precursor) into contact with the activated carbon, where it adsorbs onto the surface. The mixture is dried and heat treated (sintered) to stabilise the catalyst [96]. The role of surface oxygen complexes is also important, with catalyst dispersion and sintering increasing with the number of oxygen surface groups [97, 98].

The number of reactions mediated by activated carbon supported catalysts is extremely large. Auer et al. [99] list a "selected" 40 *classes* of reaction catalysed by Pd, Pt, Ir, Ru, and Rh supported by activated carbon. Examples dealing with the production of hydrocarbons include the Fischer-Tropsch synthesis of synthetic fuels with Mo, Co, and Fe based catalysts [100–102]; the pyrolysis of vegetable oils into a diesel-like liquid using activated carbon supported Pd [103]; and the conversion of palm oil to biodiesel using activated carbon supported KOH [104].

### 2.3.4 Activated Carbon as a Catalyst

In recent times there has been growing appreciation of activated carbon as a useful catalyst in its own right, and it is currently used commercially in the production of carbonyl chloride from carbon monoxide and chlorine [36]. While work using activated carbon alone as a catalyst is relatively sparse in the literature, there is a slowly growing body of such reactions. Trimm [37] presented a list of reactions known to be catalysed by activated carbon, which is summarised in table 2.1.

One of the areas in which concerted activated carbon research has taken place is in the oxidative removal of harmful contaminants from water and gas streams. In these applications the high porosity of activated carbon facilitates capture of

| Reactions Involving | Examples |
|---|---|
| Hydrogen | $RX + H_2 \rightarrow RH + HX$ (X = Cl, Br) |
| | $HCOOH \rightarrow CO_2 + H_2$ |
| | $CH_3CHOHCH_3 \rightarrow CH_3COCH_3 + H_2$ |
| Oxygen | $SO_2 + \frac{1}{2}O_2 \rightarrow SO_3$ |
| | $NO + \frac{1}{2}O_2 \rightarrow NO_2$ |
| | $2H_2S + O_2 \rightarrow S_2 + 2H_2O$ |
| Halogens | $CO + Cl_2 \rightarrow COCl_2$ |
| | $C_2H_4 + 5Cl_2 \rightarrow C_2Cl_6 + 4HCl$ |
| | $SO_2 + Cl_2 \rightarrow SO_2Cl_2$ |
| | $C_6H_5CH_3 + Cl_2 \rightarrow C_6H_5CH_2Cl + HCl$ |

**Table 2.1:** Reactions catalysed by activated carbon. Reproduced from [36, 37].

even low concentrations of substrate, which is then catalytically oxidised with high efficiency, resulting in a purified output stream. This process has been successfully demonstrated in the oxidative removal of $H_2S$, $SO_2$, and $NO_x$ [105–107], with these reactions proceeding along the pathways outlined in table 2.1.

The ability of activated carbon to catalyse the oxidative dehydrogenation of substances has been studied in order to produce various chemical feedstock, such as the conversion of isobutane to isobutene [108], the highly selective oxidative dehydrogenation of alkylbenzenes to produce styrene (the monomer of polystyrene) and $\alpha$-methylstyrene (the precursor to a number of plasticizers and resins) [38, 109–113], as well as the dehydrogenation and dehydration of various alcohols [114–116].

#### 2.3.4.1 Catalytic Hydrogen Production using Activated Carbon

Another area that has seen the application of activated carbon as a catalyst is the production of hydrogen from methane, according to the reaction:

$$CH_4 \rightarrow C + 2H_2 \tag{2.3}$$

This process has the potential to produce hydrogen with significantly reduced $CO_2$ emissions, and is a substantially simpler operation than many conventional hydrogen production processes such as the steam reforming of methane. Muradov et al. have successfully demonstrated this process, espousing the virtues of activated carbon as a catalyst because of its high availability and durability, low cost, and advantages over metal catalysts such as high temperature resistance, and tolerance to sulphur and other harmful impurities that often arise from natural hydrocarbon feedstock [39, 117–121]. While activated carbon has higher activity than other comparable catalysts for this purpose, it has been noted that activated carbon does deactivate over time as a result of carbon deposition from the hydrocarbon decomposition [122].

In a related application, Petkovic et al. [123] have used activated carbon to decompose hydrogen iodide to produce hydrogen, a key reaction in a wider thermochemical scheme to split water into hydrogen more efficiently than through pure thermal means.

## 2.4 Microwave Heating

The total charge of a system in an electric field is given by:

$$\mathbf{D} = \varepsilon \mathbf{E} \tag{2.4}$$

where D is the electric charge density vector ($C/m^2$), E is the externally applied electric field (V/m), and ε is the absolute permittivity (F/m) — the measure of resistance that is encountered when forming an electric field in a medium. The permittivity of a material is usually given relative to that of free space:

$$\varepsilon = \varepsilon_r \varepsilon_0 \tag{2.5}$$

where $\varepsilon_r$ is the relative permittivity, and $\varepsilon_0$ is the permittivity of free space (8.86 x $10^{-12}$ F/m). A material's polarisation does not respond instantaneously to an applied field, and is dependent on (angular) frequency (ω); it is then convenient to treat permittivity (either relative or absolute) as a complex function:

$$\varepsilon(\omega) = \varepsilon'(\omega) - i\varepsilon''(\omega) \tag{2.6}$$

where ε' is the real part of the permittivity, known as the *dielectric constant*, and is related to the ability of a material to store an electric field's energy (e.g., a microwave field inducing dipoles), and ε" is the imaginary part of the permittivity, known as the *dielectric loss factor*, which is governed by the lag between the application of an electric field and a material's polarisation, and represents the dissipation of energy (as heat) within the medium. This energy loss appears as an attenuation of the applied field and is often measured as the ratio of the dielectric loss factor to the dielectric constant, or the angle between the imaginary axis and the total current density vector (i.e., the sum of the real and imaginary components of the permittivity), the *dielectric loss tangent* or *dissipation factor*:

$$\tan\delta = \frac{\varepsilon''}{\varepsilon'} \tag{2.7}$$

Both the dielectric loss factor and the dielectric constant can vary with the frequency of the applied field and the temperature of the material, and a material with a large dielectric loss tangent (i.e., a large dielectric loss factor and moderate dielectric constant) will be a good microwave receptor, receiving and converting this energy to heat with high efficiency [124–126].

Briefly, there are three mechanisms by which microwave heating occurs. *Dipole reori-*

*entation* occurs when the chemical bonds of dipoles are realigned by the fluctuating electromagnetic field. This movement creates friction between the rotating molecules and causes heat to be generated throughout the volume of the material. The dipoles themselves can be innate to the molecule, arising from asymmetric charge distribution, or induced by the microwave field, displacing electrons or nuclei from their equilibrium position. Similar interactions with the electromagnetic field can also occur as a result of interfacial, or *Maxwell-Wagner polarisation*, where charge builds up in contact areas or interface layers in heterogeneous materials as a result of different conductivities or dielectric properties. Finally, *conductive heating* occurs when an electrically conductive material is exposed to an electromagnetic field, inducing charged particles (e.g. electrons, ions) to move. Heating occurs as a result of the material's innate resistance to this flow of current.

### 2.4.1 Dielectric Properties of Materials and Influence on Microwave Receptivity

Plastics are poor microwave receptors — the dielectric loss tangent of polyethylene is 0.0007 [127] (all such values in this text are listed at room temperature and with a microwave field at 2.45 GHz); by way of comparison, distilled water — an excellent microwave absorber — has a dielectric loss tangent of 0.118 [128]. As long non-polar molecules, plastics polarise and reorientate poorly; being homogeneous, Maxwell-Wagner polarisation does not occur with pure plastics, and with no free electrons nor does conductive heating. Clearly, plastics are very poor microwave receptors, and as such are unable to be directly targeted safely by microwave heating. Instead, when heating plastics (or indeed any microwave transparent material) with microwave radiation an intermediate receptor is used and the energy is transferred to the plastics via short-range conduction.

#### 2.4.1.1 Carbonaceous Materials as Microwave Receptors

The microwave receptivity of carbonaceous materials varies depending on their chemical composition. Diamond, for example is almost entirely microwave transparent owing to its rigid lattice-like structure deriving from its $sp^3$ bonding, and lack of free electrons. Graphite, on the other hand, with its $sp^2$ bonding and delocalised electrons, heats well when exposed to a microwave field, primarily through conductive heating. Carbonaceous materials with a high level of structural irregularity such as

coal (assuming no moisture content) are relatively poor microwave receptors (with a dielectric loss tangent of 0.02-0.08 [128]), owing to the lack of delocalised electrons; however, as the structural order increases so too does the dielectric loss tangent and microwave receptivity. Coke and activated carbon, which aside from the potential catalytic and reducing abilities that make them well suited to pyrolysis, have high dielectric loss factors of 0.35–0.83 and 0.22–2.95 respectively [128, 129], making them good microwave receptors. Furthermore, these materials are generally relatively inexpensive, and are easily available in different textures, sizes, forms, etc., all of which contributes to their selection for use in this work.

#### 2.4.1.2 Power and Penetration Depth

The power transmitted to an object in a microwave field can be calculated from the Maxwell equations: assuming a uniform electric field, E, the power, P, absorbed per unit volume is given as:

$$P = 2\pi f \varepsilon_0 \varepsilon'' \mathbf{E}^2 \tag{2.8}$$

i.e., absorbed power increases with the square of the strength of the electric field. However, as energy is absorbed by a material the electric field strength decreases, making the above equation only valid for thin materials, if they are microwave absorbent. The penetration depth of a microwave field is usually defined as the distance below the surface where the absorbed power is 1/e (i.e., approximately 37%) of that of the power at the surface of the material [125, 130]. In many cases when highly microwave-absorbent materials are placed in a “normal” strength microwave field (such as the carbonaceous microwave receptors described in this chapter) it is unlikely that the microwave field would penetrate throughout the entire material, a further reason that stirring is often in employed in these cases.

### 2.4.2 Microwave Heating Modes

#### 2.4.2.1 Single-Mode Microwave Heating

Single mode microwave heating occurs in cavities where the incident and reflected waves give rise to a single mode standing wave pattern. For simple designs this formation can be solved analytically, giving a predictable electromagnetic field distribution in the cavity. This necessitates a microwave source with very little variation in output frequency, and with one resonant mode the size of these applicators is approximately the order of one wavelength, with one “hot spot” where the microwave field strength is

very high [130]. The small size and large power intensities achieved with this form of heating lead to relatively niche applications such as joining ceramics [131], and curing thermosetting resins [132], though these properties also make it difficult to operate these reactors on anything other than small scale.

#### 2.4.2.2 Multi-Mode Microwave Heating

In multi-mode heating, microwaves are channelled into a cavity with dimensions substantially larger than that of the microwave's wavelength. This results in a large number of standing wave modes that can exist at or near to the operating frequency. To minimise the formation of "hot" and "cold" spots (high and low field strength) in the cavity as a result of constructive and destructive interference occurring it is desirable to excite as many of these modes as possible. In spite of this, heating uniformity can often be difficult to achieve in multi-mode ovens and this often promoted through the use of metallic mode stirrers or by rotating the product within the field [130]. The ability of multi-mode heating to cope with larger objects and batch operations make it by far the most common form in industrial applications.

### 2.4.3 Microwave vs. Thermal Effects

Microwave heating has been employed to facilitate a wide range of reactions (in a rather comprehensive review of microwave-assisted organic synthesis, Lidström et al. [133] individually listed over 600 separate reactions enhanced by microwave heating). Studies of microwave-assisted reactions have noted them proceeding faster (by 2–3 orders of magnitude), more cleanly, and with higher yields than their conventionally heated counterparts [134–136]. However, the source of these differences is the subject of some controversy, with some researchers positing microwave-specific effects over and above those that can be accounted for by heating and temperature profile differences alone. For example, there is some compelling evidence that microwave fields enhance sintering reactions by providing a voltage-induced driving force that increases grain boundary diffusion [137]; Marand et al. [132] have advanced explanations accounting for the microwave-enhancement of organic synthesis reactions in which preferential orientation of (dipole-containing) molecules are induced by the microwave field, or in which polar reactive groups are selectively activated (as opposed to heating the entire molecule as would be the case in externally derived conductive heating); de la Hoz et al. [138] provide a good review of various research groups' evidence in support of microwave fields providing some sort of sub-molecular selective energy transfer.

In some instances, though, the case for microwave-specific effects has been overstated, with a critical re-examination of various reactions where previous authors had claimed microwave-specific influences showing no evidence for the existence of non-thermal microwave effects [139, 140]. In this re-examination, the original discrepancies were attributed to inadequate stirring resulting in inhomogeneous temperature distribution, and/or less accurate temperature measurements such as those arising from infrared sensors, which do not provide accurate readings in the microwave heating context (by contrast, the re-examination experiments were conducted in a reactor that used multiple highly accurate fibre-optic temperature probes). In the case of liquids and gases, even highly targeted microwave energy is unlikely to cause purely thermal microwave-specific effects, as redistribution of kinetic energy between molecules occurs more rapidly than the conversion of electromagnetic energy into kinetic energy [141]. However, it should be noted that this fact does not preclude non-thermal microwave-mediated interaction.

While there is wide acceptance of the ability of microwave heating to selectively heat substances on the macroscopic (and even molecular) scale, whether this extends down to direct activation of functional groups or other non-thermal effects remains to be conclusively settled. Independent of whether this occurs, it is clear that microwave heating *does* result in different thermal heating profiles to conventional techniques (e.g., fast heating rates, volume heating, high power density, material selectivity, even heating, and good heating control) and this is of demonstrable significant value in and of itself.

#### 2.4.3.1 Microplasmas

An instance of an *observable* microwave-specific phenomenon directly applicable to this study is the formation of microplasmas [29, 142–144]. In carbon materials with graphite-like structural elements, where there are a large number of relatively mobile delocalised electrons, the microwave field may induce charge imbalances that equalise across particle boundaries in an arc that conductively ionises the intervening atmosphere. These microscopic plasmas present high temperatures and extreme (if localised) conditions that have the potential to influence the course of the bulk reaction.

## 2.5 Microwave-Assisted Pyrolysis

Microwave-assisted pyrolysis has been applied to a wide variety of inputs, resulting in products that show a range of advantages over the source material such as conversion or separation into less hazardous forms, significant volume reduction of waste, and the production of useful fuels or chemical feedstock. An illustrative set of examples of these processes is presented below.

### 2.5.1 Processing of Problematic Waste

#### 2.5.1.1 Scrap Tyres

As a complex composite material that is expendable, produced in large quantities, and potentially environmentally hazardous, automotive tyres present a challenging disposal problem. A number of research groups have examined the possibility of recycling scrap tyres using microwave-assisted pyrolysis, recovering a gas and oil fuel product, steel, and high value activated carbon or carbon black [145–148]. Furthermore, the absence of oxygen in the pyrolysis process means NOx, SOx and other harmful organic emissions are significantly reduced compared with disposal by incineration. The carbon black content in tyre rubber makes this material a sufficiently good microwave receptor that an intermediate bed need not be used.

#### 2.5.1.2 Used Automotive Engine Oil

Lam et al. [149–152] have used microwave pyrolysis to recycle used automotive engine oil, a hazardous waste containing heavy metals and polyaromatic hydrocarbons. Pyrolysis of this material using a coke bed at temperatures between 400–700°C resulted in a high recovery of the calorific and chemical value of the oil, with a condensed product consisting of aliphatics and aromatics, and a non-condensable gaseous fraction containing light hydrocarbons and some hydrogen. The microwave pyrolysis also acted as a separations process, with the majority of the heavy metals and PAHs becoming embedded in a char fraction that was separable from the reactor bed.

#### 2.5.1.3 Sewage Sludge

Sewage sludge is another hazardous waste that has been processed using microwave pyrolysis in order to generate syngas ($H_2$ + CO). In these studies, led by Menéndez et al. at the Instituto Nacional de Carbon in Spain [21, 153–155], the sludge was initially

pyrolysed with a fresh coke bed, but the char that was produced as a result of the process was also demonstrated to be an adequate microwave receptor, and was used in subsequent runs. The water content of the sludge was used to gasify the material, with a final operating temperature of 1040°C and typical yields of 62% aqueous, 25% gas, 10% char, and 3% oil. The primary components of the gas were $H_2$, CO and $CH_4$ with percentages of 22–43%, 23–30% and 2–7%, respectively. The use of microwave-assisted pyrolysis resulted in a larger gas fraction, and lower polycyclic aromatic hydrocarbon content compared with conventionally heated sludge [156, 157].

### 2.5.2 Microwave-Assisted Pyrolysis of Biomass Waste

Aside from the sewage sludge already mentioned, a wide variety of novel biomass has been the subject of microwave-assisted pyrolysis research, including wood [19, 158], coffee hulls [12], micro-algae [159], rice straw [160], waste tea [161], and wheat straw [162]. These experiments used non-catalytic carbon beds when processing materials that were poor receptors of microwaves, though others (such as the pyrolysis of wood) heated the material directly. A variety of gas, liquid and solid phase products resulted, these being determined by the characteristics of the original feedstock and the processing conditions. Potentially useful gaseous and liquid products were produced, though in many cases these would likely require further separation and/or refining before end use. The bulk heating characteristics of microwave-assisted pyrolysis allows the processing of materials without energy intensive and costly grinding/shredding (e.g., entire large wood blocks were processed by Miura et al. [158]), limited only by the size of the reactor and the ability of the microwave field to penetrate the material. This fact, combined with the more rapid reaction rate that was observed in the cases where microwave pyrolysis was compared with conventional electric heating, would result in a large overall reduction in electricity consumption compared with conventional processing.

### 2.5.3 Upgrading Naturally Occurring Hydrocarbon Sources

Microwave-assisted pyrolysis has also been applied to a number of naturally occurring hydrocarbon materials in order to produce fuels by extracting volatile components and cracking long-chain hydrocarbons. Oil shale, for example, has been subjected to microwave pyrolysis at 700°C, yielding around 6 wt.% of a highly aromatic oil and 10 wt.% gaseous products [163]. Similar yields were obtained using conventional

heating but the composition of the products differed, with more cracking occurring in the microwave-assisted pyrolysis case, and with fewer sulfur, nitrogen, and polar compounds in the resulting products.

Coal has also been processed by microwave-assisted pyrolysis at temperatures up to 1300°C in order to produce condensible tars for use as a fuel [164, 165]. While coal can be heated directly using microwave radiation, it is a relatively poor microwave-absorbent, and in this study a variety of different microwave intermediates were used to increase the pyrolysis reaction rate. Yields of condensible tars varied depending on the intermediate microwave receptor used: with coke the tar yield was 20 wt.%, using $Fe_3O_4$ resulted in 27 wt.%, and a maximum of 49 wt.% was seen with the use of CuO. The tars were primarily aliphatic (65–74% of the oil), with the remainder consisting of aromatic species.

### 2.5.4 Microwave-Assisted Pyrolysis with an Activated Carbon Bed

There have been a limited number of studies specifically using activated carbon in conjunction with microwave-assisted pyrolysis, and these are briefly discussed as follows. Ma et al. [166] have used microwave-assisted pyrolysis over activated carbon in order to remove NO from simulated combustion flue gas through conversion to $N_2$. The use of microwave heating in this context facilitated a more rapid conversion, and preserved the porous structure of the activated carbon more effectively, compared with conventional heating.

Research carried out at the Instituto Nacional de Carbon has employed microwave-assisted pyrolysis to crack glycerol into syngas at 800°C [22, 167]. Using an activated carbon bed produced slightly higher overall gaseous yields, a greater syngas yield, and a $CO/H_2$ ratio closer to one, when compared with the same procedure using an inert quartz blank.

The same group has used activated carbon as a catalyst in the microwave-assisted decomposition of methane to hydrogen [142, 168]. With an inert control bed, no decomposition of methane occurred at 800°C, though this occurred readily over the activated carbon bed. Furthermore, even when methane decomposition did occur in the non-catalytic case at higher temperatures, the selectivity for $H_2$ production was improved by nearly 100% through the use of activated carbon. The combination of activated carbon and microwave heating resulted in greater yields than pyrolysis with other carbon materials, and with conventional heating using activated carbon; this

was attributed to the formation of microwave-induced microplasmas in the bed. In longer experiments of two hours' duration some deactivation of the activated carbon was noticed, which was attributed to carbon deposits entering the pores and reducing the surface area.

Lignocellulosic biomass has also been subjected to microwave-assisted pyrolysis using activated carbon, with Douglas fir pine producing an aromatic oil at 25–35 wt.% yield. The use of activated carbon resulted in an oil with a higher content of esters and phenolic species compared with the non-catalysed case [169].

## 2.6 Pyrolysis of Plastics

The pyrolysis of plastics, with the aim of recovering valuable chemical compounds, has been carried out by a number of researchers using a wide variety of source material, though almost all of this work has been conducted with conventional heating techniques; a review of these studies is presented below. The percentages given in this section are all weight percentage of input plastic, unless specified otherwise.

### 2.6.1 Pyrolysis of Polyethylene

Research into the pyrolysis of plastics has been carried out at the University of Hamburg, led by Walter Kaminsky, since the 1970s [170]. This research has seen the development of a series of fluidised bed reactors (FBRs), in increasing sizes from laboratory plant (100 g/h), pilot plant (30 kg/h) through to prototype plant (150 kg/h). This configuration, referred to as the Hamburg process, recirculates a portion of the produced pyrolysis gas to fluidise the bed. Applying this process to polyethylene at an operating temperature of 830°C resulted in gaseous and condensed pyrolysis products, the four most prevalent species being, in order: 27.6% ethene, 23.7% methane, 16.2% benzene, and 4.0% toluene [171]. A separate study at 740°C saw the products comprise 55.8% gas, 42.4% oil and 1.8% residue (char), with the equivalent prevalent species: 23.8% methane, 20.0% ethene, 19.2% benzene, 3.9% toluene.

Within the U.K., the Williams group at the University of Leeds has led research into the pyrolysis of plastics. When pyrolysing HDPE in a fixed bed reactor, increasing from room temperature to 700°C at a rate of 25°C/min, the recovered pyrolysis products included 17% gases, 80% oil, and no char. FTIR spectra of the pyrolysis oil indicated it was primarily aliphatic [172]. Pyrolysing LDPE in a fluidised bed at a range of temperatures from 500–700°C resulted in steadily increasing gas yields with increasing

temperature from 10.8% to 71.4%, while oils and waxes fell from 89.2% to 28.6% over the same range. The gases were short-chain linear aliphatics, with methane, ethene, propene, and butene increasing the most as the reaction temperature increased. The oils and waxes were aliphatic at 500°C and 550°C, with aromatics first detected at 600°C and increasing in concentration thereafter [173].

Conesa et al. [174] have used an FBR to pyrolyse HDPE at temperatures between 500–900°C. As reaction temperature increased so did cracking and yield of gases, which reached a maximum of 94.5% at 800°C, where the main components of the pyrolysis products were ethene (37%), benzene (24%), methane (20%), and propene (4.7%). At 900°C the total yield declined slightly, a fact attributed to the cracking of input sample to soot. Comparing the FBR results to that obtained using a Pyroprobe 1000, in which secondary reactions and residence time were minimal owing to the small physical area that was heated, showed significantly less cracking than when the FBR was used at equivalent temperatures, and a change in composition with minimal aromatics present (the maximum observed yield of benzene was 2.3 wt.%), highlighting the importance of these factors in both overall cracking and aromatic formation.

Milne et al. [175] pyrolysed LDPE in an internally circulating FBR at 800°C. Changing the residence time from 400 ms to 600 ms resulted in a dramatic change in product composition, with increases in methane (10.9% vs. 23.3%) and ethene (18.7% vs. 32.3%), and decreases in heavier $C_4$ species (42.6% vs. 13.1%). Minimal char (~2%) and condensate (5–8%) were produced, though this was not analysed further.

Aguado et al. [176] used a conical spouted bed reactor to separately pyrolyse both LDPE and HDPE between 450–600°C, and found little difference between the resulting pyrolysis products. The yield of pyrolysis waxes decreased almost linearly from 80% to 49% over this range, with the gas yield making up the remaining fraction. Both of these components comprised linear aliphatic species.

Finally, Mastral et al. at the University of Zaragoza in Spain have conducted research into the pyrolysis of HDPE, using an FBR at temperatures between 640–850°C. At 640°C the obtained yields were 78.9 wt.% waxes/oils and 11.4 wt.% gases, with the waxes consisting of aliphatic hydrocarbons. Cracking and gas yields increased with temperatures to a maximum at 780°C (86.4% gases, 9.6% oils). At this temperature the most common gases identified were methane (14.2%) and ethene (41.9%). The quantity of aromatics increased with temperature, ranging from 1.5% at 640°C to 29.7% at 850°C. No char was produced in these experiments [11, 177]. A separate series of experiments [178, 179] demonstrated the importance of temperature and

residence time on the product distribution using two free-fall reactors in series. This allowed primary and secondary reactions to be studied separately, with primary pyrolysis reactions occurring in the first reactor at 600°C, and secondary cracking and recombination taking place in the second reactor at higher temperatures. With both reactors operating at 600°C aliphatic products were produced and aromatic species were insubstantial (<0.2%); however, aromatic species increased dramatically to around 50% or greater when the second reactor was raised to a high temperature (1000°C) *or*, at a lower temperature but with a longer residence time (800°C with the residence time increased from 1.8 s to 5.8 s). Greater overall cracking, including greater gas yields, was also observed with a longer residence time at a given temperature.

#### 2.6.1.1 Microwave-Assisted Pyrolysis of HDPE

With the exception of the Hamburg process, which can also be gas powered in some configurations, all the work described above used conventional electric furnaces as heat sources to supply energy for the pyrolysis. The use of microwave heating for the pyrolysis of plastic has been pioneered by Ludlow-Palafox and Chase [29, 46] at the University of Cambridge, and has been so far limited to their studies. Their investigations used a 5 kW modified catering oven, within which HDPE was pyrolysed in a quartz stirred-bed reactor. Yields of waxes and gases were found to be similar at 500°C and 600°C, at around 80% and 20% respectively. This similarity was attributed to the increased cracking rate at 600°C being counterbalanced by a decrease in residence time as a result of pyrolysis gas being more rapidly forced out of the reactor through volume expansion at the higher temperature. Both the collected gases and waxes were primarily linear aliphatics, with the waxes comprised of linear alkanes, alkenes and alkadienes, with minimal aromatic content (<2%). The microwave-assisted pyrolysis process was also successfully applied to aluminium-plastic laminate (“toothpaste tube”) with successful recovery of both the hydrocarbon and aluminium fractions, an ability attributed to the “gentle” microwave heating mode. The potential of these processes is such that a successful spin-off company has been formed to develop them commercially, securing funding for a pilot plant that is currently operational [180].

#### 2.6.1.2 HDPE Pyrolysis Overview

While the preceding review may seem something of a barrage of data, it does serve to illustrate the variety of approaches that have been taken in researching the pyrolysis of

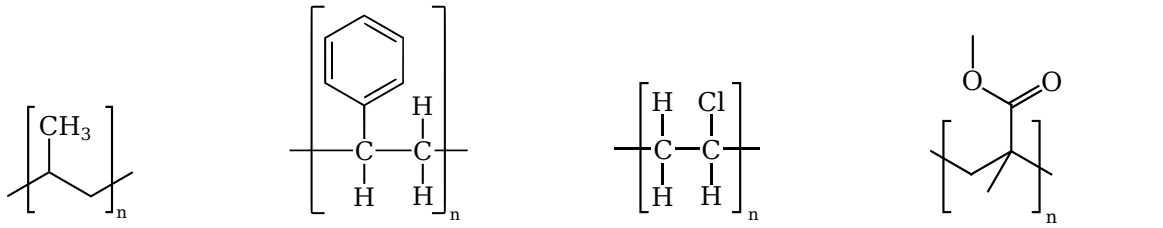


Polypropylene Polystyrene Poly(vinyl chloride) Poly(methyl methacrylate)

**Figure 2.4:** Chemical structures of some plastics.

HDPE, and the sensitivity of the pyrolysis process to a range of factors including reactor type, residence time, operating temperature, type of reactor bed, and other process variables. Nevertheless, there are certain overarching trends that can be drawn from the above survey:

- The pyrolysis of HDPE results in decomposed shorter chain hydrocarbons, comprised of gases, and waxes and oils, with small amounts of char sometimes forming at high temperatures.
- Increasing reaction temperature generally increases overall cracking, resulting in a greater yield of gases and fewer oil/wax products.
- The produced gases are comprised of $C_1$–$C_5$ aliphatics, with methane and olefins proportionally increasing the most with increased reaction temperature.
- The oils and waxes are comprised of linear aliphatic species at lower reaction temperatures, though above 600°C aromatic species are formed and can comprise a significant portion of the produced products.
- The residence time of products in the reactor has a similar effect to that of the reaction temperature, with increases in either resulting in more cracking and greater gas and aromatic yield.

The relevant data from the studies presented above are summarised in tabular form in §4.8.1, where they are compared in detail with those obtained in the course of this study, accompanied by explanations accounting for any unexpected differences between the two.

### 2.6.2 Pyrolysis of Other Plastics

While this work uses HDPE as a model plastic, it is certainly possible to pyrolyse other sorts of plastic, and work has been carried out to this end. Illustrative examples of pyrolytic recycling of some of the more common plastics are given below; the structures of these polymers is given in figure 2.4.

#### 2.6.2.1 Polypropylene

The pyrolysis of polypropylene (PP) produces aliphatic products in the same manner as HDPE; however, the branching inherent to the polymer structure results in highly branched pyrolysis products. Bockhorn et al. [181] pyrolysed PP in a crucible at temperatures between 410–460°C, resulting in a diverse variety of aliphatic pyrolysis products, comprising 7.6% alkadienes, 7.6% alkanes, and 84.8% alkenes, most of which were highly branched.

#### 2.6.2.2 Polystyrene

The pyrolysis of polystyrene (PS) is able to recover a significant fraction of the original styrene monomer. In this case the styrene monomer is a relatively stable unit, and decomposition proceeds by scission of the intervening C-C bond, which has a lower bond dissociation energy than either the benzene ring or the benzene-carbon bond. Aguado et al. [182] pyrolysed PS in a conical spouted bed reactor (CSBR) with a sand bed, and were able to recover a maximum yield of styrene monomer of 64.5 wt.% at 475°C. The remaining collected products were mostly aromatics, except for a small fraction of gases that had been cracked below $C_6$, necessarily disrupting the benzene ring. This compares with the work of Scott et al. [183], who used a fluidised bed, and gained a maximum monomer yield of approximately 76 wt.% at 532°C, with a total aromatic yield of 88 wt.%, with the remainder comprising non-condensable gases.

#### 2.6.2.3 Poly(vinyl chloride)

The chlorine in poly(vinyl chloride) (PVC) can cause significant difficulty when pyrolysing PVC. The C-Cl bond dissociation energy is lower than others in structure; as a result, degradation of the polymer proceeds via chain-stripping of the Cl [13] in a dehydrochlorination reaction that results in hydrochloric acid, which can cause corrosion and damage to apparatus [183].

Williams and Williams [172] pyrolysed PVC in a fixed bed increasing from room temperature to 700°C at a rate of 25°C/min. HCl gas from the dehydrochlorination reaction was produced from 150°C, and was the primary overall pyrolysis product at 52.9 wt.%. After the chlorine has been removed from the polymer, degradation proceeds as standard non-chlorinated vinyl, with the remainder of the pyrolysis products in this study (2.5 wt.% gas, 31.7 wt.% oil) comprising aliphatic species, with a

small quantity of aromatics. 13.8% of the input mass resulted in the formation of char due to interaction with the HCl.

The differing temperatures at which dehydrochlorination and polymer backbone scission occur allow the pyrolysis of PVC to be performed in a stepwise sequence with the HCl separated first before the remaining hydrocarbon pyrolysis products are formed. A multi-stage circulated-sphere apparatus used by Bockhorn et al. [184] was able to strip 99.6% of the Cl from the PVC at 330°C, with pyrolysis of the remaining fraction occurring at 440°C and resulting in aliphatic species.

#### 2.6.2.4 Poly(methyl methacrylate)

Poly(methyl methacrylate) (PMMA) is an example of a plastic from which especially high monomer recovery can be achieved using pyrolytic recycling. In this case the ester monomer forms a particularly stable unit, and decomposition occurs via end chain scission back into the original monomer [13].

Using the fluidised bed Hamburg process at 450°C, Kaminsky and Franck [185] were able to recover 97 wt.% of input PMMA as methylmethacrylate monomer; however, this process was highly temperature dependent, declining to 55% at 590°C, with the remaining fraction consisting of $CO/CO_2$ and short-chain gaseous hydrocarbons, indicating decomposition of the ester group had occurred.

#### 2.6.2.5 Effect of Monomer on Pyrolysis Products

The overarching observation from the above examples is that the composition of the pyrolysis products is highly dependent on the chemical structure and bond energies of the components of the polymer. While monomer recovery varies significantly from plastic to plastic, this is not to say that pyrolysis products in forms other than the monomer are not valuable; indeed, they are able to be applied to a diversity of other applications as chemical feedstock or fuels.

### 2.6.3 Catalytic Pyrolysis of HDPE

Catalysts other than activated carbon have also been used to pyrolyse plastics, with most of these deriving from the petrochemical refining industry. Most of these substances are acid-catalysts, with surface Lewis and Bronsted acid sites, which abstract hydrides and donate protons respectively, and lead to different reaction pathways than pure thermal cracking. The mechanism for the acid-cracking of

hydrocarbons is well developed and described in detail in [13]. Given the large number of publications using these catalysts, rather than present a comprehensive description of individual research, this section synthesises trends across the literature surveyed for the various catalyst types.

#### 2.6.3.1 Zeolites

Zeolites are microporous aluminosilicate minerals and are probably the most studied catalysts in the cracking of hydrocarbons. They exhibit high stability and high acid strength, and as a result of their microporous structure exhibit selectivity for smaller molecules (the porous structure acting as a molecular sieve with larger molecules physically unable to diffuse into the pores) [186]. Multiple types of zeolite exist, and these differ in chemical composition and in the structure of the underlying framework, with different resulting silicon/aluminium ratios (Si/Al). Two common types of zeolite are Y-zeolite (which has a pore formed by a twelve membered ring and a Si/Al ratio from 1.5–3.0), and ZSM-5 (which has a pore formed by a ten membered ring and a Si/Al ratio >10); both are commonly used as cracking catalysts in the petrochemical industry. The Si/Al ratio determines the surface acidity of the catalyst by altering the surface concentration of aluminium, which is the source of the acid sites that underlie catalytic activity [187].

The cracking of HDPE with zeolites is able to occur at significantly lower reaction temperatures than non-catalysed pyrolysis, with zeolite-catalysed reactions exhibiting more rapid reaction rates and greater cracking, resulting in lighter products and larger gaseous yields; these increase with increasing temperature [188]. Other characteristics of zeolite-catalysed cracking of HDPE include high yields of aromatics and olefins in the pyrolysis products, as well as isomerisation and branched products [188–190]. Aromatic species are considerably more prevalent when using Y-zeolite as opposed to ZSM-5, attributed to Y-zeolite's lower Si/Al ratio [191], but also likely resulting from the greater selectivity of ZSM-5 for smaller molecules (resulting from its smaller pore size), which preferably generates $C_3$–$C_5$ species as opposed to $C_3$–$C_8$ with Y-zeolite [192]. Ultimately the pyrolytic products produced when using zeolite are reflective of its chemical and physical make-up (i.e., surface acidity and pore size), which can be tuned towards specific desired outcomes [193].

#### 2.6.3.2 Aluminosilicates

Aluminosilicates are distinguished from zeolites by their lack of microporous structure, but they do exhibit a wide distribution of larger meso- and macropores. As a result they have lower surface area and lower strength acid sites than zeolite, with correspondingly less catalytic activity [186]. The larger pores allow larger molecules to diffuse into and out of pores, giving these catalysts less selectivity than zeolites, which has been demonstrated in the catalytic cracking of HDPE which resulted in a wider molecular mass distribution of products than when zeolite was used [194]. Cracking HDPE using aluminosilicates results in significantly more cracking compared with pure thermal pyrolysis, with very high resulting olefin yields, but little increase in aromatic compounds [190, 195].

#### 2.6.3.3 FCC Catalysts

Fluid catalytic cracking (FCC) catalysts are used commercially by the petrochemical industry to crack long-chain hydrocarbons into more useful liquid fuel products. These are generally proprietary mixes of aluminosilicates and zeolites, with a resulting cross-section of porous structure, and are highly effective at step-wise cracking, first with heavy molecules in mesopores, then lighter ones in micropores [13]. Given their industrial use, it is not surprising that these catalysts have been shown to be more selective for liquid products rather than gases when employed for pyrolytically cracking HDPE, with the products containing a greater proportion of olefins, aromatics/paraffins, and branched species than thermal cracking alone [189, 195, 196].

#### 2.6.3.4 Activated Carbon

During the course of this study, González et al. [197] conducted an investigation in which activated carbon, along with zeolite and a silica acid-catalyst were used to crack polyethylene in an electrically heated fixed bed reactor. The highest yield of products of 49.2% of input mass was obtained with activated carbon at 450°C. At this temperature the products were comprised of aliphatic species in all cases except with the activated carbon, where the condensed products also contained around 6% aromatics. This study used only small amounts of catalyst (a 1:10 ratio of catalyst:plastic), and exhibited across-the-board low conversion rates from plastic into products.

#### 2.6.3.5 Summary of Catalytic Cracking

The catalytic cracking of plastics shares a number of common features; it is able to occur at lower temperatures than pure thermal cracking, and for a given temperature proceeds at a more rapid rate, resulting in greater cracking than in the non-catalytic case. As a result of the greater cracking a more narrow range of lighter products is produced, with a greater gaseous fraction. The primary pyrolysis products resulting from the catalytic cracking of HDPE are olefins, with aromatics produced in much greater quantities than thermal cracking in many cases. As a result of the different catalytic reaction pathways, isomerisation and branching are more prevalent than with thermal cracking. Overall, the physical and chemical properties of the catalyst determine the activity and selectivity with which the reaction proceeds.

## 2.7 Summary

Activated carbon is a polycrystalline form of carbon with a very high level of porosity and adsorptive ability. These properties arise from a complex three-dimensional structure that is formed as a result of defects that alter the carbon lattice away from the regular graphene formation, with pores existing as the interstices. The activation process, which involves either gasification at high temperatures, or the addition of chemicals, creates new porosity, widens existing porosity, opens access to previously inaccessible pores, and modifies the surface of the carbon, to its final highly porous configuration.

Activated carbon is currently used in a wide range of applications that revolve around its highly developed porous structure, such as treatment and purification, product recovery, and the enhancement of the catalytic ability of other substances by increasing the interface between catalyst and substrate over a wider physical area.

Activated carbon has also shown promise as a catalyst in its own right in reactions involving hydrogen, carbon, and combinations thereof (including the decomposition of short-chain hydrocarbons such as methane) which indicate that it may have the potential to act as a catalyst in the pyrolysis of plastics.

The pyrolysis of plastics has been carried out by a number of researchers, producing lighter hydrocarbon products that have potential value as a fuel or chemical feedstock. The pyrolysis of HDPE produces primarily linear aliphatic species, with aromatics becoming more prevalent at temperatures above 600°C. The pyrolysis of HDPE using acid-catalysts allows the reaction to proceed at a lower temperature with greater

cracking, an increase in aromatic and olefin yields, and species containing a greater level of branching.

Microwave-assisted pyrolysis has been used to process materials such as hazardous and problematic waste, as well as various kinds of biomass and hydrocarbon-based materials. In these applications it has shown several advantages over pure thermal pyrolysis such as higher yields, faster reaction time, less emission of harmful undesirable products, and reduction in overall energy consumption. Whether these results arise from the characteristics of microwave heating (fast heating rates, volume heating, high power density, material selectivity, even heating, and good heating control) or microwave-specific effects over and above these (such as from direct interaction with functional groups or alignment of molecules) is the subject of some debate.

The microwave-assisted pyrolysis of plastic is currently poorly studied, though its possibility has been successfully demonstrated with the use of a carbon bed acting as a microwave-receptive intermediate. Activated carbon has also seen limited study as a catalyst in its own right, and has not before been been used in combination with microwave heating. Given the promise that pyrolysis has shown as a recycling technique for plastic, the advantages of microwave heating, the requirement of using a microwave-receptive intermediate when targeting microwave-transparent materials such as plastics, and the catalytic potential that activated carbon has shown in hydrocarbon reactions, there is a clear opportunity to combine these by investigating the microwave-assisted pyrolysis of plastic using an activated carbon bed, and it is this topic that the remainder of this dissertation comprehensively examines.

Given the paucity of literature in this specific area (this being the first study to combine activated carbon as catalytic bed with the microwave-assisted pyrolysis of plastic), the initial focus of this research is on demonstrating the feasibility of the concept, i.e., developing the necessary experimental apparatus to carry out the process, and employing it for proof of concept studies. This will allow a comparison to the existing body of microwave-assisted pyrolysis literature, an evaluation of the catalytic abilities of activated carbon in this context, and an evaluation of the chemical composition of the produced products. Assuming these initial results are sufficiently promising the ultimate goal of this project is to further the understanding of the microwave-assisted pyrolysis of plastic, and the use of activated carbon as a catalyst, with a view towards developing a sustainable process that could be employed in an industrial context.

# 3

# Development of Microwave-Assisted Pyrolysis Equipment

## 3.1 Introduction

Many of the key pieces of microwave equipment used in this work existed in the lab, and had been used for exploratory work involving the pyrolysis of liquid hydrocarbons some years prior to this work. However, considerable time and resources were invested into developing, refining, and adding to the apparatus, so that it was suitable for processing solid HDPE, and moreover ensuring that safe, reliable, and optimal operation was possible. This chapter describes the equipment, as received, after assembling and recommissioning, and outlines the most significant developments and improvements to the equipment undertaken throughout the course of this research.

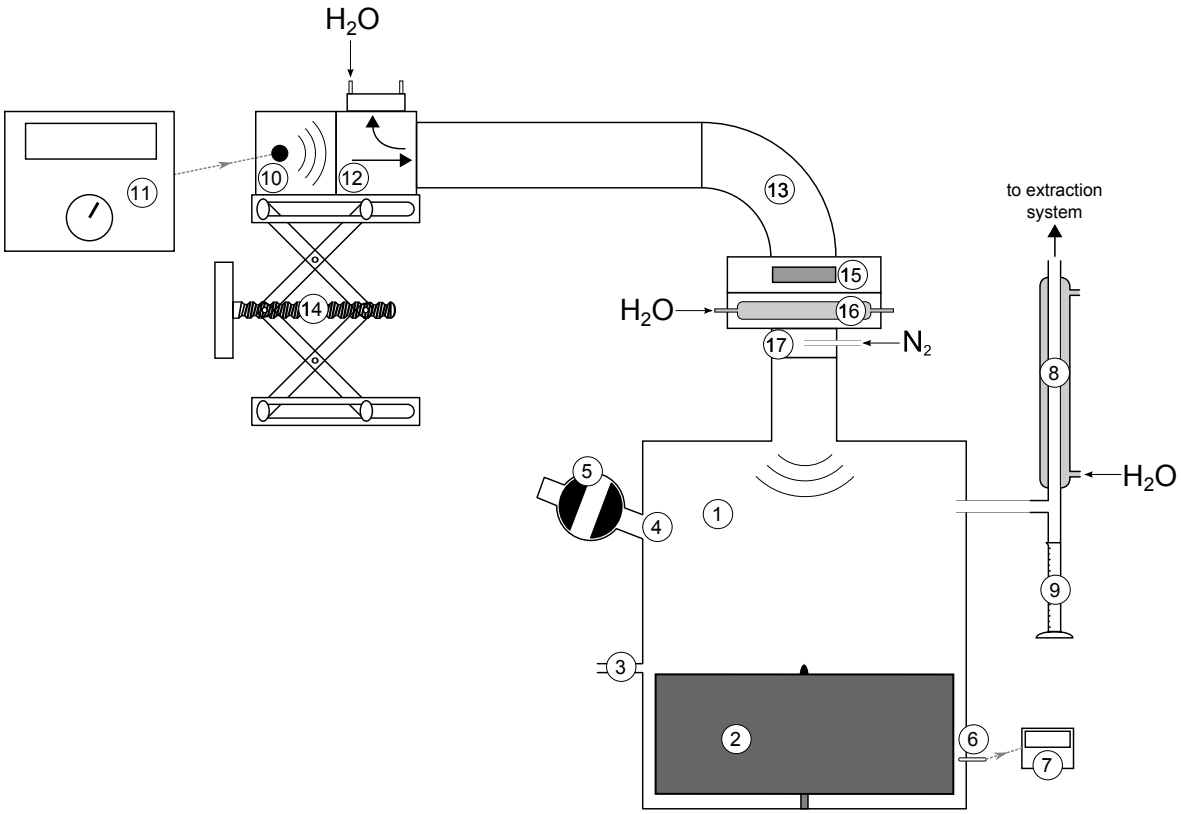


**Figure 3.1:** Microwave-assisted pyrolysis apparatus as received. Numbered components are described in the text.

## 3.2 Description of the Apparatus as Received

Figure 3.1 shows the microwave heating equipment and reactor as received at the commencement of this research. The reactor vessel itself (1) was a custom-built cylinder constructed of cast iron, with an internal diameter of 250 mm, a height of 250 mm and a wall thickness of 25 mm. The reactor contained a stirrer (2) that measured 80 mm from the bottom of the reactor, and extended across its entire width. The stirrer blades slanted at 30° from vertical (to ensure vertical mixing as well as radial), and it rotated at a variable speed from 0–10 r.p.m. The reactor possessed two inlets, one 2 mm I.D. inlet (3) suitable for pumping liquids in, and a larger 40 mm I.D. inlet (4) sealed with a ball valve fitting (5). Four K-type iconel-sheathed thermocouples (6; RS Components) were distributed throughout the inner surface of the reactor wall and were connected to digital read outs (7; RS Components) to monitor the temperature of the reactor contents. Gases generated in the reactor exited to a Liebig condenser (8); condensate collected in a measuring cylinder below (9), and non-condensable gases vented to the extraction system.

The microwave heating system consisted of a magnetron head (10; MH3000S-

210BA, Muegge) that operated at at 2.450 GHz (+/- 10 MHz) and was driven by a 3 kW air-cooled power supply (11; MS3000D-110EF, Muegge) that could be adjusted by hand to a power level between 10–100%. An isolator (12) prevented any energy that was reflected back from the reactor from returning to (and damaging) the magnetron; the reflected energy was safely diverted into a continuously supplied water load, and the magnitude of the reflection was continuously measured so that the effective power output (i.e., that reaching the reactor) at any given time could be calculated. The magnetron and isolator were connected to the reactor via a series of IEC R26 / EIA WR340 standard waveguides, including a 90° H-bend (13) (bent in the plane of the magnetic field component of the electromagnetic wave), which was necessary in order for the magnetron head and isolator to be physically supported (by a lab jack (14)), while directing the microwaves into the vertical waveguide port in the reactor lid.

The microwave heating system was hermetically separated from the reactor by a quartz window (15), which prevented pyrolysis products from entering and damaging the sensitive electromagnetic components, while still allowing microwaves to pass through to the reactor. The window was cooled by a water jacket (16) below. A gas inlet (17) allowed nitrogen to enter the reactor to purge any oxygen to maintain an inert atmosphere throughout operation. Gas-tight seals between components were achieved with a milled groove in the flange of the waveguide pieces in which a graphite gasket was located, with each join placed under sealing pressure by 10 M5 bolts.

## 3.3 Maximising Transmission of Microwave Power to the Reactor

One of the main concerns identified when using the equipment, as received, to perform initial feasibility testing of the pyrolysis of HDPE, was the high level of microwave energy emitted from the magnetron that was not being absorbed by material in the reactor. This was due to high amounts of energy being reflected back from either the reactor itself, or components between the magnetron and the reactor; or, by components between the magnetron and the reactor absorbing energy before it could reach the reactor. Power that was reflected back to the magnetron was measured by a microwave detector diode (MM1001B-110AB, Muegge), and then diverted into a water load by the return isolator, preventing it from reaching and damaging the magnetron. When first tested, the measured reflected power under normal operation was 50–60%,

an inefficient and dangerous condition that required rectifying before pyrolysis work could commence.

### 3.3.1 Arc Prevention

When dealing with high powered electromagnetic fields such as the microwaves used for heating in this work, there exists the risk of arc formation, where high voltage ionises the normally non-conductive air across a voltage gap, causing a current to flow, and effectively creating a "short-circuit". The very high temperature plasma that results in this arc is highly destructive, capable of melting or vaporising most materials. Unchecked, an arc will cause pitting damage, and travel up the waveguide back towards the power source; if it reaches the magnetron it will short and shatter this sensitive and expensive piece of equipment. Microwave energy not dissipated in the reactor is spurious energy that might potentially start an arc, providing an additional motivation to ensure that as much of the emitted energy was transmitted to the reactor bed as possible.

### 3.3.2 Minimising Energy Lost in Transmission to Reactor

#### 3.3.2.1 Locating Energy Loss Source

In the first instance, components of the pyrolysis rig (other than the reactor) that were absorbing microwave energy were located by gradually ramping up the power output of the magnetron, and feeling by hand areas that increased in temperature. This soon revealed that the primary location absorbing power outside the reactor was the 90° waveguide H-bend (see figure 3.1). In spite of the bend being an off-the-shelf component, the changes in the magnetic field required to rotate the microwave beam were causing reflections, and resulting in a significant amount of energy being absorbed by the bend itself. The high levels of energy reflected back from further downstream in the microwave transmission system may have resulted in constructive interference occurring, exacerbating the situation further.

#### 3.3.2.2 Simplifying the Power Transmission System

Several possibilities were considered to overcome the reflection and absorption issues presented by the waveguide H-bend. For reasons of time and economy, it was decided to focus on the magnetron head support system to see whether an alternative design could be employed to eliminate the bend entirely. With the goal of simplifying the

number and type of components in the system, every piece between the magnetron and the reactor was evaluated as essential to operation or not, and those regarded as extraneous were set aside. Discarding the spacing and routing waveguide sections resulted in a reduction of the transmission path length between the magnetron and reactor from 1200 mm to 400 mm. With only the core components of the transmission path (magnetron head, isolator, quartz window, water jacket, and gas inlet) remaining, a new approach to supporting the magnetron head was tried, in which the components of the transmission path themselves acted as supports in a vertical stack; with a full complement of ten M5 nuts and bolts at each join, this approach indeed proved to be feasible.

The elimination of the waveguide bend, and the simplification of the power transmission pathway, served to reduce the reflected microwave power to around 30–40%. Sustained testing at maximum power in this linear configuration identified no further components in the transmission pathway absorbing microwave energy, and it was subsequently assumed that all energy emitted from the magnetron was either absorbed in the reactor, or reflected back to the isolator where it was measured by the detector diode.

### 3.3.3 Window Development

In order to determine the contribution the remaining components in the microwave transmission path made to the reflected power, each component was removed in turn and the pyrolysis rig was run without the input of any sample. The only significant drop in reflected power (of 10–15%) was observed when the quartz window (separating the dirty/hot section of the pyrolysis rig from the clean electromagnetic components) was removed from the transmission path. In addition to causing a substantial portion of the microwave power reflection, the existing window had several other problems, many of which were a result of the fact that the design consisted of a number of separate physical and functional components; these are outlined below:

- Every segment of the window required a graphite gasket in order to maintain a gas-tight seal; this not only made it more difficult to maintain a good seal, but the distinct materials presented barriers to electrical continuity, acting as potential sources of arcs and reflections.
- The multiple pieces of the window were difficult to dis- and re-assemble — when assembled they had to be in exact alignment along the inner surface in order to

act as an effective waveguide and prevent arcs and reflections occurring at the junctions.

- The water-cooling jacket was physically separate from the window-surround, meaning the window itself was subject to sub-optimal cooling. This could lead to heat damage and sometimes even shattering of the quartz window, especially when deposits built up, making it more microwave-absorbent.
- The quartz windows themselves were very expensive to replace, requiring custom fabrication, with correspondent long manufacturing lead-times.

#### 3.3.3.1 Miniaturisation: Integration of Water Cooling and Gas Inlet

A redesign of the window (figure 3.2) was undertaken to remedy the problems outlined above. Given the opportunity, it was decided to incorporate as many pieces of the transmission pathway as practicable into one unified structure. As such, a new piece was designed and fabricated, incorporating the window support, internal channels for water cooling, and a four-point inlet structure for nitrogen purge gas to enter the reactor. This design was considerably more compact, and was made of one unified milled aluminium piece, ensuring a smooth internal structure throughout, dramatically reducing the possibility of arcs forming, and ensuring significantly better performance of the water cooling.

#### 3.3.3.2 Investigating Alternative Window Materials

Testing with new window support in place, but with the actual quartz glass removed, indicated that it was the quartz itself, and not the support structure that was the major cause of microwave reflection, implying that it was not as microwave transparent as originally assumed. Given the expensive and sometimes fragile nature of the quartz, an extensive search for a suitable replacement window material was undertaken, with the requirements that it be microwave transparent, robust under high temperatures, electrically insulating, and preferably inexpensive. After testing a range of materials including HDPE, PTFE (Teflon), PVC, rubber, and borosilicate glass, it was eventually determined that silicone polymer exhibited the greatest number of desirable properties: it is thermally stable up to 300°C, chemically resistant, almost completely microwave transparent, an insulator, inexpensive, and does not reflect microwave energy in the way the quartz window did. Furthermore, on a practical level, using silicone as the window material eliminated the need to have sealing O-rings on either side of the window: the compression provided by making the window slightly thicker than

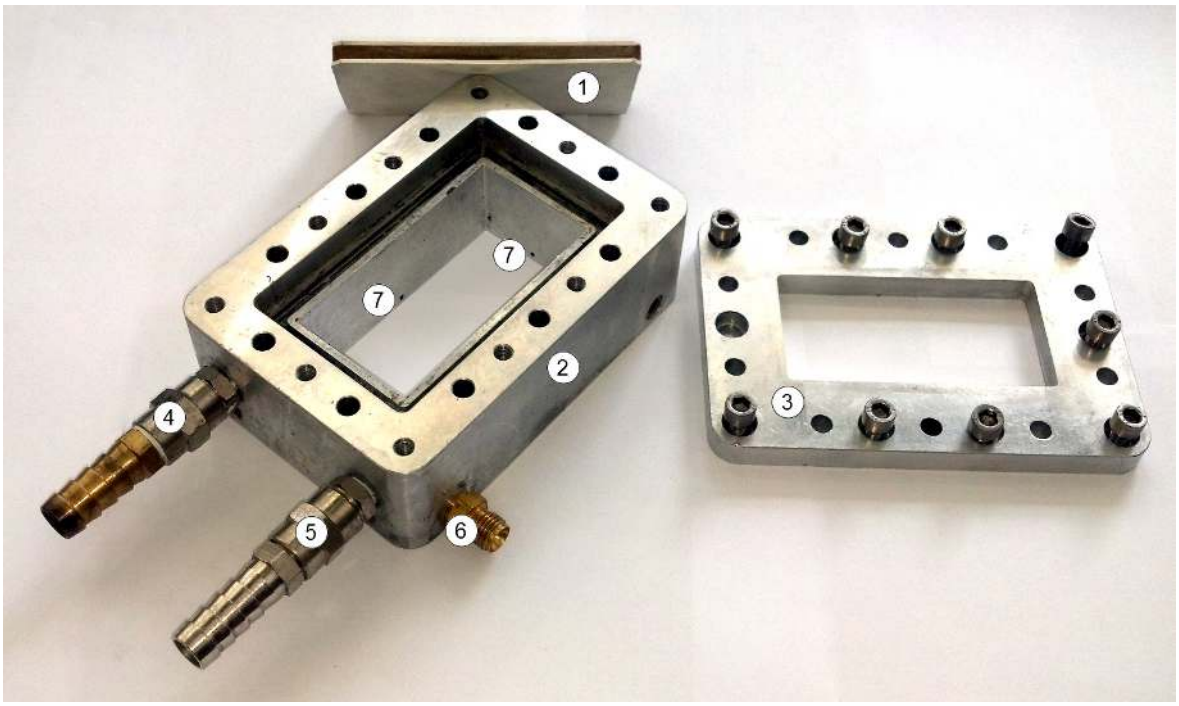


**Figure 3.2:** Final design of the microwave-transparent window, which separated the microwave heating system from the reactor and its associated heat and harmful pyrolysis products. The mica and silicone sandwich window (1) slotted into the milled aluminium window support (2), with the silicone providing a good seal due to compression from the window support cover (3). Water travelled from external inlet (4) to outlet (5), through internal passages in the window support walls, providing cooling. Nitrogen purge gas entered through an external swagelok inlet (6) and was distributed to outlets on each of the four internal walls (7).

the space in the window support structure allowed the window itself to maintain an excellent seal.

#### 3.3.3.3 Reduced Carbon Deposition from Silicone Material

An additional benefit to using silicone as the window material revealed itself after prolonged use, when it was noticed that significantly less carbonaceous deposit was present on the window after a number of pyrolysis tests. These deposits generally accumulated over a number of runs, and arose from cracked hydrocarbon settling or condensing on the window, where, directly in the path of the microwave beam, it would be carbonised owing to the high energy flux present. This presented a problem, as the carbonaceous material itself was highly microwave absorbent and, without regular cleaning, the energy absorbed by the build-up would melt or crack the window itself. The silicone window, however, if not actively repulsive to hydrocarbon, was not conducive to hydrocarbon settling, and use of this material reduced the carbonaceous build-up problem significantly.

#### 3.3.3.4 Final Window Design Refinements: Added Strength from Central Mica Layer

A final enhancement to the silicone design was made some time later, when mica was trialled as an alternative window material. This pseudo-hexagonal crystalline sheet silicate mineral exhibits excellent electrical insulation properties and microwave transparency, and remains structurally rigid and thermally stable up to 900°C. The added strength and hardness of the mica provided an additional backup in the event that arcing or high temperatures did occur: silicone by itself would decompose relatively rapidly, allowing damaging pyrolysis gases into the sensitive electromagnetic components; mica gave an additional safety factor and was much more resistant to decomposition. However, mica did not exhibit the same resistance to carbonaceous deposits as silicone, and required an extra sealing system as it could not make gas-tight joins with the support structure in the way that silicone could. Combining the best of both materials was possible by using sheets of silicone on the top and bottom of a central mica layer. This final "mica-sandwich" design (see figure 3.2 on the preceding page) was strong, gas-tight, microwave transparent, all-but-impenetrable even to sustained electrical arcs, resistant to carbon deposition, economical, and easy to maintain owing to the cheap and disposable nature of the silicone layers.

### 3.3.4 Maximising Power Transfer through Impedance Matching

Impedance is the property of a component to oppose to the passage of current when an alternating voltage (such as a high frequency microwave source) is applied. In microwave heating, the impedance of the source and the load (i.e., the carbon bed in the reactor) are particularly important — the better the impedance of the load is matched to that of the source, the better the power transfer from source to load. A short illustrative background on why this is the case is given in the following section, followed by a description of the steps taken to optimise the power transfer of the microwave pyrolysis rig.

#### 3.3.4.1 Background: Impedance Matching Theory

Consider a simplified circuit (figure 3.3) in which the microwave source, of voltage $V_S$, feeds a load of impedance $Z_L$, and the combined impedance of the source and transmission pathway is $Z_S$. $Z_S$ and $Z_L$ effectively form a voltage divider circuit, which gives the voltage across the load, $V_L$ (equation 3.1).

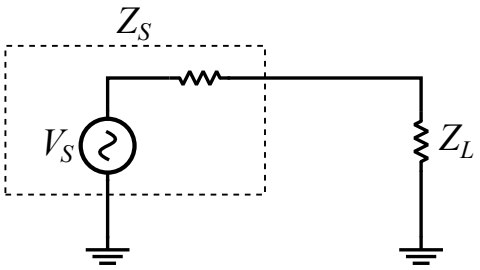


**Figure 3.3:** Simplified circuit used to illustrate the impedance matching principle. $V_S$ is the source voltage, $Z_S$ is the combined impedance of the source and transmission pathway, and $Z_L$ is the load impedance.

$$V_L = V_S . \frac{Z_L}{Z_L + Z_S} \tag{3.1}$$

Substituting into the formula for power $P$ in terms of voltage and impedance (equation 3.2) gives the power dissipated in the load, $P_L$ (equation 3.3).

$$P = \frac{V^2}{Z} \tag{3.2}$$

$$P_L = \frac{{V_S}^2 . Z_L}{(Z_L + Z_S)^2} \tag{3.3}$$

Considering the power transferred to the load as a function of the load impedance (figure 3.4 on the next page), it is clear that the maximum power transfer load occurs when the load impedance matches the source impedance.

This can also be shown analytically — differentiating equation 3.3 and setting this to zero gives equation 3.4:

$$\frac{dP_L}{dZ_L} = \frac{{V_S}^2 . Z_S}{(Z_L + Z_S)^3} - \frac{{V_S}^2 . Z_L}{(Z_L + Z_S)^3} = 0 \tag{3.4}$$

$$\text{i.e. } Z_L = Z_S \tag{3.5}$$

In reality a more complex wave-based analysis would be required for a fully descriptive model of the microwave pyrolysis setup, where waves have the potential to be reflected or transmitted at the junction of each component (or indeed at any given material change within a component), and the standing waves that result would produce a variable voltage along the transmission line; however, such an analysis is beyond the scope of this document and, in any case, the principle illustrated here of greatest power transfer occurring with matched impedances nevertheless holds true.

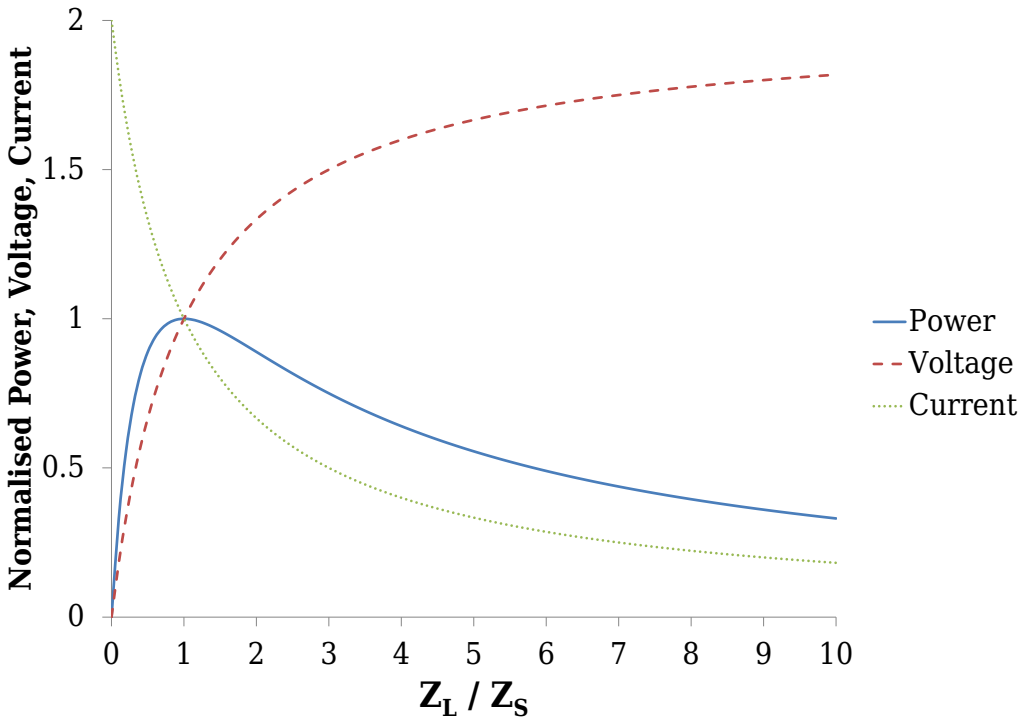


**Figure 3.4:** Power transferred to the load as a function of the load impedance. Load impedance is normalised to the source/transmission impedance. Load voltage and current are also shown for illustrative purposes. Maximum power transfer occurs at $\frac{Z_L}{Z_S} = 1$, i.e., $Z_L = Z_S$ where the load impedance is matched with that of the source and transmission path.

#### 3.3.4.2 Tuning the Microwave Circuit

It is possible to alter the impedance of the load through the use of a stub tuner. This device inserts stubs of capacitive material into the waveguide, at various positions along a wavelength, close to the load. These stubs act as electrical shunts, and alter the combined impedance of the tuner and load. Power not dissipated in the load is reflected back to the source where it is diverted by the isolator. By measuring the reflected energy and altering the impedance of the load it is possible to "tune" the circuit so as to minimise reflected energy and maximise power transfer to the load. To this end, a three-stub tuner (MW2009A-260ED, Muegge) was acquired and added to the microwave transmission pathway immediately before the window. Appropriately set through manual experimentation, the tuner was able to reduce the overall reflected energy; however, the reflected energy was not static over time, making it difficult to optimise.

#### 3.3.4.3 Time-Domain Impedance Optimisation

In order to gain a greater understanding of the variation in reflected power, software was written (see §3.6) to sample the reflected energy from the detector diode and track

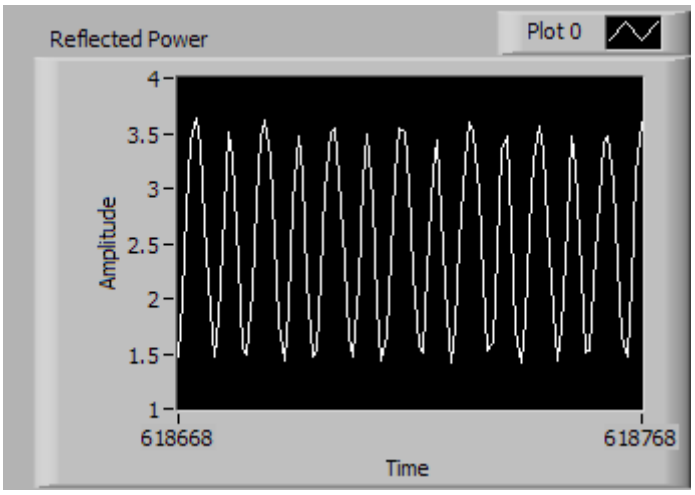


**Figure 3.5:** Microwave energy reflected back from the reactor, exhibiting exactly twice the frequency as that of the carbon bed stirrer.

it over time. This revealed that the variation in reflected power was periodic, and semi-sinusoidal (see fig 3.5).

It was soon noticed that the period of the reflected power function was exactly half that of the period of the carbon bed stirrer. The connection between the two was determined when the reactor bed was examined with the stirrer running: the motion of the stirrer created a crest in the carbon that rotated along with the stirrer (see figure 3.6 on the following page). The microwaves incident to the reactor were polarised along a directionally constant axis, but the amount of carbon present along this axis (and thus the impedance of the load) varied as the crest of the carbon induced by the stirrer rotated.

While it was possible to adjust the tuner to minimise reflected power for any specific static configuration when the stirrer was stopped, this resulted in an overall much higher reflectance when the stirrer was running. Instead, by charting the reflected power over time it was possible to tune the rig such that the area under reflected power curve was minimised, optimising for the average state of the load impedance. Using this technique, and the improvements described in the previous segments of this section, it was possible to reduce the reflected power to an average of less than 10%. Fully optimised, even the peak of the reflected power curve remained well within acceptable and safe operating limits, ensuring that by far the majority of the microwave power was successfully transferred to the carbon bed.

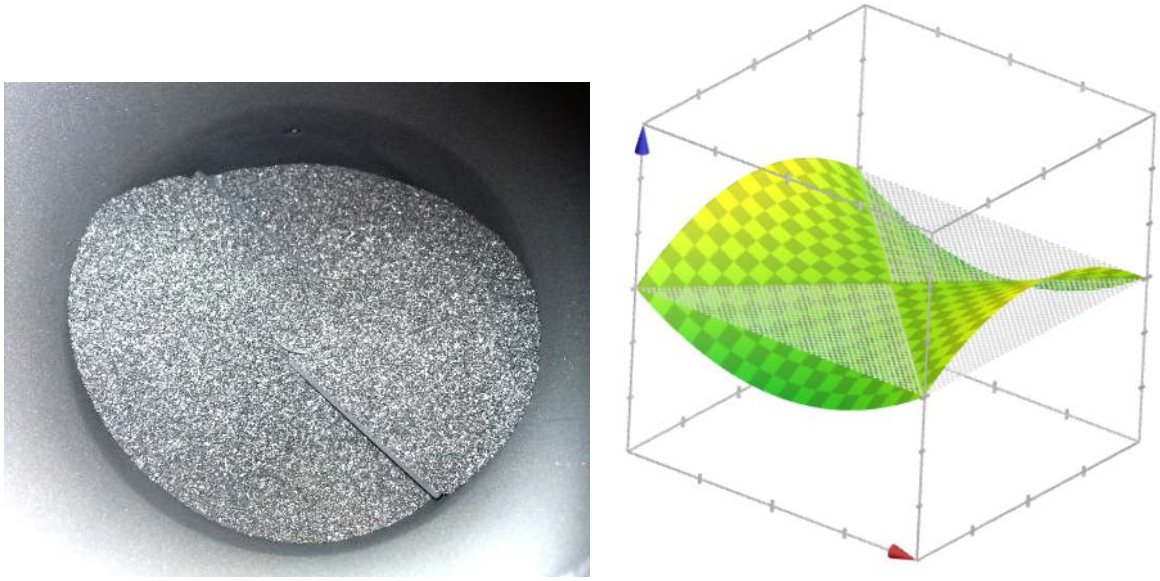

**Figure 3.6:** Crests in the carbon bed were induced by the stirrer as it rotated, causing periodic variation in load impedance and microwave power reflectance (left); in this image the volume of carbon bed has been reduced until the top of the stirrer is just visible. For clarity, an abstract approximation of the form of the top surface of the carbon bed induced by the stirrer is given at right, with the average bed height denoted by the checked grey plane.

## 3.4 Sample Injection System

Prior to this work, the microwave pyrolysis rig had been used only for processing liquids, which were injected directly into the carbon bed through a small side inlet. In order for HDPE to be processed, a system had to be developed that could inject solid pellets into the reactor under operating conditions. Requirements for the injection system included that it be gas tight, microwave impenetrable, and temperature resistant.

### 3.4.1 Plunger Injection

A simple mechanical plunger apparatus was constructed (figure 3.7), with a stainless steel tubular barrel of the same internal diameter (40 mm) as the top inlet of the reactor lid. The plunger fitted precisely inside the inner diameter of the barrel, and had a hand-operated shaft that was sufficiently long to allow the plunger head to extend all the way into the reactor itself. This ensured that all of the sample mass entered the reactor, that no blockages occurred, and that sample pellets did not stick to the inlet tube walls. In order to operate, the ball valve was closed, and a measured mass of HDPE pellets was added to the barrel. The plunger was then fitted and lowered to the level of the HDPE pellets so that minimal air was injected at the same time as the sample. A gas-tight

**Figure 3.7:** Batch addition plunger injection apparatus ready for injection. The PTFE cap at the top end is screwed down creating a gas-tight seal once the sample has been added; an O-ring and ball valve seal the bottom of the system until the sample is injected into the reactor.

seal was ensured with a silicone O-ring at the ball valve end of the plunger casing, and a PTFE cap that screwed on at the open end of the barrel after the sample and plunger were added. When the reactor reached the desired temperature the ball valve was opened, the plunger was quickly extended into the reactor and withdrawn, and the ball valve closed behind it.

#### 3.4.1.1 Problems with Plunger System

The plunger injection system proved invaluable in providing initial exploratory results for the microwave-assisted pyrolysis of HDPE using coke and activated carbon reactor beds (see chapter 4). However, a number of problems soon became apparent. The plunger system was only able to add a maximum of around 100 g of HDPE to the reactor for any given experiment. This mass was limited by the length of the plunger barrel — given the small diameter of the injection port, the length of the barrel and plunger handle would quickly become unwieldy were the mass of the injected sample increased. The plunger system was only able to inject sample instantaneously, en masse. Not only

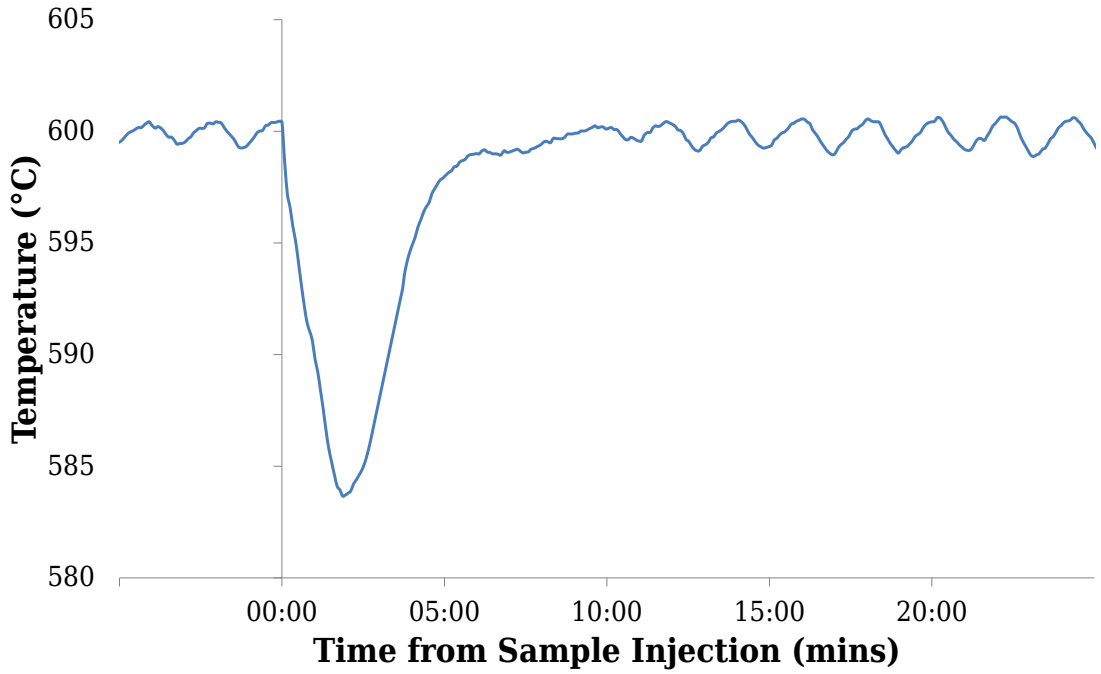


**Figure 3.8:** With a target reactor temperature of 600°C, the microwave heating system was unable to maintain operating temperature when 100 g of HDPE pellets were injected, leading to an 18°C drop in temperature lasting for several minutes.

was this batch addition not a good approximation to any inevitably continuous process that might be developed were the system to be scaled up, but the quantity of mass entering the reactor over such a short period of time could overwhelm the ability of the microwave heating system to maintain the reactor bed at the desired temperature (see figure 3.8), making the characterisation of the products at a given process temperature less reliable than desired.

### 3.4.2 Continuous Rotary Feeder

A continuous feeder was designed, based around a rotary airlock; HDPE pellets would gravity feed from a 12 L inverted pyramidal hopper into a constantly rotating eight-spoke feed wheel. The rotational speed of the feed wheel determined how quickly pellets were transferred from the hopper into the reactor's top inlet, where they would fall under gravity into the reactor itself. A Parvalux SD1BSS DC shunt-wound motor was combined with a worm gearbox in order to provide a sufficiently low revolutionary speed for the feed wheel. This reduction also provided sufficient torque to shear HDPE pellets in the event that they became stuck between the feeder spokes and the casing, ensuring the feeder did not become immobilised during operation. The quantity of pellets remaining in the hopper could be monitored through an air-tight polycarbonate

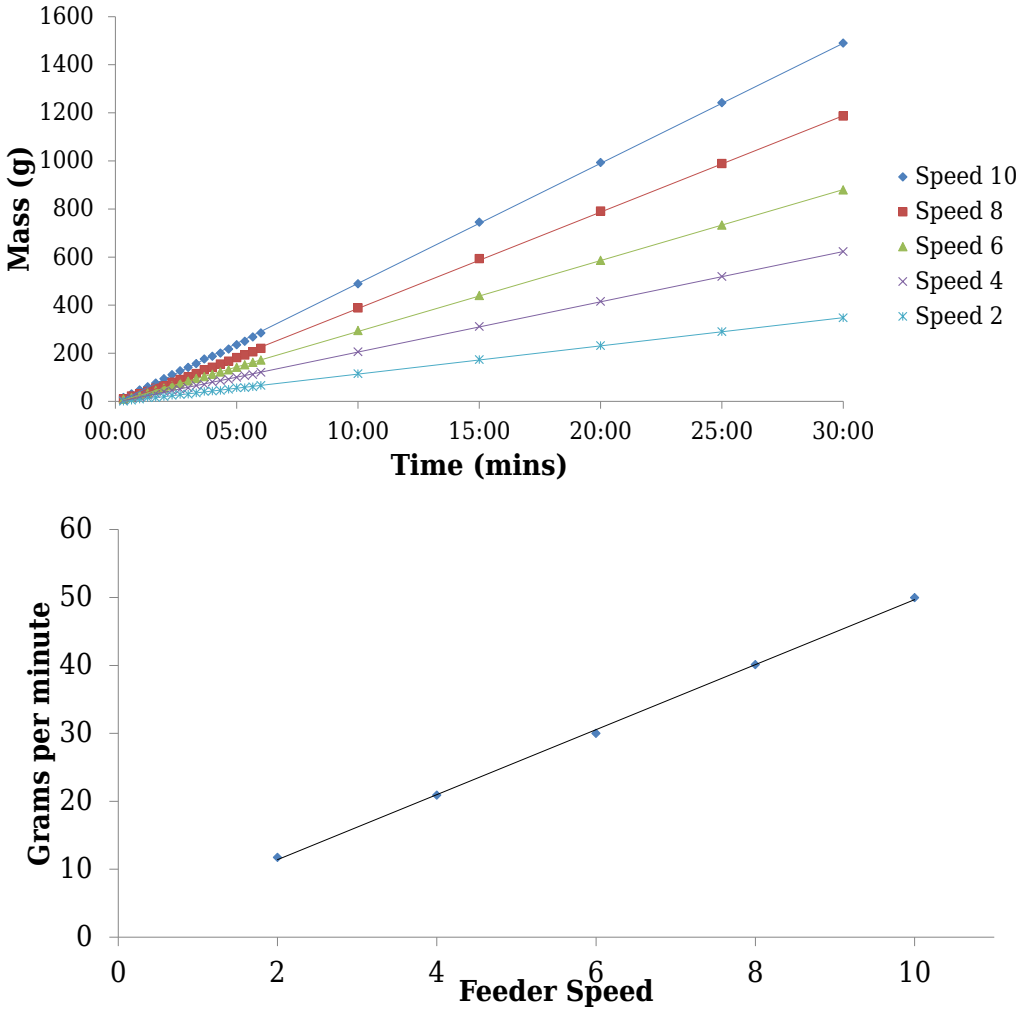


**Figure 3.9:** Calibration of the continuous HDPE pellet rotary feeder. Feeder throughput was constant and accurate over time (top); furthermore, feeder throughput scaled linearly and accurately with the feeder motor controller settings (bottom). Coefficient of determination, $R^2$, was greater than 0.999 in all cases.

view port on the top face of the hopper. The diameter of the feed tube was much less than the wavelength of the microwaves, effectively isolating the feeder mechanism and preventing any microwave radiation from leaving the reactor.

#### 3.4.2.1 Calibration of Rotary Feeder

The feeder motor controller operated only in discrete states, with speeds 0–10 available. With no existing information on the output rotational speed at the various motor settings, a comprehensive calibration of the feeder was required over the full range of feeder speeds (see figure 3.9). With this calibration it was possible to calculate an appropriate running time for any desired mass of sample to be introduced to the reactor, at any feeder speed.

#### 3.4.2.2 Co-addition of Air with HDPE Pellets

With the necessity to maintain an oxygen-free atmosphere within the reactor for pyrolysis to occur, there was some concern that air from the hopper would travel into the reactor along with HDPE. As such, the hopper was designed and fitted with vacuum and purge gas feeds, so that it could be purged with a vacuum pump and back-filled with nitrogen gas before the feeding process began. In practice, experimentation showed that these steps were unnecessary, and no significant quantity of air entered the reactor with the HDPE pellets — no oxygenated species were observed in subsequent GC/MS analysis of products created under these conditions. It is thought that the volume between HDPE pellets was so minimal as to be insignificant, and what little air was present may have been prevented from entering the reactor owing to the positive pressure from the nitrogen purge gas feed, and gas production reactions, within the reactor itself. Correspondingly, the air-lock nature of the feeder minimsed the return of pyrolysis gases to the hopper, which was in any case gas tight itself, and thus prevented any pyrolysis gas escaping to the external environment.

#### 3.4.2.3 Pellet Adherence to Reactor Inlet

One problem occasionally encountered when using the continuous feeder was the adhering of pellets to the inlet tube downstream of the feeder, where sticky pyrolysis products would sometimes condense. In the event that this did occur, it usually involved a minimal amount of mass relative to the total added. Pellets that did not enter the reactor were recovered at the end of a run and subtracted from those calculated to have been added. Regular cleaning of the inlet minimised this occurrence.

## 3.5 Pyrolysis Product Condensing Apparatus

The performance of the condensing apparatus acted as the primary limiting factor in collecting non-gaseous pyrolysis products, and a number of design iterations were undertaken in an attempt to maximise the condensed pyrolysis yield.

### 3.5.1 Liebig Condensers

Initial testing was carried out with a single Liebig condenser, which was present in the rig configuration as received (figure 3.10a). It quickly became clear that the rapid production of pyrolysis products when HDPE was added to the reactor completely

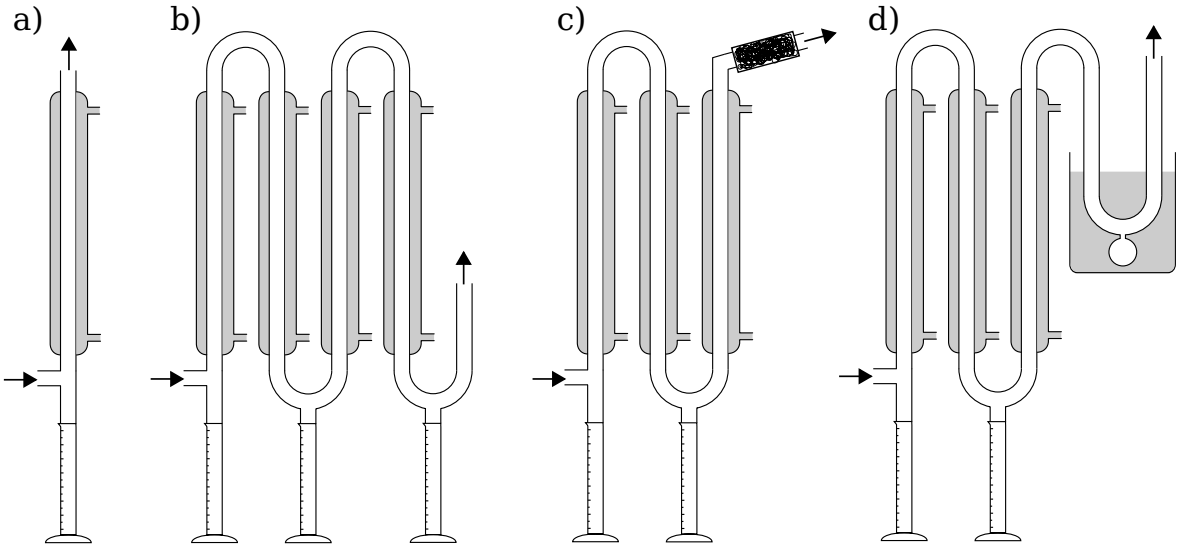


**Figure 3.10:** Configurations of several tested designs used to condense pyrolysis products as they exited the reactor. a) Single Liebig condenser. b) Four Liebig condensers in series. c) Three Liebig condensers with a mesh particle trap. d) Three Liebig condensers with a dry ice / acetone cold trap. Arrows mark the entry of pyrolysis gases, and the exit of non-condensable gases to the extraction system.

overwhelmed this single condenser, resulting in a low yield of condensed products, and necessitated finding a more effective condensing solution.

#### 3.5.1.1 Multiple Condensers

Additional Liebig condensers were added in series, up to a maximum of four (figure 3.10b), with the condensing system tested after each addition. No extra condensed pyrolysis product was collected when a fourth Liebig condenser was added, so it was removed in subsequent design iterations. With three condensers in place the system showed a substantial improvement in performance; however, a significant portion of the pyrolysis products that could be condensed were still passing through the system. This was clear both from the yields, which at 35% were still significantly below that observed in literature [29], and from the presence of a visible white aerosol mist, comprising fine particles of uncollected pyrolysis product, that exited the condensing system.

#### 3.5.1.2 Temperature Variation

Using recirculating water heater/chiller units, a number of different operating temperatures for the condensers were investigated to increase the yield of condensed product. In accordance with the findings of Ludlow-Palafox [46], the temperature of the condensers was raised to 60°C to aid collection. With further experimentation additional improvements were made; the optimal configuration was found to be 60°C

for the first condenser, 25°C for the second, and 0°C for the third. Overall, however, the condenser temperature had a relatively small effect on yield, making a difference of only a few percent at most.

#### 3.5.1.3 Attempts to Collect Aerosol Mist Using a Particle Trap

A significant portion of the pyrolysis products exiting the reactor condensed into fine aerosol droplets, which were light enough that they were swept along by the continuous flow of gas exiting the reactor. This meant that they travelled down the centre of the condenser tube and did not make contact with the cold condensing walls. In order to capture these particles and prevent them from leaving the condensing system, a mesh of steel wool was introduced at the exit of the Liebig condensers (figure 3.10c), the idea being to disrupt the laminar flow of the pyrolysis gas and present a greater cooling surface area onto which any particles could settle. Unfortunately, despite experimenting with several different materials of varying density (non-absorbent fibre wool, tissue, wire mesh, etc.), the filter material soon became overwhelmed and clogged with the throughput of the pyrolysis gas; the pressure build-up would then push the filter out of its holder and the system would become ineffective. While unsuccessful as an attempt to collect the mist, this apparatus did at least validate the idea that there was still a significant quantity of product leaving the system in aerosol form.

#### 3.5.1.4 Difficulties with Sample Extraction

When heavier pyrolysis products were produced they would accumulate on the inner surfaces of the condenser system. Extracting them required gently warming them with a heat gun until they reached their melting point and ran into the collecting measuring cylinders below. Using a complex condensing system comprising many different individual components required joining each of these components together. The off-the-shelf Liebig condensers and U-bends used in this work employed standard QVF flange seals between each component. Unfortunately, the QVF supports around each join could be damaged by the heat from the heat gun required to melt and collect the pyrolysis waxes; the use of these types of joints prevented access to a portion of the condensing system until the extremely time-consuming process of disassembly and reassembly could be undertaken.

### 3.5.2 Alternative Condenser Designs

A number of alternative condenser designs were considered in order to increase surface contact area between the pyrolysis gas and the condenser system; unfortunately, most of these were deemed impractical for one reason or another. Condensers such as coiled condensers, which packed a greater contact surface area of condenser into a smaller volume, presented difficulties with internal access for cleaning and sample extraction. A cyclone vortex was considered as a possibility to settle hydrocarbon particles caught up in the gas stream; however, the gas velocity was insufficient to exert adequate centripetal force to be effective. Introducing a forcing system to increase the velocity posed issues of altering reaction pressure, to say nothing of procuring a pump with the ability to process, and not be clogged by, gas containing hydrocarbons.

### 3.5.3 Dry Ice Cold Trap

A cold trap chilled by a dry ice and acetone bath to -78°C was introduced in an attempt to enhance the effectiveness of the condensing system (figure 3.10d); the cold trap incorporated a small spherical vessel that condensed product could collect in, so as not to block transmission of gases through the wider system. While the cold trap did effectively increase the condensed yield by several percent, it still provided a smooth bore through which the pyrolysis gases could travel, and thus did not address the issue of hydrocarbon particles travelling in the gas stream, preventing them from settling.

### 3.5.4 Dry Ice Percolating Condenser

A final, successful, design that incorporated low temperatures, high surface area, and non-laminar pyrolysis gas flow, was created with a condenser that employed dry ice as a cooling agent, but on the *inside* surface of the condenser. In this way, pyrolysis gas entering the reactor would have to pass through the spaces between the dry ice pellets — an innately tortuous path that disrupted the laminar flow of the pyrolysis gas. The pellets themselves, approximately cylindrical in shape, with a diameter of 8–9 mm and a length of 5–20 mm, also provided a very large surface area, maximising heat transfer from the gas to the condensing system. The condenser itself (figure 3.11 on the following page) was fabricated out of thermal-shock-resistant borosilicate glass, and was funnel-like in shape — the initial wide 150 mm diameter entrance provided a large area for the incident pyrolysis gas to settle over, preventing blockages from occurring as the condensed hydrocarbon accumulated on the surface of the dry ice pellets (though

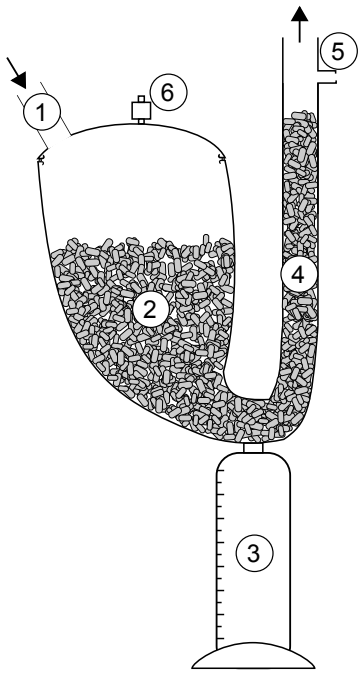


**Figure 3.11:** Final design of dry ice percolating condenser. Pyrolysis gases entered from the reactor through a port on the lid (1), and passed through the dry ice (2), where they condensed, and were collected in a measuring cylinder below (3). Gas exited through a vertical tail (4), which ensured maximum heat transfer and condensed yield. The remaining non-condensable gases were sampled at a monitoring port (5) just prior to entering the extraction system. A pressure release valve on the lid (6) prevented excess pressure building up in the event of blockages. Arrows mark pyrolysis gas entry point and exit to extraction system.

it was found that this was somewhat self-regulating as the dry ice sublimated as the warmer condensate deposited). The condenser then progressively narrowed in diameter down to 35 mm, at which point a 1 L collecting vessel was attached below in which liquid pyrolysis product accumulated. From here the condenser extended upwards with a 500 mm long tail which was also filled with dry ice, and which ensured maximum contact between the ice and the traversing pyrolysis gas. The lid of the condenser was sealed by an O-ring and compression seal, and incorporated both the inlet through which the pyrolysis gas entered, and a pressure release valve, which would allow any excess gas to vent into the extraction system if the pressure inside the condenser exceeded one bar.

Having one, large, condenser rather than a system comprised of several separate units provided several advantages. The size of the condenser, with its entire top a removable lid, afforded easy access for cleaning, while the single unit provided a simplified system, with fewer potential points of failure from seals and joins, and made it ideal for the recovery of longer chain waxes using a heat gun.

#### 3.5.4.1 Operation

The condenser was filled with dry ice and connected to the outlet of the reactor immediately prior to HDPE sample being added to the reactor to avoid the dry ice sublimating while the condenser was not in use. When pyrolysis was under way, gas passed through and condensed on the surface of the dry ice pellets. Depending on the melting point of the condensate, small molecule liquids would drip down into a 1 L measuring cylinder collection vessel, and larger molecules would freeze to the pellets and gradually make their way down as the dry ice beneath sublimated. No aerosol particles were observed leaving the condenser (though sublimated $CO_2$ gas was visible) — the tortuous convection path and high surface area ensured all particles settled in the condenser. At the completion of the experiment, the dry ice in the condenser was allowed to sublimate away, leaving any previously frozen pyrolysis products to melt into the collecting vessel (with the assistance of a heat gun in the case of sufficiently long-chain waxes).

It is recognised that a dry ice condenser as described would not be appropriate for use were the process to be scaled up significantly in size and operational throughput. It does, however, maximise collection in the laboratory context, and provide useful information on maximum yield expectations for the process applicable on any scale. An alternative condensing system design that might be more suitable on a larger scale is outlined in §7.2.6.

#### 3.5.4.2 $CO_2$ Interaction with Condensate

Concerns that the hot pyrolysis products might react with the $CO_2$ in the condenser to form new species were allayed through a comparison of the products collected with this condenser and previous condensing systems. While some differences in the relative proportions of species in the products were noted (e.g., a better retention of smaller molecules), this was to be expected with the more efficient condensing system. Significantly, no oxygenated species were present when using the dry ice condenser other than $CO_2$ in the non-condensable gases, implying that no chemical interaction occurred. The rapid cooling of the pyrolysis products upon leaving the hot zone of the carbon bed in the reactor, and the very low temperature of the dry ice, no doubt ensured this.

#### 3.5.4.3 $CO_2$ Contamination in Collected Gas

While the evaporation of the dry ice from the condenser did add a significant quantity of $CO_2$ to the gas samples collected for later analysis, testing with previous condensers had convincingly demonstrated that no $CO_2$ was actually generated from the pyrolysis of HDPE under normal operation. As such, the $CO_2$ peak in GC/MS analysis of samples collected using the internal dry ice condenser was discarded (with no loss in resolution for the analysis of the remaining gases), and no $CO_2$ component was included in the gaseous product composition analyses.

## 3.6 Control Software Development

As received, control of the magnetron power supply was effected via a rotary potentiometer, which was set by hand and allowed the variation of power from 0–100%.

### 3.6.1 Problems with Existing Control Setup

The existing manual setup suffered from a number of limitations, including:

- requiring significant time and attention, forcing the operator to constantly adjust the power at the expense of other important tasks
- performing inconsistently between runs
- unpredictability — if the operator was not paying close attention to the power output a wide variety of temperatures could result
- no mechanism for recording the power output, or the reflected power
- limited diagnostic output and feedback when errors occurred
- slow human response in the event of a problem

Given the large number of experimental runs required for the work in this project, a more robust system remedying these flaws was required; as such, a computerised automatic controller was developed as described in the following section.

### 3.6.2 Hardware Interface

The magnetron power supply included the facility for control by an external programmable logic controller. An in-depth analysis of the control mechanism and thermocouples resulted in the requirements for a computer-based control system, set forth in table 3.1. Digital input and output was provided by an Audon PCX-4264 PCI card with 32 channels; analog input and output was provided by a Measurement

**Table 3.1:** Input and output requirements for computer control of the microwave power supply. Input and output is defined relative to the computer controller, i.e., *input* signals are readings from the power supply or thermocouples to the computer, and *output* signals are controls sent from the computer to the power supply.

| Analog | | Digital (24 V) | |
|---|---|---|---|
| Input | Output | Input | Output |
| Power supply monitor (0–10 V) | Magnetron power (0–10 V) | Ready | Remote control on |
| Reflected power (0–10 V) | | Magnetron status | Filament heating on |
| Thermocouple 1 (0–50 mV) | | High voltage supply | Magnetron on |
| Thermocouple 2 (0–50 mV) | | Safety interlock | Reset |
| Thermocouple 3 (0–50 mV) | | Failure | |
| Thermocouple 4 (0–50 mV) | | Magnetron cooling failure | |
| Thermocouple 5 (0–50 mV) | | Power supply cooling failure | |
| | | Input failure | |
| | | Overload | |

Computing PCI-DAS6014 16-bit PCI card with eight input channels and two output channels. The 16-bit resolution provided by the analog input board was judged to be of sufficient depth, when operating in the 50 mV range mode (providing a theoretical 0.76 µV resolution), to read the thermocouples directly without amplification. A custom-built daughter board was also constructed to handle switching from the low voltage digital I/O to the 24 V system used by the power supply.

### 3.6.3 Software Controller

National Instruments' Labview 8.6 was selected as a programming environment in which to develop control software for the microwave system owing to its strengths in rapid development, real-time capabilities, and data input/output interfacing. Figure 3.12 on the next page shows a simplified schematic of the main control program, the components of which are described below. A screenshot of the final configuration of the software interface is given in figure 3.13 on page 67.

#### 3.6.3.1 Analog Input

The analog signals (thermocouple voltages, magnetron power, reflected power) were read in at a sampling rate of 40 kHz. Digital signal processing was applied to the signals to reduce background noise (e.g., a notch filter was applied to remove 50 Hz mains interference). The thermocouple voltages were converted into temperatures using the NIST PB93-190338 standard [198] (a ninth-order polynomial approximation with $\leq$0.05°C error over the measuring range).

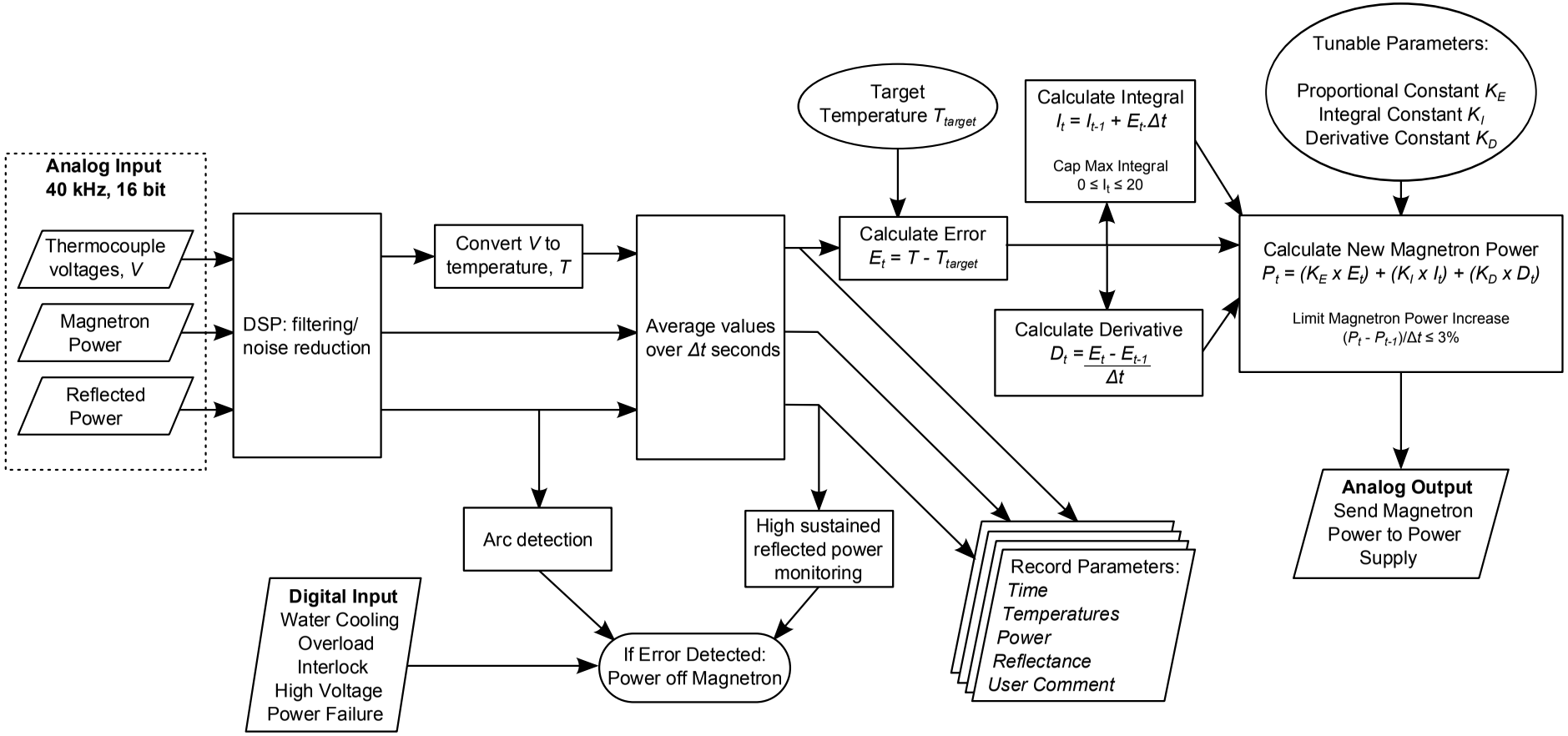


**Figure 3.12:** Simplified PID controller software schematic. Components are described in §3.6.3.

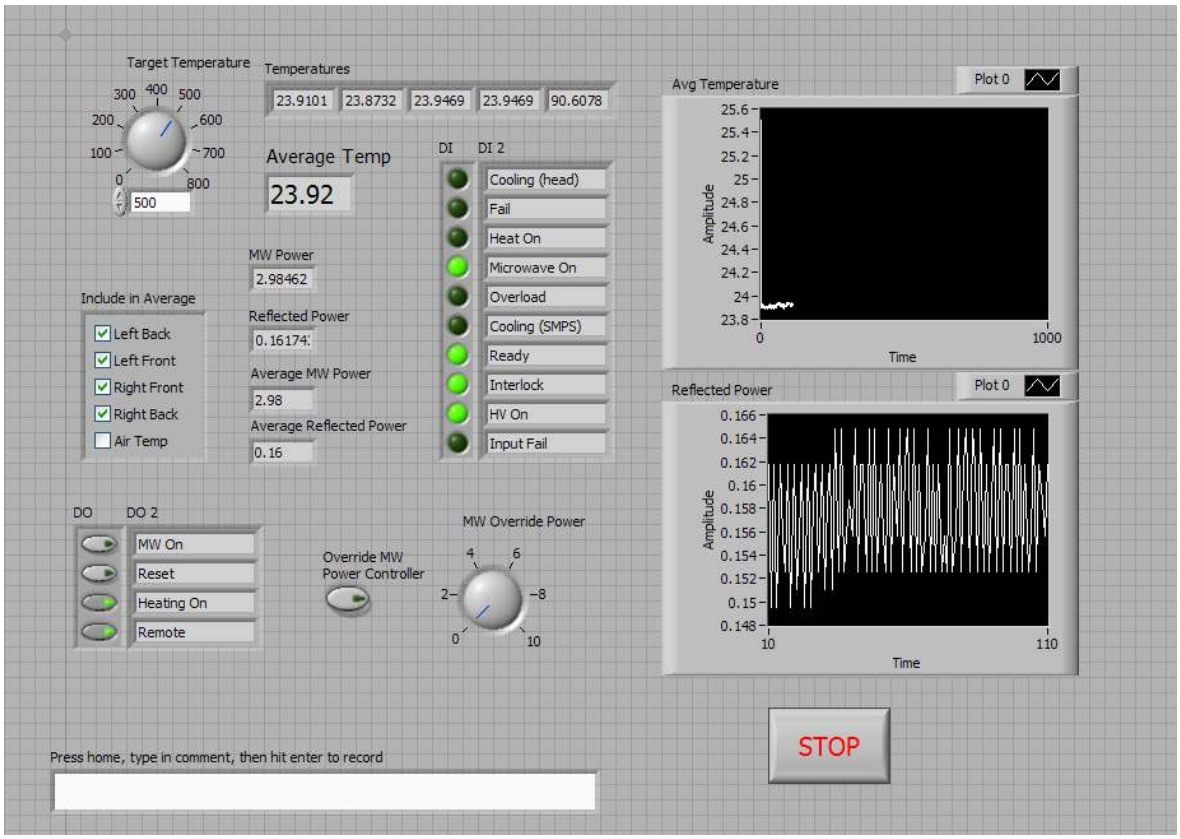


**Figure 3.13:** Screenshot of the final configuration of the PID controller software interface.

### 3.6.3.2 PID Controller

A software proportional-integral-derivative (PID) feedback controller [199] was constructed according to equation 3.6.

$$P(t) = K_E.E(t) + K_I.\int_0^t E(\tau).d\tau + K_D.\frac{d}{dt}E(t) \tag{3.6}$$

In this system, the power output to the magnetron ($P(t)$) at any time ($t$) is calculated as a weighted sum of the current error ($E(t)$) — the difference between the current operating temperature and the reactor target temperature; a "backward looking" integral term ($\int_0^t E(\tau).d\tau$) which corresponds to the accumulation of previous errors; and a "predictive" derivative term ($\frac{d}{dt}E(t)$) — the current rate of change of the error. The respective contribution of the proportional, integral, and derivative terms to the final power output is controlled using user-tunable constants ($K_E$, $K_I$, $K_D$ respectively).

Applying equation 3.6 to a computer system requires converting the continuous equation into a discrete form in the time domain, applicable to individual data points. This was done for the integral term as follows:

$$\int_0^t E(\tau).d\tau = I_t = I_{t-1} + E_t.\Delta t \tag{3.7}$$

where $I_t$ is the current accumulated integral error, which comprises the previous integral error ($I_{t-1}$), and the error ($E_t$) accumulated over the previous time step ($\Delta t$). The term is initialised to 0 at the commencement of operation ($I_{t=0} = 0$).

The derivative term was approximated using backward finite differences, as the change from the error at the previous sampling time ($E_{t-1}$) to the current error ($E_t$) over the sampling time ($\Delta t$).

$$\frac{d}{dt}E(t) \approx \frac{E_t - E_{t-1}}{\Delta t} \tag{3.8}$$

Combining these gives the overall discretised PID equation for microwave output power ($P_t$):

$$P_t = K_E.E_t + K_I.(I_{t-1} + E_t.\Delta t) + K_D.(\frac{E_t - E_{t-1}}{\Delta t}) \tag{3.9}$$

#### 3.6.3.3 Practical Implementation Issues

*Integral windup* occurs when the integral term accumulates to a very large value as the reactor temperature differs from the set point for a prolonged period of time (e.g., when the reactor is heating up at the beginning of an experiment). In order to prevent this occurring, a hard limit was imposed on the maximum value the accumulated integral error could take. An absolute value of 20 for this limit was found to provide plenty of head-room for the integral parameter during normal operation (around the target temperature), while preventing integral windup from deleteriously affecting operation.

The selection of a suitable time period, $\Delta t$, over which to sample the temperature inputs (and thus error), and between which to update the magnetron power, involved a trade-off between providing a sufficiently rapid response to changing conditions (e.g., the addition of HDPE sample requiring greater power input to maintain the bed at the target temperature), and introducing instability owing to the inherent time delay between changing the power input and the resultant change in measured reactor bed temperature. Manual experimentation with this parameter resulted in the selection of a five-second update period that proved both responsive and stable.

Translating the boundless PID function into a practical power output required limiting the absolute value of the output $0 \leq P_t \leq 10$ so that it fell between the 0–10 V of the power supply input. It was also considered prudent to avoid large increases in

power output at each update interval to prolong the life of the magnetron filament. Without limitation, when the PID was first turned on the power would jump from 0% to 100% instantaneously, potentially damaging the magnetron with the sudden increase in power. As such, an upper limit was imposed in software with the maximum power increase confined to 3% per second.

Tuning of the PID constants ($K_E$, $K_I$, $K_D$) was achieved using the Ziegler-Nichols method [200] initially, then manually optimised for stability and sensitivity of the system. The fully tuned system exhibited excellent performance, and was able to maintain the average reactor temperature within ±1ºC of the target.

#### 3.6.3.4 Arc Prevention and Safety Systems

As described in §3.3.1, arcing is a destructive threat present when operating high power electromagnetic sources such as the microwave reactor used in this work. When arcing does occur, the key to preventing damage is to recognise that it is occurring, and to cut power to the power source as quickly as possible. It was found that a reliable indicator that an arc was occurring was a sudden spike in reflected power, far beyond the normal levels usually observed. Accordingly, a detection subroutine that monitored the magnitude of the reflected power was incorporated into the programme; the routine triggered when it breached a safety threshold, and instantly powered down the magnetron. Under computer automation, with a 40 kHz sampling rate (i.e., a 0.025 ms response time), monitoring was far more effective, and action taken far more rapidly, than when it was left to a human operator.

In addition to monitoring high transient reflectance, the software also monitored for a sustained higher-than-normal average reflected power, which could indicate an arc occurring deeper in the reactor (as opposed to in the waveguide) or some other malfunction, and would also trigger a rapid safety shutdown so the cause could be investigated.

The software also had a number of digital inputs from sensors distributed around the power supply and magnetron head that would indicate if a fault had occurred (e.g., overload, low water cooling rate, power failure, etc.) and would shut down the system to prevent damage in the event that any of these were triggered.

#### 3.6.3.5 Data Logging

Throughout execution, the software continuously logged operating parameters (current time, thermocouple temperatures, microwave power output, reflected power). The

software interface also contained the facility to record comments from the operator, which were time-stamped, and recorded in the log file along with the other parameters. In the event of catastrophic failure the software was designed to prevent information loss as much as possible by writing data to disk as soon as possible. In the event that such failure did occur, the software was designed for rapid resumption of controller duties so as to minimise disruption to the experiment, and was able to append to the log file starting from the last data point written.

## 3.7 Safety Systems

The combination of microwave radiation, high temperatures, and flammable gases presented a unique series of safety challenges, as our beleaguered department health and safety officer would no doubt attest.

### 3.7.1 Microwave Safety

British Standard 5175 states that the maximum safe level of power density permissible outside the shielding of a microwave device is 50 W $m^{-2}$ at a distance of 5 cm. Conformance with this specification was tested every time after the pyrolysis rig was assembled, by gradually increasing the power output of the magnetron and sweeping the entire rig with a Robin TX90 hand-held microwave leakage detector. Use of industry standard IEC R26 / EIA WR340 waveguides and flanges for all components in the microwave transmission path meant that leakage was rarely above background and the safety standard was never breached.

### 3.7.2 Preventing Equipment Leaks

Given the potential toxicity of the gases produced during pyrolysis it was important to have completely gas-tight equipment. A common design approach employed throughout improvement of the pyrolysis rig was to simplify components, and combine them where possible, to reduce the number of failure points due to joins and seals. In spite of this effort, the rig was still tested after each modification and assembly by perfusing with nitrogen gas, and testing at each seal with a hand-held Restek thermal-conductivity leak detector for the presence of nitrogen gas in concentrations above background.

### 3.7.3 Extraction System

Any pyrolysis gases that were not able to be condensed were sampled and then entered the extraction system. The extraction system totally surrounded the exit of the condenser, but was not directly coupled to it, in order to avoid applying negative pressure to the reactor and condensation equipment. This also allowed the exiting gases to be substantially diluted by the concurrently admitted air, reducing the concentration of any toxic components, and diluting the hydrocarbons below the minimum concentration required for combustion.

### 3.7.4 Additional Safety Systems

Additional safety systems installed throughout the course of this work include:

- An emergency stop button installed within arm's reach of the operator that would immediately cut power to the magnetron.
- An audible and visual alarm which would alert the operator in the event of extraction failure.
- Additional $CO_2$ fire extinguishers — given the criticality of timeliness when it comes to fire control it was decided to install several supplementary extinguishers, such that at least one would be within arm's reach of the operator at all times.

## 3.8 Final Configuration of Microwave-Assisted Pyrolysis Apparatus

The final configuration of the microwave pyrolysis apparatus, incorporating all of the improvements described thus far, is detailed overleaf in figures 3.14 and 3.15 in schematic and photographic form respectively.

## 3.9 Summary

A number of problems presented in the microwave-assisted pyrolysis equipment as received, including high levels of reflected power, transmission losses, and the formation of damaging arcs. These problems were tackled with an overall design approach involving simplifying and combining components where possible, to reduce the number of potential failure points. This resulted in a rethink of the transmission pathway — linearising it and eliminating a substantial number of components, and a

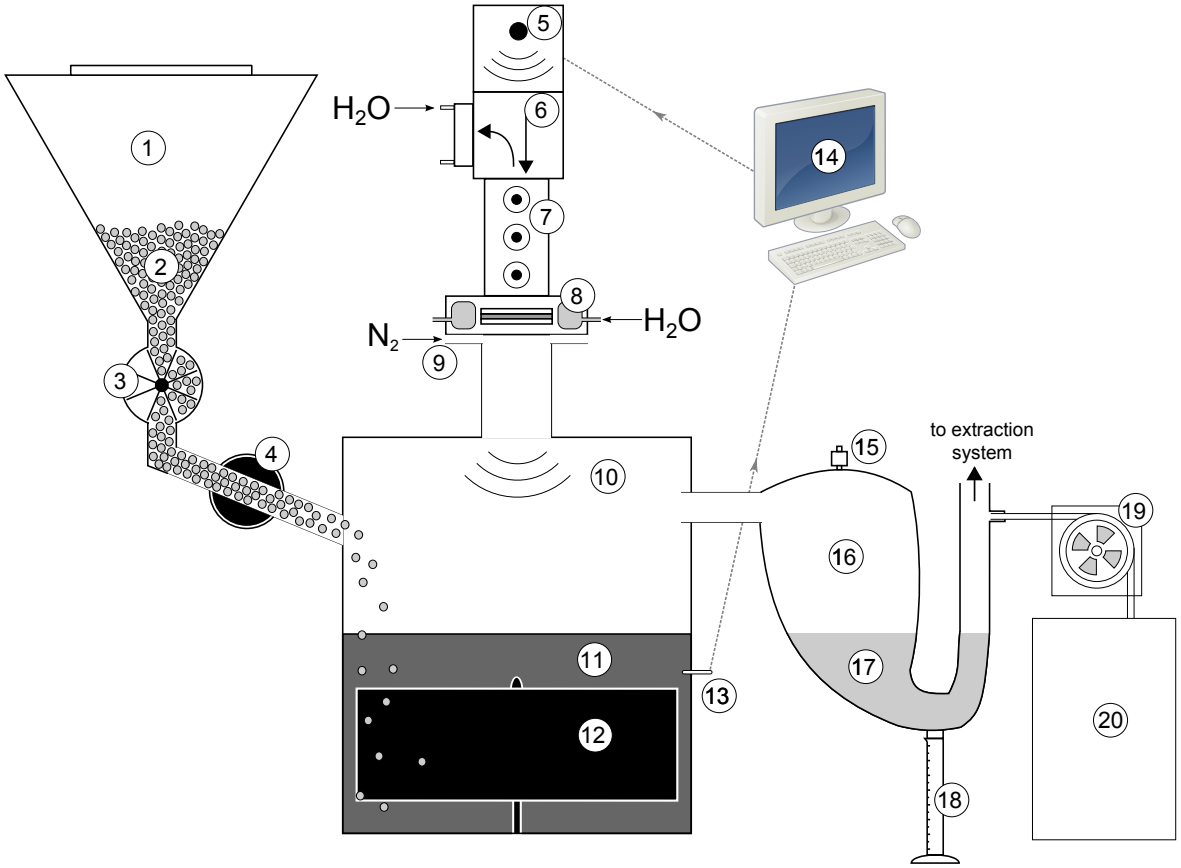


| | | | |
|---|---|---|---|
| 1 | Feeder hopper | 11 | Carbon bed |
| 2 | HDPE pellets | 12 | Stirrer |
| 3 | Rotary feeder mechanism | 13 | Thermocouple |
| 4 | Ball valve isolator | 14 | Computer control system |
| 5 | Magnetron | 15 | Pressure release safety valve |
| 6 | Isolator | 16 | Condenser |
| 7 | Three-stub tuner | 17 | Dry ice |
| 8 | Window | 18 | Collecting vessel |
| 9 | Nitrogen inlet | 19 | Peristaltic sampling pump |
| 10 | Reactor | 20 | Gas collecting bag |

**Figure 3.14:** Schematic of the final configuration of the microwave-assisted pyrolysis apparatus.

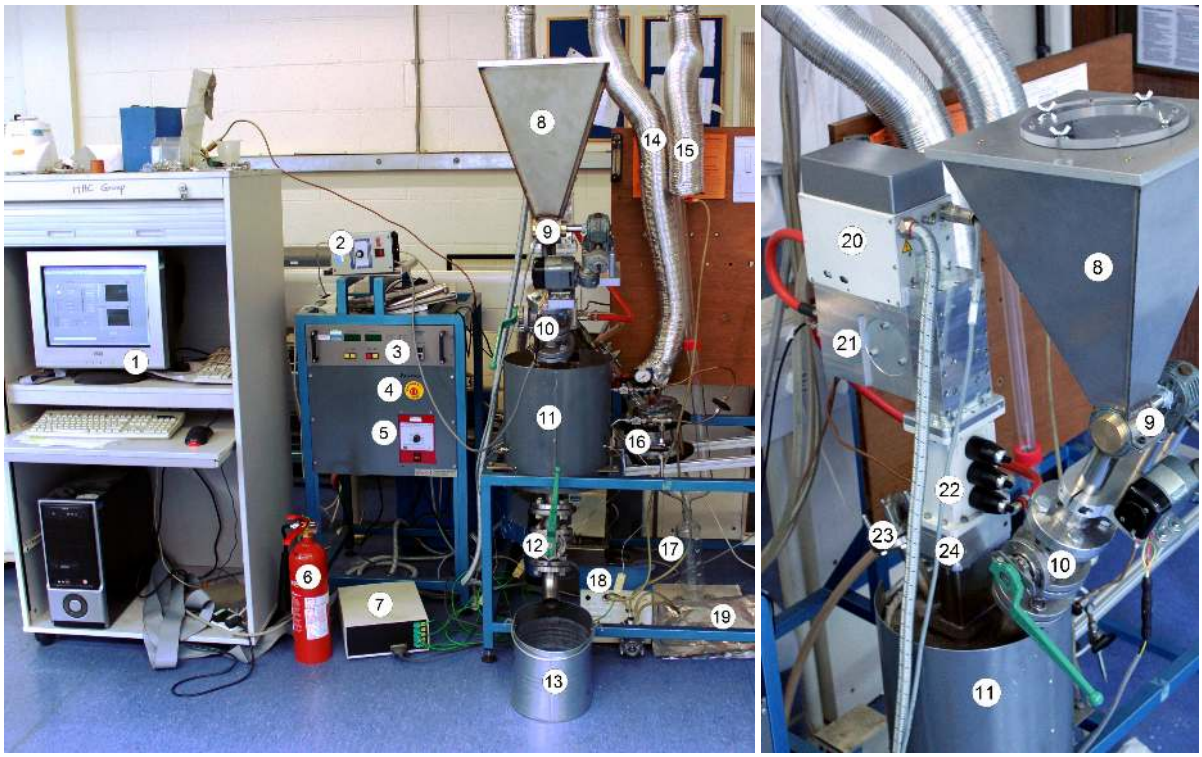


| | | | |
|---|---|---|---|
| 1 | Computer control system | 13 | Bed collection container |
| 2 | Feeder motor controller | 14 | Pressure release valve extraction |
| 3 | Magnetron power supply | 15 | Condenser extraction |
| 4 | Emergency stop button | 16 | Condenser |
| 5 | Stirrer motor controller | 17 | Collecting measuring cylinder |
| 6 | Fire extinguisher | 18 | Peristaltic sampling pump |
| 7 | Control system daughter board | 19 | Gas bag |
| 8 | Feeder hopper | 20 | Magnetron |
| 9 | Rotary feeder mechanism | 21 | Isolator |
| 10 | Inlet isolator ball valve | 22 | Three-stub tuner |
| 11 | Reactor | 23 | Reactor gas outlet pipe |
| 12 | Reactor emptying ball valve | 24 | Window |

**Figure 3.15:** Final configuration of the microwave pyrolysis apparatus in overview (left), and close-up on the transmission path (right). Numbered components are consistent between both images, though may not be present in both cases.

redesign of the window — integrating it with the nitrogen gas inlet and incorporating more effective internal cooling. A re-examination of the window material itself resulted in changing it from expensive, fragile, and microwave-reflecting quartz, to a mica and silicone composite, which had the advantages of strength, self sealing, the elimination of microwave reflection, and a reduction in damaging carbonaceous deposits. These improvements, combined with tuning the microwave system through impedance matching, reduced reflected power from greater than 50% to below 10%, and greatly improved system reliability.

An initial plunger-type feeder allowed HDPE pellets to be added to the reactor at pyrolytic temperatures; however, the discrete addition of sample limited the quantity of material that could be pyrolysed at once and overwhelmed the microwave heating system's ability to maintain a constant reactor temperature. Correspondently a continuous rotary feeder was designed and built, which solved these issues, and allowed the pyrolysis rig to operate effectively indefinitely, and process arbitrary quantities of input material.

Manual control of the magnetron power output required significant operator time and attention, and proved inconsistent and slow to respond to damaging arcs occurring in the system. A computer-based PID controller was developed that automated control of the magnetron, improved reliability, and was able to detect and respond to arcs and other faults safely and far more rapidly than a human operator.

The condensing apparatus proved a significant limitation on extracting condensible pyrolysis products from the gaseous stream exiting the reactor. A number of design iterations based around Liebig condensers failed to prevent a hydrocarbon-containing aerosol mist from being carried along by the continuous flow of gases through the system. A final, effective design passed the pyrolysis gas through a condenser containing dry ice pellets, which disrupted the laminar flow of the gas and provided a very high surface area to maximise heat transfer.

While presented as a single block of work, the improvements outlined in this chapter represent the continuous evolution and refinement of the microwave-assisted pyrolysis rig over a prolonged period of time. Nevertheless, unless the equipment changes had no impact on results, or it has been otherwise noted, it is the final form of the microwave pyrolysis equipment that, along with the protocol developed alongside, was used to generate the results that comprise the remainder of this dissertation.

# 4

# Batch Pyrolysis of HDPE using an Activated Carbon Reactor Bed

## 4.1 Introduction

Activated carbon is a relatively unstudied catalyst, completely so in the context of the microwave-assisted pyrolysis of HDPE. Having developed a reliable set of equipment and operating procedures to pyrolyse HDPE using microwave heating and a carbon bed, it was next important to evaluate the utility of activated carbon as a catalyst in this context, i.e., to establish the feasibility of using activated carbon as a catalyst in this process, and to determine the characteristics, chemical make-up, and economic value of the products resulting from its use, so that the overall process could be assessed as worthwhile or not.

In order to evaluate the performance of activated carbon as a catalytic bed, a series of exploratory experiments were undertaken using the reactor and equipment described in the previous chapter, in semi-batch mode (i.e., with the batch input of

HDPE and continuous removal of pyrolysis gases as they were produced), using the plunger injector (see §3.4.1), hereafter referred to as “batch” mode. The thermal sensitivity of the process was characterised with a series of experiments conducted over the widest possible range of operating temperatures: from the lower threshold of pyrolysis occurring at 400°C, to the maximum temperature sustainable by the magnetron with the addition of the HDPE at 600°C, with the resulting yields, mass distribution, and chemical composition of the products examined. Control experiments were conducted with the same parameters but using a coke bed to provide a baseline from which to compare the effects of the activated carbon. While the microwave-assisted pyrolysis of HDPE using a coke bed has been studied previously [29, 46], specific outcomes are often sensitive to the exact reactor type and configuration. Accordingly, it was considered prudent to generate control results with the coke bed for direct comparison, in order to eliminate as many variables as possible.

This chapter describes the methodology, results, and analysis undertaken in order to establish the utility of activated carbon for microwave-assisted pyrolysis, and places this in context with the wider body of pyrolysis literature.

## 4.2 Materials

### 4.2.1 HDPE

HDPE was chosen as a model material for pyrolysis over the course of this research, owing to its simple, pure hydrocarbon molecular structure, which avoided adding any further complication to the already complex pyrolytic breakdown reaction pathway. HDPE is also one of the relatively few materials on which microwave pyrolysis research has already been conducted [29, 46], and thus offered an external point of comparison to this research. Liten ML 71 HDPE was acquired from Unipetrol RPA; this particular form of HDPE has a wide variety of applications derived from its intended use in injection moulding manufacturing. It was chosen for use in this research because of its lack of additives, wide availability, and ease of handling owing to its pelleted form (cylinders approximately 2 mm in diameter and 3–4 mm long). The material properties of Liten ML 71 are given in table 4.1.

**Table 4.1:** Typical material properties of Liten ML 71 HDPE. Provided by Unipetrol RPA.

| Property | Value | Test Method |
|---|---|---|
| Density | 963 kg/m$^3$ | ISO 1183 |
| Yield Stress | 26 MPa | ISO 527 |
| Tensile Strain at Yield | 8.50% | ISO 527 |
| Flexural Modulus | 1100 MPa | ISO 178 |
| Charpy Notched Impact Strength, 23°C | 6.5 kJ/m$^2$ | ISO 179 |
| Charpy Notched Impact Strength, -30°C | 5.5 kJ/m$^2$ | ISO 179 |
| Shore Hardness | 58 | ISO 868 |
| Vicat Softening Temperature | 126 C | ISO 306 |
| Melt Flow Rate (190°C / 2.16 kg) | 8.5 g / 10 mins | ISO 1133 |
| Melt Flow Rate (190°C / 5 kg) | 23.0 g / 10 mins | ISO 1133 |

### 4.2.2 Coke

High purity FC-250 petroleum coke (Timcal Ltd) was obtained for use as the reactor bed. The high calcination temperature used in production ensured that it contained no volatile hydrocarbons, and minimal other impurities, which might contaminate the pyrolysis products. Typical material properties are given in table 4.2. Approximately 2.0–2.5 kg of coke was used for the reactor bed — sufficient to completely cover the stirrer while in operation. Before the coke was first used for pyrolysis it was heated in the reactor to 700°C for 30 minutes to ensure any trace compounds were burnt off, and to remove any moisture from the material before it was first weighed. Heating the coke to 100°C higher than it would be used at during pyrolysis provided a safety margin that ensured no contaminants would evolve during the actual pyrolysis experiments.

**Table 4.2:** Typical material properties of Timrex FC-250 coke (Timcal Ltd), and Aquacarb 207EA (Chemviron Carbon); data provided by the manufacturers.

| Property | Coke | Activated Carbon |
|---|---|---|
| Ash | 0.07 wt% | <1 wt% |
| Moisture | 0.02 wt% | <5 wt% |
| Sulfur | 1.3 wt% | - |
| Bulk density | 0.80 g/cm$^3$ | 0.48-0.52 g/cm$^3$ |
| Bulk volume | 125 mL / 100g | - |
| Tapped density | 0.91 g/cm$^3$ | - |
| Plastic deformation | 0.21% | - |
| Elastic deformation | 0.10% | - |
| Surface area | - | 950–1100 m$^2$/g |
| Particle Size Distribution | 2% >250 µm<br>75% >125 µm<br>85% >90 µm | 0.42–1.68 mm |

### 4.2.3 Activated Carbon

Aquacarb 207EA was acquired from Chemviron Ltd. This high-activity carbon originally derives from bituminous coal, and is steam activated. Typical material properties are given in table 4.2. Similar to the coke bed, sufficient activated carbon was used as the reactor bed to cover the stirrer while in operation (2.0–2.5 kg), and an identical initial heat treatment process was applied to ensure moisture and impurities were removed.

## 4.3 Microwave Pyrolysis Method

The microwave-assisted pyrolysis apparatus used in this chapter is the final configuration described in §3.8, with the exception that the continuous feeder had not yet been developed during these experiments. As such, the reactor operated in batch mode, with the plunger injection system adding HDPE sample in one quantity, and the pyrolysis products exiting the reactor to the condensing system as they were produced. All experiments were conducted at atmospheric pressure.

At the commencement of an experimental run, the nitrogen supply was turned on and allowed to vent through the apparatus at a rate of 0.7 L/min. The stirrer was set to a speed of 8 revs/min — a speed sufficiently rapid to maintain an even temperature distribution throughout the carbon bed. The water cooling system was started, and the computer was set to the target temperature. The magnetron was switched on, and the reactor bed was heated to the target temperature, a process that took 1–2 hours. Once the bed had reached the desired temperature it was allowed to equilibrate for a minimum of 15 minutes to ensure a homogeneous heat distribution. At this point, the percolating condenser was filled with dry ice and it was connected to the outlet of the reactor. HDPE pellets were added to the reactor using the plunger injector system (described in §3.4.1), and the peristaltic pump which sampled the gas exiting the condenser was switched on.

The pyrolysis of HDPE produced a mixture of gaseous hydrocarbons, some of which, once they left the hot zone of the reactor, condensed into a suspension of liquid droplets. This aerosol was visible entering the condenser, and provided a visual cue as to the progress of the pyrolysis reaction: the reactor was maintained at the target temperature until more of the pyrolysis aerosol was generated. At this point the microwave heating was switched off, and the reactor was allowed to cool. During this time the dry ice in the condenser sublimed, and any frozen condensed

sample melted into the collecting cylinder. Non-condensable gases continued to be collected throughout this time (with the $CO_2$ peak arising from the dry ice condenser subsequently discarded in later analysis). In the event that any solid pyrolysis products remained in the condenser after all the dry ice had sublimed it was gently warmed with a heat gun until it melted into the collecting vessel.

Once the reactor bed reached approximately 150°C (a process usually taking 2–3 hours) the carbon was removed from the reactor and weighed; the reactor bed was always weighed at >100°C so that moisture absorbed from the air was not included in the mass.

### 4.3.1 Experimental Conditions

Pyrolysis experiments were conducted with the activated carbon bed, and a control bed of coke, at 400°C, 450°C, 500°C, 550°C, and 600°C. These temperatures represented the effective limits of the pyrolysis equipment used: below 400°C pyrolysis either did not occur or occurred so slowly as to make experiments impractically long; 600°C was the maximum reactor temperature that the 3kW microwave heating system could sustain without an unacceptable drop of temperature occurring when the HDPE was injected. In all experiments 100 g of HDPE pellets was added to the reactor in each sample injection.

### 4.3.2 Pyrolysis Product Mass Measurement

The mass of the condensed pyrolysis products was assessed by weighing the full collecting cylinder at the conclusion of an experiment, then subtracting the mass of the empty, clean, and dry cylinder. The mass of the input sample retained in the reactor was measured by the increase in mass of the reactor bed between runs. The amount of non-condensable gas generated in the pyrolysis was determined through the principle of conservation of mass, and was calculated by the mass of sample added, less the mass of the condensed products, less the increase in mass in the carbon bed.

## 4.4 GC/MS Analysis

Samples were analysed by gas chromatography coupled with mass spectrometry (GC/MS) using an HP 6890 gas chromatograph and an HP 5973 mass selective system

(Agilent Technologies). Compounds were identified using Agilent Chemstation version G1701DA and the NIST 2005 mass spectral library.

### 4.4.1 Condensed Product Analysis

Condensed pyrolysis products were analysed with an SGE HT5 30 m x 0.25 mm x 0.1 μm capillary column (5% Phenyl equiv. polycarborane-siloxane). Any samples containing solid waxes were heated before being injected to ensure they were entirely liquid and homogeneous. 1 μL of sample was injected into a split inlet operating at 250°C at a ratio of 100:1, a pressure of 5 psi, and a gas flow of 1.2 mL/min. The oven was initially set at 30°C, at which temperature it was held for 3 minutes after injection, and it was then ramped at 8°C/min to 350°C, where it was held for 30 minutes. 6.0-grade helium (99.9999% pure) was used as the carrier gas.

### 4.4.2 Gas Analysis

Gas samples were analysed with an Agilent GS-Gaspro 60 m x 0.32 mm porous layer open tubular capillary column. 100 μL of gas was injected into a split inlet operating at 250°C at a ratio of 20:1, a pressure of 5 psi, and a gas flow of 1.1 mL/min. The oven was initially set at 30°C, a temperature at which it was held for 10 minutes after injection, and it was then ramped at 5°C/min to 150°C. 6.0-grade helium (99.9999% pure) was used as the carrier gas.

### 4.4.3 Quantification of Compounds by Peak Area

The large number of individual compounds present in the pyrolysis products (up to several hundred) meant that quantitative calibration of each of these in the GC/MS analysis was impractical; instead, a measure of proportional peak area is used throughout this work. With this metric, each compound is quantified by the integrated area of the corresponding peak on the mass spectrometer chromatogram. This is then given as a percentage of the total area of all peaks in the analysis. This method allows a descriptive and quantitative analysis of products that gives a good approximation to mass percentage.

**Figure 4.1:** Condensed pyrolysis products generated using activated carbon (left) and coke (right) reactor beds. The activated carbon derived condensate is entirely liquid at room temperature and clear — notice that it is sufficiently transparent that the sample label is clearly visible at the rear of the glass sample bottle. The condensate produced using a coke bed, by contrast, is mostly solid at room temperature and entirely opaque.

## 4.5 Analysis of Condensed Pyrolysis Oils and Waxes

### 4.5.1 Visual Assessment

Figure 4.1 shows samples of the condensed pyrolysis products produced with activated carbon and coke beds. A dramatic visual difference is obvious: the condensate produced using a coke bed is viscous, waxy, and of mixed consistency; when using an activated carbon bed a clear, homogeneous product resulted that was entirely liquid at room temperature.

### 4.5.2 GC/MS Analysis and Peak Identification

Figure 4.2 on the next page shows typical examples of GC/MS chromatograms of the condensed pyrolysis products produced using activated carbon and coke reactor beds. The coke derived chromatogram is similar to those produced by other researchers investigating the pyrolysis of polyethylene [29, 173, 201]. Of particular note is the regular series of peaks, with each peak grouping further along the chromatogram corresponding to the group of hydrocarbons with one additional carbon atom in their molecular formula. The largest and most clearly identifiable of these peaks is composed of, for each carbon number, a terminal alkadiene (with the double bonds located at

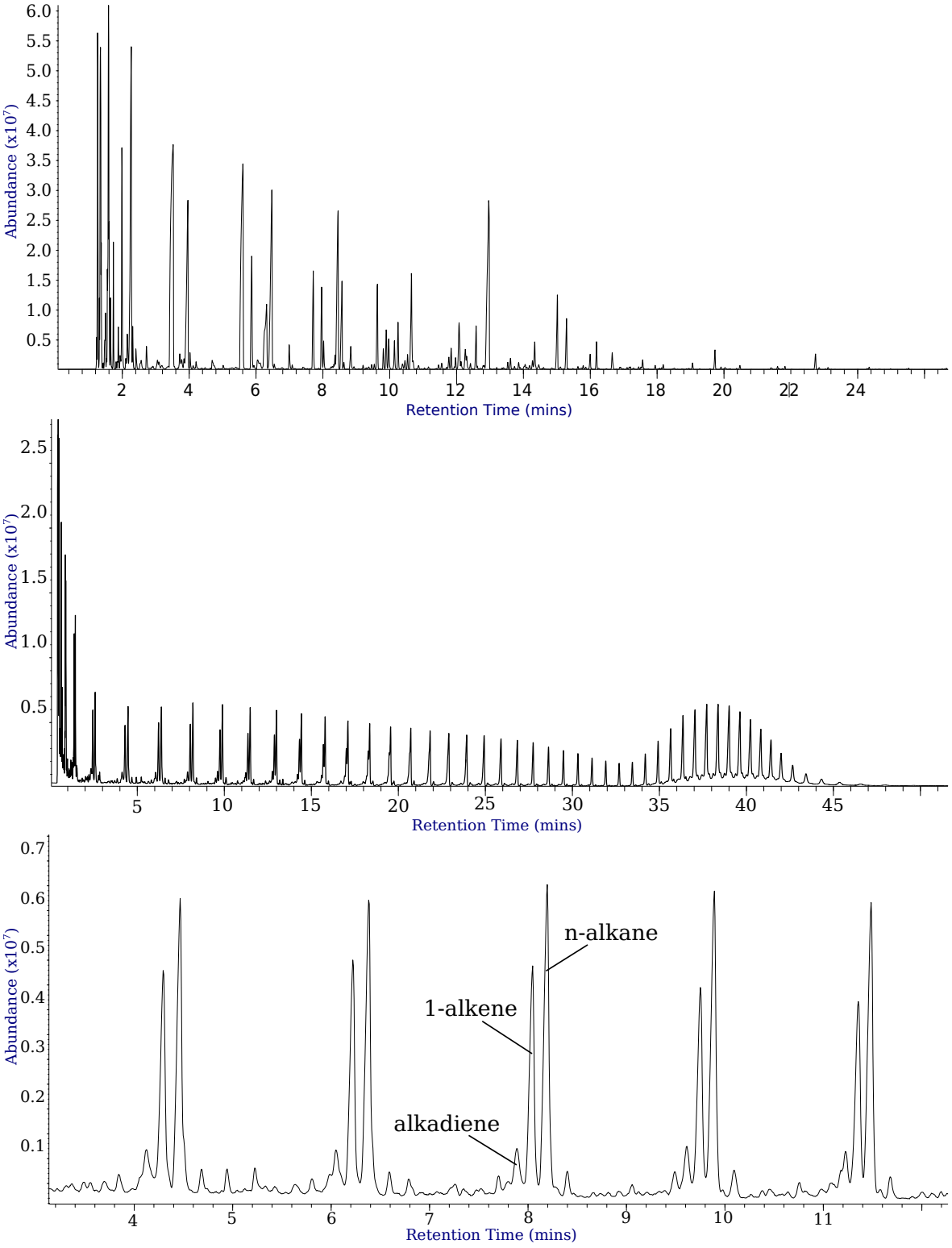


**Figure 4.2:** Typical GC/MS chromatograms generated from the analysis of condensate from activated carbon (top) and coke (middle) reactor beds. A magnified view of the characteristic alkadiene, 1-alkene, and n-alkane triple peaks is shown in the bottom sub-figure; the regularity of these peaks makes them useful as markers for compound identification.

the peripheries of the molecule), followed by a 1-alkene, followed by an n-alkane (in order of increasing retention time); this "triple peak" grouping has been identified by researchers conducting similar analyses of the condensed pyrolytic products of polyethylene [46, 173, 191, 201]. These regular triple peaks provided valuable information that could be used to identify compounds in the event that they were either not contained in the spectral database, or if the match to the database for a peak was unclear (generally molecules larger than $C_{25}$ were not present in the NIST database). Fortunately, the regularity with which the triple peaks occur (a grouping is present for every carbon number in the sample) provided a consistent goalpost with which to measure the carbon numbers of unidentified peaks; furthermore, the order with which different molecules elute remains consistent between (and within) each triple peak marker, e.g., the alkane form always immediately follows the 1-alkene, allowing the identification of the specific hydrocarbon from the relative retention time.

In contrast to the coke bed, the activated carbon derived chromatograms show a much shorter total elution time, with correspondingly smaller molecules on average. The regular triple peaks are still present, though they are interspersed with a much larger number of other (mostly aromatic) compounds. The smaller maximum molecular size of the condensate produced with an activated carbon bed means that the peaks could be identified using the NIST database alone. Histograms and statistics derived from the GC/MS analyses are presented in §4.5.3.

### 4.5.3 Mass Distribution of Condensed Pyrolysis Products

Figure 4.3 on the following page shows the size of the compounds in the condensed pyrolysis products as measured by carbon number, and determined by GC/MS analysis. The dramatic difference in the composition of the products is clearly visible, with the oil produced using the activated carbon bed consisting of much smaller molecules, distributed over a smaller range of molecular masses. The distribution of the condensed products produced using an activated carbon bed is uni-modal, centred around $C_8$. By contrast the distribution of products produced with a coke bed is less regular, with a far greater spread of molecular masses that encompasses a second grouping of products in the $C_{40}$–$C_{50}$ range (discussed further in §4.5.3.4). Summary statistics quantifying average molecular mass and spread across all reaction temperatures are given in table 4.3 on page 85. The pyrolysis oil produced using an activated carbon bed is far lighter, with an average carbon number of 10.0 to 11.5 compared with that produced with a coke bed of 25.0 to 33.0 — approximately three times larger. Furthermore,

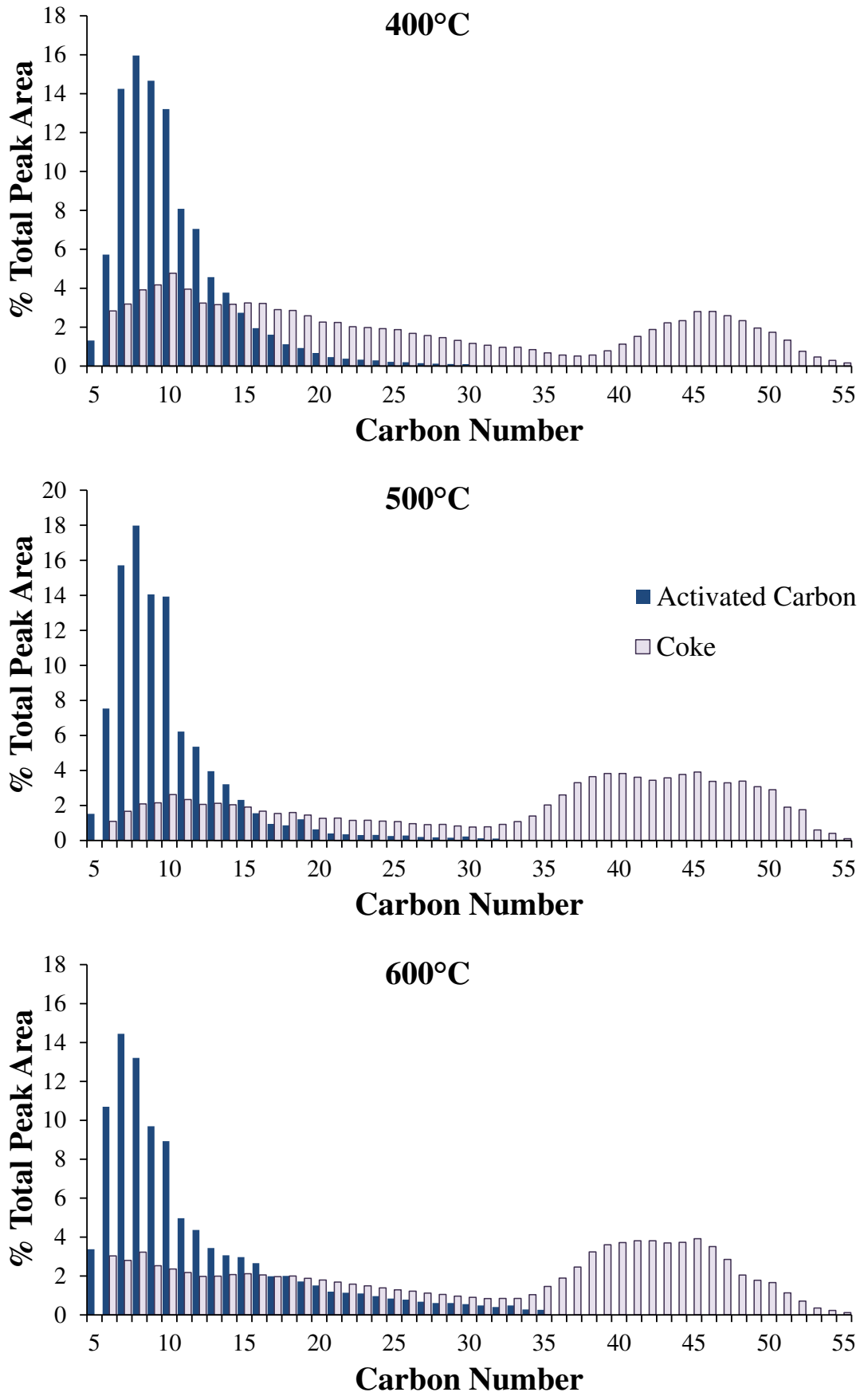


**Figure 4.3:** Distribution of compounds in condensed pyrolysis oil by number of carbons in molecule from batch pyrolysis of HDPE. Figures for 450°C and 550°C have been omitted to conserve space, but show no significant deviations from interpolating between those figures shown. Summary statistics for all temperatures are presented in table 4.3.

**Table 4.3:** Comparison of the condensed pyrolysis products produced with activated carbon and coke reactor beds. Both carbon number (CN) and molecular weight (MW, g $mol^{-1}$) are compared, and the mean, standard deviation (SD) and maximum for the analysed samples are given. The proportion of condensed products that fall into the liquid transport fuel range (C≤21 — a carbon number of 21 or less) as a proportion of total peak area is also given. Mean and standard deviation were calculated using weightings based on peak area percentages.

| | Activated Carbon | | | | | Coke | | | | |
|---|---|---|---|---|---|---|---|---|---|---|
| | 400°C[a] | 450°C | 500°C | 550°C | 600°C | 400°C[a] | 450°C | 500°C | 550°C | 600°C |
| $\overline{CN}$ | 10.3 | 10.5 | 10.0 | 10.6 | 11.5 | 25.0 | 33.0 | 32.7 | 32.2 | 29.9 |
| $\overline{MW}$ | 142.0 | 143.5 | 137.5 | 145.3 | 159.0 | 351.1 | 462.4 | 456.2 | 450.9 | 418.4 |
| CN SD | 3.7 | 3.8 | 4.0 | 5.2 | 6.3 | 14.6 | 13.5 | 14.2 | 14.5 | 14.5 |
| MW SD | 52.9 | 52.5 | 56.9 | 74.2 | 89.2 | 204.7 | 189.7 | 198.4 | 203.8 | 203.4 |
| CN Max | 30 | 30 | 32 | 32 | 35 | 55 | 53 | 55 | 55 | 55 |
| MW Max | 422.5 | 422.5 | 450.5 | 450.5 | 492.6 | 772.9 | 742.8 | 772.9 | 772.9 | 772.9 |
| C≤21 | 98.1% | 98.3% | 97.5% | 94.0% | 90.8% | 51.7% | 25.5% | 28.9% | 30.8% | 35.7% |

[a]400°C was the lower threshold at which pyrolysis occurred; the resulting prolonged reactor residence time increased cracking, though operating batch apparatus at this temperature would not be practical or efficient in reality, and these figures should be read in this context.

the hydrocarbons produced with an activated carbon bed lie within a much smaller range ($C_5$ to $C_{35}$ vs. $C_5$ to $C_{55}$, also reflected by the lower standard deviations). These characteristics — lighter products over a smaller range of sizes — account for the visual differences observed in the products described earlier.

#### 4.5.3.1 Operation at the Temperature Threshold for Pyrolysis

The oil produced at 400°C using a coke reactor is significantly lighter than that produced at other temperatures. Operating at 400°C using either bed resulted in the pyrolysis process occurring extremely slowly — at or near the threshold of it occurring at all, and the process was still not complete even an hour after the HDPE sample was added. The same lower threshold has been observed by other researchers pyrolysing HDPE [186, 202], and is consistent with thermogravimetric analyses, which show that the thermal degradation begins at, or just below this temperature [203]. In the coke bed case, the low reactor temperature dramatically increased the time the input sample spent in the reactor; the pyrolysed compounds were heated to a lower temperature, thus requiring them to be cracked to a greater extent before they entered the gaseous state and could leave the reactor — accounting for the lighter oil produced at this temperature. In the activated carbon case, this effect is small in comparison with the extra cracking from the catalytic effect. In practice, the dramatically longer reaction time would make operating at this temperature with the batch addition of sample infeasible.

#### 4.5.3.2 Influence of Reactor Temperature on Cracking Rate and Residence Time

In most pyrolysis work, reaction temperature has consistently been found to be the operating parameter that has had the greatest impact on the make-up of the pyrolysis products [46, 204, 205]. Increasing the reactor temperature has two primary, yet opposing effects: it increases the reaction rate of the thermal cracking process, so more pyrolysis occurs in the same period of time; but it can also decrease the residence time of the process, decreasing the amount of cracking that occurs.

The input sample undergoes pyrolysis only when it has sufficient energy by being above the threshold temperature at which thermal breakdown occurs — in microwave-assisted pyrolysis this effectively means that the sample must be in the “hot zone” of the reactor bed, where it is conducting heat energy from the carbon.

Sample *leaves* the reactor bed only when it has been cracked sufficiently that it enters the gaseous state and physically egresses to the condensing system. A higher bed temperature means that sample will enter the gaseous state sooner, and may thus leave the reactor bed with less cracking. This reduced residence time has been shown to be a large determinant of pyrolysis product composition [46, 206]. Furthermore, at higher temperatures, the increased rate at which cracking occurs means there is greater positive pressure generated as solid sample enters the gaseous state and expands, which provides a second impetus for sample to leave the hot zone of the reactor bed.

In microwave-assisted pyrolysis the targeted bulk heating of the carbon bed exaggerates the contrast in temperatures between the reactor hot zone (it being the only microwave receptive material in the reactor) and anything present outside this area. Overall, then, it is the balance of cracking rate and residence time that determines the composition of the products for a particular temperature. This can vary depending on reactor configuration: almost all researchers report that the increased cracking effect dominates, and the average molecular mass decreases with increasing reactor temperature [173, 204, 205, 207]; however, in the only comparable microwave-assisted pyrolysis work, Ludlow-Palafox observed an increase in molecular mass of the pyrolysis condensate when reactor temperature was increased from 500°C to 600°C, which he attributed to a decrease in sample residence time [29].

#### 4.5.3.3 Influence of Reactor Temperature on Molecular Mass Distribution of Products

While it is clear that in this work the use of a catalytic reactor bed resulted in changes to the pyrolysis products that far outweighed any temperature-induced variation, there are, nevertheless, temperature-dependent trends within each bed type. At increased reactor temperatures, shorter residence time and greater rate of cracking act in concert to increase the range of molecular weights in the products (an increase in smaller products from the greater cracking, and an increase in larger products from the higher temperature causing molecules to enter the gaseous state and exit the reactor sooner). This is observed in both the activated carbon and coke cases, with the range of molecular masses increasing most at 550–600°C.

Generally, the similarity of the profiles of the compounds produced using an activated carbon bed across the temperatures studied is remarkable, though the tail of the distribution begins to lengthen and encompass longer molecules at temperatures over 550°C, with a corresponding increase in average molecular mass and standard deviation. For condensed products produced using a coke bed, a similar distribution of products is observed between 450–550°C, with the average molecular mass decreasing beyond this point as reactor temperature increases. While this increase in cracking dominates in the coke bed case, consistent with the research described in §4.5.3.2, the average molecular mass increases at higher temperatures in the activated carbon case. Because of the catalytic activity of the activated carbon, the cracking rate is already high even at lower tempatures; the increase in range of molecular masses facilitated by operating at a higher reactor temperature (i.e., from causing larger molecules to enter the gaseous state and leave the reactor, and from reduced residence time due to faster phase change volume expansion of the cracked HDPE) must then cause the overall average to increase.

#### 4.5.3.4 Bimodal Molecular Mass Distribution with Coke Reactor Bed

The bimodal distribution of molecular masses in the condensed pyrolysis products produced using a coke bed suggests the possibility that more than one mechanism may have resulted in the presence of the heavier modal grouping in the condensate. Furthermore, this grouping contains within it at least some hydrocarbons with a boiling point greater than the reactor temperature, and must have therefore arisen through a different means than vaporizing in the reactor and re-condensing in the condensing

system. One possible mechanism accounting for the presence of these compounds is that they are concurrently physically transferred by the continuous flow of gases exiting the reactor. This may be through physical transfer processes such as chain entanglement, surface tension where gaseous and longer liquid molecules are held together (analogous to the fluid present around a soap bubble), or convection; or alternatively via chemical recombination, with chains re-polymerising, as suggested by Williams and Williams [173], who also observed a significant fraction of condensed product that exhibited a boiling point higher than the reactor temperature would have reached.

That this mechanism does not apparently occur in the activated carbon case could be due to the smaller molecules produced that do not entangle, the formation of a large portion of more chemically stable aromatic species, which would not re-polymerise, or simply the greater bed surface area, leading to greater (simultaneous) cracking of the HDPE so that the resulting pyrolysis products all fall below the molecular mass where secondary physical transport becomes an issue. In any case, with or without the additional heavy molecular grouping it is clear that the condensate produced using an activated carbon bed is considerably lighter and has undergone substantially more cracking.

#### 4.5.3.5 Production of Liquid Transport Fuels

The fraction of condensed products that fall within the range of the liquid transport fuels ($C_5$–$C_{21}$) particularly emphasises the increased cracking that the input HDPE undergoes when the activated carbon bed is used. Indeed, as table 4.3 shows, >98% of the oil produced using an activated carbon bed at temperatures of 450°C and lower falls within this liquid transport fuel range. With the standard coke bed, an increase in these useful $C \leq 21$ products is observed as increased reaction temperature (and thus energy expenditure) promotes increased cracking (the 400°C scenario being a special case discussed in 4.5.3.1); nevertheless, as reaction temperature increases with an activated carbon bed, the proportion of condensed product that lies within the valuable liquid transport fuel range actually decreases, as hydrocarbons are produced across a wider range of masses. In other words, activated carbon produces a narrower and more useful range of products as reactor temperature is reduced (with a lower bound of sufficient thermal energy being input for the pyrolysis process to occur in a reasonable amount of time).

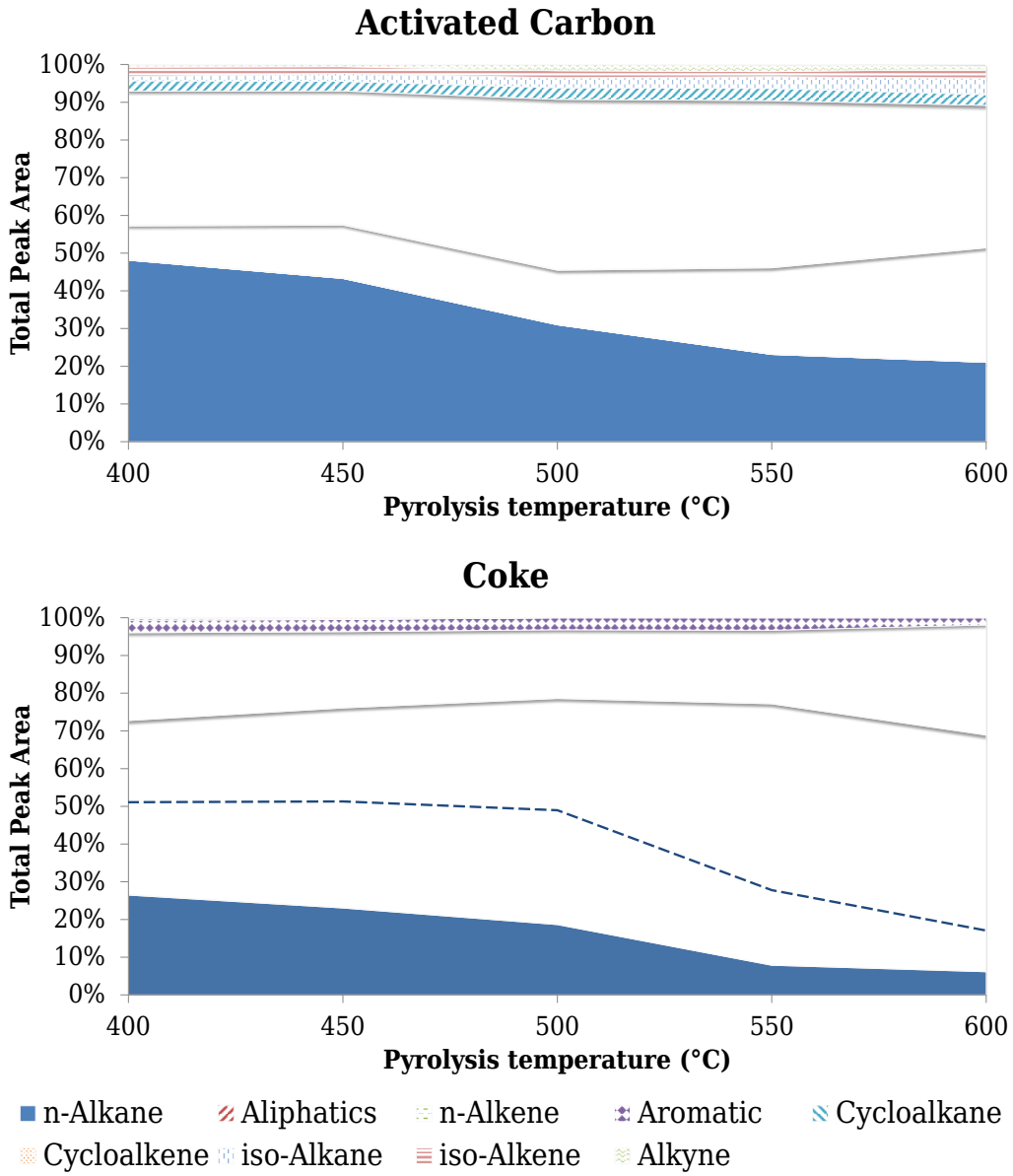


**Figure 4.4:** Chemical composition of condensed pyrolysis products produced using activated carbon (top) and coke (bottom) reactor beds with batch introduction of sample. Here, "alkenes" encompass species containing one or more double bonds. "Aliphatics" includes linear alkanes and alkenes which were unable to be distinguished from one another in the GC/MS analysis owing to their large molecular mass (>$C_{23}$), though dashed line represents best estimate of the division of this grouping between n-alkanes and n-alkenes based on identified species.

### 4.5.4 Chemical Composition of Condensed Pyrolysis Products

Figure 4.4 compares the composition of the condensed products from the microwave-assisted pyrolysis of HDPE using activated carbon and coke beds. As the hydrocarbon chain length gets longer, it becomes more difficult to distinguish between different types of aliphatic species with the same carbon number, because the distinguishing moiety of the molecule (e.g., two carbons connected by a double bond) becomes an increasingly small proportion of the whole (and correspondingly the similarity

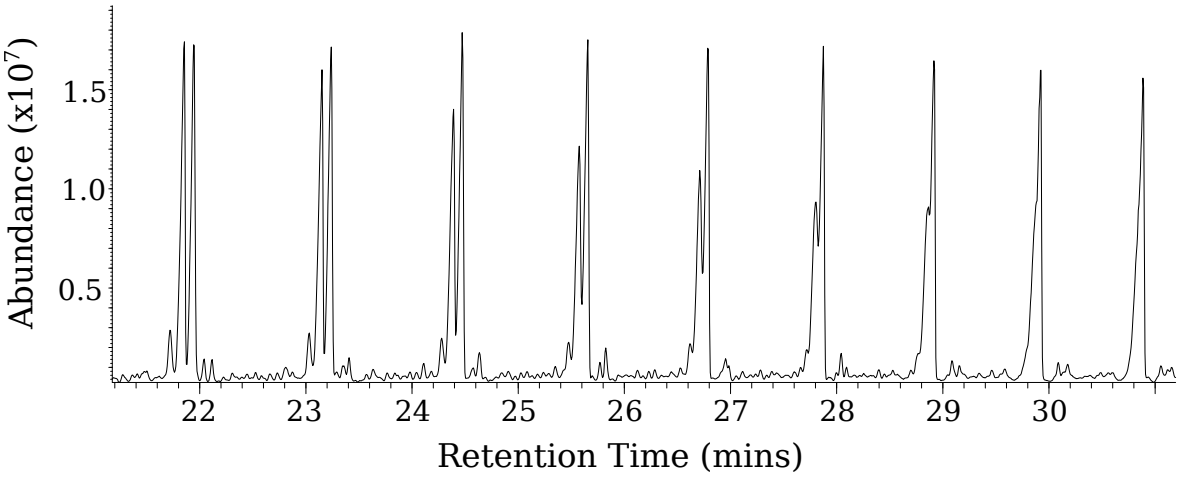


**Figure 4.5:** Merging of aliphatic gas chromatograph peaks at larger molecular masses. While the alkadiene, alkene, and alkane peaks are clearly separate at a retention time of 22 minutes, they slowly merge and become indistinguishable by the 29–30 minute mark.

between molecules grows, with increased chain length coming in the form of identical alkyl groups). As shown in figure 4.5, the gas chromatography column becomes progressively less able to separate these species (as their chemical properties and retention times converge), until around $C_{23}$ the peaks merge completely. These species, comprising linear alkanes and alkenes, have been grouped together in this analysis as "aliphatics".

With a standard coke bed the condensed oil is comprised of straight chain alkanes and alkenes, with around 3% or less of the total comprising aromatic species. This agrees with the observed consensus in the literature that linear aliphatic hydrocarbons comprise the bulk of the condensed products resulting from the pyrolysis of HDPE (in an inert medium), regardless of reactor type.

In FTIR analysis of the condensate produced from the conventional pyrolysis of polyethylene using a fluidised bed reactor, Williams and Williams [173] noted the significant formation of aromatic species only at 700°C (these temperatures were beyond the operating maximum for the rig used in this work).

Also using a fluidised bed, Hernández et al. [208] did not see any aromatic species in the condensed pyrolysis products at all, with linear aliphatics comprising the entire oil; a large increase in the alkene to alkane ratio of the pyrolysis condensate from 500°C to 600°C was also observed, consistent with this work, where although the proportion of alkanes to alkenes is approximately even from 400°C to 500°C, above this temperature the proportion of alkenes increases.

In the only directly comparable microwave-assisted pyrolysis experimental work, Ludlow-Palafox and Chase [29] observed similar trends to this work using a coke bed,

with the alkene:alkane ratio increasing with increasing reactor temperature; however, the overall proportion of species other than linear aliphatics was higher in their work, varying from 18.9–7.2% peak area from 500–700°C. The exact make-up of this fraction is not given, though some of this no doubt comprises branched and cyclic aliphatics. Nevertheless, the results of this work using a coke bed fall well within Ludlow-Palafox's "general statement that the pyrolysis of HDPE yields little aromatics (<5%)" [46].

Each pyrolytic scission of the polyethylene backbone creates two highly reactive radicals that stabilise themselves predominantly through intermolecular or intra-molecular hydrogen transfer, creating alkanes and alkenes respectively (for a full discussion of the molecular mechanisms underlying the pyrolytic breakdown of HDPE see §6.2). Based on McCaffrey et al. [209], who showed that intermolecular hydrogen abstraction is blocked by an increase in hydrogen abundance, Ludlow-Palafox theorised that the observed increase in proportion of alkenes with increased reaction temperature was due to an increase in hydrogen content (though not necessarily in the form of molecular hydrogen gas) in the pyrolysis gas [46], possibly resulting from an increase in repolymerisation reactions at higher temperatures [206, 210]. While this link remained unproven in that research owing to inadequate GC column resolving ability at the low molecular masses these hydrocarbon gases exhibit, further evidence in partial support of this theory is presented in §4.6.2.

The catalytic activity of the activated carbon bed is clearly evident in the pyrolysis oil produced from it. While simple straight chain alkanes and alkenes still make up a significant fraction of the oil, there is a dramatic increase in proportion of aromatic compounds (35.5–45.3%), and the presence of other types of hydrocarbons is observed (cyclo- and branched alkanes and alkenes, as well as alkynes), increasing to 10% peak area of the oil at 600°C. These figures are in excess of any non-catalytic derived results reported in the literature at equivalent temperatures.

The increase in alkenes at the expense of alkanes as reaction temperature increases is also observed using an activated carbon bed, likely as a result of the reasons outlined above, and it is exactly this reducing environment coupled with a dearth of hydrogen as the HDPE is progressively cracked that promotes the formation of the more "complex" hydrocarbons previously mentioned.

The variety of compounds produced by the activated carbon bed relative to the coke bed is also notable: more than 150 different compounds are present in the activated carbon derived oil compared with typically around 100 for coke-bed derived oil, and these compounds occur over a smaller range of carbon lengths. Much of this

extra variety derives from the greater quantity of aromatic compounds present in the activated carbon derived oil, though many of these are present only in very small quantities (the three main aromatic species are toluene, ethylbenzene, and xylene, with peak areas of 4.8–8.8%, 3.6–5.4%, and 1.6–5.3% respectively; the peak area percentages decline rapidly after this point). Indeed, in general the pyrolysis products exhibit a "long tail" distribution, with many different compounds present in small quantities as a result of the stochastic decomposition process. The aromatic compounds are primarily single ring benzene derivatives, made up of varying and/or multiple alkyl groups bonded to a central benzene ring; the presence of these compounds in such quantities points to activated carbon catalysing the formation of these aromatic rings.

## 4.6 Analysis of Non-condensable Pyrolysis Gases

### 4.6.1 Mass Distribution of Non-condensable Pyrolysis Gases

The bulk of the non-condensable pyrolysis gases (table 4.4) are two or three carbons in length, independent of the type of reactor bed used. As the reactor temperature increases, more cracking occurs and smaller gases are produced; this is the case when using both activated carbon and coke beds, though the activated carbon pyrolysis gases are overall very slightly heavier, with longer chains, than the coke ones at the same reactor temperature. In spite of this, methane (the only $C_1$ compound) is not produced in large quantities at any temperature, and hydrogen gas is not produced at all (no ions of the appropriate mass were found in scans of the chromatogram). As the hydrocarbon with the highest hydrogen to carbon ratio, the formation of methane is selected against

**Table 4.4:** Comparison of the non-condensable pyrolysis products produced with activated carbon and coke reactor beds by carbon number and peak area percentage. Average carbon number (CN) and molecular weight (MW, g $mol^{-1}$) are calculated using the weightings derived from peak area.

| | Activated Carbon | | | | | Coke | | | | |
|---|---|---|---|---|---|---|---|---|---|---|
| | 400°C[a] | 450°C | 500°C | 550°C | 600°C | 400°C[a] | 450°C | 500°C | 550°C | 600°C |
| $C_1$ | 2.8 | 2.9 | 3.1 | 5.3 | 6.8 | 4.6 | 3.6 | 4.2 | 4.5 | 5.8 |
| $C_2$ | 28.8 | 27.2 | 30.9 | 37.6 | 40.5 | 46.1 | 39.9 | 42.9 | 45.6 | 54.0 |
| $C_3$ | 55.2 | 59.0 | 55.9 | 49.6 | 49.0 | 45.1 | 49.6 | 44.1 | 36.4 | 31.5 |
| $C_4$ | 13.3 | 9.4 | 9.2 | 4.8 | 3.8 | 4.3 | 6.9 | 8.8 | 13.5 | 8.6 |
| $C_5$ | 0.0 | 1.6 | 1.0 | 2.7 | 0.0 | 0.0 | 0.0 | 0.0 | 0.0 | 0.0 |
| $\overline{CN}$ | 2.8 | 2.8 | 2.7 | 2.6 | 2.5 | 2.5 | 2.6 | 2.6 | 2.5 | 2.4 |
| $\overline{MW}$ | 40.8 | 40.6 | 39.8 | 38.0 | 36.2 | 35.7 | 37.3 | 38.0 | 36.7 | 34.5 |

[a]400°C was the lower threshold at which pyrolysis occurred; the resulting prolonged reactor residence time increased cracking, though operating batch apparatus at this temperature would not be practical or efficient in reality, and these figures should be read in this context.

in the hydrogen-deficient environment of the reactor. Molecular hydrogen is not present, owing to the highly reducing carbon bed, and the fact that hydrogen radicals would quickly bond to the myriad of newly cracked hydrocarbon radicals present (C=C bond formation is more energetically difficult than C-H). This finding is consistent with other researchers who produced little to no molecular hydrogen when pyrolysing polyolefins at the temperatures considered in this study [11, 29, 202, 207], though Cozzani et al. [206] observed a significant quantity of hydrogen in the gas resulting from the pyrolysis of polyethylene in a fixed bed (20–30% gas vol. at 500°C and 600°C). This particular experimental configuration had a very low residence time caused by the constant high flow of nitrogen gas directly through the (horizontal) reactor; this separated out pyrolysis products immediately as they were produced, preventing the recombination of hydrogen-rich species into an overall more stable configuration, and resulting in a comparatively high char formation (2–10% wt.) from the remaining hydrogen-deprived species.

Ludlow-Palafox [46] analysed the non-condensable gases produced from pyrolysis of HDPE at temperatures of 500°C and 600°C, but was unable to extend the analysis below $C_3$ owing to insufficient column resolving power. Small quantities of compounds up to $C_7$ were also present in their samples, with the proportion of gases declining as the carbon number increased, as seen in the present work. The narrower range of compounds present in this work is likely due to the superior efficiency of the condensing system.

The pyrolysis gases generated at 600°C using a coke bed were very similar to those reported in Donaj et al. [207] when pyrolysing a mixture of polyolefins (76% PE, 24% PP) at 650°C with $C_2$ and $C_3$ molecules making up the bulk of the gases. The higher proportion of methane generated in this case is attributable to the presence of the polypropylene, with its methyl group side chain.

### 4.6.2 Chemical Composition of Non-condensable Pyrolysis Gases

The non-condensable pyrolysis gases are composed entirely of alkanes and alkenes (table 4.5 on the next page). By virtue of their small molecular size the compounds are simple — almost all linear, with trace quantities of branched molecules. As reactor temperature increases a greater proportion of alkenes are produced, with a corresponding decrease in alkanes, analogous to the change observed in the condensed pyrolysis products. Given the same absolute number of hydrogen atoms, the increased cracking at higher temperatures seen in the analysis of molecular masses necessitates

**Table 4.5:** Percentage chemical composition of the non-condensable pyrolysis gases produced with activated carbon and coke reactor beds, with batch introduction of HDPE. Figures given are peak area percentages. H/C is the overall proportion of hydrogen to carbon calculated for each gas based on the proportional peak area of each compound.

| | Activated Carbon | | | | | Coke | | | | |
|---|---|---|---|---|---|---|---|---|---|---|
| | 400°C[a] | 450°C | 500°C | 550°C | 600°C | 400°C[a] | 450°C | 500°C | 550°C | 600°C |
| n-Alkane | 85.0 | 69.7 | 67.8 | 62.7 | 56.9 | 40.7 | 41.5 | 38.8 | 33.5 | 27.8 |
| n-Alkene | 15.0 | 26.3 | 28.4 | 32.8 | 39.6 | 57.9 | 51.6 | 55.5 | 62.4 | 66.9 |
| iso-Alkane | 0.0 | 2.4 | 2.9 | 1.8 | 1.6 | 1.4 | 2.6 | 3.2 | 1.6 | 1.2 |
| iso-Alkene | 0.0 | 1.6 | 1.0 | 2.6 | 1.9 | 0.0 | 4.3 | 2.5 | 2.5 | 4.0 |
| H/C | 2.68 | 2.57 | 2.57 | 2.58 | 2.56 | 2.41 | 2.37 | 2.31 | 2.28 | 2.28 |

[a]400°C was the lower threshold at which pyrolysis occurred; the resulting prolonged reactor residence time increased cracking, though operating batch apparatus at this temperature would not be practical or efficient in reality, and these figures should be read in this context.

the formation of individually less hydrogen-dense molecules (i.e., alkenes instead of alkanes).

The marked increase in alkanes over alkenes in the non-condensable gases produced using an activated carbon bed is due to the greater proportion of “complex” unsaturated molecules formed in the corresponding condensate, with the resulting hydrogen-containing radicals forming fully saturated gases. The higher H/C proportion of the activated carbon gases compared with the coke gases supports this, with the only other hydrocarbon pyrolysis product (the condensate) therefore having a correspondingly lower H/C proportion, resulting from the greater proportion of these more complex molecules with a lower H/C proportion (aromatics, cycloalkanes, cycloalkenes, alkynes) described in §4.5.4.

Interestingly, the H/C proportion remains approximately constant across reactor temperatures for gases produced using an activated carbon bed (the 400°C case excepted), in spite of the increase in proportion of alkenes. This can be explained by the greater overall proportion of alkenes at higher temperatures being balanced by the greater cracking occurring, which results in smaller molecules, with higher individual hydrogen content.

In contrast, the H/C proportion of the non-condensable gases produced with a coke bed reduces somewhat with increasing temperature, as there is both less change in molecule size and a greater proportional increase in alkenes. This observation is initially apparently in opposition to the earlier discussed relationship Ludlow-Palafox proposed regarding an increase in hydrogen abundance in the pyrolysis gases causing a blocking of intermolecular hydrogen abstraction, and the observed decrease in alkanes and increase in alkenes in the condensate at higher temperatures — certainly, the proportion of hydrogen in the gases produced using a coke bed falls. However, while

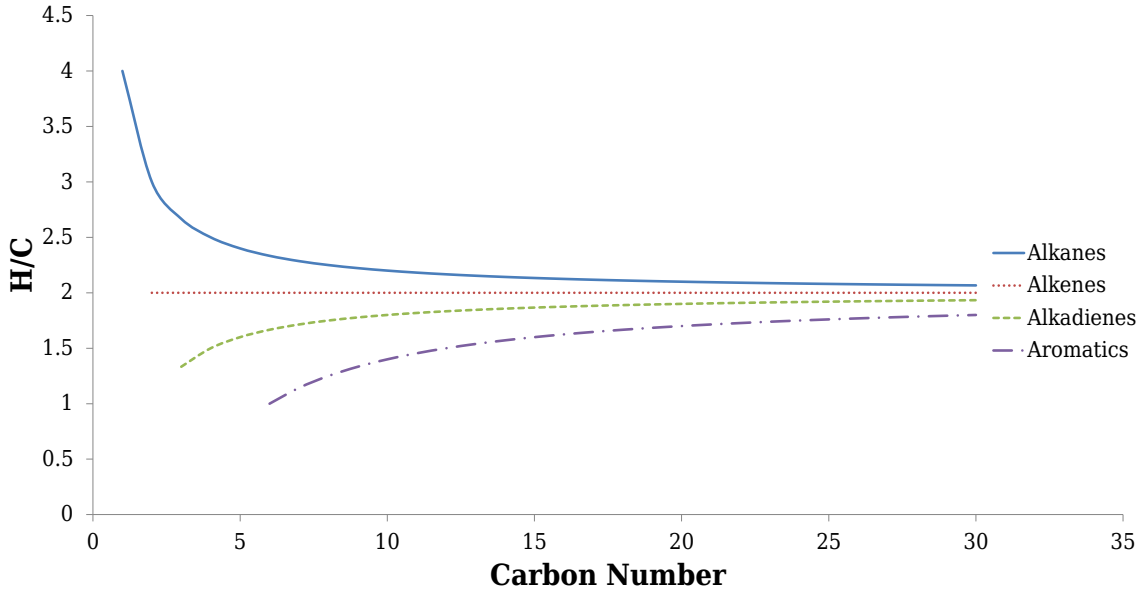


**Figure 4.6:** Hydrogen to carbon proportion of unbranched hydrocarbons by carbon number. The aromatics in this case are the most common class observed in the condensate: benzene derivatives with alkyl groups that increase in length with carbon number.

the relative amount of hydrogen per unit mass is smaller, the absolute amount of hydrogen-rich gas is in fact much greater, owing to a higher overall amount of non-condensable gas being produced, as shown in §4.8. Furthermore, it is difficult to establish a causative relationship in this case, as an increase in the formation of alkadienes would equally result in an increase in hydrogen-rich radicals and ultimately gases.

## 4.7 Conservation of Mass and Hydrogen Transfer

The principle of conservation of mass requires there to be the same total number of carbon and hydrogen atoms in the unprocessed HDPE as in all the pyrolysis products. The stoichiometry of polyethylene is such that H/C = 2 in the input product. As figure 4.6 shows, a pyrolytic decomposition of HDPE into pure alkenes would not change the H/C balance (and would approach a return to the ethene monomers from which HDPE is produced as cracking continued). Alkanes are more hydrogen-rich than polyethylene, and alkadienes less, and this imbalance is amplified as the molecules become shorter and the functional group comprises a larger relative proportion of the molecule as a whole. Nevertheless, for every hydrogen-rich molecule that is produced, an equally hydrogen-deficient one must also be, in order that the overall number of atoms is conserved. Indeed, if, for every alkane produced an equivalent alkadiene (of the

same carbon number) were also produced the H/C balance would remain satisfied. Given that these three classes of hydrocarbon are the simplest breakdown products of HDPE (reaction pathways discussed in §6.2) it is no surprise that they are also the most common species produced when pyrolysing HDPE through conventional means, as demonstrated in §4.5.4.

This conservation of mass, and hydrogen transfer, underlies all of the final pyrolysis product compositions, and the mechanisms by which they are produced. Indeed, the whole system exists in a dynamic equilibrium where thermal scission, inter- and intra-molecular hydrogen abstraction, and further secondary reactions interplay to create the complex array of species observed in the final pyrolysis products.

By comparing the products produced with an activated carbon bed with those produced using a coke bed, it is clear that the activated carbon promotes secondary reactions and the creation of aromatics and other complex products. As the aromatics are hydrogen poor (relative to polyethylene), their formation “frees up” hydrogen and allows the formation of a greater portion of alkanes in the gaseous state, as previously observed, implying that a dearth of hydrogen is a limiting factor influencing the chemical make-up of the gaseous fraction (especially in the coke bed case). This is further emphasised when it is considered that only alkanes can exist below $C_2$; alkadienes cannot physically form below $C_3$, nor aromatics below $C_6$, thus as products are cracked into progressively smaller molecular sizes they are forced to assume more hydrogen-rich conformations, resulting in the high H/C make-up of the non-condensable gases previously described.

## 4.8 Pyrolysis Product Component Yields

Table 4.6 shows the component product yields from the microwave-assisted pyrolysis of HDPE. Consistent with other work in the microwave pyrolysis field [29, 149], reactor temperature is the parameter that has the largest single effect on the constituent make-up of the pyrolysis products. As reaction temperature increases, more cracking occurs: more gaseous products result, with a corresponding decrease in condensed products. Given that the gaseous products have a high H/C ratio, as discussed, the greater cracking and increased proportion of gases at higher reaction temperatures impacts the make-up of the condensate, necessitating the formation of a greater portion of lower H/C species, which explains the presence of these species in higher proportions observed in §4.5.4.

**Table 4.6:** Percentage yields of retained, condensed, and non-condensable pyrolysis products with batch introduction of sample. *Retained* refers to the portion of input mass left in the reactor at the conclusion of the experiment, *condensed* product is the oil/wax collected in the condenser, *condensed C≤21* is the subset of the condensed products with a carbon number less than or equal to 21, non-condensable (gaseous) product accounts for the remaining mass (and is calculated as such). All percentages are expressed on a mass basis as a proportion of the input HDPE, using peak area as a determinant of the proportion of products that lie at or below $C_{21}$.

| | Activated Carbon | | | | | Coke | | | | |
|---|---|---|---|---|---|---|---|---|---|---|
| | 400°C[a] | 450°C | 500°C | 550°C | 600°C | 400°C[a] | 450°C | 500°C | 550°C | 600°C |
| Retained | 10.3 | 9.0 | 6.0 | 7.3 | 11.3 | 2.0 | 1.0 | 0.0 | 0.0 | 0.0 |
| Condensed | 54.9 | 50.3 | 41.0 | 30.7 | 27.3 | 59.1 | 69.0 | 42.0 | 42.3 | 31.4 |
| Cond. C≤21 | 53.8 | 49.5 | 40.0 | 28.8 | 24.8 | 30.6 | 17.6 | 12.1 | 13.0 | 11.2 |
| Gases | 34.8 | 40.7 | 53.0 | 62.0 | 61.3 | 38.9 | 30.0 | 58.0 | 57.7 | 68.6 |
| Overall C≤21 | 88.6 | 90.2 | 93.0 | 90.8 | 86.1 | 69.5 | 47.6 | 70.1 | 70.7 | 79.8 |

[a]400°C was the lower threshold at which pyrolysis occurred; the resulting prolonged reactor residence time increased cracking, though operating batch apparatus at this temperature would not be practical or efficient in reality, and these figures should be read in this context.

In spite of the higher percentage of condensible products produced with a coke bed (reaching a maximum of 69.0% of input mass at 450°C), much of these are less useful long-chain waxes (as shown in §4.5.3); when only products in the liquid transport fuel range (C≤21) are considered, using the activated carbon bed results in significantly higher yields at all temperatures. This is also the case if the same criterion is applied to all products (both gases and condensibles), with the bulk of the "useful" products comprising gases produced at high temperatures when using a coke bed, in any case. In other words, more useful products are produced using an activated carbon reactor bed than with a coke one, and this is possible at lower temperatures.

At low temperatures using a coke bed the retained fraction represents un-pyrolysed HDPE. The significant increase in the retained fraction when using an activated carbon bed required further investigation (see §6.6), though it may be that the activated carbon catalyses not only hydrocarbon cracking but also the formation of char, which remains within the reactor.

### 4.8.1 Comparison with Other Published Work

Table 4.7 on the following page presents a comparison of the yields of the products resulting from the pyrolysis of polyethylene, in batch operation, between this work and all other identified comparable peer-reviewed publications. There is considerable variation in the results reported across the literature, a fact that emphasises the importance of the reactor type and specific configuration, both of which themselves vary considerably across the published work. This reinforces the need to perform control experiments in this work using the same reactor but with a coke bed, in order to

**Table 4.7:** Comparison of PE pyrolysis yields in batch operation from 400–600°C. Percentage yields of non-condensable gases, condensed product, and mass retained in the reactor at the conclusion of the experiment, are all reported on a mass basis as a proportion of the input sample. N.R. = not reported; FBR = fluidised bed reactor; CSBR = conical spouted bed reactor; TGA = thermogravimetric analysis.

| Reference | Reactor Type | Reactor Volume | Sample Volume | Heating Method | Bed Type | Temperature | Retained | Condensed | Gases |
|---|---|---|---|---|---|---|---|---|---|
| This Work | Stirred Bed | 12 L | 100 g | Microwave | Activated Carbon | 400°C | 10.3 | 54.9 | 34.8 |
| | | | | | | 450°C | 9.0 | 50.3 | 40.7 |
| | | | | | | 500°C | 6.0 | 41.0 | 53.0 |
| | | | | | | 550°C | 7.3 | 30.7 | 62.0 |
| | | | | | | 600°C | 11.3 | 27.3 | 61.3 |
| This Work | Stirred Bed | 12 L | 100 g | Microwave | Coke | 400°C | 2.0 | 59.1 | 38.9 |
| | | | | | | 450°C | 1.0 | 69.0 | 30.0 |
| | | | | | | 500°C | 0.0 | 42.0 | 58.0 |
| | | | | | | 550°C | 0.0 | 42.3 | 57.7 |
| | | | | | | 600°C | 0.0 | 31.4 | 68.6 |
| Achilias et al. [211] | Fixed Bed | N.R. | 1 g | Electric | None | 450°C | 61.0 | 38.5 | 0.5 |
| Al-Salem and Lettieri [212] | TGA | N.R. | 15 mg | Electric | None | 500°C | 0.1 | 79.7 | 20.2 |
| | | | | | | 550°C | 0.2 | 67.0 | 32.8 |
| | | | | | | 600°C | 0.2 | 56.0 | 43.7 |
| Cozzani et al. [206] | Fixed Bed | 1.2 L | 15–20 g | Electric | None | 500°C | ~2–5 | ~83–90 | ~8–12 |
| | | | | | | 600°C | ~6–10 | ~55–74 | ~20–35 |
| Elordi et al. [205] | CSBR | 3 L | N.R. | Electric | Sand | 600°C | N.R. | ~94 | ~6 |
| Hernández et al. [208] | FBR | 1.9 L | 2 g | Electric | Sand | 500°C | 36.5 | 48.3 | 15.2 |
| | | | | | | 600°C | 24.6 | 43.0 | 32.4 |
| Kumar and Singh [186] | Semi-batch | 156 mL | 20 g | Electric | None | 400°C | 4.6 | 11.2 | 84.2 |
| | | | | | | 450°C | 3.8 | 24.0 | 72.2 |
| | | | | | | 500°C | 3.0 | 72.2 | 24.8 |
| | | | | | | 550°C | 2.5 | 79.1 | 18.4 |
| Ludlow-Palafox and Chase [29] | Stirred Bed | 4 L | 50 g | Microwave | Coke | 500°C | 0.0 | 81.0 | 19.0 |
| | | | | | | 600°C | 0.0 | 79.1 | 20.9 |
| Marcilla et al. [213] | Crucible | N.R. | 600 mg | Electric | None | 550°C | 0.0 | 84.7 | 16.3 |
| Williams and Williams [173] | FBR | 5.5 L | 3 g | Electric | Silica Sand | 500°C | 0.0 | 89.2 | 10.8 |
| | | | | | | 550°C | 0.0 | 78.6 | 21.4 |
| | | | | | | 600°C | 0.0 | 75.8 | 24.2 |

derive useful comparative results. Very few results were reported below 500°C, likely due to the longer reaction time when operating below this temperature.

#### 4.8.1.1 Temperature Dependent Gas Production and Influence of Reactor Configuration

Several trends are evident across the results considered, such as the increase in the proportion of non-condensable gases produced as reactor temperature and cracking correspondingly increase. The one exception to this trend is the work presented by Kumar and Singh [186], the examination of which serves a useful purpose in demonstrating the importance of reactor configuration. In this study, HDPE was heated in a reaction vessel with a long vertical exit pipe that reached sufficiently high to allow room for the condenser to fit in the space below. In this case it is thought that the length of the pipe, and its lack of heating or insulation, would present a high "barrier to exit" for pyrolysis products leaving the reactor. As such, they would likely continually reflux and crack into progressively smaller products until they were sufficiently small that they could remain in the gaseous state for a sufficient period of time that they could leave the reactor. Most other experimental configurations used the continual flow of an inert gas to ensure an oxygen-free environment, but which also served to convectively force the pyrolysis gases from the reactor. In this case the only impetus for evolved gases to leave the reactor was the volume expansion pressure generated from cracking the HDPE into gaseous molecules, and this had to overcome both gravitational and thermodynamic pressures, potentially increasing the residence time of the reaction as products were unable to escape the reactor. Indeed, in this extreme case, the reactor configuration influenced the residence time to the point that it became the dominant process parameter, evidenced by the extremely long reaction times reported (well over 12 hours at 400°C decreasing to a minimum of 54 minutes at 550°C) — far in excess of those reported by any other researcher. By contrast, the conical spouted bed reactor used by Elordi et al. [205] gave a "residence time of the volatiles in the range of centi-seconds", and resulted in the highest reported recovery of condensed products of 94%.

#### 4.8.1.2 Minimal Retained Portion

Most experiments showed very little mass retained in the reactor at the end of the experiment, with the exceptions to this trend apparently deriving from the experiment not running through to completion for one reason or another. In Achilias et al. [211], where 61% of the input sample was retained in the reactor at the end of the pyrolysis,

the methods mention “the time of the experiment was 17 min”, an apparent externally imposed constraint given that the range of plastics considered in this work would require different times to pyrolyse. Here, the residue fraction is not discussed further.

In the work of Hernández et al. [208], which saw 25–37% of the input sample retained in the bed at the conclusion of the experiment, the entirety of the fluidising and pyrolysis gas “flow [was] shifted to the sampling bag” for collection and later analysis. Given a reported fluidising gas flow of 3.5 L/min, and a 25 L gas sampling bag, this constrains the maximum experimental run time to seven minutes, even if no pyrolysis gas were produced, and this time constraint is likely the source of the high retained portion.

In this work, the pyrolysis was allowed to run through to completion; the minimal retained product remaining in the coke bed case is consistent with other researchers. The higher retained fraction in the activated carbon case is investigated further in §6.6.

#### 4.8.1.3 Relative Gaseous and Condensed Product Yields and the Influence of Reactor Configuration used in This Work

A maximum condensed product yield of around 70–90% was seen across the examined body of research; this most commonly occurred at a reactor temperature of 500°C. In this work, in the comparable coke bed case, a maximum condensed product yield of 69% at 450°C was observed, which is at the lower end of the range reported in the literature. Indeed, generally an increase in the yield of gaseous products was observed in this work for any given temperature; this can be explained when the specific characteristics of the reactor used to undertake this work are taken into account.

The reactor used in this work is the largest reactor in this literature comparison, by volume, by a factor of greater than two. The larger volume reactor creates a greater intervening space between the hot reactor bed and the condenser system — a space in which the pyrolysis products may cool, recondense, and undergo secondary reactions, and a scenario exacerbated by the targeted microwave heating mode used in this work where only the reactor bed is heated. Furthermore, the reactor in this work does not operate in a direct “pass-through” mode whereby the products are directly forced out of the reactor hot zone, unlike many of the compared reactors. Instead, the inert nitrogen gas necessarily enters from the top of the reactor (see figure 3.14), and may pass over the reactor bed when pyrolysis is under way. In this way the pyrolysis products must crack sufficiently to travel up and out of the reactor before condensing. It is

the combination of these factors and the higher barrier to exit that resulted that likely caused the greater cracking and comparably larger portion of non-condensable gaseous products.

In addition, in this work, partially as a consequence of operating a larger reactor, the flow-rate of inert gas in proportion to reactor volume of 0.06 L/min/L, is considerably less than that of others such as Hernández et al. [208] with 1.84 L/min/L, or 0.25 L/min/L in the more directly comparable work of Ludlow-Palafox and Chase [29]. The egress of pyrolysis products is therefore likely to be primarily driven by phase change volume expansion of the products themselves. It should be noted that a full-scale pyrolysis plant is unlikely to use inert carrier gas at all, though it was used in this case for safety purposes, and to create an initial oxygen-free environment before pyrolysis started.

When primary products are forced to egress from the reactor quickly, captured products provide information about the initial chemistry of the pyrolytic breakdown. However, many of the reactor configurations required to achieve this state are only practical on a laboratory scale, and provide little information about the behaviour of larger systems required for scale-up, and the secondary reactions and subsequent products that result. Indeed, these secondary reactions have been shown to be critical when dealing with larger reactors [202, 214], and when optimising for a particular product [215], and are discussed further in §6.2.

#### 4.8.1.4 Comparison to Other Activated Carbon Work

As the only other work using activated carbon to catalytically crack polyethylene, the work of González et al. [197] bears some discussion. In this study, polyethylene supermarket bags were catalytically cracked (with a 1:10 mass ratio of activated carbon:plastic) using a small electric fixed bed furnace through which flowed inert nitrogen gas. The highest yield of total products of 49.2% of input mass (corresponding to 50.8% retained in the reactor) was obtained with activated carbon at 450°C. At this temperature the products comprised all aliphatic species except for around 6% aromatics.

The remarkably large proportion of char retained in the reactor (this is not likely to have been unpyrolysed HDPE as the experiment was run over two hours) is likely because of a combination of the activated carbon and the flow-through design of this reactor, where the nitrogen carrier gas results in a very low residence time for the produced pyrolysis products. This constant flow combined with the small size of the

reactor means that almost as soon as products entered the gaseous state they would leave the hot zone and not undergo further cracking. As such, hydrogen-rich alkanes (formed through activated carbon catalysed hydrogen transfer reactions as described in §6.3.1) are swept out of the reactor, resulting in the greater production of char as the remaining input mass has less hydrogen with which to form cracked pyrolysis species. This is supported by the higher methane content of the evolved gases in this study (22% vs. 2.9%), and the lower aromatic content (6% vs. 30%), as aromatic and non-linear species require a greater formation time in the hot zone than linear aliphatics [178, 179].

The use of microwave heating and a stirred bed as in this dissertation, and the introduction of sample when the reactor was at the target temperature as opposed to heating from room temperature, may have also contributed to a more even heat distribution and less resulting char formation. In any case, the work of González et al., like those studies discussed above, may provide information about pyrolysis breakdown in a specific low-residence configuration, but such configurations are less useful as models for larger industrial processes.

## 4.9 Utility of Products Produced Using an Activated Carbon Bed

### 4.9.1 Condensed Pyrolysis Oil

The condensed pyrolysis oil produced at lower temperatures using activated carbon comprises more than 98% hydrocarbons $C \leq 21$, and suggests that it would be very easy to use this microwave-assisted pyrolysis to produce a high value, saleable product from the pyrolysis oil with a minimum of extra processing. Given the tunability of diesel engines and the breadth of fuels that they can be run on [216–219], it should be possible to run a suitably configured engine on the pyrolysis oil directly. The carbon length profiles suggest that it would be possible to directly separate the pyrolysis oil into petrol and diesel fractions, though the appropriate standards [220, 221] would also have to be met before it could be sold on the open market.

Compared with the condensed product produced using the conventional coke bed, it is clear that the activated carbon bed has, in effect, performed *in situ* upgrading of the pyrolysis oil, resulting in a much lighter and potentially more useful liquid product. Indeed, the heavier aliphatics present in the coke bed derived oil have little value by

themselves and would usually be actively detrimental to any product containing them, though they can be used as a feedstock in crackers to produce other shorter chain products. All of the produced pyrolysis products could be used as fuels in conventional fossil fuel boilers, though this does not maximise the potential chemical value that could be extracted from the plastic.

#### 4.9.1.1 Aromatic Content

The condensed products produced using an activated carbon bed contained a high proportion of aromatic compounds; for example, the four most common aromatics present in the oil were, in order, toluene, ethyl-benzene, xylene, and benzene. While the addition of aromatics to liquid transport fuels increases the octane/cetane rating and reduces knocking, the maximum aromatic content permissible in petrol and diesel has been capped in many countries in recent times for environmental reasons [222]. If the pyrolysis oil were to be used as a liquid transport fuel, it is likely that these components would have to be separated out — by solvents and liquid-liquid extraction, or extractive distillation. Fortunately, these compounds can have an even greater value than aliphatics [223], finding use as solvents, and as precursors for a wide variety of compounds including drugs, lubricants, detergents, plastics (e.g., polystyrene, polycarbonate), and explosives.

### 4.9.2 Gases

The non-condensable gases produced during the microwave-assisted pyrolysis of HDPE are also economically important, the primary constituents being ethane, ethene, propane, and propene (these making up over 85% peak area of the gas). These high-energy gases could be used on-site in a generator, in order to power the microwave heating and make the process energetically self-sustaining. Alternatively, the pyrolysis gases could be split into the relevant fractions and fed into the existing distribution network for LPG, natural gas, and natural gas liquids. Ethene and propene in particular have a multitude of uses, and indeed are the single most used organic chemical feedstocks worldwide [224], with the creation of virgin HDPE and PP amongst their uses.

## 4.10 Summary

This chapter presents the most complete characterisation of the products resulting from the microwave-assisted pyrolysis of HDPE to date, and represents the first characterisation of the microwave-assisted pyrolysis of HDPE using an activated carbon bed. Large differences were observed between the products resulting from the different reactor beds, with the condensed pyrolysis oil produced using an activated carbon bed approximately three times lighter than that produced using a coke bed (with an average carbon number of 10–11.5 vs. 25.0–33.0); furthermore, the activated carbon oil contained hydrocarbons with a much narrower range of molecular masses. The molecular masses of the oil derived from an activated carbon bed matched those of the liquid transport fuels petrol and diesel ($C_5$–$C_{21}$), with over 98% of the condensed product, and 50% of the total input mass converted into these fractions when operating at a reactor temperature of 450°C, a temperature lower than most conventional pyrolysis is performed at. Increasing the reactor temperature above this point increased the cracking and lowered the exit threshold for pyrolysed molecules, resulting in a product containing an increased average and range of molecular masses.

The pyrolysis products produced using a coke bed were almost all linear aliphatic compounds, in agreement with other researchers. Indeed, the condensed fraction contained a high proportion of less useful long-chain waxes. By contrast, using an activated carbon bed resulted in a large increase in “complex” molecules in the condensed products, primarily aromatics (35.5–45.3% peak area of the condensate), which were themselves mostly single ring benzene structures and derivatives (the most common being toluene, ethyl-benzene, xylene, and benzene itself).

The non-condensable gases were mainly two or three carbons long, independent of reactor type, and were comprised of simple linear aliphatics by virtue of their small molecular size. Methane was not present in large amounts owing to the molecule’s high proportion of hydrogen to carbon (hydrogen being a rate-limiting reactant owing to the stoichiometry of HDPE); hydrogen gas itself was not observed. The conservation of mass meant that with an activated carbon bed, the formation of less hydrogen-dense aromatics in the condensate “freed up” hydrogen, and a greater alkane content was observed in the activated carbon derived gases.

Overall, it is clear that microwave-assisted pyrolysis of HDPE with an activated carbon bed produces a narrower range of products that are potentially more valuable and useful, than when a conventional coke bed is used. The larger reactor configuration

used in this work promotes secondary reactions, resulting in a greater proportion of gaseous products, though it is important to understand the influence of these reactions as they are likely to become more important in any process scale-up. Indeed, the results presented in this chapter were sufficiently promising to warrant further investigation into the microwave-assisted pyrolysis of HDPE. Accordingly, as a further step towards scale-up, a more industrial-like operation was developed where the reactor operated in a continuous throughput mode and was able to process much larger volumes of sample; this work is presented in the following chapter.

# 5

# Continuous Pyrolysis of HDPE using an Activated Carbon Reactor Bed

## 5.1 Introduction

Having established in the previous chapter that using activated carbon as a catalytic bed in the microwave-assisted pyrolysis of HDPE was feasible, and having identified the resulting pyrolysis products as possessing sufficient utility and economic value as to make the process worthwhile, it was decided to more fully characterise the pyrolysis process, with the intention of determining whether it would be suitable for scale-up and operation on a larger, industrial scale. In order to achieve this, it was necessary to change the configuration of the pyrolysis equipment so that it could process larger quantities of material, and in a continuous mode with a constant input of HDPE and collection of products, as the capacity, efficiency, and economic demands of a potential commercial industrial facility would necessitate.

Furthermore, while microwave-assisted pyrolysis has been demonstrated in continuous operation when processing input gases [168] and liquids [152], there is a dearth of reports in the literature dealing with the continuous processing of solid material. This is likely due to the still burgeoning nature of the microwave-assisted pyrolysis field, and the inherent difficulties in processing solids in this context — they can quickly become tacky and difficult to handle when heated; an appropriate feeding mechanism must allow solid particles to enter the reactor while remaining impervious to returning pyrolysis gases; to say nothing of the difficulties of designing suitable mechanisms to operate within the confines of a "microwave friendly" space. Nevertheless, this study presented an excellent opportunity to investigate the differences between batch and continuous processing using microwave-assisted pyrolysis, and pioneer the continuous input of solid material.

Another necessary step towards scaling up the activated carbon catalysed pyrolysis process was evaluating and quantifying the repeatability of the process and the products it produced over time, and between independent runs, to determine how consistent these were, and to investigate the performance of the catalyst over time — this, in particular, required the ability to process larger masses of HDPE afforded by the continuous input of sample.

This chapter presents the results and analysis obtained from the continuous processing of HDPE with activated carbon catalysed microwave-assisted pyrolysis, comparing the process and products to those produced using the batch mode operation described in the previous chapter, and relates the associated discovered difficulties resulting from the scale-up of the process to handle larger quantities of input material.

## 5.2 Method

Continuous feed operation required a redesign of the sample injection apparatus, and resulted in the continuous rotary feeder described in §3.4.2. HDPE was added to the reactor at a rate of 11.8 g/min. This speed was selected so that the microwave heating system could easily maintain the reactor temperature throughout the course of the experiment, even when operating at the highest studied temperature, thus avoiding the pitfalls of the batch investigation where at high temperatures the introduction of sample overwhelmed the microwave heating capability and caused the reactor temperature to drop. The same addition rate was used across all experiments carried out. The typical mass of HDPE added throughout an experiment was around 500 g.

The continuous addition study was primarily conducted at 450°C — the reaction temperature with the greatest yield and without a prolonged residence time — though a more limited set of comparative data was collected at 400°C, 500°C, and 600°C. A fresh bed was used when beginning each set of experimental runs at the same temperature (i.e., those experiments conducted sequentially at the same reactor temperature). Other than the described changes, the same materials, experimental apparatus, methodology, and analytical techniques were applied as those described in the previous chapter (§4.2–4.4).

## 5.3 Pyrolysis Product Component Yields

### 5.3.1 Coke Bed Control Yields

The continuous pyrolysis process was first applied to the coke bed in order to establish consistency data for the control non-catalytic state; three experimental repeats were performed at each temperature. Table 5.1 shows the average yields obtained at each temperature. The maximum yield of condensed products of 84.1% was obtained at 450°C. This yield then rapidly dropped off with increasing reaction temperature as the fraction of input HDPE converted to non-condensable gases increased, until the ratio of condensed to non-condensable gases reversed at 600°C, with 81.5% of the input HDPE converted to non-condensable gas. Almost no input sample was retained within the reactor, and the yield between runs was relatively consistent, with a maximum standard deviation of 3.5%.

The larger quantity of HDPE processed in these runs, combined with the relatively heavy products produced when using the coke bed, caused issues in some cases where the percolating dry ice condenser became blocked. In the event that this occurred, the experiment was cut short, and the yield percentages were calculated from the quantity of HDPE that was actually added during the experiment.

**Table 5.1:** Percentage yields of retained, condensed, and non-condensable pyrolysis products produced using a coke reactor bed with a continuous input feed of HDPE. *Retained* refers to the portion of input mass left in the reactor at the conclusion of each experiment, *condensed* product is the oil/wax collected in the condenser, *gases* refers to the remaining non-condensable gaseous fraction and is calculated by difference. All percentages are expressed on a mass basis as a proportion of the input HDPE ± the standard deviation.

| | 400°C | 450°C | 500°C | 600°C |
|---|---|---|---|---|
| Retained | 0.1 ±0.1 | 0.0 ±0.0 | 0.0 ±0.0 | 0.0 ±0.0 |
| Condensed | 80.4 ±3.0 | 84.1 ±3.5 | 52.5 ±3.2 | 18.2 ±3.3 |
| Non-condensable gases | 19.5 ±3.1 | 15.9 ±3.5 | 47.5 ±3.2 | 81.5 ±3.3 |

As with the batch experiments, greater cracking occurs at higher pyrolysis temperatures, resulting in an increased yield of non-condensable gases. At 400°C this trend is countered by an increase in residence time as the reactor temperature approaches the lower temperature limit for pyrolysis to occur. However, even at this temperature with the longer residence time the reactor did not become "overwhelmed" with input solids undergoing processing. A comparison between the results generated in batch and continuous input mode is given in §5.7.

### 5.3.2 Activated Carbon Yields

A similar procedure of attempting to determine the consistency of the microwave-assisted pyrolysis process was applied using the activated carbon bed; however, it quickly became clear that large differences in the component yields were occurring between runs. Figure 5.1 shows the changes in yields with each successive run as more HDPE was processed with the activated carbon bed. Testing at 500°C and 600°C was stopped after six experiments each, as the resulting condensed product was highly viscous and began to clog the condenser.

#### 5.3.2.1 Retained Fraction

The mass fraction of the input HDPE that is retained in the reactor bed is initially very large (ranging from 15–28% depending on temperature, with a larger fraction retained as the operating temperature increases), but rapidly reduces as the cumulative mass of HDPE processed by the bed increases. Indeed, from the extended 450°C case the retained fraction seems to tend towards an asymptote of zero.

#### 5.3.2.2 Condensed Products

The proportion of condensed pyrolysis products is also temperature dependent, and follows a similar order to that observed in the coke bed case, with the greatest yield observed at 450°C, and the yield rapidly declining as the reaction temperature increases from here. As more sample is processed with the activated carbon bed, the yield of condensed products increases; in the 450°C case the yield appears to be approaching that of the coke bed equivalent and, given the similar progression of the other temperatures for the examined data, it is likely that they too would approach their coke bed yield equivalents in time.

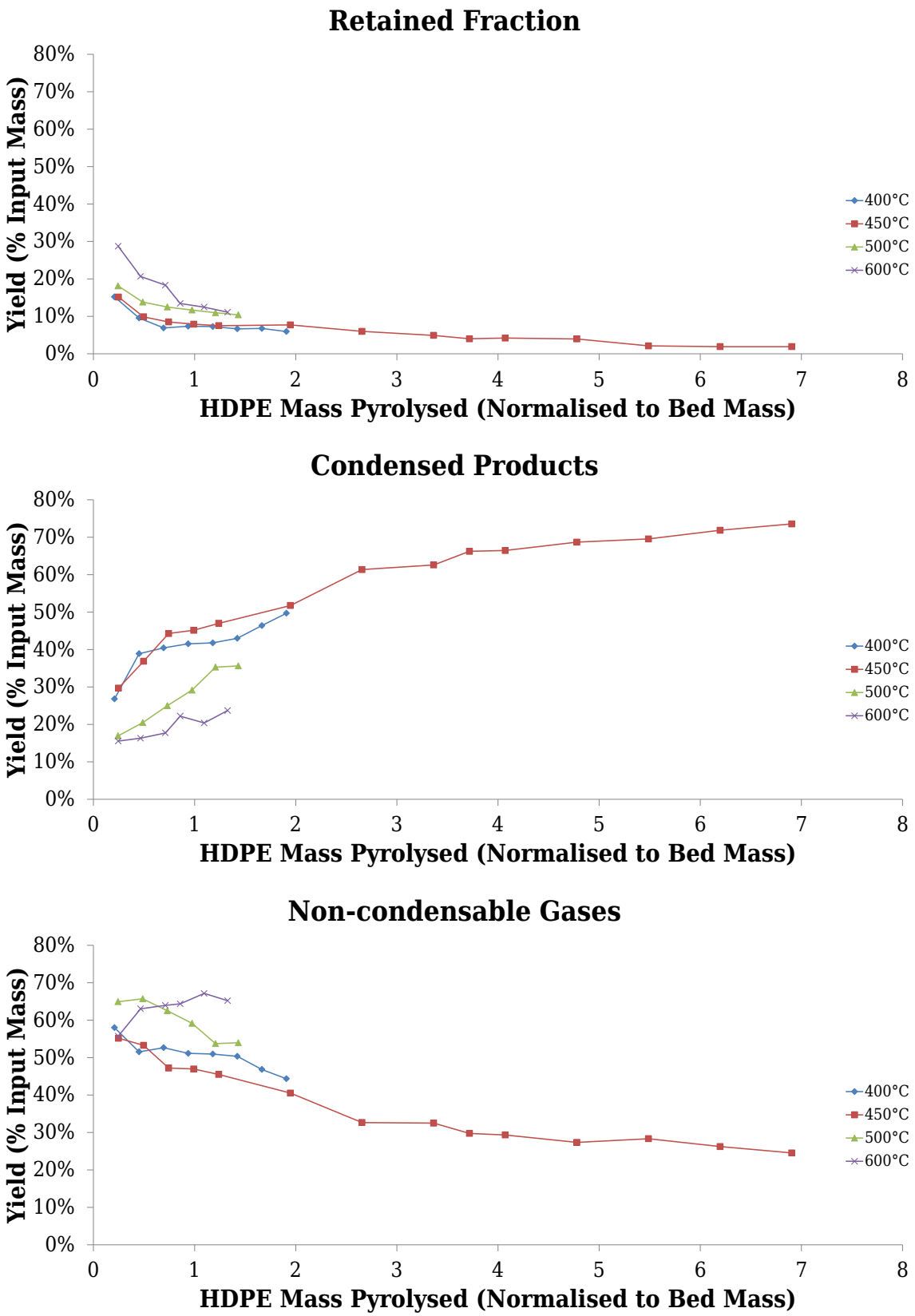


**Figure 5.1:** Percentage yields of retained, condensed, and non-condensable pyrolysis products produced using an activated carbon reactor bed with a continuous input feed of HDPE. The *retained* fraction refers to the portion of input mass left in the reactor at the conclusion of the experiment; *condensed* product is the oil/wax collected in the condensing system; the remaining fraction comprises *non-condensable gases* and is calculated by difference. All percentages are expressed on a mass basis as a proportion of the input HDPE.

#### 5.3.2.3 Non-condensable Gases

For the most part the yield of the non-condensable gases declines over time as the mass of HDPE processed increases, as would be expected given the increase in condensed products. The seeming counter-example to this trend is the initial increase in proportion of non-condensable gases produced at the 600°C reaction temperature — this is the result of the comparatively larger decrease in the proportion of sample that is retained in the reactor over this period: the 18% drop in retained mass represents additional material that is converted to condensed and gaseous products, such that the net effect on the non-condensable gases is to increase over this period. If the experiments at this temperature had been able to be continued and more HDPE was processed, the non-condensable fraction would likely decrease in line with the results obtained for the other temperatures, and the final data point gathered shows initial evidence of this occurring. When the retained fraction is excluded, independent of the amount of HDPE processed, the non-condensable yields show a temperature dependence consistent with all the data observed thus far, with the greatest portion of gases produced at 600°C, and this decreasing as reaction temperature is reduced to 450°C, before slightly increasing at 400°C.

#### 5.3.2.4 Change in Activity of Bed

From these longitudinal studies, conducted with significantly larger quantities of HDPE than the initial batch input investigation of the previous chapter, it is clear that a constitutive change in the nature of the pyrolysis products produced using the activated carbon bed is occurring as more HDPE is processed. The increase over time in the proportion of heavier condensed products, and decrease in the lighter non-condensable gases that have undergone greater cracking, is consistent with a reduction in catalytic activity of the activated carbon bed. This is supported by a visual observation of the condensed pyrolysis products, which over time became more viscous, and less clear and homogeneous. That a significant proportion of the input mass remains in the reactor (the “retained” fraction) even after being subject to temperatures that would normally drive off any volatiles present, suggests the production of char, where the catalyst has effectively stripped the hydrocarbon of hydrogen, leaving a carbonaceous residue. In this way, the retained fraction is effectively hydrocarbon that has been cracked “beyond” the non-condensable gases stage (and deposited on to the surface of

the bed particles), explaining the initial increase in these gases (and decline in retained fraction) at 600°C as catalytic deposition reduces.

This accumulation of mass retained in the reactor over time, the corresponding apparent loss of catalytic activity of the activated carbon bed, and the decrease in the rate of accumulation as the activity of the bed itself declines, suggests that the catalytic deactivation may be occurring via coking, with the deposition of non-active carbon on the surface of the activated carbon particles. This is supported by the lack of any significant mass retained in the reactor when operating with the non-catalytic coke bed. Indeed, by the end of the experimental series conducted at 450°C, the activated carbon bed had accumulated (non-catalytic) material equivalent to 25% of its mass. If nothing else, assuming this material is non-catalytic, this accumulation of mass would "dilute" the reactor bed and reduce the proportion of catalyst that the HDPE substrate is exposed to. A detailed investigation into the specific nature of the retained fraction was later conducted and is presented in §6.6. A general trend from these results, though, is as more mass is processed by the activated carbon bed, yields tend more closely towards those obtained when using a coke bed — consistent with the catalytic deactivation of activated carbon, and with the coke bed representing the ultimate non-active state.

## 5.4 Analysis of Condensed Pyrolysis Oils and Waxes

### 5.4.1 Mass Distribution of Condensed Pyrolysis Products

A complete GC/MS analysis of the condensed products produced in the continuous mode was carried out, and from this the distribution of molecular masses for each experiment was obtained. Figure 5.2 on the next page shows the average molecular mass, and the range of the molecular masses of the compounds present in the condensate (delineated by 5th and 95th percentile so as to eliminate the non-representative influence of any small concentration outliers).

#### 5.4.1.1 Coke Bed

The distribution of condensed products produced using a coke bed with a continuous input of sample follow a similar pattern to those produced with batch input. Both the average molecular mass and the range of masses present in the condensate increases with increasing reactor temperature, up to 550°C, at which point the average

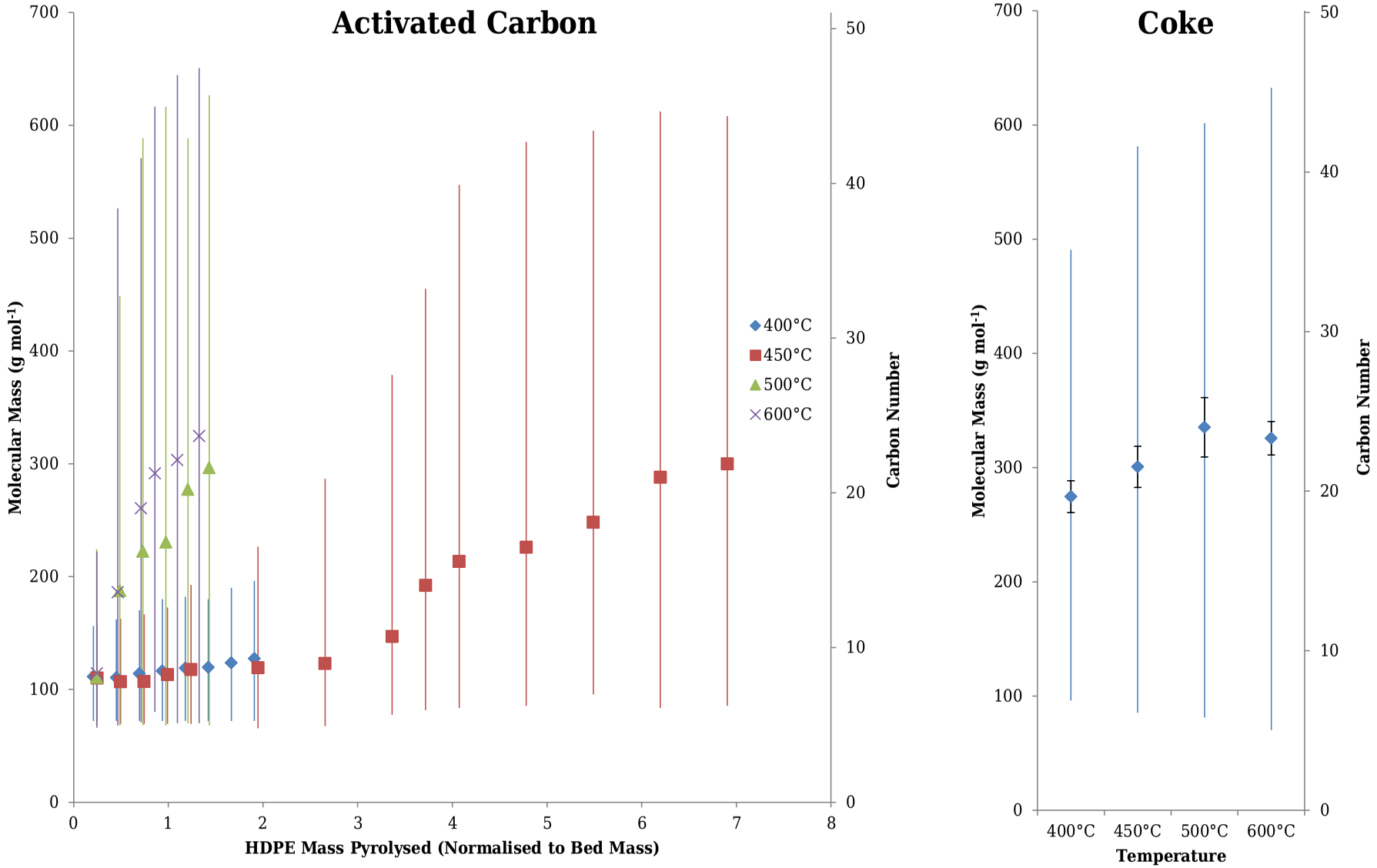


**Figure 5.2:** Average molecular mass of condensed pyrolysis products with continuous introduction of HDPE. Capped central error bars show standard deviation of mean. Non-capped longer bars show 5th and 95th percentile of the range of the molecular masses. All results are calculated on peak area basis. Carbon number axis is based on the average correlation to molecular mass.

molecular mass reduces slightly. The average molecular mass of the condensed products is determined by the amount of cracking these products undergo, which itself is determined by temperature and residence time. Up to 550°C the increase in temperature reduces the amount of time the HDPE spends in the hot zone of the reactor so it is overall cracked less, and has a higher average molecular mass. At 600°C the increase in the speed of the cracking process dominates and the average molecular mass is reduced. The range of products increases with reaction temperature as the hotter temperatures allow larger compounds to enter the gaseous state and exit the reactor, and the more rapid cracking (and thus production of pyrolysis gas which drives exit from the reactor through phase change volume expansion) reduces residence time.

While this residence time based explanation of the increase in average molecular mass of condensed products between 400–500°C certainly holds true, it is important to remember that this average only encompasses the condensed fraction of the pyrolysis products produced, and that while the condensed products may have a greater average molecular mass at 500°C than 450°C, overall, more cracking occurs at 500°C (and indeed overall cracking consistently increases with reactor temperature), as is clear from the increased yield of shorter chain non-condensable gases seen in figure 5.1.

#### 5.4.1.2 Activated Carbon Bed

When the activated carbon bed was used, while the temperature and residence time effects described for the coke bed case are no doubt present, the composition of the condensed product is primarily determined by the catalytic nature of the activated carbon. It is clear that over time, as more HDPE is processed by a given activated carbon bed, both the average molecular mass and the range of masses of the condensed pyrolysis products increase, consistent with a reduction in bed catalytic activity. The rate of this increase is highly temperature dependent: at 450°C the initial increase in average mass of the condensed pyrolysis products is almost negligible, remaining at around 110–120 g $mol^{-1}$ (corresponding to around $C_8$–$C_9$) until around 3.5 times the mass of the bed itself has been processed, after which it increases to a maximum of 300 g $mol^{-1}$ (around $C_{14}$), and at which time the rate of increase plateaus. The results obtained at 400°C follow a similar trend to the 450°C case. However, at 500°C the average molecular mass increases far more rapidly as more HDPE is processed, with no initial plateau as in the lower temperature cases; the range of the molecular masses of the products produced at this temperature increases equally quickly. These increases

occur even more rapidly at 600°C, and are consistent with the visual observation of the products produced at these temperatures, which showed inhomogeneity and high viscosity (from the greater range and mass of hydrocarbons respectively), and caused problems with blocking the percolating dry ice condenser.

#### 5.4.1.3 Temperature Dependent Change in Activated Carbon Bed Activity

It is clear that the molecular mass time profile of the products with an activated carbon bed varies considerably depending on the temperature at which pyrolysis is conducted. The rapid change in average molecular mass and range of products shown at 500°C and 600°C, contrasted with the equivalent seen at 400°C and 450°C, implies that the process leading to the deactivation of the activated carbon bed is highly non-linear with temperature.

Based on the extended study made at 450°C, as the deactivation of the activated carbon progresses the profile of the resulting condensed products grows increasingly similar to those produced using the non-catalytic coke bed. In the 500°C and 600°C cases the composition of the condensed products is still undergoing change; interestingly, from the third set of experiments (HDPE/Bed Mass $\approx 0.75$) the average molecular mass of the products produced at 600°C is considerably greater than those produced at 500°C, in contrast with their equivalents produced using the coke bed, where the average molecular mass is somewhat smaller at 600°C. This may be a result of the catalytic cracking effectively magnifying the non-linear reduction in residence time that, with increased reaction temperature, increased the average molecular mass of the condensed products in the batch mode (§4.5.3.2). If, in the non-catalysed case, the increase in rate of production of pyrolysis gases at higher temperatures was sufficient to increase the pressure within the reactor to cause said pyrolysis gases to leave more quickly (resulting in the higher average molecular mass of the condensed products), then in the *catalysed* case the reaction rate will be quicker still, the exit pressure even greater, the residence time less, and the average molecular mass of the products greater. Note that it is not the ultimate yield of non-condensable gases that determines the exit pressure and residence time, but rather the *rate of production* of the pyrolysis gas (which includes all products in the gaseous state in the reactor). Hence, it would be entirely possible for the changes that occurred after those recorded at 600°C to include a lower average molecular mass in the condensate, and a higher total proportion of non-condensable gases, as a result of a reduction in catalytic activity causing an overall slower reaction rate and reducing the residence time.

#### 5.4.1.4 Change in Carbon Number Distribution

The initial condensed pyrolysis products produced using an activated carbon bed with continuous addition of HDPE all have very similar molecular mass distributions, regardless of the temperature at which they were produced, though the upper bound of the range does increase somewhat with increasing temperature. They are uni-modal, with the largest peak at $C_8$; the distribution produced at 450°C is shown in figure 5.3 on the following page.

As more HDPE is processed by the activated carbon bed, for all temperatures, the distribution of the molecular masses changes considerably as the tail grows to encompass larger molecules. An examination of the extended study conducted at a reactor temperature of 450°C is useful as this case not only presents the most data, but the changes in mass distribution happen sufficiently slowly that the snapshots of each experimental run allow a complete picture of changes to be built up. Data gathered at 500°C and 600°C is consistent with similar changes taking place but much more rapidly; at 400°C the change is similar but slower.

At 450°C as more HDPE is processed by the activated carbon bed the distribution remains similar for some time, until there is a rapid increase in the maximum molecular mass in the condensed pyrolysis products when the quantity of HDPE processed is equal to around 3.5 times the mass of the bed: going from 2.9 times the mass of the bed processed to 4.1 times, the maximum carbon number increases from $C_{20}$ to $C_{45}$, accounting for the rapid rate of increase in average molecular mass in this period observed in figure 5.2. These heavier compounds are initially present in small quantities, but as more HDPE is processed by the bed they are produced in increasing quantities, until a clear second grouping becomes evident.

This emergent second grouping resembles that observed in the condensate produced with the coke bed in the batch mode, is also comprised of long-chain aliphatic species, and likely derives from the same origin, possibilities of which are discussed in §4.5.3.4. The increase in prominence of these heavier compounds results in a corresponding reduction in the lighter grouping and an increasingly flat distribution. By the time 6.9 times the mass of the bed has been processed, the carbon number distribution is clearly bi-modal, and highly resembles that produced using the coke bed at the same temperature, as seen in the lower two graphs of figure 5.3.

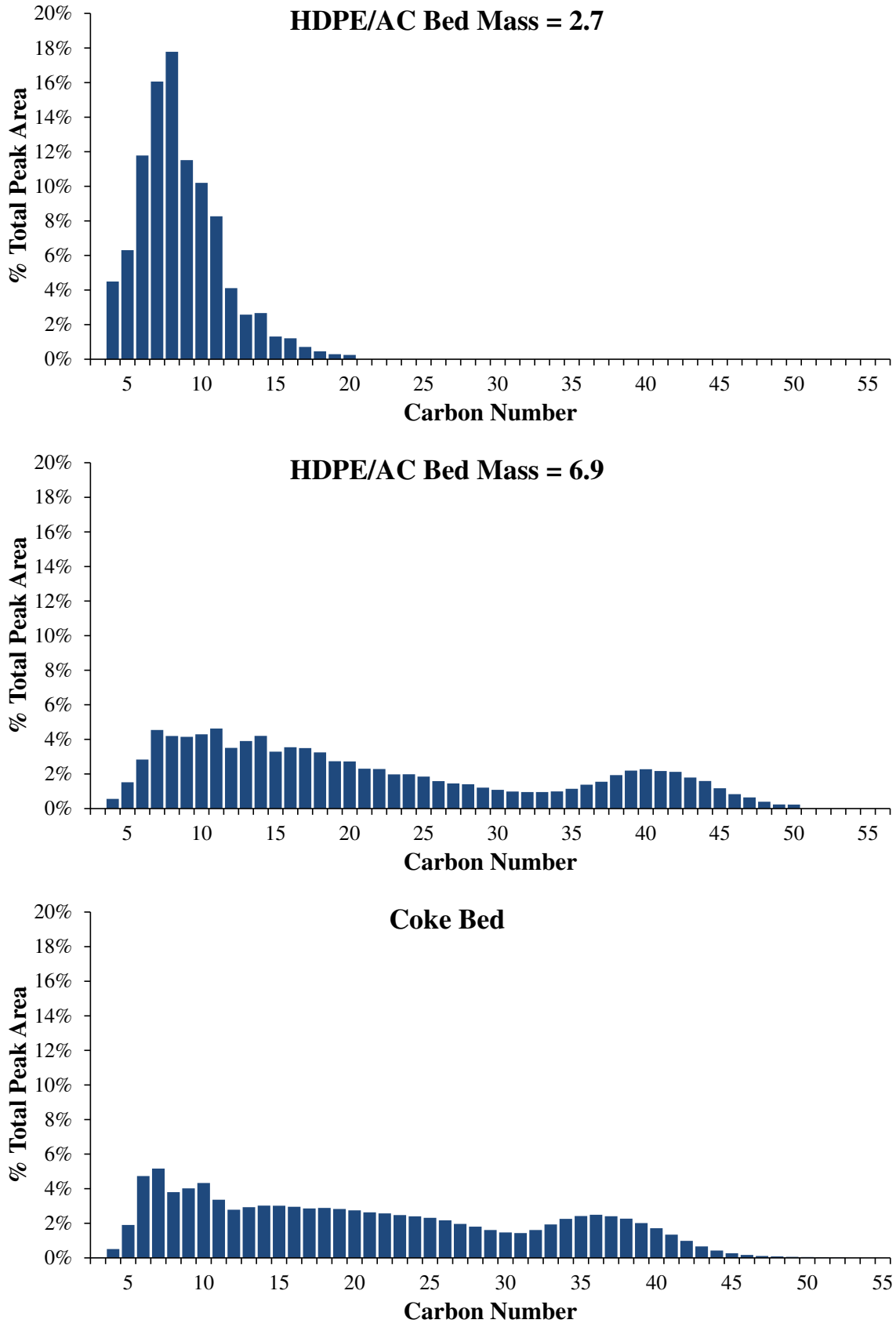


**Figure 5.3:** Change in carbon number distribution of condensed products due to deactivation of activated carbon. The condensed products analysed here were all produced at a reactor temperature of 450°C with the continuous addition of sample. The top figure represents the initial mass distribution produced using activated carbon having processed up to 2.7 times its mass of HDPE; by the end of the experimental series after the bed has processed 6.9 times its mass of HDPE the mass distribution has changed considerably (middle), and resembles that resulting from the control coke bed (bottom).

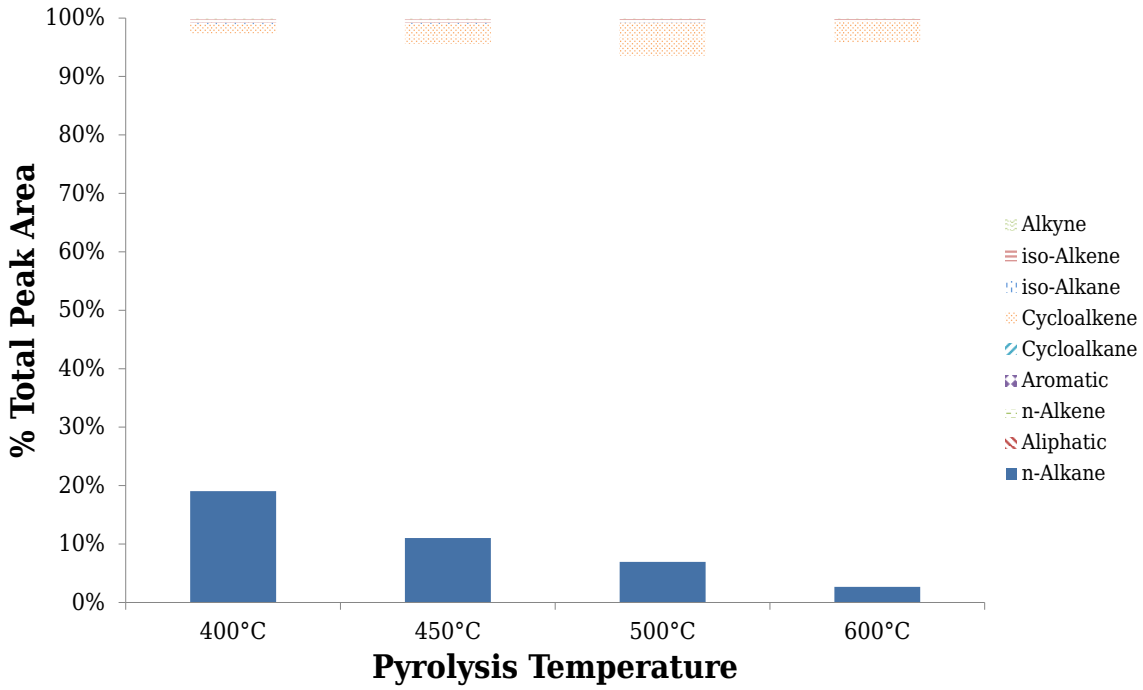


**Figure 5.4:** Chemical composition of the condensed pyrolysis products produced using a coke bed with a continuous input of HDPE. "Alkenes" encompasses species containing one or more double bonds. "Aliphatics" includes linear alkanes and alkenes which were unable to be distinguished from one another in the GC/MS analysis owing to their large molecular mass ($>C_{23}$).

## 5.4.2 Chemical Composition of Condensed Pyrolysis Products

### 5.4.2.1 Coke Bed

Figure 5.4 shows the chemical composition of the condensed pyrolysis products produced using a coke bed. The bulk of the products comprise linear alkanes and alkenes (over 90% peak area at 400°C and 450°C), with small quantities of cyclic compounds. As the reaction temperature increases there is a reduction in the linear alkanes and alkenes, and an increase in cyclic and aromatic species, which make up around 25% of the peak area at 600°C.

The proportion of heavier aliphatics (comprising linear alkanes and alkenes, though indistinguishable from each other in this analysis owing to their large molecular mass) increases with reaction temperature, as does the ratio of (separable) alkenes to alkanes. The greater thermal energy at 500°C and 600°C also facilitates secondary reaction mechanisms (described in §6.2) that lead to the production of aromatics.

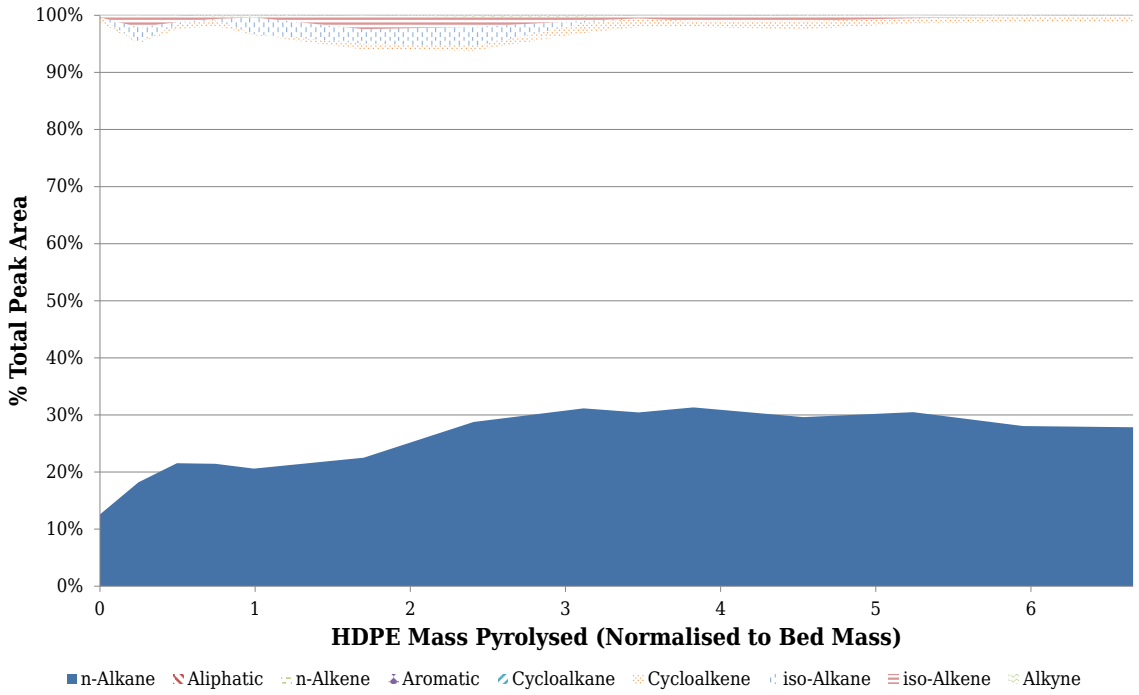


**Figure 5.5:** Change in chemical composition of the condensed pyrolysis products produced using an activated carbon bed at 450°C with a continuous input of HDPE. "Alkenes" encompasses species containing one or more double bonds. "Aliphatics" includes linear alkanes and alkenes which were unable to be distinguished from one another in the GC/MS analysis owing to their large molecular mass ($>C_{23–25}$).

#### 5.4.2.2 Activated Carbon Bed

The change in the chemical composition of the condensed pyrolysis products produced using an activated carbon bed at 450°C, as it processes progressively more HDPE, is shown in figure 5.5. The most dramatic change across the range tested is in the proportion of aromatics, which initially comprise the majority of the condensed product (around 85% peak area), but as the activated carbon bed processes more HDPE decrease steadily. The decrease in aromatic content is matched by an increase in linear alkane and alkene species. After the bed has processed around 3 times its mass in HDPE we see the appearance of the longer chain indistiguishable aliphatics, which coincides with the increase in average molecular mass seen in §5.4.1.2. The remaining classes of compounds (branched aliphatics, cyclics, and alkynes) are never present in any large quantity, remaining well under 10% peak area at all times even when summed together.

Figure 5.6 shows the effect of reaction temperature on the change in chemical composition of the condensed pyrolysis products produced using an activated carbon bed. The depicted range of masses processed by the beds has been limited in the 450°C case for comparative purposes; however, over this range it is clear that very

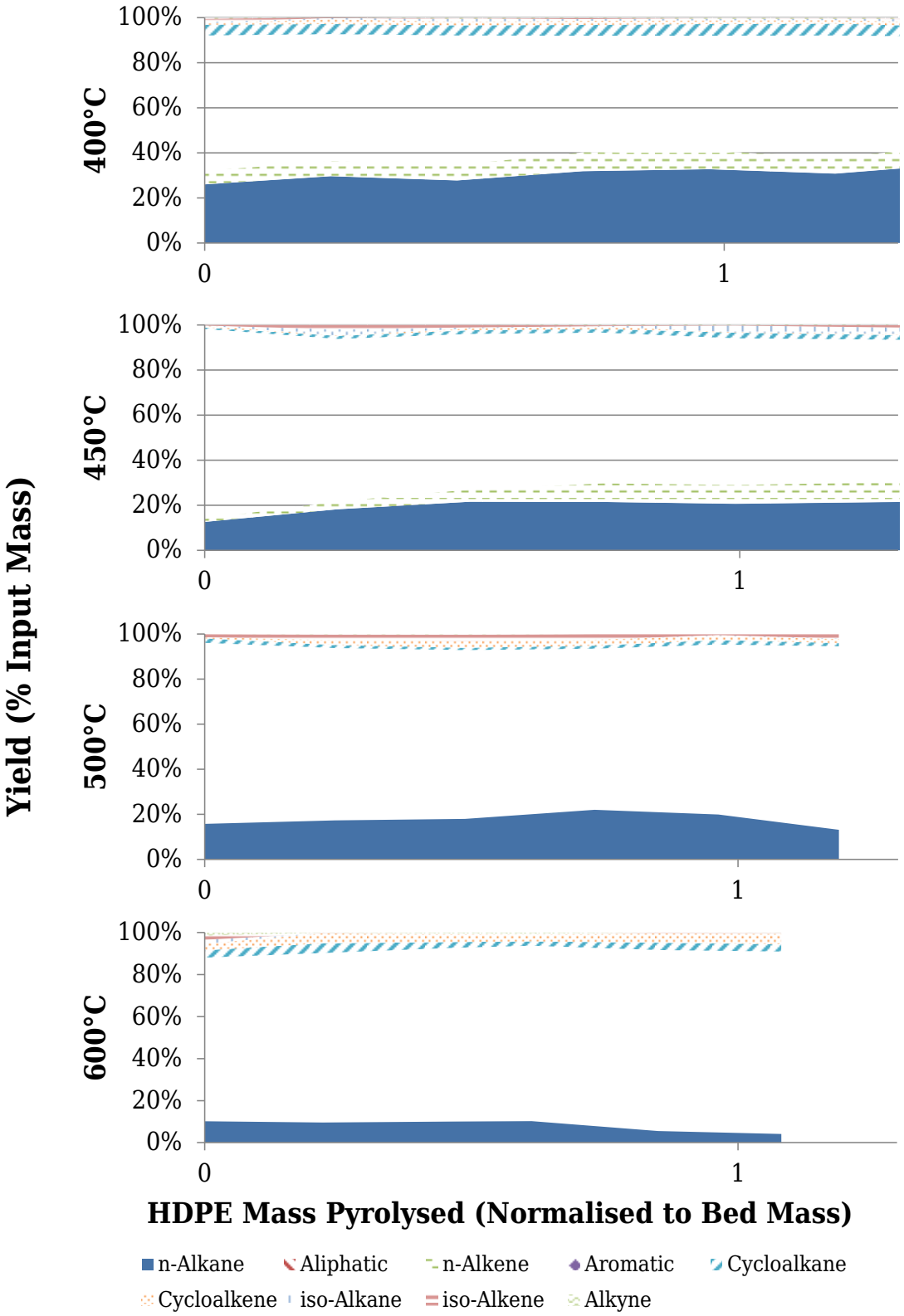


**Figure 5.6:** Change in chemical composition of the condensed pyrolysis products produced using an activated carbon bed with a continuous input of HDPE at all studied temperatures. The 450°C case has been foreshortened in this figure for comparative purposes, but is given in full in figure 5.5. "Alkenes" encompasses species containing one or more double bonds. "Aliphatics" includes linear alkanes and alkenes which were unable to be distinguished from one another in the GC/MS analysis owing to their large molecular mass (>$C_{23–25}$).

little change occurs at reactor temperatures of 400°C and 450°C. In contrast, with an increase in reactor temperature of just 50°C, the change in species present in the condensed product over the course of the bed processing its own mass in HDPE is significant: heavier aliphatic species are immediately apparent, and aliphatics generally increase over time as the aromatic content declines. In other words, the same changes observed with the 450°C bed occur, but much more rapidly, consistent with the activated carbon deactivating more quickly at higher temperatures.

Across the entire range of temperatures and reactor beds, linear aliphatics and aromatics comprise the vast majority of the pyrolysis products (>90% peak area), with the ratio of aromatic to aliphatic declining depending on reactor temperature and, with an activated carbon bed, how much HDPE has been processed. The primary breakdown products of the pure thermal scission of HDPE are linear aliphatics [225]. Given that aromatics are only present in any significant quantity at high temperatures (600°C) in the non-catalytic coke bed case, and that they decline as the activated carbon bed processes more HDPE and becomes deactivated, it is clear that activated carbon catalyses the formation of aromatic species. Potential reaction mechanisms accounting for this, and the formation of all other major species observed in the pyrolysis products are discussed in detail in §6.2.

#### 5.4.2.3 Specific Compound Analysis and Examples

Thus far the chemical analysis of pyrolysis products has focused on general categories of compounds; tables 5.2 and 5.3 present lists of the most five most common individual species within each of these categories produced using the coke and activated carbon beds respectively, with the latter of these also detailing how the proportion of species changes as the activated carbon progressively processes more HDPE. The stochastic nature of the pyrolytic breakdown of HDPE results in an extremely large number of separate compounds produced, making listing all of them impossible given any reasonable space constraint, and which is not especially instructive in any case given the category-based analysis already presented. In spite of this, the most common compounds make up a disproportionately large percentage of the total: the top 24 species across all analyses performed with an activated carbon bed make up 50% of the total peak area, while the remaining 50% consists of around 550 other species (though not all of these are present in each analysis). As such, the data presented in these tables on the most common compounds observed does add informative value, and provides a representative flavour of the compounds present in each pertinent category.

**Table 5.2:** Five most prevalent compounds for each chemical grouping (averaged across all experiments) in the condensate produced using a coke bed continuously fed with HDPE. All figures are percent peak area derived from GC/MS analysis. Positional isomers (e.g. o-, m-, p-xylene) are grouped. *Aliphatics* are long-chain linear alkanes and alkenes that were not distinguishable from each other owing to their length; as a grouped category these present a proportionally larger fraction than the equivalent single species would.

| Pyrolysis Temperature | 400°C | 450°C | 500°C | 600°C |
|---|---|---|---|---|
| Alkane | | | | |
| Eicosane | 1.5 | 0.9 | 0.3 | 0.2 |
| Docosane | 1.5 | 0.9 | 0.3 | 0.1 |
| Octadecane | 1.4 | 0.8 | 0.3 | 0.2 |
| Hexadecane | 1.3 | 0.8 | 0.3 | 0.2 |
| Heneicosane | 1.4 | 0.9 | 0.3 | 0.1 |
| Alkene | | | | |
| Decene | 2.6 | 2.6 | 2.3 | 1.6 |
| Undecene | 2.2 | 2.2 | 1.7 | 1.3 |
| Heptene | 1.5 | 1.5 | 1.9 | 1.1 |
| Tetradecene | 2.3 | 2.0 | 1.4 | 1.1 |
| Hexene | 1.4 | 1.4 | 1.6 | 1.4 |
| Aliphatic | | | | |
| $C_{36}$ | 1.9 | 2.2 | 4.1 | 3.7 |
| $C_{37}$ | 1.6 | 2.1 | 4.0 | 3.8 |
| $C_{38}$ | 0.8 | 1.9 | 3.9 | 3.9 |
| $C_{35}$ | 1.2 | 2.1 | 3.9 | 3.2 |
| $C_{39}$ | 0.5 | 1.8 | 3.4 | 3.5 |
| Aromatic | | | | |
| Toluene | 0.1 | 0.4 | 1.2 | 4.6 |
| Benzene | 0.0 | 0.2 | 0.7 | 4.4 |
| Naphthalene | 0.0 | 0.0 | 0.1 | 2.0 |
| Ethylbenzene | 0.0 | 0.1 | 0.3 | 1.0 |
| Benzene, 1,3-dimethyl- | 0.0 | 0.1 | 0.5 | 0.7 |
| Other | | | | |
| Cyclopropane, ethyl- | 0.7 | 0.8 | 1.0 | 0.8 |
| Cyclohexene | 0.1 | 0.2 | 0.5 | 0.4 |
| Cyclopentene | 0.1 | 0.2 | 0.4 | 0.4 |
| 1,3-Cyclopentadiene | 0.0 | 0.1 | 0.4 | 0.8 |
| 1,3-Cyclohexadiene | 0.0 | 0.1 | 0.6 | 0.0 |

The most prevalent alkanes produced using a coke bed are dominated by the distribution of compounds at 400°C, which has a higher proportion of alkanes than the other temperatures. As a result of being so close to the pyrolysis threshold, the distribution of compounds is also different at this temperature — while the average and upper molecular mass is smaller than at higher temperatures, the mode is larger as a result of the flatter distribtuion, accounting for the larger alkanes listed in this table. Aromatics are not present in large quantities until 600°C, with benzene and derivates

**Table 5.3:** Five most prevalent compounds for each chemical grouping (averaged across all experiments) in the condensate produced using an activated carbon bed continuously fed with HDPE. All figures are percent peak area derived from GC/MS analysis. Positional isomers (e.g. o-, m-, p-xylene) are grouped. Selected representative runs are presented as the beds have processed more HDPE (*HDPE/Bed Mass* = mass fraction of HDPE to that of the bed). *Aliphatics* are long-chain linear alkanes and alkenes that were not distinguishable from each other owing to their length; as a grouped category these present a proportionally larger fraction than the equivalent single species would.

| Pyrolysis Temperature | 400°C | | | | 450°C | | | | | | 500°C | | | 600°C | | |
|---|---|---|---|---|---|---|---|---|---|---|---|---|---|---|---|---|
| HDPE/Bed Mass | 0.45 | 1.18 | 1.42 | 1.91 | 0.50 | 0.99 | 1.95 | 3.36 | 4.78 | 6.91 | 0.48 | 0.97 | 1.43 | 0.47 | 0.86 | 1.33 |
| Alkane | | | | | | | | | | | | | | | | |
| Hexane | 6.4 | 5.6 | 5.2 | 4.8 | 5.2 | 4.4 | 4.9 | 2.4 | 1.1 | 0.9 | 2.7 | 2.4 | 1.9 | 2.1 | 1.4 | 1.0 |
| Pentane | 6.3 | 5.1 | 4.7 | 4.2 | 4.8 | 3.4 | 5.4 | 1.7 | 1.1 | 1.1 | 3.9 | 3.0 | 2.8 | 2.1 | 1.3 | 0.9 |
| Heptane | 4.9 | 4.8 | 4.6 | 4.7 | 3.9 | 4.0 | 3.6 | 3.0 | 1.3 | 1.0 | 2.5 | 2.0 | 1.5 | 1.4 | 0.9 | 0.4 |
| Octane | 3.5 | 3.9 | 3.8 | 4.3 | 2.5 | 2.4 | 2.5 | 2.4 | 1.8 | 1.1 | 1.9 | 1.5 | 1.3 | 1.1 | 0.7 | 0.3 |
| Nonane | 2.2 | 2.9 | 2.9 | 3.4 | 1.5 | 2.4 | 1.8 | 3.2 | 2.2 | 1.1 | 1.5 | 1.0 | 1.1 | 0.9 | 0.6 | 0.3 |
| Alkene | | | | | | | | | | | | | | | | |
| Hexene | 2.0 | 2.0 | 1.9 | 1.6 | 0.5 | 1.1 | 1.3 | 2.9 | 1.3 | 4.0 | 4.7 | 3.9 | 6.2 | 9.1 | 5.5 | 7.2 |
| Heptene | 1.6 | 1.8 | 1.6 | 1.5 | 1.6 | 2.4 | 3.0 | 1.2 | 0.9 | 0.6 | 2.5 | 1.9 | 2.9 | 3.5 | 1.6 | 2.1 |
| Octene | 1.1 | 1.6 | 1.5 | 1.5 | 1.2 | 2.2 | 2.1 | 0.4 | 1.3 | 1.4 | 2.2 | 2.2 | 2.1 | 2.9 | 1.3 | 1.9 |
| Decene | 0.3 | 0.3 | 0.4 | 0.8 | 1.0 | 0.6 | 0.7 | 2.1 | 1.0 | 0.6 | 1.1 | 1.7 | 1.5 | 2.2 | 1.4 | 1.4 |
| Undecene | 0.2 | 0.5 | 0.4 | 0.4 | 0.4 | 0.6 | 0.5 | 2.3 | 1.4 | 1.8 | 1.0 | 1.3 | 1.3 | 1.7 | 1.6 | 1.8 |
| Aliphatic | | | | | | | | | | | | | | | | |
| $C_{40}$ | 0.0 | 0.0 | 0.0 | 0.0 | 0.0 | 0.0 | 0.0 | 1.0 | 0.7 | 2.3 | 1.3 | 1.6 | 2.0 | 0.2 | 2.0 | 2.4 |
| $C_{39}$ | 0.0 | 0.0 | 0.0 | 0.0 | 0.0 | 0.0 | 0.0 | 0.9 | 0.6 | 2.2 | 1.4 | 1.5 | 1.9 | 0.2 | 2.4 | 2.5 |
| $C_{38}$ | 0.0 | 0.0 | 0.0 | 0.0 | 0.0 | 0.0 | 0.0 | 0.7 | 0.5 | 1.9 | 1.5 | 1.3 | 1.8 | 0.2 | 2.8 | 2.6 |
| $C_{41}$ | 0.0 | 0.0 | 0.0 | 0.0 | 0.0 | 0.0 | 0.0 | 1.0 | 0.7 | 2.2 | 1.2 | 1.6 | 2.0 | 0.3 | 1.5 | 2.1 |
| $C_{37}$ | 0.0 | 0.0 | 0.0 | 0.0 | 0.0 | 0.0 | 0.0 | 0.6 | 0.5 | 1.5 | 1.5 | 1.1 | 1.5 | 0.2 | 3.2 | 2.3 |
| Aromatic | | | | | | | | | | | | | | | | |
| Toluene | 13.1 | 7.7 | 7.5 | 5.5 | 13.6 | 11.2 | 9.2 | 3.0 | 1.6 | 0.9 | 14.7 | 5.7 | 3.6 | 6.3 | 3.2 | 3.1 |
| Xylene | 6.6 | 4.9 | 5.1 | 4.1 | 9.9 | 9.7 | 8.1 | 5.4 | 2.2 | 0.2 | 4.5 | 3.6 | 2.4 | 1.8 | 1.7 | 1.1 |
| Ethylbenzene | 7.6 | 5.3 | 5.4 | 3.8 | 9.9 | 8.6 | 7.3 | 2.8 | 1.7 | 0.6 | 4.1 | 3.3 | 2.2 | 2.3 | 1.3 | 0.7 |
| Benzene | 3.9 | 1.7 | 1.6 | 1.0 | 3.2 | 2.1 | 4.8 | 1.4 | 0.6 | 0.5 | 4.7 | 3.3 | 2.0 | 4.4 | 2.4 | 2.6 |
| Naphthalene | 4.5 | 0.4 | 0.0 | 0.0 | 7.1 | 5.8 | 6.3 | 2.3 | 1.5 | 0.2 | 3.6 | 2.8 | 1.9 | 2.7 | 1.6 | 0.9 |
| Other | | | | | | | | | | | | | | | | |
| Cyclopropane, ethyl- | 0.8 | 0.7 | 0.7 | 0.6 | 0.4 | 0.6 | 1.0 | 0.0 | 0.0 | 0.0 | 1.1 | 0.0 | 0.0 | 0.0 | 1.0 | 1.5 |
| Cyclopentane, methyl- | 1.1 | 0.9 | 0.9 | 0.8 | 0.1 | 0.0 | 0.0 | 0.7 | 0.2 | 0.2 | 0.2 | 0.4 | 0.3 | 0.4 | 0.1 | 0.0 |
| Cyclopropane, dimethyl- | 1.5 | 1.3 | 1.2 | 1.0 | 0.0 | 0.0 | 0.3 | 0.0 | 0.6 | 0.4 | 0.4 | 0.0 | 0.0 | 0.2 | 0.0 | 0.0 |
| Cyclopentane, ethyl- | 0.4 | 0.5 | 0.5 | 0.5 | 0.3 | 0.4 | 0.3 | 0.5 | 0.2 | 0.1 | 0.1 | 0.1 | 0.1 | 0.1 | 0.0 | 0.0 |
| Cyclohexane, methyl- | 0.0 | 0.4 | 0.4 | 0.4 | 0.2 | 0.3 | 0.0 | 0.7 | 0.3 | 0.2 | 0.2 | 0.3 | 0.2 | 0.3 | 0.2 | 0.0 |

most prevalent, though bi-cyclic napthalene is also present at 600°C. Aliphatics make up a large proportion of the condensate, though have larger absolute values as this is a category that groups alkanes, alkenes, alkadienes, etc.

In the condensate produced using fresh activated carbon, toluene is the single most common species, and remains the most common aromatic species across almost all testing performed. By far the majority of all the aromatic species are single-ring benzene derivatives with aliphatic side chains, though benzene itself is also present. PAHs are present though not in large quantities; naphthalene is by far the most abundant of these, with the three-ring anthracene the largest PAH observed across all samples, and this only in small amounts. The quantity of PAHs present declines quickly as the activated carbon bed processes more HDPE. The most common alkanes and alkenes are linear, from $C_5$–$C_{11}$, though as more HDPE is processed by the bed heavier aliphatics become more common, with a concurrent proportional reduction in the lighter alkanes and alkenes. Cycloalkanes comprise the majority of the remaining species, though these are not present in large quantities.

Generally as species contain an increasing number of side chains, or as the side chains become increasingly branched, they are less prevalent: in order for these more complex species to form they must undergo a greater number of reaction steps from the linear primary decomposition products of HDPE. As the number of secondary reaction steps in a sequence grows, the potential number of possible end-products grows extremely rapidly, with the probability of a particular individual end-product forming falling concurrently. Further, the number of secondary reactions a molecule is likely to undergo is itself probabilistically determined, with a greater number of reactions in sequence progressively less likely to occur. This combination of facts accounts for the large number of individual species observed across all the experiments conducted, and the overall distribution of species, with the smaller numerical subset of those that occur most frequently making up by far the greatest portion of the whole.

### 5.4.3 Economic Value and Consistency Over Time of Condensed Products

From the analysis presented thus far, it is clear that the composition of the condensed products varies significantly as the activated carbon bed processes progressively more HDPE. While in the initial studies presented in chapter 4 the condensate showed significant promise for use in liquid transport fuels, it is necessary to re-evaluate this in light of the new information on the deactivation of activated carbon and consequent

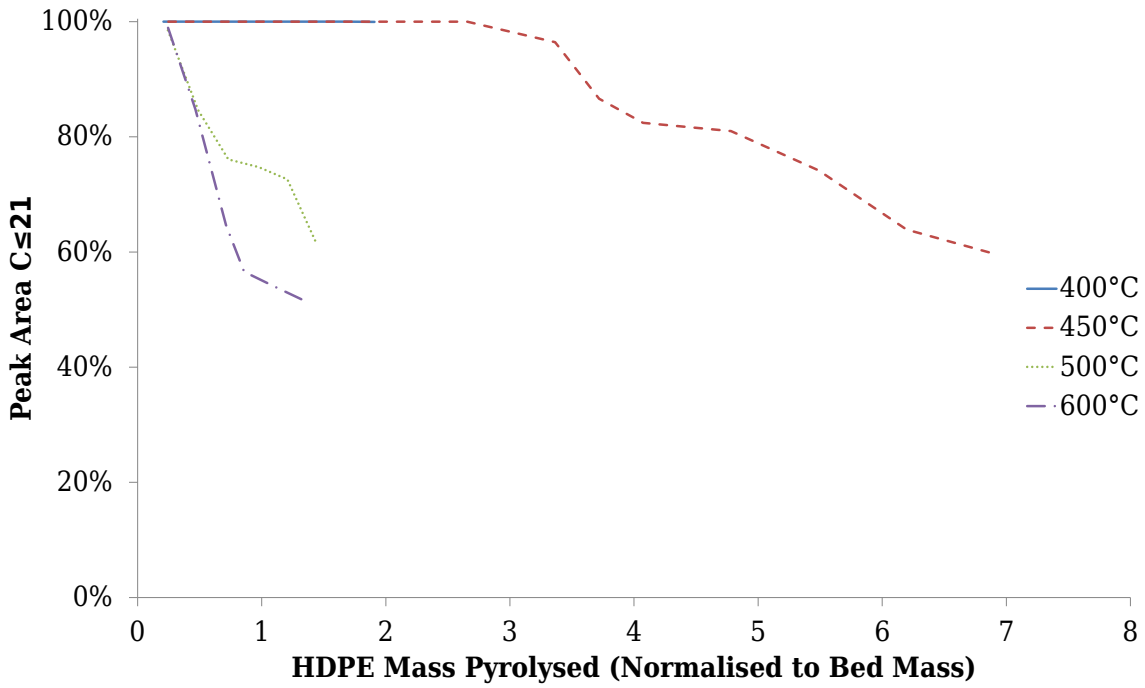


**Figure 5.7:** Proportion of condensate produced using an activated carbon bed with a carbon number in the liquid transport fuel range ($C_{\leq 21}$). Percentages are derived from peak areas in GC/MS analysis of the samples.

change in composition of the products presented in this chapter. Figure 5.7 shows the proportion of the condensed product, produced at various reaction temperatures with an activated carbon bed, that lies in the liquid transport fuel range ($C_5$–$C_{21}$). The rapid deactivation that occurs at operating temperatures of 500°C and greater results in a swift drop-off of liquid transport fuel range products, making operating at these temperatures infeasible. At 450°C the entire condensate is initially in the liquid transport fuel range, and remains so until the bed has processed approximately three times its mass. As shown in the previous section, over this period the resulting condensate is highly consistent in chemical make-up and would be ideal for separation into two valuable output streams: the aromatic BTX fraction, and the aliphatic liquid transport fuels, as described in the previous chapter. A similar, if slightly slower, deactivation and processing ability would be expected at 400°C given the relative similarity observed between these two temperatures. That 450°C is the optimal temperature for the liquid transport fuel production is reinforced when the yield of condensed product is considered, which is greatest at this temperature.

Over the long term, however, the value of the catalytic microwave-assisted pyrolysis process is tempered by the deactivation of the activated carbon and its inability to produce a consistent output product. In the 450°C case, after the activated carbon has processed approximately three times its mass of HDPE, heavier aliphatics begin to

appear in the condensed product. These would require separating out from potential liquid transport fuel end products, increasing the expense of the overall process. The balance of desirable shorter chain molecules to heavier products steadily worsens as the activated carbon processes more HDPE. If the activated carbon bed required replacement every time after processing only three times its weight of HDPE, the process would be uneconomical: given the expense of activated carbon, its replacement cost alone would far outweigh the value of the products produced throughout its lifetime. A potential solution to this problem would be to maintain catalytic activity by regularly regenerating the activated carbon. This could potentially be undertaken *in-situ* in the reactor itself, a possibility explored in §7.2.4.

## 5.5 Analysis of Non-condensable Pyrolysis Gases

### 5.5.1 Chemical Composition

#### 5.5.1.1 Coke Bed

The compounds comprising the non-condensable gases produced using the non-catalytic coke bed in continuous mode are presented in table 5.4 on the next page. Alkenes are the most common class of compounds, in line with the non-catalytic breakdown of HDPE, these being the closest to the monomer from which HDPE is formed. Compared with the activated carbon case (below), alkanes, with a higher H/C ratio, are less likely to be present owing to the formation of far fewer catalytically derived “hydrogen freeing” aromatic species in the condensate.

#### 5.5.1.2 Activated Carbon Bed

Table 5.5 on page 129 presents the results of the GC/MS analysis of the non-condensable gaseous products produced using the activated carbon bed with a continuous input of HDPE. The gases are mostly linear alkanes and alkenes, the bulk of which have a carbon number between $C_2$–$C_4$. The primary factors determining the make-up of the non-condensable gases are the reaction temperature and the activity of the activated carbon, which influences cracking and, by altering the make-up of the larger condensed molecules into more or less hydrogen-dense forms, determines the quantity of atomic hydrogen “available” for the shorter chain gases as described in §4.6.2.

As the activated carbon deactivates, there is an increase in the average molecular

**Table 5.4:** Chemical composition of the non-condensable gases produced using a coke bed using a continuous input of HDPE. Figures are percent peak area derived from GC/MS analysis.

| Pyrolysis Temperature | 400°C | 450°C | 500°C | 600°C |
|---|---|---|---|---|
| **$C_1$** | **2.1** | **2.6** | **3.9** | **5.2** |
| Methane | 2.2 | 2.6 | 3.9 | 5.2 |
| **$C_2$** | **25.1** | **28.4** | **38.8** | **38.5** |
| Ethane | 7.9 | 8.4 | 9.0 | 7.1 |
| Ethene | 17.1 | 20.0 | 29.8 | 31.4 |
| **$C_3$** | **65.6** | **62.5** | **49.2** | **44.6** |
| Propane | 23.0 | 18.8 | 7.6 | 1.5 |
| 1-Propene | 42.7 | 43.6 | 41.6 | 43.0 |
| **$C_4$** | **6.7** | **6.1** | **8.1** | **11.4** |
| Butane | 2.3 | 1.7 | 0.6 | 0.3 |
| 1-Butene | 4.1 | 4.0 | 5.5 | 5.0 |
| 1-Propene, 2-methyl- | 0.3 | 0.0 | 0.2 | 0.9 |
| 2-Butene | 0.0 | 0.1 | 0.5 | 1.2 |
| 1,3-Butadiene | 0.0 | 0.3 | 1.3 | 3.9 |

mass of the non-condensable gases, with a decrease in the smaller gases (e.g, methane, ethane) and an increase in heavier $C_4$–$C_5$ gases. The proportion of hydrogen-rich alkanes also decreases as the activated carbon processes more HDPE, mirroring the decline of aromatic species in the condensed products, from which the hydrogen was freed that allowed the formation of gaseous alkanes in the first place. This shift is particularly evident in the shorter chain molecules of the non-condensable gases, as the hydrogen to carbon ratio necessary for the formation of alkanes increases drastically as the chain length reduces. Overall, as the activated carbon bed processes more HDPE the non-condensable gases produced show a steady convergence towards those produced using a coke bed (in terms of alkene:alkane ratio, average molecular mass, and relative proportion of species). $C_4$ compounds are more prevalent in the activated carbon produced gases, the primary component of which is butane; however, it may be that these compounds decline to the levels seen in the coke produced bed as the activated carbon becomes more inert — there is evidence of a decline in the sum total of $C_4$ compounds in the last captured data point at all operating temperatures.

Generally as the reaction temperature increases, greater cracking results in the gases having a lighter average molecular mass, though this becomes more evident as the activated carbon deactivates and pure thermal cracking becomes dominant over catalytic effects.

**Table 5.5:** Composition of non-condensable gases produced using an activated carbon bed using a continuous input of HDPE. All figures are percent peak area derived from GC/MS analysis. Representative selected runs are presented for comparative purposes as the beds have processed more HDPE (*HDPE/Bed Mass* = mass fraction of HDPE to that of the bed).

| Pyrolysis Temperature | 400°C | | | | 450°C | | | | | | 500°C | | | 600°C | | |
|---|---|---|---|---|---|---|---|---|---|---|---|---|---|---|---|---|
| HDPE/Bed Mass | 0.45 | 1.18 | 1.42 | 1.91 | 0.50 | 0.99 | 1.95 | 3.36 | 4.78 | 6.91 | 0.49 | 0.97 | 1.43 | 0.47 | 0.86 | 1.33 |
| **$C_1$** | **5.5** | **4.1** | **4.1** | **4.7** | **5.6** | **5.7** | **4.9** | **3.1** | **3.2** | **2.1** | **12.9** | **8.4** | **6.0** | **13.0** | **9.1** | **6.4** |
| Methane | 5.5 | 4.1 | 4.1 | 4.7 | 5.6 | 5.7 | 4.9 | 3.1 | 3.2 | 2.1 | 12.9 | 8.4 | 6.0 | 13.0 | 9.1 | 6.4 |
| **$C_2$** | **19.8** | **17.7** | **11.3** | **10.8** | **32.1** | **35.0** | **25.8** | **20.3** | **18.9** | **19.1** | **33.5** | **20.9** | **20.6** | **26.1** | **24.1** | **27.9** |
| Ethane | 16.3 | 15.3 | 8.9 | 7.7 | 28.1 | 28.9 | 22.2 | 16.1 | 13.8 | 8.9 | 24.8 | 14.2 | 12.0 | 9.3 | 10.9 | 8.8 |
| Ethene | 3.5 | 2.4 | 2.3 | 3.1 | 4.0 | 6.1 | 3.6 | 4.2 | 5.2 | 10.2 | 8.7 | 6.8 | 8.5 | 16.8 | 13.3 | 19.1 |
| **$C_3$** | **53.8** | **51.2** | **48.1** | **56.9** | **51.3** | **52.5** | **53.3** | **50.6** | **50.6** | **58.1** | **42.0** | **44.6** | **48.8** | **41.2** | **43.3** | **42.0** |
| Propane | 43.1 | 41.9 | 39.0 | 45.4 | 40.4 | 36.9 | 38.7 | 31.6 | 29.7 | 23.8 | 18.8 | 21.3 | 24.0 | 9.8 | 10.4 | 4.9 |
| 1-Propene | 10.7 | 9.3 | 9.1 | 11.5 | 10.9 | 15.5 | 14.6 | 19.0 | 20.9 | 34.2 | 23.2 | 23.2 | 24.8 | 31.4 | 32.9 | 37.1 |
| **$C_4$** | **20.9** | **27.0** | **36.1** | **26.8** | **9.3** | **6.0** | **14.8** | **23.4** | **24.1** | **16.8** | **11.6** | **24.6** | **20.3** | **17.7** | **21.7** | **19.3** |
| Butane | 17.1 | 23.9 | 29.4 | 20.9 | 7.0 | 4.6 | 9.8 | 14.5 | 14.3 | 8.2 | 6.7 | 9.7 | 8.4 | 3.1 | 3.6 | 1.3 |
| 1-Butene | 1.4 | 3.1 | 4.0 | 2.9 | 0.4 | 0.4 | 2.1 | 3.4 | 7.7 | 4.4 | 4.9 | 7.0 | 6.0 | 6.5 | 8.3 | 9.3 |
| 1-Propene, 2-methyl | 0.0 | 0.0 | 0.0 | 0.9 | 1.4 | 0.9 | 2.9 | 5.5 | 2.7 | 4.2 | 0.0 | 6.3 | 1.9 | 0.0 | 0.0 | 1.9 |
| 2-Butene | 2.4 | 0.0 | 2.7 | 1.4 | 0.0 | 0.0 | 0.0 | 0.0 | 0.0 | 0.0 | 0.0 | 0.0 | 2.9 | 3.5 | 4.8 | 1.3 |
| 1,3-Butadiene | 0.0 | 0.0 | 0.0 | 0.0 | 0.0 | 0.0 | 0.0 | 0.5 | 0.0 | 0.6 | 0.0 | 0.0 | 0.0 | 3.9 | 4.9 | 5.6 |
| Propane, 2-methyl- | 0.0 | 0.0 | 0.0 | 0.7 | 0.5 | 0.0 | 0.0 | 0.0 | 0.0 | 0.0 | 0.0 | 0.0 | 0.0 | 0.7 | 0.0 | 0.0 |
| Cyclobutene | 0.0 | 0.0 | 0.0 | 0.0 | 0.0 | 0.0 | 0.0 | 0.0 | 0.0 | 0.0 | 0.0 | 1.5 | 1.2 | 0.0 | 0.0 | 0.0 |
| **$C_5$** | **0.0** | **0.0** | **0.5** | **0.8** | **1.7** | **0.8** | **1.2** | **2.1** | **2.6** | **3.3** | **0.0** | **1.4** | **4.3** | **2.0** | **1.8** | **4.4** |
| Pentane | 0.0 | 0.0 | 0.5 | 0.8 | 1.3 | 0.8 | 1.2 | 1.6 | 2.6 | 1.5 | 0.0 | 1.4 | 3.1 | 2.0 | 1.8 | 3.6 |
| 1-Pentene | 0.0 | 0.0 | 0.0 | 0.0 | 0.0 | 0.0 | 0.0 | 0.5 | 0.0 | 1.2 | 0.0 | 0.0 | 1.2 | 0.0 | 0.0 | 0.8 |
| Cyclopropane, 1,2-dimethyl- | 0.0 | 0.0 | 0.0 | 0.0 | 0.0 | 0.0 | 0.0 | 0.0 | 0.0 | 0.5 | 0.0 | 0.0 | 0.0 | 0.0 | 0.0 | 0.0 |
| 2-Pentene | 0.0 | 0.0 | 0.0 | 0.0 | 0.4 | 0.0 | 0.0 | 0.0 | 0.0 | 0.0 | 0.0 | 0.0 | 0.0 | 0.0 | 0.0 | 0.0 |

### 5.5.2 Economic Value of Non-Condensable Gases

The non-condensable gases produced with the continuous pyrolysis of HDPE consist of simple alkanes and alkenes, with similar chemical composition to those produced in batch mode, and as such retain the same economic potential in terms of use as chemical feedstock (including for the synthesis of virgin HDPE) and combustion fuels (see §4.9.2). Indeed, the non-condensable gases by definition encompass a much smaller range of molecular masses and compounds, and furthermore comprise a smaller subset of types of hydrocarbon (aromatics, for example, cannot be present owing to the molecules containing too few carbon atoms to form these rings). There is therefore less variation in the make-up of the non-condensable gases in spite of potentially significant underlying changes in bed activity. What variation does exist would not present any barriers to their utilisation (unlike, for example, the longer chain liquid hydrocarbons that result when the activated carbon deactivates).

Given the added expense of separating out higher mass aliphatics and aromatics from any potential liquid fuel product (produced using a coke bed or activated carbon bed after it has partially deactivated), the natural (and thus free) phase separation ability of molecules in the gaseous state, the greater uniformity of their chemical composition, and the still substantial economic value of these resulting gases, it may be possible to alter the production focus of the pyrolysis process and optimise it such that hydrocarbon gases are the primary targeted product. This possibility is discussed in depth as a potential course of further study in §7.2.6.2.

## 5.6 Temperature Dependence of Rate of Change of Catalytic Activity

From the analysis of the pyrolysis products presented in this chapter thus far, it is clear that activated carbon deactivates relatively quickly when used in the microwave-assisted pyrolysis of HDPE, but further, that this deactivation process itself is highly temperature dependent: the change in yields and composition of the pyrolysis products at 500°C and 600°C is far more rapid than that which occurs at 400°C and 450°C. Assuming the deactivation derives from coking of the pores and/or active sites of the activated carbon, it may be that the dehydrogenation or equivalent process that drives this coke formation has an activation energy that causes it to rapidly increase in rate when this energy threshold is reached. This would explain the large change

in deactivation rate over the relatively small temperature change between 450°C and 500°C. A full investigation into the nature of the molecular changes in the activated carbon accompanying the change in output pyrolysis products, the catalytic consequences of these changes, and the effect of reaction temperature on the rate of these changes is given in the following chapter.

## 5.7 Batch and Continuous Operation Comparison

The development of the continuous rotary feeder allowed the investigation of microwave-assisted pyrolysis operating in continuous throughput mode as outlined thus far in this chapter. The results of the previous chapter, using the same procedure and apparatus operating in batch mode, present an opportunity to compare the characteristics and product differences between the two modes of operation. Given that the catalytic nature of the activated carbon bed dramatically impacts on the outputs, and varies depending on its state of deactivation, the bulk of this comparison focuses on data generated using the coke bed, though where relevant conclusions can be drawn, the impact of the differences in addition mode when using activated carbon is also detailed.

### 5.7.1 Coke Bed Yields

Significant differences in yields were observed between pyrolysis using batch injection and a continuous feed of HDPE. When operating with a continuous feed, the maximum yield of condensed products (84.1% at 450°C) is approximately 15% higher than when operating in batch mode (69.0% at 450°C). A similar deviation was observed in the maximum non-condensable gases yield (81.5% vs. 68.6% continuous and at batch respectively at 600°C). At low temperatures relatively more cracking of the HDPE occurred in the batch mode compared to continuous, but at high temperatures the reverse was true, and more cracking occurred in the continuous mode. Overall then, the difference in yields attributable to reaction temperature was considerably larger when HDPE was added in a continuous fashion.

### 5.7.2 Chemical Composition of Products Produced using Coke Bed

The chemical composition of the condensed products is broadly similar between batch and continuous modes, consisting almost entirely of linear alkanes and alkenes.

**Table 5.6:** Comparison between condensed product properties produced in batch and continuous reactor modes with a coke reactor bed. Yields of condensed products and non-condensable gases are given, along with the average molecular mass (MW) and standard deviation (SD) of the condensed products and overall molecular mass of all combined pyrolysis products as an indicator of overall cracking.

| | Batch | | | | Continuous | | | |
|---|---|---|---|---|---|---|---|---|
| | 400°C | 450°C | 500°C | 600°C | 400°C | 450°C | 500°C | 600°C |
| Condensed (% wt.) | 59.1 | 69.0 | 42.0 | 31.4 | 80.4 | 84.1 | 52.5 | 18.2 |
| Non-condensable Gases (% wt.) | 38.9 | 30.0 | 58.0 | 68.6 | 19.5 | 15.9 | 47.5 | 81.5 |
| Overall Average MW (g $mol^{-1}$) | 221.4 | 330.2 | 213.6 | 155.0 | 228.4 | 258.9 | 193.5 | 89.1 |
| Condensed Product MW (g $mol^{-1}$) | 351.1 | 462.4 | 456.2 | 418.4 | 274.6 | 300.6 | 335.4 | 325.7 |
| Condensed Product SD (g $mol^{-1}$) | 204.7 | 189.7 | 198.4 | 203.4 | 127.1 | 141.4 | 182.2 | 199.0 |

However, at reactor temperatures of 500°C and over, the condensate produced in the continuous mode diverges, with aromatic and cyclic species becoming prevalent (14% and 25% at 500°C and 600°C in continuous mode vs. 2–4% throughout the batch mode).

#### 5.7.2.1 Molecular Mass Distribution and Heavy Aliphatic Grouping

The average molecular mass of all combined pyrolysis products (i.e., both condensed and non-condensable gases) is the best indicator of how much cracking of the input HDPE has occurred over the course of an experimental run. As seen in table 5.6, which compares batch and continuous modes, it is clear that at temperatures of 450°C and above the pyrolysis products produced in batch mode are significantly heavier on average (and thus have undergone less cracking) than those produced in continuous mode. Furthermore, the spread of the pyrolysis products' molecular masses is significantly greater in the batch regime for any given reaction temperature. A significant proportion of this difference derives from the grouping of heavier aliphatic compounds, which in batch mode are both more numerous, and longer in chain length (this group having a mode of around $C_{45}$ in batch configuration compared with $C_{36}$–$C_{40}$ in the continuous equivalent).

### 5.7.3 Residence Time Differences due to Pyrolysis Rate and Exit Pressure

The fact that the pyrolysis products produced with a continuous input of HDPE have undergone more cracking than those produced with a batch input can be explained by considering the pyrolysis rates and residence times of the respective sample introduction modes. The egress of pyrolysis products from the reactor is primarily driven by phase change volume expansion of the products themselves as they change from solid to gas. With the bulk introduction of sample at higher reactor temperatures,

an initial sudden "explosive" rush of pyrolysis gases was observed entering the condenser soon after the HDPE was added to the reactor, which then tailed off over time. Here, the large quantity of introduced material is rapidly pyrolysed and converted to gaseous form, which expands and provides a large driving pressure differential forcing gases out of the reactor ("exit pressure"). As the mass of material present in the reactor declines, the absolute rate of conversion to the gaseous state declines, and so does the driving force causing pyrolysed material to leave the reactor. This effect was reduced when operating at 400°C in batch mode, while with the continuous addition of HDPE, the rate of pyrolysis gas entering the condenser was relatively constant, and no initial high-velocity "explosive exit" occurred.

#### 5.7.3.1 Simplified Mathematical Model of Input Modes

These observations are perhaps best explained using a simple mathematical model of the kinetics of the different addition scenarios. Assuming the pyrolysis of HDPE follows first-order kinetics, i.e., the rate of pyrolysis is proportional to the amount of sample in the reactor (an approximation used by other researchers [46, 226]), then in batch mode the pyrolysis process can be modelled by:

$$\frac{dH}{dt} = -k(T).H$$

where $H$ is the amount of HDPE in the reactor, $t$ is time, and $k$ is the reaction rate constant (itself primarily dependent on reaction temperature ($T$), and often empirically modelled using the Arrhenius equation [212, 227]). Separating variables and integrating gives:

$$H = H_0 e^{-kt}$$

Thus an initial batch injection of HDPE gives an exponentially declining pyrolysis rate, and an equivalently declining exit force and residence time. Assuming the same kinetics, but with the continuous addition of HDPE sample gives:

$$\frac{dH}{dt} = -k(T).H + A$$

where $A$ is the rate at which sample is added to the reactor. By examining the steady state configuration it is clear that the pyrolysis rate is limited by (and at steady state equal to) the rate of sample addition.

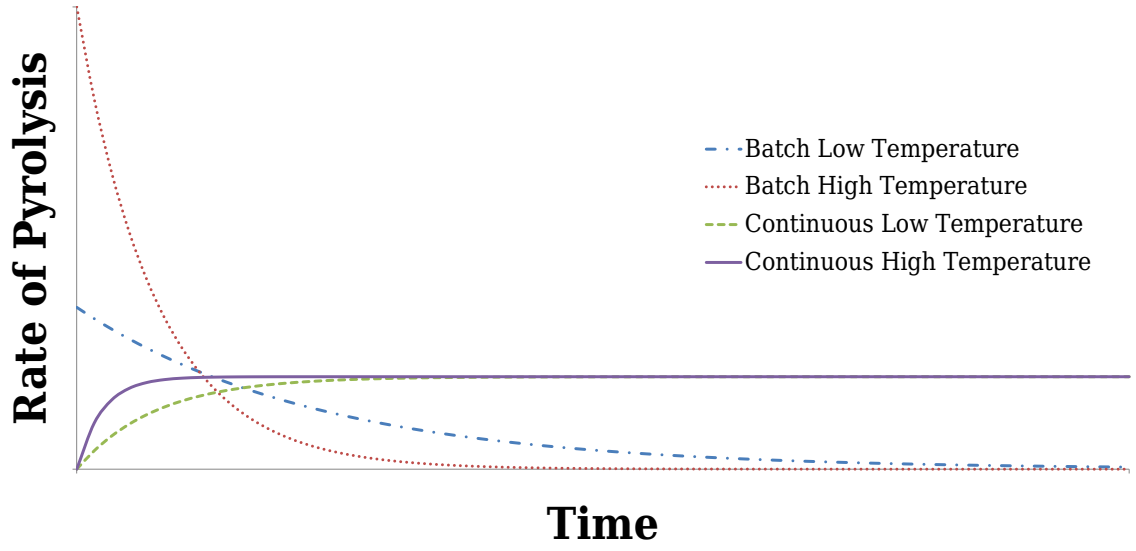


**Figure 5.8:** Examples of theoretically derived pyrolysis rates in batch and continuous modes at high and low reaction temperatures.

Figure 5.8 uses the above equations and compares the resulting overall pyrolysis rate under demonstrative high and low temperature configurations between a single initial batch introduction of sample and continuous addition scenarios. With the continuous addition of sample, independent of temperature, the pyrolysis rate quickly stabilises to the rate of HDPE addition. It is worth noting that even though the pyrolysis rate stabilises to the same value regardless of temperature, the residence time will still have a temperature-dependent component, with a longer residence time at lower temperatures (and a greater mass in the reactor at any given time).

With batch addition, in the high temperature case (demonstrating the scenario likely occurring when the reactor operates at 450°C and above), the larger reaction rate constant, and the large initial mass of HDPE present, results in a high initial pyrolysis rate, which would in turn result in a short residence time for the period in which the majority of the HDPE is pyrolysed, as large quantities of gas are produced and forced out of the reactor by volume expansion. In this scenario the low residence time results in less cracking compared with the continuous addition of sample, where there is a lower average rate of pyrolysis, longer residence time, and ultimately greater cracking of the HDPE.

In the low temperature case (corresponding to the 400°C, where operating temperature approaches the threshold of pyrolysis), with a smaller corresponding value for the reaction rate constant, the pyrolysis rate is much slower, and undergoes slower decay, potentially remaining below that of the continuously fed case for much of the experimental run. As such, in spite of the larger amount of sample present in the

reactor in the batch case, the production of pyrolysis gases is still relatively slow, and they create less exit pressure to force themselves out of the reactor, and thus have a longer residence time. So with a slow reaction rate at lower temperatures, the batch mode results in a longer residence time and greater cracking, with a greater yield of non-condensable gases and less condensed products compared with continuous addition.

Not only does this account for the observed differences in cracking, but a second consequence of the different HDPE addition modes is that while the reaction rate and residence time quickly stabilise in the continuous addition case, they are very variable over the course of an experimental run in the batch mode, with the exponential decay resulting in a long slow rate tail, in contrast to the initial high reaction rate upon sample addition. The distribution of the molecular masses for the respective products resulting from these two addition modes should therefore show significant differences at the same operating temperature, and indeed this is the case. As seen in table 5.6, at any given reaction temperature the range of molecular masses of the condensed products produced using a coke bed is considerably larger in batch mode compared with those produced in the continuous mode.

#### 5.7.3.2 Effect of Residence Time on Chemical Composition of Pyrolysis Products

Differences in residence time are also able to account for some of the observed differences in chemical composition between the two reactor modes. In the continuous mode at reactor temperatures of 500°C and above, significant quantities of aromatic species were observed in the condensate; these are only present in very small amounts in the condensate produced in batch mode. The formation of aromatics in the pyrolysis of hydrocarbons is dependent on both temperature and time: the pyrolysis of decane by Cypres [228] did not yield any aromatic species below 700°C with a 2 s contact time, but with increasing contact time the minimum formation temperature decreased and quantity of aromatic species increased. The described short residence time in batch mode for the majority of HDPE processed, would, at the operating temperatures investigated, explain the lack of aromatic species observed in the resulting condensed products. In the tail of the exponential decay of the pyrolysis rate, as the amount of HDPE in the reactor declines and the residence time increases, the little hydrocarbon left may account for the small quantity of aromatics observed, though as the residence time increases, produced species are more likely to be non-condensable gases in any

case due to greater cracking. The longer average residence time resulting from the continuous mode would also allow for the formation of the observed aromatics at higher temperatures.

#### 5.7.3.3 Convective Transfer of Pyrolysis Aerosol Particles Owing to Exit Pressure

The exit pressure generated by the pyrolysis gases not only affects the residence time in the reactor, but also acts in part to determine which products are able to exit the reactor in the first place. At least some convective transfer of molecules from the reactor to the condenser must occur; this is evident from the presence of hydrocarbons up to $C_{55}$, which have boiling points of around 600°C, in the condensate, even when the reactor was operating at a temperature of 400°C. For an aerosol particle (i.e., a small drop of liquid or solid) to leave the reactor, a sufficiently large force must act upon it so that it can overcome gravity and escape. This force comes in the form of convection, where the particle has directional force imparted on it from the collective movement of the gaseous particles in which it is suspended towards the reactor exit. The greater the movement of gases (i.e., pressure derived from the pyrolysis induced phase change volume expansion of the HDPE), the greater convective force will be exerted, allowing particles with greater mass to overcome gravity and escape the reactor. Given the pyrolysis rate is much greater as the bulk of the HDPE is cracked into pyrolysis gas in batch mode, with the large introduction of HDPE to the reactor the convective transfer will also be greater during this period, with larger heavy-mass molecules able to be transferred, and in greater quantities. This is borne out by an examination of the mass distributions of the products produced in the different reaction modes: the grouping of heavier aliphatic compounds are both more numerous, and longer in chain length in batch mode compared with the continuous equivalent, and as a result the condensed products in batch mode are considerably heavier (see table 5.6).

### 5.7.4 Differences in Reaction Mode for Activated Carbon Studies

#### 5.7.4.1 Deactivation Across Batch Experimental Set

For the continuous mode experiments detailed in this chapter, a fresh bed of activated carbon was used at the start of each set of experiments for every reaction temperature studied. For the initial investigation in the batch mode, before it was clear that the

activated carbon deactivated relatively rapidly, the same bed was used across all the experiments (though the bed was fresh at the beginning of these). In spite of this, the relatively small mass pyrolysed in these experiments compared to the continuous case should mean that the change in catalytic activity across this set of experiments was relatively small.

A quick, highly qualitative evaluation of the processed masses involved supports this argument: each experiment in the batch mode involved 100 g of carbon; the first experiments at 400°C and 450°C would have seen little change in catalytic activity due to the slow rate of deactivation at these temperatures. The subsequent three experiments at 500°C, 550°C, and 600°C involved processing a total of 300 g of HDPE, a quantity approximately equal to the first data point gathered at each temperature in the continuous processing case. The results presented in this chapter (e.g. figure 5.1) indicate little change from baseline with this quantity of HDPE processed. The order of experiments (lowest temperature to highest) also helps to minimise the total deviation in catalytic activity from the virgin state. A quantitative theoretical exploration and validation of this concept is given in §6.5.4.1.

#### 5.7.4.2 Yield and Composition Differences

Comparing the pyrolysis products produced using the activated carbon bed in the batch mode with the first set of data at each temperature in the continuous mode reveals similar trends to those observed in the non-catalytic coke bed case. More cracking of the HDPE occurs in the continuous mode (with a greater yield of non-condensable gases, and a lighter condensed fraction), with a greater proportion of aromatic species present in the pyrolysis products. This is consistent with the faster pyrolysis rate and shorter residence time for the bulk of the HDPE pyrolysed in the batch mode as described above.

The reduced contact time resulting from the batch mode would also lower the extra catalytic cracking that occurs with activated carbon, accounting for the smaller quantity of aromatics, and mass (char) retained in the reactor in the batch case. This factor is also potentially exacerbated by the better mixing between HDPE and catalyst that would likely result from the slower continuous addition of sample. That the observed differences between the two sample addition modes result from the kinetics underlying these reaction modes, and not the deactivation of the activated carbon over the course of the batch runs, is supported by the fact that these differences were still

observed in the 400°C and 450°C cases, where the activated carbon would be in, or very close to, virgin condition.

## 5.8 Summary

The development of the continuous rotary feeder allowed the investigation of the microwave-assisted pyrolysis of HDPE in continuous throughput mode, facilitating the processing of an arbitrarily large quantity of sample — a necessary requirement in any realistic industrial scale-up of the process. This facility was then used to investigate the variability of the pyrolysis products produced over multiple experimental runs. For each temperature investigated, using the coke bed resulted in relatively consistent yields of pyrolysis products, with unchanging chemical composition. By contrast, with the activated carbon bed, dramatic changes in the pyrolysis products were observed over time, with the overall cracking reducing (resulting in less non-condensable gases and more condensed products) and the chemical composition changing (with fewer aromatics and more aliphatics produced over time). With a fresh activated carbon bed, a significant proportion of the input HDPE mass was retained within the reactor at the end of the experimental run. This accumulation of mass, the correlated loss of catalytic activity of the activated carbon bed, and the decrease in rate of accumulation as the activity of the bed itself declined, suggested the activated carbon was deactivated by coking. Indeed, it seems that activated carbon catalyses not only the cracking of hydrocarbon, but also its dehydrogenation, leaving a carbonaceous remainder that interferes with the catalytic ability of the bed.

The deactivation process itself was temperature dependent, though in a highly non-linear fashion, occurring very rapidly at temperatures of 500°C and above, but significantly slower at 450°C and below. At 450°C the bed was able to process around 3.5 times its own mass in HDPE before any significant changes in pyrolysis product composition were noticeable. The pyrolysis products were almost entirely unbranched aliphatic, and aromatic species, with the balance between the two changing over time: aromatics were observed in large quantities with virgin activated carbon, and these declined as the activated carbon deactivated. Using a coke bed the pyrolysis products were comprised almost entirely of linear aliphatics, up until the highest temperatures tested where aromatic species started to be produced. Generally, as more HDPE was processed by the activated carbon bed and it deactivated, the characteristics

of the pyrolysis products in terms of both molecular mass distribution and chemical composition tended towards those obtained when using the non-catalytic coke bed.

The differences arising from the batch and continuous addition of sample were investigated using the coke bed, in order to avoid the catalytic influence of the activated carbon which changed over time. While at 400°C slightly more cracking of HDPE occurred in batch mode, generally the average molecular mass across all pyrolysis products was less when operating in continuous mode, i.e., more cracking occurred with the continuous addition of sample. This was thought to result from different residence times arising from the fundamental kinetics underlying the two different addition modes, a conclusion supported by the development of a simple illustrative mathematical model using first order kinetics. The abrupt introduction of a large quantity of HDPE in the batch mode caused large quantities of pyrolysis gas to be rapidly produced; the resulting increase in volume from the solid to gas phase change rapidly forced pyrolysis gas from the reactor, decreasing residence time. While this declined exponentially as the quantity of HDPE remaining in the reactor also declined, the average residence time across a batch run was still shorter in all but the lowest temperature cases, resulting in the pyrolysis products undergoing less cracking compared to the continuous case, where the residence time was longer and quickly reached a steady state governed by the rate of introduction of sample.

While the condensed pyrolysis products resulting from the microwave-assisted pyrolysis of HDPE using an activated carbon bed in continuous mode initially all lay within the desirable molecular mass range suitable for use as liquid transport fuels, as the activated carbon deactivated heavier aliphatics began to form, with the bed able to process around 3.5 times its mass in HDPE before these became evident. The relatively rapid deactivation of the activated carbon, and the resulting inconsistency of the output products beyond this point, calls into question the economic feasibility of the overall process, unless an inexpensive method of reactivating the activated carbon could be found.

The in-depth examination of the pyrolysis products' yields and chemical composition revealed that while activated carbon is a useful catalyst in the microwave-assisted pyrolysis of HDPE, it deactivates relatively rapidly in continued use. Thus far, the data gathered on the catalyst itself has been indirect — resulting from examination of the products produced using the catalyst. In order to build up a more complete understanding of the catalytically assisted cracking, and the observed changes in the activated carbon's catalytic ability, it was next necessary to examine the activated

carbon itself. As such, the remainder of this work investigates the catalytic mechanisms of the activated carbon accounting for the differences in the pyrolysis process and produced products that have been outlined over the last two chapters, with a particular emphasis on the physical and chemical changes in the activated carbon over time that underlie its observed decline in catalytic activity.

# 6

# Mechanisms of Pyrolysis, Catalysis, and Deactivation

## 6.1 Introduction

Over the previous two chapters it has been established that pyrolysing HDPE over fresh activated carbon produces products with a considerably different chemical composition, and which are considerably more cracked, than those produced using a non-catalytic bed. This was achieved by first establishing that this difference existed at all (chapter 4), and then by attempting a more detailed characterisation by processing larger quantities of HDPE in a continuous input mode (chapter 5), during which time it became clear that the activated carbon deactivated as this process continued, with the resulting pyrolysis products gradually approaching the non-catalytic coke bed profile over time as this occurred. Having investigated the activated carbon catalysed pyrolysis of HDPE in some depth, and detailed the changes in the carbon bed and pyrolysis products (the “what”), it was then necessary to investigate the causes of these

changes and the mechanisms that underlie them (the “why” and “how”).

This chapter presents a set of plausible reaction pathways that are able to account for the species observed in the pyrolysis products; first, those produced with the non-catalytic coke bed; this is then followed by an attempt to establish reaction mechanisms and pathways for the catalytic case, deriving these from first principles from the known and observed structural characteristics of activated carbon.

A similar process is applied to understanding the mechanism underlying the deactivation of the catalyst, with a detailed examination of the changes in the activated carbon bed, and the physical, structural, and chemical properties of the retained fraction informing a thesis that accounts for the deactivation of the activated carbon over time.

## 6.2 Pyrolysis Reaction Mechanisms

Any discussion of the pyrolysis of HDPE would be incomplete without dealing with the reaction mechanisms that underlie its breakdown into smaller hydrocarbons. Accordingly, this section applies theory taken from the literature, and data gathered during the course of this work, to describe both the thermal and catalytically enhanced breakdown of HDPE into useful shorter chain hydrocarbon products.

### 6.2.1 Thermal Decomposition of HDPE

Thermal decomposition of HDPE proceeds via a free-radical mechanism, with much of the pioneering work developing the theory of radical-mediated decomposition of hydrocarbons undertaken by Rice and co-workers in the 1930s and ’40s [229–235]. The following summary applies the current working model of this theory to the decomposition of HDPE to account for the species observed in the pyrolysis products over the previous two chapters.

#### 6.2.1.1 Initiation

Beginning with an arbitrary HDPE segment:

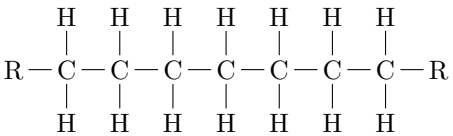

(6.1)

Initiation of the thermal degradation of HDPE occurs by random scission: decomposition of hydrocarbons occurs through the homolytic rupture of covalent C–C bonds, rather than C–H bonds, owing to the lower bond dissociation energy of the former (at 347 kJ/mol compared with 413 kJ/mol) [14, 229]. This results in the formation of two shorter hydrocarbon chains with free radical termini [230]:

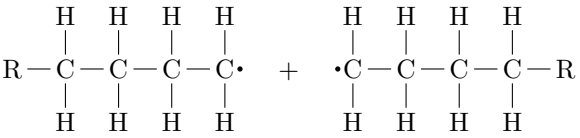

(6.2)

However, it has been shown that in an open reaction system where all pyrolysis gas is continuously removed as soon as it is produced, random scission alone is not able to reduce the molecular size of hydrocarbon molecules below approximately $C_{72}$. Below this point, the energy required to cleave the C–C polymer backbone is greater than that required to vaporise the molecule itself [236, 237]. Clearly other mechanisms are necessary to explain the further cracking of hydrocarbon These are thought to involve free radical hydrogen transfer reactions.

#### 6.2.1.2 Inter- and Intra-molecular Hydrogen Transfer

The probability that the two radicals produced in equation 6.2 collide again is negligibly small, therefore the free radicals produced in this way stabilise by reacting with themselves or surrounding hydrocarbon molecules [229]. This can occur through inter-molecular hydrogen transfer, where an atom of hydrogen is abstracted from a neighbouring molecule, forming a stable saturated alkane and a secondary radical in the middle of the neighbouring molecule:

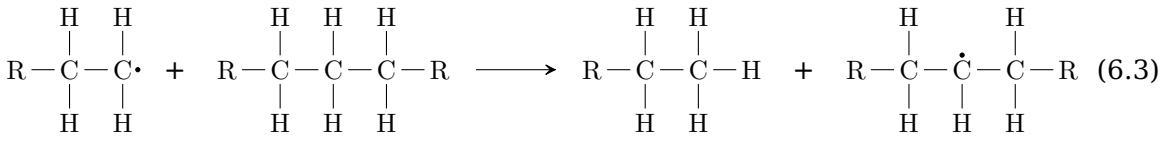

(6.3)

Alternatively, intra-molecular hydrogen transfer may occur (equation 6.4 on the next page), where the hydrocarbon backbone “coils back” to form a transient 5- or 6-membered ring intermediate [238], before free radical hydrogen transfer occurs between carbons in the terminal and 5th positions [239] (though 1,4- and 1,6-transfer are also possible [240]). These molecules may then undergo consecutive isomerisations, each time changing the position of the radical on the hydrocarbon

backbone — the likelihood of this phenomenon increases with the chain length as the polymer gains more “flex” [235].

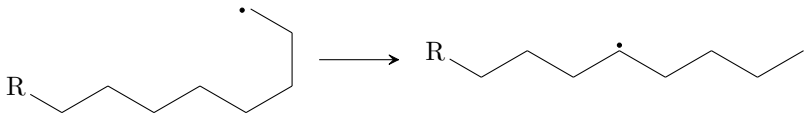


(6.4)

The secondary intra-molecular radicals formed through inter- and intra-molecular hydrogen transfer are thought to be considerably more stable than the terminal radicals formed initially by thermal scission, and the rates of both of these forms of free radical transfer are very fast in comparison with the rate of random scission [209, 241], accounting for the pyrolysis products having a mass less than the $C_{72}$ limit imposed by thermal random scission alone.

#### 6.2.1.3 Beta-scission

The intra-molecular radicals formed through inter- and intra-molecular hydrogen transfer most commonly stabilise through the process of beta scission [181, 235] (equation 6.5), forming two smaller hydrocarbons: a terminal alkene and a new terminal radical. This new terminal radical then initiates a new cycle of hydrogen transfer reactions, and the cracking process continues in a chain reaction fashion until the resulting molecules are sufficiently small that they enter the gaseous state and leave the hot zone of the reactor. When an existing alkene is attacked by a radical, an alkadiene and second radical results [242].

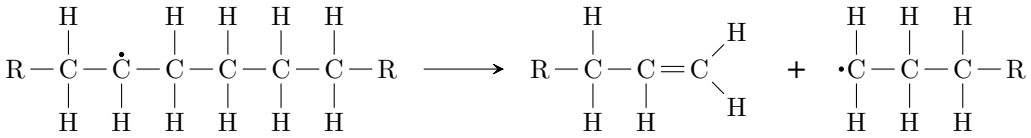

(6.5)

#### 6.2.1.4 Termination

The decomposition chain reaction can terminate with the recombination of two radicals to form an alkane:

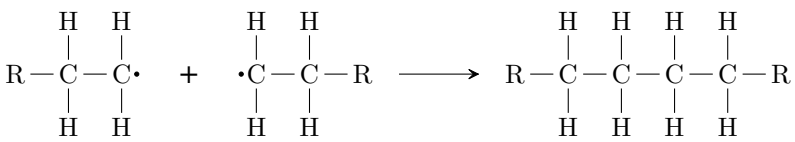

(6.6)

An alternative termination pathway is through disproportionation, resulting in an alkane and alkene [177]:

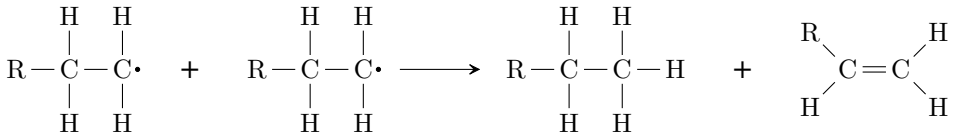


(6.7)

#### 6.2.1.5 Non-Catalytic Pyrolysis of HDPE

The reactions detailed thus far are thought to be the primary mechanisms for the pure thermal decomposition of HDPE. These reactions alone are able to account for the vast majority of species observed in the pyrolysis products produced using the non-catalytic coke bed, in particular the alkadiene (eq. 6.5), alkene (eq. 6.5, 6.7), alkane (eq. 6.3, 6.6, 6.7) triple peaks described in §4.5.2. Of the two hydrogen transfer mechanisms, intramolecular transfer is thought to dominate, especially at higher temperatures, owing to the hydrogen-rich nature of the HDPE polymer backbone, and the flexibility of the C-C bonds.

The activation energy of beta-scission is higher than both the hydrogen transfer and the termination reactions. The proportion of beta-scission reactions will therefore increase with reaction temperature [173]; this accounts for the observed distribution of alkenes and alkanes in the pyrolysis products, particularly the temperature-dependent increase in alkene prevalence.

### 6.2.2 Cyclic and Aromatic Formation

#### 6.2.2.1 Diels-Alder Reactions

The formation of aromatic and cyclic compounds has traditionally been ascribed to Diels-Alder reactions [228, 243], schematically shown in figure 6.1 on the following page. In this thermally driven cyclo-addition reaction, a conjugated alkadiene and alkene react to form a substituted cyclohexene intermediate. In conventional Diels-Alder reactions the aromatic then forms from successive dehydrogenation, or loss of substituted groups, from the cyclic alkene; this dehydrogenation is likely to occur at least in part through the hydrogen transfer mechanisms already outlined, given the large number of radicals that will be present at pyrolysis temperatures in the reactor.

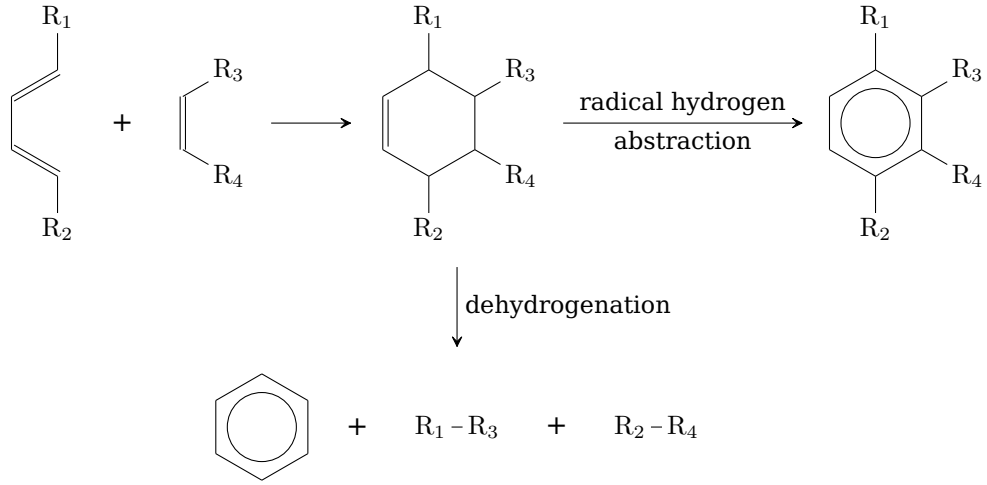


**Figure 6.1:** The formation of aromatic species through the Diels-Alder reaction. In traditional Diels-Alder the aromatic species forms by consecutive dehydrogenation of the cycloalkene, though this can also occur through radical-mediated hydrogen abstraction, leaving the functional groups attached to the benzene ring.

Equation 6.8 presents a specific example of the generic reaction presented in figure 6.1, giving the formation of toluene, the most common aromatic observed in the pyrolysis products:

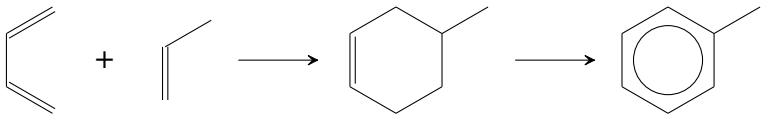


(6.8)

In this reaction, toluene is produced from 1,3-butadiene reacting with propene; the four hydrogen atoms could be abstracted from the cyclohexene ring by radicals, but this reaction is unlikely to proceed through bi-molecular recombination as no molecular hydrogen was observed in the produced non-condensable gases. The concentration of 1,3-butadiene observed in the pyrolysis gas produced using a coke bed increases with temperature, correlating with the concentration of aromatics observed in the condensed products. More generally, this scheme is representative of the class of reactions that is able to account for the bulk of aromatic species observed: benzene rings with variable length substituted alkyl groups. The terminal alkene reactants required for this pathway are produced through the beta-scission mechanism already outlined. In the case of longer alkene reactants, the resulting longer alkyl groups would not be immune to further cracking and radical attack for as long as they were present in the reactor. However, the methyl group in the toluene structure is largely immune to this form of attack, as stabilisation of any radical that forms here, other than by hydrogen abstraction back to the methyl group, requires the disruption of the benzene

ring — a process with a considerably higher activation energy than maintaining the methyl group; this accounts for the stability of the toluene molecule and its status as the most abundant aromatic species observed in the pyrolysis products.

#### 6.2.2.2 Radical-Mediated Aromatic Formation

More complex radical-mediated mechanisms are also likely to result in the formation of aromatic species, and indeed these pathways may represent the dominant mode of aromatic formation. However, defining these exact reaction pathways is an area of ongoing research, with a multitude of possible mechanisms proposed to explain aromatic ring formation. Many of these pathways are bimolecular, deriving from the combination of short-chain alkenes in the gaseous state, though mono-molecular pathways are also posited, where a terminal radical coils back and reacts intra-molecularly [244–247]. Equation 6.9 presents a simple example of cyclisation and aromatisation derived from a terminal alkene and radical [14]; the existence of these initial reactants is easily explainable using the mechanisms already discussed.

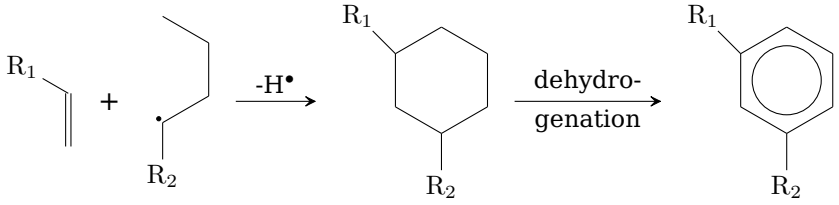


(6.9)

Indeed, given the stochastic decomposition of long-chain hydrocarbons, and the plethora of species that result, it is unlikely that formation of aromatic species is limited to any one particular scheme. It is worth noting, though, that some of these schemes offer alternative radical stabilisation and chain reaction termination pathways to those detailed in §6.2.1.4. Given the complexity, uncertainty, and preponderance of these secondary pathways, cataloguing them lies outside the scope of this work, though the interested reader is directed toward a comprehensive review by Richter and Howard [248], which covers some of these schemes.

## 6.3 Catalytic Activity of Activated Carbon

From the lighter molecular masses and different chemical make-up of the pyrolysis products produced using an activated carbon bed, it is clear that the cracking of HDPE occurs more rapidly, and with altered pathways, compared with the use of a non-catalytic coke bed. The mechanism of activated carbon catalysis of hydrocarbons

(in isolation, and not as a support material in conjunction with, e.g., metal ions) is generally not well characterised, and suffers from conflicting evidence in the literature. While the elucidation of a complete catalytic mechanism for activated carbon is beyond the scope of this work, the subject does bear discussion. As such, several different possible mechanisms accounting for the observed catalytic activity of activated carbon, when used in a microwave-heated environment, are presented below. The mechanisms discussed here are by no means mutually exclusive, and indeed it is quite possible that they act together in concert to produce the cracking and product profile observed when using the activated carbon bed.

### 6.3.1 Catalytic Cracking Reaction Mechanisms

While carbon is usually thought of as an inert material, the surface of activated carbon has a number of active sites, deriving from unsaturated valencies at the edges of graphene layers, heteroatoms, and defects within the graphene structure. The quantity of all of these kinds of active sites increases with the surface area and porosity of a sample [52], and these sites are likely to underpin activated carbon's catalytic ability, with the activity of carbon catalysts linearly correlating with the concentration of these surface groups [38].

#### 6.3.1.1 Microporous Structure

The very microporous structure of the activated carbon itself is also likely to play a role in the catalytic activity observed in the formation of the described pyrolysis products, with micropores themselves showing an ability to stabilise free radicals, and promote bimolecular reactions in the pore space (such as the radical mediated formation of aromatic species described previously) [249–251].

#### 6.3.1.2 High Energy "Defect" Sites Facilitating Hydrogen/Radical Transfer

Greensfelder et al. [252] theorised that the high surface area of the activated carbon acts to abstract hydrogen from hydrocarbons (generating radicals), and return hydrogen to free radicals. In other words, the activated carbon acts as a catalyst to reduce the activation energy of hydrogen and radical transfer reactions. While Greensfelder et al. proposed no mechanism for this transfer to occur, a possibility arises when the structure of activated carbon is considered. Semi-amorphous, "disordered" carbons such as activated carbon consist of layers that exhibit short-range hexagonal

graphene lattice structure, but with the “defective” remaining structure resulting in folds, discontinuities, and irregular morphology, from which the 3D structure of the pores derives [52].

The defects in the graphene structure, with the associated disruptions in the regular array of carbon bonds, result in a range of energetic abnormalities such as unsaturated and “free” valencies, including unpaired and/or delocalised electrons [36, 39]. These high energy sites may act to donate or accept electrons (radical transfer) and/or hydrogen (on to and from free valencies). Certainly, the disrupted lattice as described would be able to accept and donate these species far more readily than a fully saturated graphene lattice. Indeed, it is widely accepted that the more disorder present in a carbonaceous material, the greater the exhibited catalytic activity [119, 120, 253], i.e., it is the structural disorder in the form of high energy active sites and pores from which the catalytic activity of carbonaceous materials derives. The boundary cases of highly ordered graphite, diamond powder, and carbon nanotubes show little to no catalytic activity (the edge area of graphite where unsaturated carbon atoms occur is small compared with the basal plane, which in any case does not exhibit the defects discussed), while amorphous “glassy” carbon shows catalytic activity (though its smaller surface area compared with activated carbon makes it overall a less effective catalyst per unit mass) [39].

By acting as a hydrogen and/or radical acceptor/donor/transfer agent, the activated carbon lowers the activation energy for the reactions that are mediated by these mechanisms, speeding them up considerably. In this method, then, dissociative adsorption of hydrocarbons on high energy active sites occurs with an initial adsorption of a molecule onto the surface of the active site, arising from intense van der Waals forces owing to the near proximity of multiple carbon atoms. Cracking initiation, or transfer reactions (by which chain reaction propagation occurs), are then facilitated by the proximity of the hydrocarbon to the high energy sites, which reduce the activation energy of electron/hydrogen transfer. Given the van der Waals forces holding the hydrocarbon to the activated carbon surface, it is likely to maintain physical contact for sufficient time to effect intra-molecular transfer (with a conformation change or small movement in the hydrocarbon molecule); alternatively, the hydrocarbon may desorb, with another molecule taking its place, facilitating a potential future intra-molecular transfer. A final possibility is the molecule progressing from physisorption of the hydrocarbon to chemisorption, with the molecule bonding to the basal structure of the catalyst; this would also present a consistent mechanism for deactivation and

elimination of these high energy sites, the possibility of which is explored further in §6.9.

It is acknowledged that the detailed mechanism for this catalysis is complex and requires significant additional research before it is completely characterised and understood. However, this theory is consistent with the current knowledge of the structure of activated carbon, and with the products of activated carbon mediated catalytic cracking of HDPE observed in this work.

#### 6.3.1.3 Accounting for Activated Carbon Product Spectrum by Catalytic Mechanism

The major differences between the products produced using the activated carbon bed and the coke bed are the increase in total cracking, and the increase in the proportion of aromatic species. From the mechanisms and research outlined above, it is clear that activated carbon catalyses dehydrogenation [99], which is a central requirement in the formation of aromatics through the mechanisms discussed. Generally, aromatic species are highly stable products, but which have a relatively large activation energy for the formation from aliphatics. The catalysis of hydrogen and radical transfer would lower this activation energy considerably and allow the formation of aromatics as a stable end product, and the consequent higher production of alkanes owing to the "freed" hydrogen. More generally, an across-the-board enhancement of the radical and hydrogen transfer mechanisms discussed in §6.3.1 would account for the overall greater cracking observed when the catalytic activated carbon bed was used.

#### 6.3.1.4 Oxygen Active Sites and Acid-Activated Catalysis

The presence of heteroatoms within the carbon lattice (e.g., oxygen, hydrogen, and nitrogen) also introduces active sites into the activated carbon structure. Of these, oxygen active sites are thought to play by far the largest role in catalysis, providing acid sites that are able to crack molecules through acid-activated catalysis [36]. This process (using different catalysts such as zeolites) underpins fluid catalytic cracking (FCC), one of the most important processes in the petrochemical industry, which is used to convert high molecular weight hydrocarbons into more valuable lighter products. Acid catalysis involves the transfer and acceptance of protons, as originally outlined by Whitmore [254] (with contemporary mechanistic theory summarised by Corma and Orchilles [255], and Cumming and Wojciechowski [256]), as opposed to the radical-based mechanisms proposed thus far.

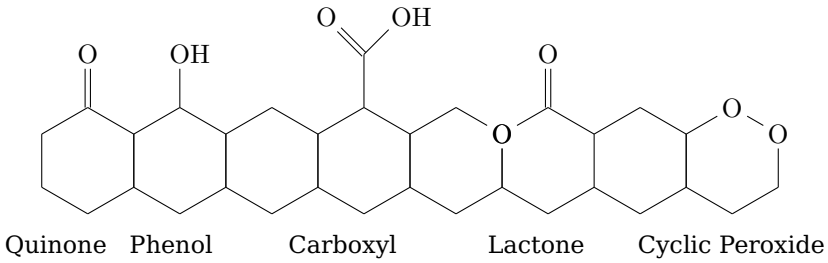


**Figure 6.2:** Some oxygen-based functional groups present on the surface of activated carbon. Adapted from [36].

Oxygen-based surface active sites in activated carbon may arise from the original oxygen-containing source material from which the activated carbon is derived, through the presence of oxidising species during activating treatment or post-treatment or, most commonly, oxygen may be chemisorbed onto high-energy sites on the surface of the activated carbon after exposure to oxygen-containing species in the atmosphere (e.g., $O_2$ or $CO_2$) [52]. At least some of these oxygen activate sites would still be present in the activated carbon even after the pre-treatment in inert nitrogen atmosphere at 700°C (these sites requiring temperatures greater than 1000°C before they are completely removed [52]).

Zawadzki [257] and Ishizaki and Marti [258] used infrared spectroscopy to identify oxygen sites on the surface of activated carbon; these included carboxylates, phenols, quinones, and lactones, though many different possible configurations for these oxygen active sites exist, some of which are presented in figure 6.2.

Szymanski and Rychlicki [114] presented evidence for the centrality of these oxygen-based surface active sites to activated carbon's catalytic ability by freshly preparing samples of activated carbon and treating them with hydrogen at 1223 K to remove any oxygen sites, then using this as a bed with which to dehydrogenate butan-2-ol. The activated carbon prepared this way showed little ability to catalyse this reaction. In contrast, activated carbon prepared in the same way but with an extra treatment of highly oxidising concentrated nitric acid effectively catalysed both dehydration and dehydrogenation.

Pereira et al. [38] identified carbonyl/quinone surface functional groups as responsible for the catalytic activity of activated carbon in the oxidative dehydrogenation of ethylbenzene by first introducing oxygen surface groups by treatment of activated carbon with oxygen gas, then selectively removing functional groups through progressive heating of the carbon to high temperatures. After heating to 1023 K, a temperature at which only carbonyl/quinone groups remained, the reaction remained catalysed. A further heat treatment to 1373 K removed all oxygen functional groups, after which the

reaction showed no difference compared with activated carbon that had not undergone the initial oxygen treatment.

It should be noted, however, that both of these studies involve either the decomposition of an oxygen-containing species, or the undertaking of a reaction in an oxygen-supplied environment, which may reflect an oxidative mechanism different from the pyrolysis considered in this work. There may also be differences in the functional groups of the activated carbon used in these experiments: functional groups formed on activated carbon in the presence of oxygen at high temperatures are significantly different from “conventional” activated carbon where any oxygen chemisorption occurs at room temperature [259–261]. Furthermore, in these studies the oxygenated active sites were artificially induced, either by treatment with oxygen gas or with nitric acid. Certainly, the acid sites created with nitric acid are significantly stronger than those evolving through reaction with oxygen present in the atmosphere [52], as occurs with conventional activated carbon. As such, the oxygen acid sites present in these samples may have resulted in additional catalytic ability over and above that naturally occurring in untreated activated carbon; this additional catalytic ability was then removed with heat treatment returning the carbon to the base state.

A contrasting perspective is presented by Muradov et al. [39], who removed oxygen-based surface functional groups from activated carbon by treatment with pure hydrogen at 1123 K, and noted only a small decline (of around 2% vol.) in the production of hydrogen from methane over this bed compared with the untreated equivalent. A far more significant drop in catalyst performance and reduction in yield (of around 40%) was observed over time, which correlated with the reduction in surface area of the carbon. Muradov et al. concluded that the catalytic activity of activated carbon could not be solely attributed to oxygen surface functional groups, and that the majority of catalytic activity derives from surface defects, dislocations, vacancies, and other high-energy sites as described previously.

Further evidence towards this conclusion was assembled by Petkovic et al. [123], who, while decomposing hydrogen iodide to produce hydrogen using an activated carbon catalyst, found no correlation between numbers of any particular type of acid site (i.e., carboxylic, lactonic, phenolic, etc) and catalyst activity across several different types of activated carbon tested. Indeed, the carbon with the highest measurable total acid sites displayed only intermediate catalytic activity in this context.

Acid catalytic cracking proceeds through proton transfer and the generation of intermediate carbenium ions, which typically result in high levels of isomerisation

and branched products [256]. The fact that these species were not observed in large quantities in the products produced from cracking HDPE with activated carbon in this work, suggests that the acid-catalysis pathway plays a smaller role in comparison to the radical mechanisms already outlined [252]. This is not to say that acid catalytic cracking does not occur at all, nor indeed, that surface oxygen active sites cannot act in non-acidic cracking as previously proposed: they are high energy sites in and of themselves; however, the evidence presented here indicates that it is unlikely that these high energy locales consist solely of oxygen-based active sites, and further suggests that activated carbon catalyses hydrocarbon cracking through a different, or at least an additional, mechanism to that of traditional commercial petrochemical acid-catalysts such as zeolite.

## 6.4 Microwave-Mediated Catalysis

### 6.4.1 Coupling to Free Radicals

Given their prominence in the pyrolysis process, free radicals will be present in abundance in the reactor as the breakdown of the HDPE occurs. As charged species, the microwave field will interact not only with the microwave intermediate bed but also with the radicals themselves as they are produced. The extra targeted energy imparted to these molecules by the microwave field may enhance the pyrolysis process, and contribute to further HDPE breakdown above that of a conventionally heated configuration; though in order to fully test this a direct comparison of the same reactor configuration with microwave and non-microwave heating sources would be required, as proposed in the further study possibilities presented in §7.2.1.

### 6.4.2 Generation of Microplasmas through Microwave Irradiation

While heating the activated carbon with microwaves, it was noticed that a plethora of small sparks were present within the bed (see figure 6.3 on the following page). These sparks, which have also been observed by other researchers [142–144] were of extremely short duration but were continually formed throughout all visible areas of the bed whenever it was irradiated by the microwaves. It is thought that these electrical discharges, or “microplasmas” were created by the interaction of the rapidly oscillating electromagnetic microwave field with the activated carbon bed, which

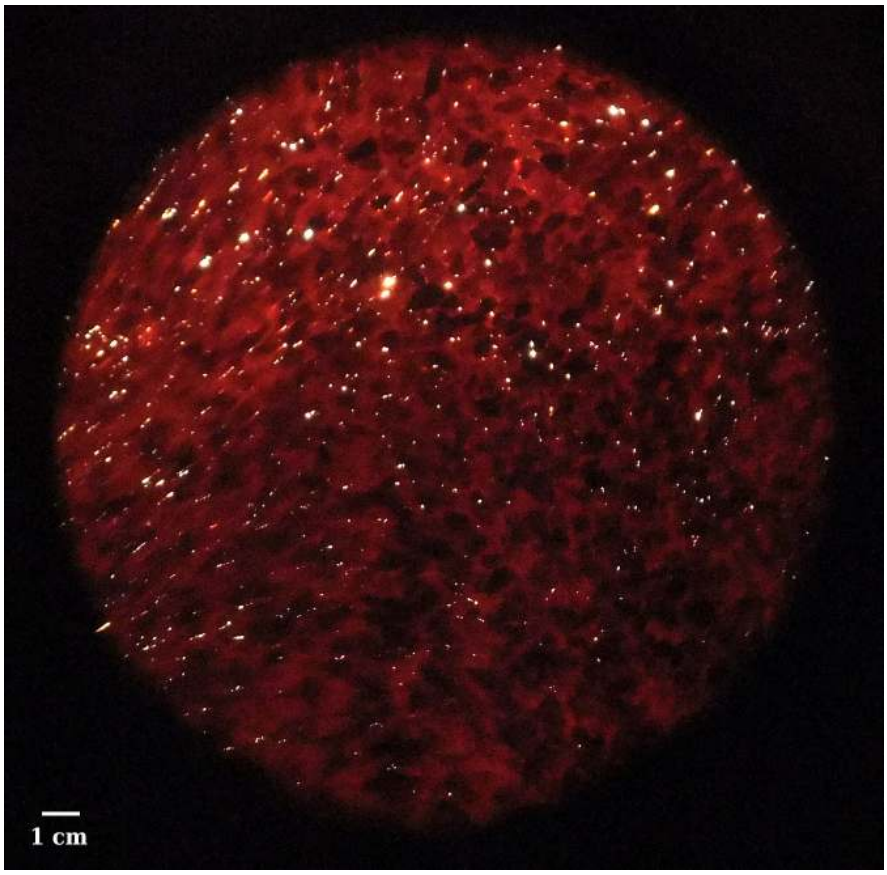


**Figure 6.3:** Photograph of the activated carbon bed, ready to process HDPE, taken from the continuous rotary feeder input port. The red colour of the bed is from thermal radiation; the bright spots are microplasmas of ionised gas induced by the irradiation of the bed by microwave energy.

contains relatively free delocalized π-electrons, which experience electromotive force from the microwave field; this created charge imbalances that were restricted by the physical boundaries of the carbon particles. In order to equalise the induced charge imbalance, a small arc (both in distance and duration) would form between the points of high and low voltage, ionising the gas between the points as charge is transferred.

While these microplasmas were observed whenever the activated carbon bed was used, they were not seen with the coke bed. This is thought to arise from structural differences between the two types of particle. The activated carbon had extensive networks of pores throughout the particle structure — these presented physical gaps which prevented the flow of charge and allowed voltage to build up to the point at which it would equalise via a microplasma arc. The size of the activated carbon particles and their irregular shape would also allow this phenomenon to occur in the gaps between individual particles. In contrast, the coke particles were not only approximately spherical with no porous structure, but also considerably smaller (90–250 µm vs. 0.52–1.68 mm), with the size and regularity resulting in sufficient physical contact

between granules that flow of charge could occur unimpeded, thus never building up to the levels required to form the microplasma arcs.

The extremely high energy of these microplasmas is evident by their ability to ionise nitrogen gas (with which the bed was pervaded during the capture of figure 6.3): the nitrogen-nitrogen triple bond has dissociation energy of 945 kJ/mol. Accordingly, the temperature of these microplasmas is considerably in excess of that of the bulk reactor bed, and hydrocarbon localised in this area will be correspondingly cracked to a greater extent. This effect results from the juncture of the microwave heating mode and the activated carbon structure, and is not technically a catalytic one, though is still expected to increase hydrocarbon cracking over and above the coke bed case, and may enhance the initiation of chain-reaction cracking through the creation of radicals in the hydrocarbon plasma. The lack of any nitrogen containing species in the pyrolysis products can be attributed to rapid displacement of the nitrogen by the generated hydrocarbon pyrolysis gas.

## 6.5 Changes in Porous Structure of Activated Carbon

Physical adsorption studies were carried out on the activated carbon, as a method for measuring its surface area and characterising the pore volume and area. This analysis was carried out in order to understand the physical and structural changes to the activated carbon occurring as it was used in microwave-assisted pyrolysis, and to determine whether a relationship existed between these changes and the loss of catalytic activity of the carbon.

### 6.5.1 Physical Adsorption Analysis Method

Automatic sorption analysis of the carbon samples was carried out using a Micrometrics ASAP 2010 Automatic Sorption Analyser (Micrometrics U.K. Ltd, Bedfordshire). The carbon particles were first degassed, then exposed to varying pressures of nitrogen gas at a temperature of 77K, with the volume of gas that was adsorbed onto the surface of the sample at each pressure recorded. Nitrogen adsorption and desorption isotherms were constructed from the data, which allowed the characterisation of the porous structure, and calculation of the surface area of the sample according to BET theory [262]. Pore volume and area distributions were determined according to BJH analysis [263]. The analytical and technical aspects of this analysis were performed under the guidance and supervision of Zlatko Saracevic, an instrumentation support

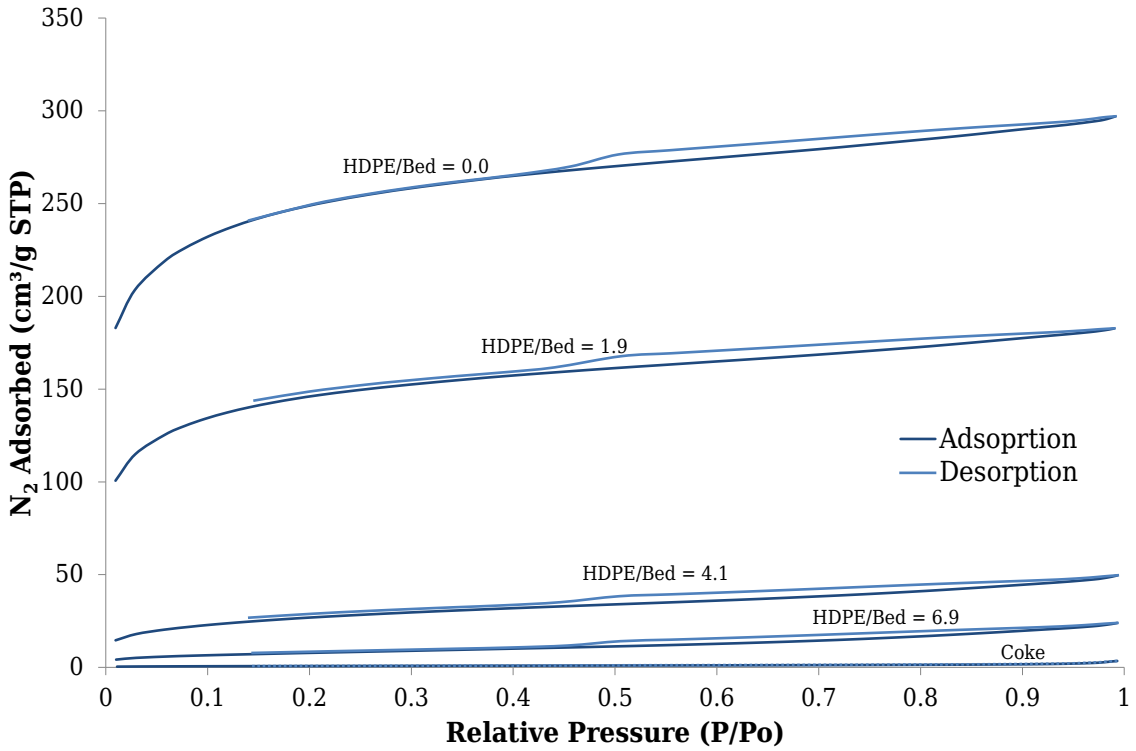


**Figure 6.4:** Nitrogen adsorption/desorption isotherms from activated carbon and coke reactor beds. For the activated carbon beds the mass of HDPE processed relative to the bed mass is indicated by *HDPE/Bed*; the pyrolysis of the HDPE occurred at 450°C.

technician in the Department of Chemical Engineering and Biotechnology, University of Cambridge.

### 6.5.2 Adsorption/Desorption Isotherms

Figure 6.4 shows examples of the adsorption/desorption isotherms from the nitrogen sorption analysis of the activated carbon. The isotherms can be classified as type I according to the standard IUPAC system [264, 265]: the rapid adsorption at low pressure followed by the flattening out indicates the activated carbon has microporous properties, with the bulk of the absorptive extent occurring with these small diameter pores. A small amount of type $H_4$ hysteresis [266] between the adsorption and desorption isotherms results from capillary condensation of the nitrogen and indicates the presence of mesopores.

It is clear that the absorptive ability of the activated carbon declines dramatically as it processes more HDPE, with an approximate 10-fold decrease in nitrogen absorbed after the activated carbon has processed 6.9 times its own mass. This indicates the surface area of the activated carbon (including catalytic active sites) accessible to

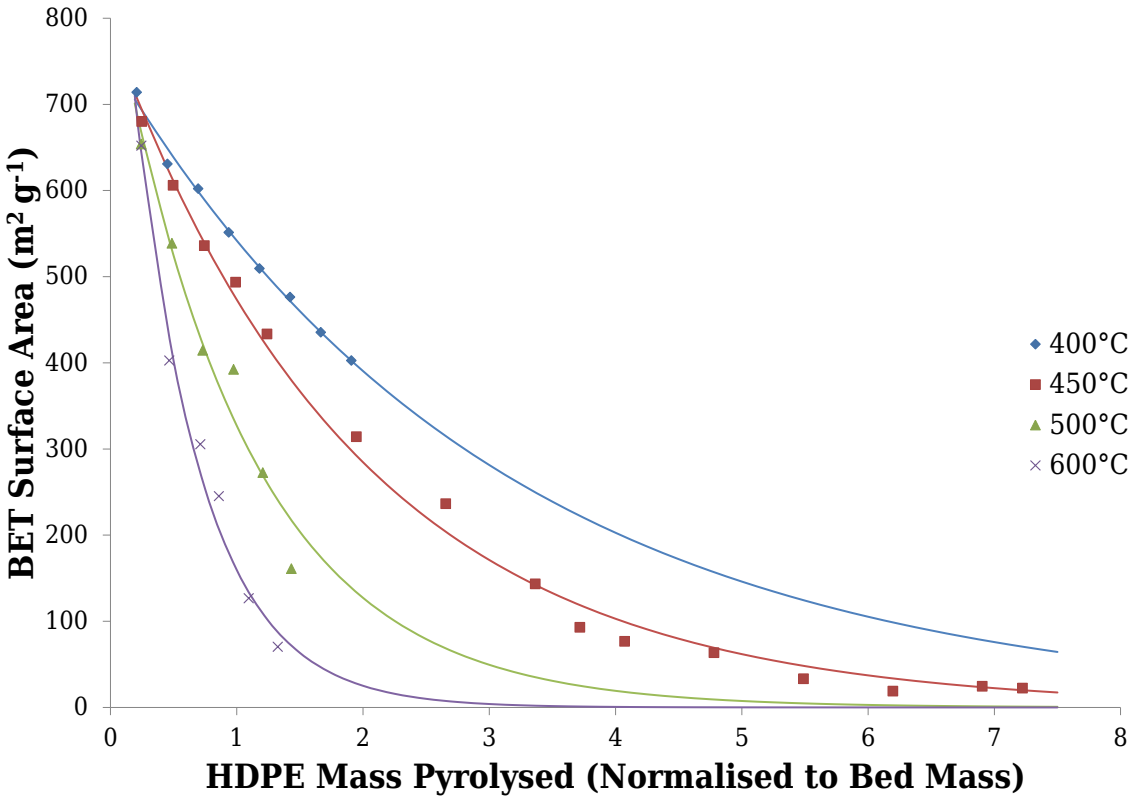


**Figure 6.5:** Change in surface area of the activated carbon as it processes progressively more HDPE, at different reaction temperatures. Lines of best fit are fitted to a first-order kinetic model of deactivation described in the text.

molecules decreases as the bed processes HDPE, as demonstrated with the following BET surface area analysis.

### 6.5.3 BET Surface Area

Virgin activated carbon has a BET surface area of around 750–800 $m^2/g$; by comparison, the non-catalytic coke used in the experiments conducted in this work has a surface area of just 1–3 $m^2/g$. Figure 6.5 shows the change in surface area of the activated carbon bed over time as it has processed progressively more HDPE. As expected from the observed changes in produced pyrolysis products, the process is highly temperature dependent, occurring extremely rapidly at 600°C, and progressively more slowly as the reactor temperature decreases. The decline in catalytic activity of the bed correlates well with the reduction in surface area of the activated carbon, in agreement with the results of Muradov et al. [39] when cracking methane to hydrogen. Independent of temperature, the quantity of mass retained in the reactor correlates well with the reduction in surface area of the activated carbon; given the non-volatile nature of the

deposited mass (see §6.6), this correlation is consistent with the deactivation arising from coking of the activated carbon pores/active sites.

#### 6.5.3.1 Mathematical Accuracy of BET Model

The BET model of surface adsorption assumes a "monolayer coverage" of molecules, which does not account for cooperative effects or multilayer absorption that is thought to occur in the micropores of activated carbons [267]. The calculated values presented in this work thus represent a monolayer coverage "effective surface area" which, even though it is acknowledged that multilayer adsorption would be occurring, are nevertheless regularly used to quantify the surface area of activated carbons [268–272], and are useful for comparative purposes. Indeed, no adsorption instrument exists that is able to give a "true" measurement of atomic surface area; rather, it is adsorption capacity that is always measured and only afterwards converted, through the selection of an appropriate mathematical function, into a calculated surface area equivalent [52]. The BET model is simple, effective, widely used, and employed here with full transparency.

### 6.5.4 Kinetics of Deactivation/Surface Area Loss

The reduction in surface area of the activated carbon, as a proxy for the deactivation of the activated carbon, is able to be modelled well using first-order kinetics: the rate of decrease in surface area, with respect to the (normalised) mass of HDPE processed by the bed, is proportional to the surface area of the activated carbon at any given time:

$$\frac{dB}{dm} = -k.B \tag{6.10}$$

where $B$ is the BET surface area of the activated carbon, $m$ is the mass of the HDPE pyrolysed, normalised to the mass of the reactor bed, and $k$ is the reaction rate constant. Separating variables and integrating gives:

$$B = B_0 e^{-k.m} \tag{6.11}$$

Curve fitting this equation to the data gives the lines of best fit depicted in figure 6.5. The temperature dependence of the reaction rate constant was modelled using the empirical Arrhenius equation:

$$k = Ae^{-\frac{E_a}{RT}} \tag{6.12}$$

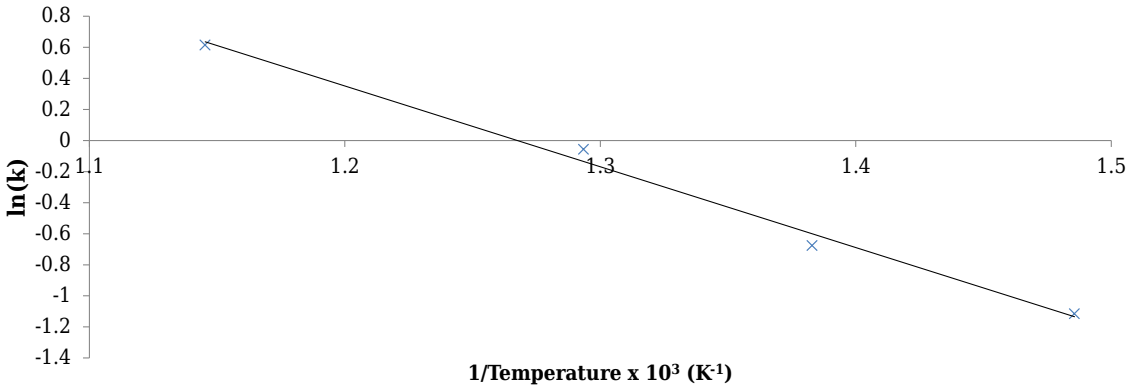


**Figure 6.6:** Arrhenius plot to determine activation energy of deactivation process. $R^2 > 0.99$

where $A$ is the pre-exponential factor, $E_a$ is the activation energy, $R$ is the universal gas constant, and $T$ is temperature. Taking the natural logarithm of this equation, gives:

$$\ln(k) = -\frac{E_a}{R}.\frac{1}{T} + \ln(A) \tag{6.13}$$

Thus, the gradient of the plot of $\ln(k)$ versus $T^{-1}$ shown in figure 6.6 gives the activation energy of the deactivation process, at 43.2 kJ/mol. As should be clear from the derivation thus far, the activation energy derived from this calculation cannot be compared with the activation energy derived from the Arrhenius equation in its standard use. Traditional application of the Arrhenius equation relates: the rate of change in concentration of a species with respect to time; the reaction rate constant — thought of as the number of collisions between reactants, per second, that result in a reaction (i.e., a change in concentration of reactants); the pre-exponential factor — the total number of collisions (successful or not) per second; and $e^{-\frac{E_a}{RT}}$ — the probability that any given collision will result in a reaction, with the activation energy determining the temperature (i.e., thermal energy) sensitivity of this likelihood.

With the derivation carried out in this case the reaction rate constant is the number of collisions between reactant and activated carbon, per unit mass of HDPE processed by (an equivalent mass of) the activated carbon bed, that result in the deactivation of the activated carbon (i.e., the decrease in BET surface area); the pre-exponential factor is the total number of collisions between reactant and activated carbon per unit mass HDPE processed by (an equivalent mass of) the activated carbon bed; and $e^{-\frac{E_a}{RT}}$ is the probability that any of these given collisions as described will result in a successful deactivation / loss in surface area, with the activation energy determining the temperature (i.e., thermal energy) sensitivity of this likelihood. Ultimately, though, it should be remembered that the Arrhenius equation is inherently an empirical relation

in any case.

The purpose of undertaking this calculation is not necessarily to derive a specific activation energy parameter for external comparison, but rather to demonstrate the properties of the underlying deactivation reaction: it is well described with a first-order kinetic model, and demonstrates temperature sensitivity in a mathematically consistent manner that is well described by the Arrhenius relation. Indeed, this analysis suggests that the apparent step change in the rate of deactivation of activated carbon observed between 450°C and 500°C and described in §5.6 is not in fact derived from a fundamental change in reaction chemistry, but rather is the result of the increase in deactivation rate resulting from the exponential nature of the temperature sensitivity of the reaction.

#### 6.5.4.1 Calculated Deactivation Over Batch Experiments

Using this model of BET surface area decline, it is possible to calculate the theoretical drop in BET surface area that would have occurred over the course of the batch experiments throughout chapter 4. Figure 6.7 shows the change in BET surface area over the course of these experiments, progressively applying the calculated rates of change in surface area for each temperature. While the deviation in surface area of the consecutive-use bed does grow over time relative to that of a fresh bed, the overall magnitude of the deviation is not large, owing to the smaller quantity of material processed in the batch investigation. As an indication of the magnitude of these

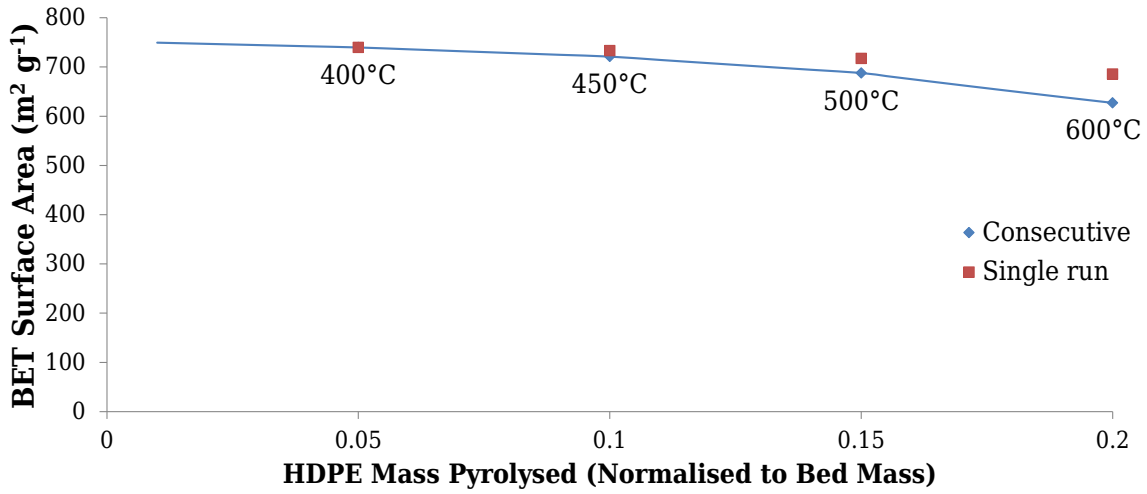


**Figure 6.7:** Calculated change in BET surface area throughout batch experiments. The loss in surface area of the activated carbon bed throughout the batch experiments, where the same bed was across all runs, is shown as the *consecutive* data set; the *single run* data, where a fresh bed would have been used for every experiment, is shown for comparative purposes.

changes, extrapolating backwards from the calculated BET surface area to the mass of HDPE processed equivalent, for the batch consecutive tests, the change in catalytic activity of the bed for all of the experiments except the final 600°C case lies within the first data point collected during the continuous experiments. Within this range of HDPE processed, the composition of the pyrolysis products produced is similar (see figure 5.2), i.e., there is little difference in the catalytic activity of the bed. Even for the 600°C consecutive case the calculated BET is very close to the first observed data point in the continuous case at the equivalent temperature, with a surface area of 652 $m^2$ $g^{-1}$ vs. 627 $m^2$ $g^{-1}$.

In fact the change in catalytic activity / BET surface area for the batch consecutive case is likely to be less than that calculated in this comparison, as this model assumes the same rate of deactivation across batch and continuous addition modes, where the reduction in average residence time in the batch case would likely reduce the deactivation of the bed (owing to less contact time between the HDPE and catalyst for any given quantity of HDPE processed). Overall, then, the deactivation across the batch experimental set is unlikely to have been substantial.

### 6.5.5 Distribution of Pore Volume

Figure 6.8 on the following page shows representative examples of the change in cumulative pore volume of the activated carbon bed as it processes more HDPE. The pore size distribution was determined from the adsorption branch of the isotherm, to avoid artefacts from hysteresis and desorption pore network effects [273, 274]. This analysis confirms the initial impressions garnered from the isotherms, with the vast majority of the activated carbon's absorptive ability deriving from microporous volume (note the steep increase in pore volume that occurs with the smallest diameters in figure 6.8, a point only emphasised by the fact that the diameter scale here is *logarithmic*). The coke exhibits little porosity and no microporous structure. These results are consistent with other studies characterising the porosity and adsorption of activated carbon [275–277].

The bulk of the porosity present in virgin activated carbon is 3 nm or less, approximately twenty times the length of a C-C bond [278]. Interestingly, with virgin activated carbon, the largest products produced had a carbon number of $C_{20}$, suggesting a possible correlation between the size of the pores and that of the final products. Indeed, microporous carbon has been shown to exhibit molecular sieve properties — the ability to separate molecules based on size and shape [277, 279, 280],

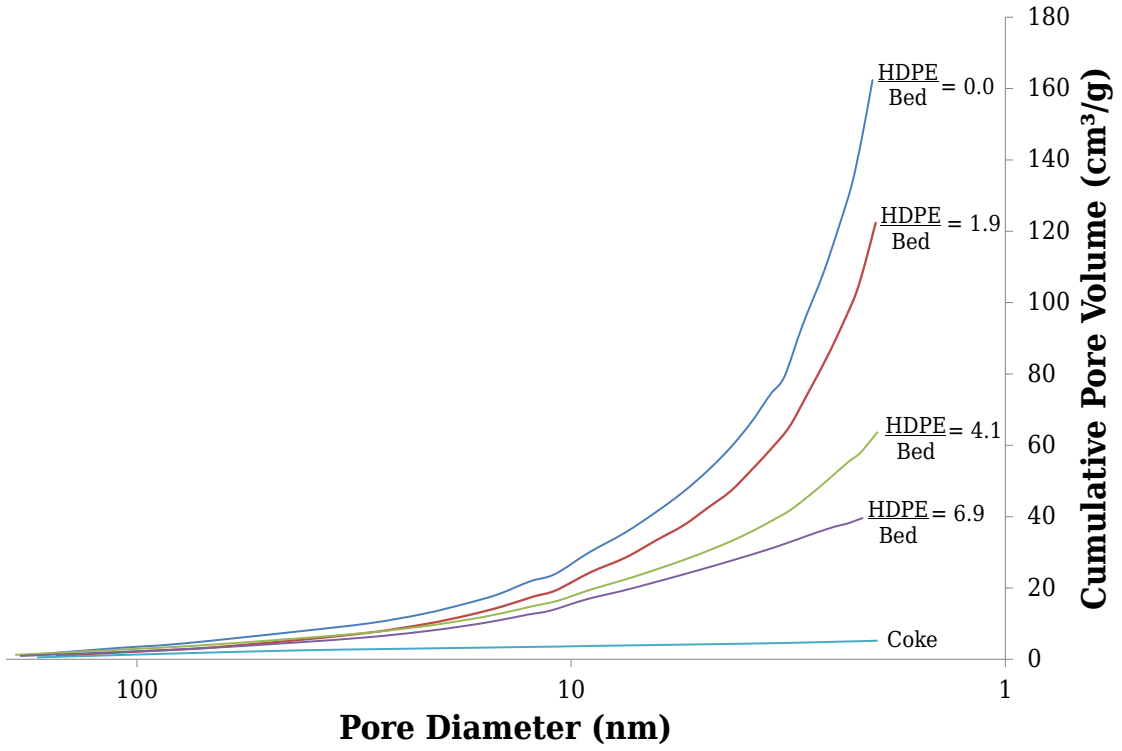


**Figure 6.8:** Cumulative pore volume of activated carbon and coke reactor beds, as pore diameter decreases. For the activated carbon beds the mass of HDPE processed relative to the bed mass is indicated by *HDPE/Bed*; the pyrolysis of the HDPE occurred at 450°C. Pore diameter is presented on an inverted logarithmic scale.

and this property may also contribute to the final make-up of the pyrolysis products produced using the activated carbon bed; in particular the fixed range of molecular masses observed in the products initially produced using activated carbon (i.e., up until the bed had processed around 3.5 times its mass of HDPE at 450°C).

The loss of porosity and surface area that occurs as the activated carbon processes more HDPE occurs primarily from the micropores. However, while the bulk of the loss derives from pores of this size, there is an across the board reduction in pore volume, independent of pore diameter, roughly in proportion to the volume present. Not only does this marry extremely well with the first-order kinetic model of surface area loss developed in §6.5.4, but furthermore it provides an insight into the nature of the underlying mechanism for the loss: that the loss in pore volume is experienced across all pore diameters, and in proportion to the pore volume at that diameter, is consistent with individual stochastic molecular deposition of material across the activated carbon surface.

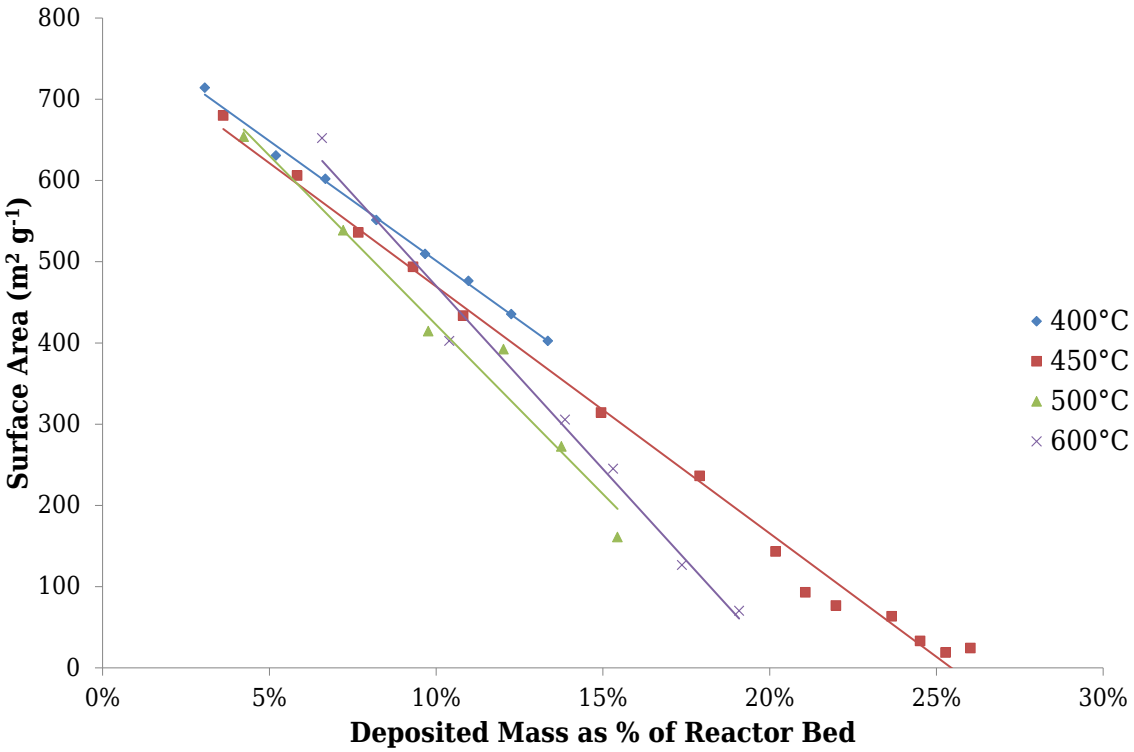


**Figure 6.9:** Temperature dependence of coke deposition, and effect on surface area of activated carbon.

#### 6.5.5.1 Temperature Dependence of Deposition Distribution

While the preceding description of deposited material accumulating across the entire surface area of the activated carbon holds true at 400°C and 450°C, at higher temperatures the relationship between deposited mass and porous surface area does change somewhat. As seen in figure 6.9, the rate of reduction in porous surface area, per unit mass deposited, increases with increasing reactor temperature; however, at high temperatures, the surface area does not initially reduce as much, for the amount of mass deposited, as at lower temperatures. These observations can be explained by considering the processes involved in the deposition of coke in porous media.

At low temperatures, where the reaction rate is relatively slow, the pyrolysis gas perfuses throughout the entire porous structure and deposits evenly across the entire surface of a particle (as in figure 6.10b). At high temperatures, the deposition reaction rate is fast compared with the rate at which the hydrocarbon molecules diffuse into the pores, resulting in deposition occurring more quickly at the mouth of the pores, as in figure 6.10c. Initially, this results in a higher available surface area under nitrogen adsorption testing than when coke is deposited across the entire surface area, as the inner pore network, with little deposition, is still accessible as long as the outer pore

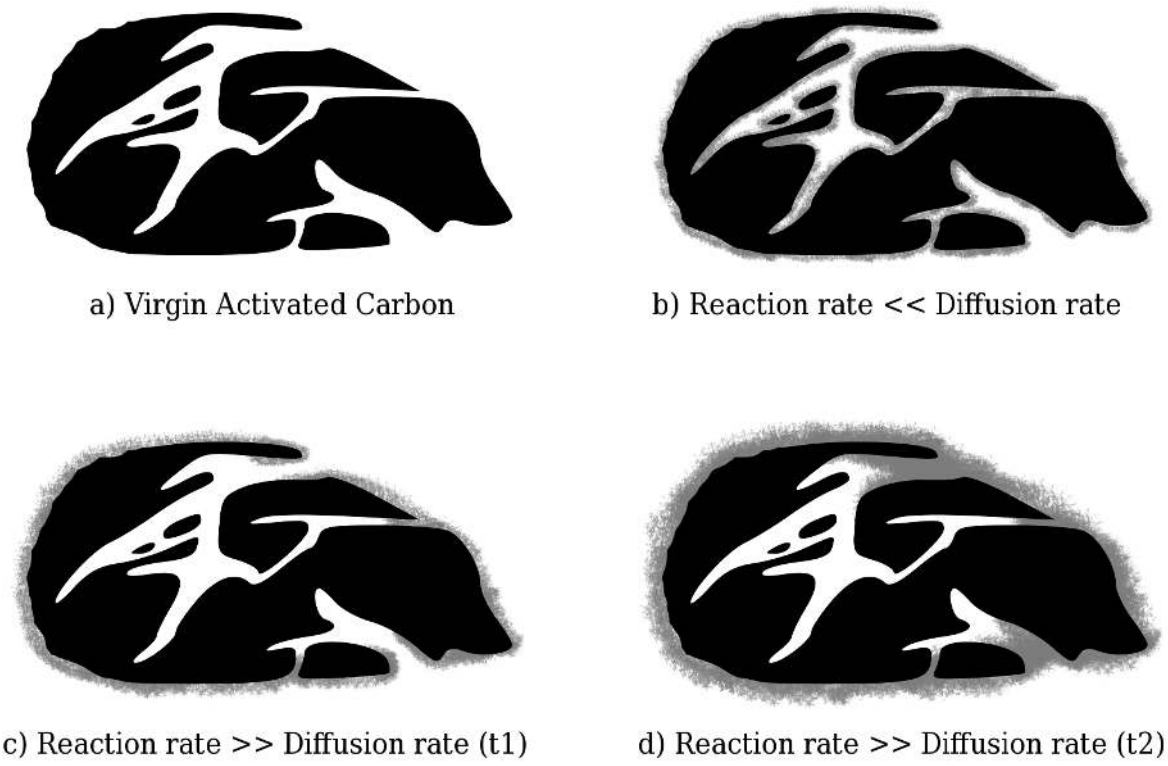


**Figure 6.10:** Influence of reaction rate and diffusion rate of pyrolysis gas on spatial distribution of coke deposition. Grey represents deposited material, black represents original activated carbon particle. Starting with a virgin activated carbon particle (a), if the reaction rate is slow (i.e., at low temperatures) compared with the diffusion rate, then coke is deposited across the entire surface of the particle (b). If the reaction rate is fast (i.e., at high temperatures) compared with the diffusion rate, then deposition occurs more at the mouth of the pores than inside the particle (c), though over time (t2, d) deposition at the pore mouth will close off the inner surface completely.

mouths have not been closed off completely. However, the build-up of material at the pore mouth progresses until access to the inner structure is completely lost (shown in figure 6.10d) with a corresponding sharp decrease in measured surface area. The spacio-diffusion aspects of the deposition and deactivation effectively act to magnify the thermal dependence of the process, though it should be noted that these effects are incorporated into the empirical rates derived in the deactivation model outlined previously in §6.5.4.

Evidence supporting the occurrence of this pore-mouth deposition mechanism has been developed by Gonçalves et al. [281], who measured the adsorption ability of activated carbon after exposure to propene at various temperatures. Measuring the ability of the treated activated carbon to adsorb both nitrogen and carbon dioxide showed that the adsorption of the smaller molecule decreased far less than the larger one, as the temperature at which the propene exposure occurred increased (and the rate of reaction dominates over diffusion speed), i.e., a narrowing of the pores occurred

at the mouth through which the smaller molecule could still pass and “access”/adsorb onto the inner porous structure. This effect was particularly noticeable at temperatures of 500°C and above, supporting the observations of this work.

## 6.6 Chemical Composition of Mass Retained in Reactor

### 6.6.1 Thermogravimetric Analysis

The chemical composition of the deposited material was examined by thermogravimetric analysis, with the evolved gases analysed by infrared spectroscopy. This was intended to determine whether the deposited material was comprised of hydrocarbons and/or volatile substances that had been adsorbed onto the surface of the bed, or, as suspected, carbonaceous material resulting from coking and dehydrogenation of the HDPE pyrolysis products.

#### 6.6.1.1 Method

Analysis of the carbon samples was carried out on a Q500 Thermogravimetric Analyser (TA Instruments, West Sussex). Samples were heated in the presence of nitrogen carrier gas from room temperature up to 1000°C at a rate of 20°C/min, and the change in weight recorded. As there was no obvious method to physically separate the deposited material from the reactor bed, the two were tested together, with a bed sample from the end of the series of HDPE pyrolysis experiments conducted at 450°C analysed (representing the bed with the greatest proportion of deposited material by mass, at around 25%) compared with a sample of virgin activated carbon that had not been used to pyrolyse any HDPE. The evolved gases produced during the thermogravimetric testing were analysed by Fourier transform infrared spectroscopy (FT-IR) with a Nicolet IS-10 Infrared Spectrometer (ThermoFischer Scientific, USA) to determine their composition.

#### 6.6.1.2 Thermogravimetric Analysis

Figure 6.11 on the next page shows the thermogravimetric curves of the virgin activated carbon (0% deposited mass) and the deposited material mix. The decrease in mass up to 100°C seen in the virgin activated carbon case results from the loss of water vapour adsorbed by the carbon. This is not seen to any significant level

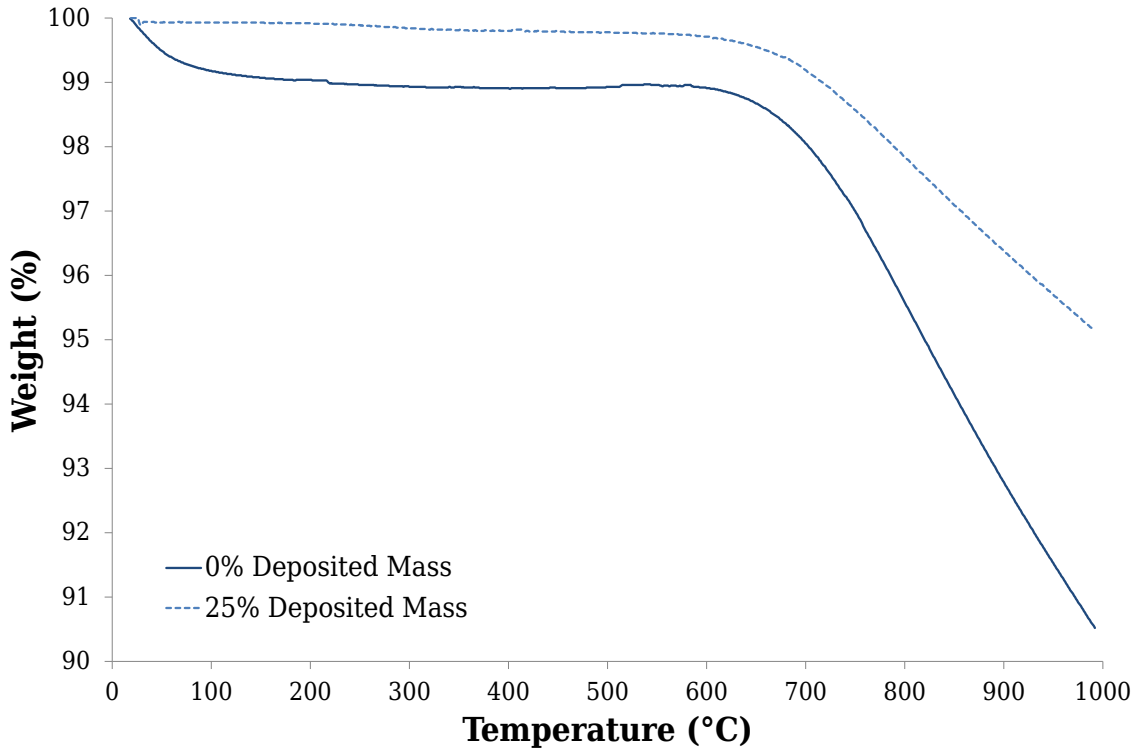


**Figure 6.11:** Thermogravimetric curves for virgin activated carbon, and the activated carbon reactor bed at the end of the series of HDPE pyrolysis experiments conducted at 450°C, by which time the bed comprised approximately 25% deposited material by mass.

with the deposited mass mix owing to the loss of adsorption capacity and reduction in surface area, as described in §6.5.3. Between 100°C and around 650°C there is no significant change in mass for either sample. At temperatures of greater than 650°C both samples start to decrease in mass at a constant rate. This resulted from the carbon samples oxidising to $CO_2$, owing to the small amount of oxygen present in the nitrogen carrier gas. Given a constant concentration of oxygen in the carrier gas, and this being the rate limiting reactant in the oxidisation process, the absolute rate of mass reduction should be constant. The difference in rate of reduction between the two samples can be explained given their differences in initial mass: the absolute rate of oxidation (as limited by the concentration of oxygen in the carrier gas) is in fact the same between both samples, with the greater *percentage* decline in the virgin activated carbon sample arising from its smaller initial mass.

Tests conducted where the mass decline of the samples was allowed to continue through to conclusion showed no significant difference between the virgin activated carbon and the deposited mix, with almost the entirety of the sample mass eliminated through oxidation, though both left a small quantity of residual ash (<10% wt.).

From the point of view of this analysis, the virgin activated carbon and deposited

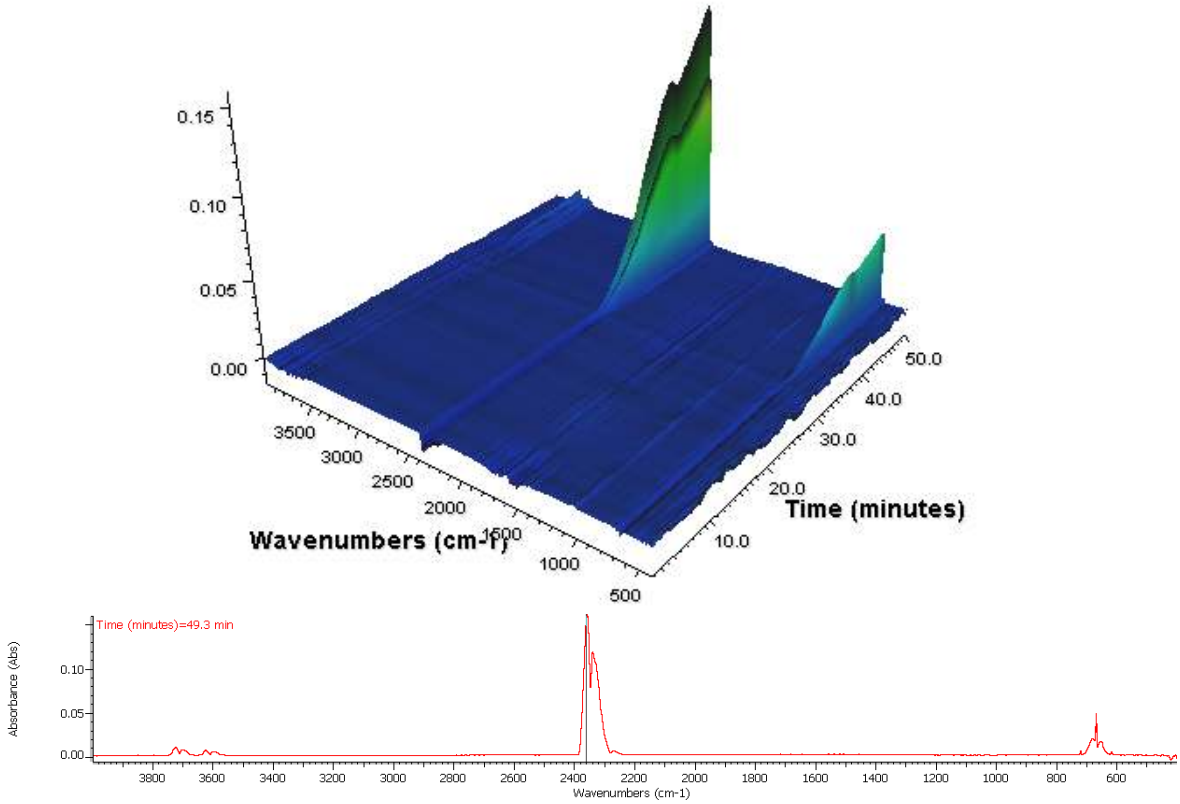


**Figure 6.12:** Typical FT-IR spectrum of evolved gases during TGA of carbon samples. Top figure shows the spectrum over time, with the only significant signal arising at the same time the carbon begins to decrease in mass as it is oxidised. Bottom signal shows a snapshot of the FT-IR spectrum at its peak strength; the signal is consistent with that of $CO_2$.

material mix may be considered effectively equivalent, at least to the extent that any differences between them have been easily explained, and do not arise from underlying differences in chemical composition. This similarity implies that the deposited material comprises the same carbonaceous chemical composition, and is not made of volatile hydrocarbons or any other non-similar material as, even were this matter “trapped” behind a pore blockage, a deposit with a different chemical composition would exhibit different thermogravimetric and oxidation patterns.

#### 6.6.1.3 Infrared Spectrometry of Evolved Gases

The infrared spectrometry analysis of the evolved gases is consistent with the account of the thermogravimetric analysis advanced thus far: figure 6.12 shows the FT-IR spectrum over the course of the thermogravimetric analysis. The only significant signal is temporally coincident with the decrease in carbon mass due to oxidation, and was identified as $CO_2$.

## 6.7 Electron Microscopy

The activated carbon samples were analysed using scanning electron microscopy (SEM) to visually investigate any structural changes that occurred as a result of the deactivation process. This was then coupled to energy-dispersive X-ray spectroscopy (EDS) in order to perform an elemental chemical analysis of the carbon.

### 6.7.1 Method

Imaging was performed using an XL30 Field Emission Gun SEM (FEI, Oregon, USA), operated at 5 kV; in EDS mode the SEM operated at 20 kV, and was coupled with an Oxford Instruments Si/Li atmospheric thin window detector; data collection and analysis was performed using Oxford Instruments' INCA software. The analytical and technical aspects of this analysis were performed under the guidance and supervision of Dr Jeremy Skepper, Technical Director of the Multi-Imaging Centre, Department of Physiology, Development, and Neuroscience, University of Cambridge, whose assistance is gratefully acknowledged.

### 6.7.2 SEM Images

Figure 6.13 shows the SEM micrographs of the activated carbon particles. Of necessity, a limited number of images are presented in this dissertation; however, while carrying out the microscopy several areas were scanned and examined for consistency. No significant deviations in structure were observed throughout the microscopy work, and these micrographs are fully representative of the observed structure.

Broadly speaking, two types of morphology were seen in the activated carbon particles: planar, relatively flat surface (figures 6.13 a and b), and porous areas that extended into the particle (figures 6.13 c and d). It should be noted that at this micrometer resolution the only pores visible will be macropores; micropores, which account for the bulk of the activated carbon's porosity and absorptive ability, have a diameter of 2 nm or less, and are difficult to image without specialised setup including high-resolution transmission electron microscopy and significant image processing [269, 282]. Nevertheless, significant differences were observed between the virgin activated carbon and that which had been used to process HDPE. The virgin activated carbon had a relatively smooth exterior, with some loose carbon/dust particles evident on the surface. By contrast, the texture of the used activated carbon (which in this

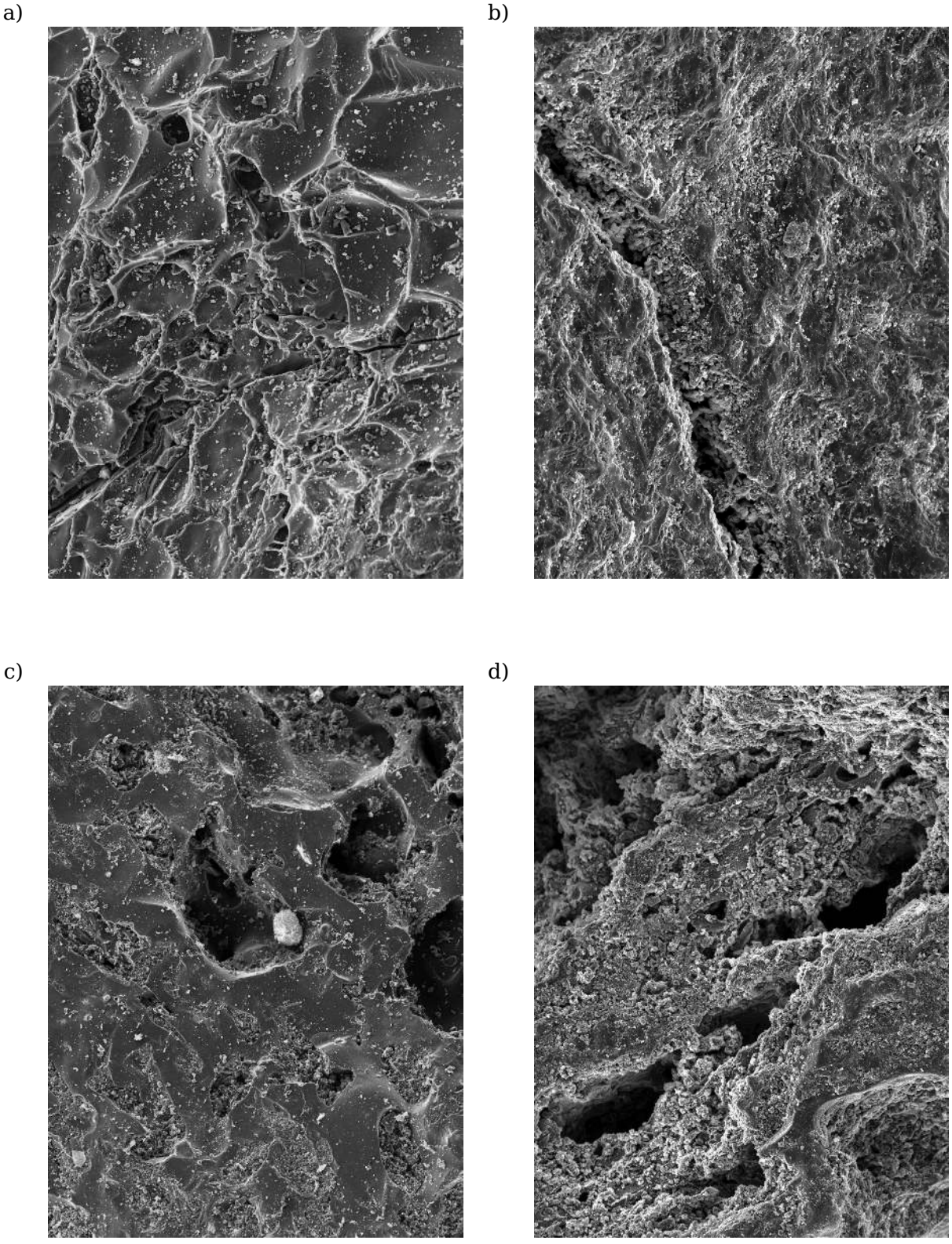


**Figure 6.13:** SEM micrographs of virgin activated carbon (a,c) and activated carbon that has processed 6.9 times its mass of HDPE at 450°C, resulting in significant surface deposition (evident from its textural change). While larger macropores are still evident (though reduced in diameter), the deposition of material on the surface of the carbon would effectively block micropores (which result from the structure of the surface itself). Images a and b show mostly planar particle surface and are 75 μm across, images c and d show macroporous structure and are 160 μm across.

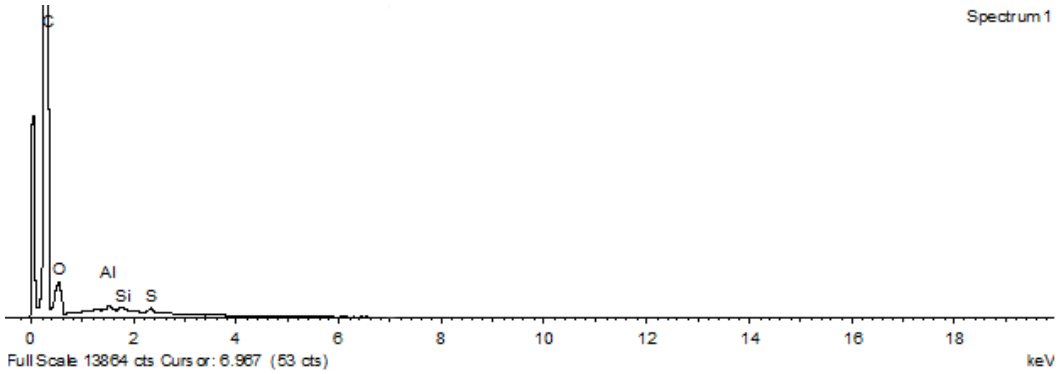


**Figure 6.14:** Typical energy-dispersive X-ray spectrum of activated carbon sample. Y-axis has been shortened so that elements other than carbon are visible (though carbon is by far the dominant element).

case had processed 6.9 times its mass of HDPE and lost most of its porous adsorptive ability) is quite different, with a rough, amorphous surface as a result of stochastically deposited material. Given the size and extent of the accumulated deposits, which cover the entire imaged surface of the carbon particle, it is clear that any microporous catalytic surface of the original activated carbon particle would be almost completely subsumed by the deposited material (evident from the surface texture change), with the chemical properties of the bed reflecting its new surface coating.

### 6.7.3 EDS Elemental Analysis

EDS analysis showed no substantive differences between the activated carbon and the deposited material, with multiple physical points compared on both virgin and used activated carbon samples. Figure 6.14 shows a typical spectrum derived from this analysis. In all cases carbon comprises by far the main element in the samples. Small quantities of oxygen are present, deriving from oxygenated surface functional groups (carbon surfaces are never free from oxygen except under extreme conditions such as heating to >950°C under vacuum [52]). Small quantities of silicon, sulfur, and aluminium were observed in some cases, though these were present in both the virgin and used activated carbon samples so were thought to derive from the bituminous origin of the activated carbon.

## 6.8 Attrition and Thermal Cycling

In order to attribute the deactivation of the activated carbon solely to coke deposition, physical and thermal deactivation methods were considered and tested as potential contributors to the deactivation process. Given the bed was continually stirred

throughout the experiments, deactivation through attrition of the activated carbon particles remained a possibility, and was tested for by running the stirrer with a fresh batch of activated carbon, regularly measuring the mass of the bed, and taking samples to test for any changes in surface area; figure 6.15 presents the results of this attrition test. A very small quantity of extremely fine dust was generated, which left the reactor; this occurred during the first 20 hours of continuous stirring and accounted for around 0.3% of the initial mass, an insignificant quantity in the context of the large mass changes observed through coke deposition. The BET surface area varied by around ±2% over the course of the test, but no clear trend was evident over this period; this variation was thought to represent the precision of the measuring instrument.

The activated carbon beds underwent multiple intense thermal cycles throughout their use; however, testing conducted on a fresh bed with no HDPE added showed no significant change in mass or BET after the first burn-off that all activated carbon underwent before first use, in spite of undergoing six subsequent cycles where the carbon was heated to 700°C for one hour. These results effectively eliminate attrition and thermal decomposition as deactivation mechanisms for the activated carbon.

## 6.9 Mechanism of Activated Carbon Deactivation

From the observed change in product yields, the decrease in cracking, increase in molecular masses of the pyrolysis products, and the change in chemical make-up of the products themselves, it is clear that activated carbon rapidly loses its catalytic

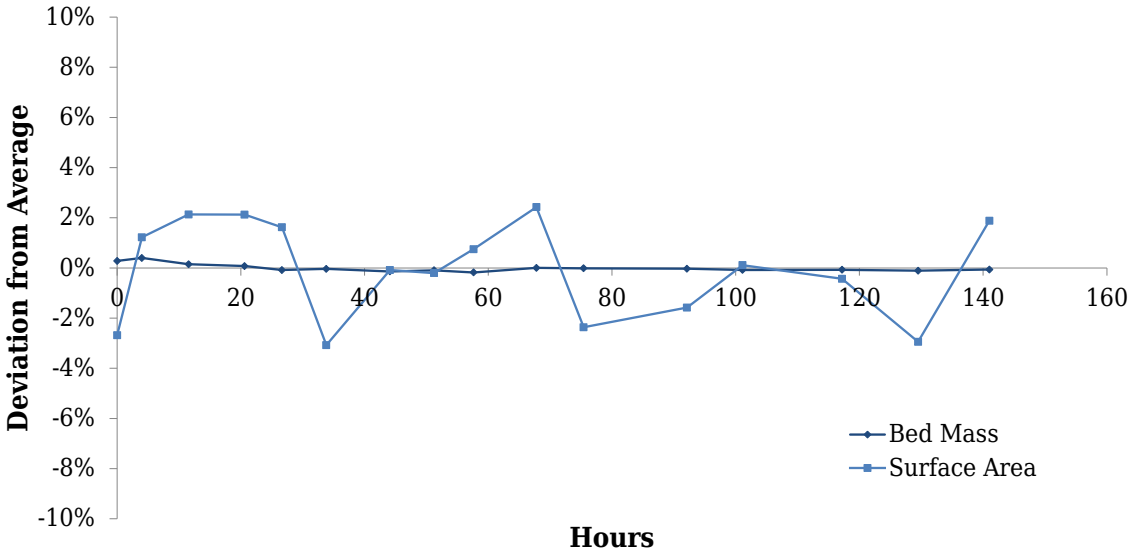


**Figure 6.15:** Testing for attrition by change in bed mass and surface area over time.

ability as it processes HDPE. The elimination of attrition and thermal decomposition as mechanisms, and the correlation between mass accumulated in the bed and reduction in catalytic ability, combined with the inability to separate this material retained in the reactor from the activated carbon bed, points to the deposition of a substance directly on to the surface of the activated carbon in a way that either eliminates or blocks off the active sites from which the catalytic ability derives. Thermogravimetric and energy-dispersive X-ray spectroscopy established that the deposited substance was carbon — indistinguishable from the activated carbon bed from the point of view of these analyses. From a chemistry perspective, though, it is clear that the carbon deposited during the catalytic decomposition of HDPE does not possess catalytic activity itself, otherwise the cracking process would become auto-catalytic and stabilise rather than rapidly decline to the level observed with no catalyst present. There must therefore be a substantial difference in structure of the deposited carbon compared with that of the activated carbon; the nature of this difference is suggested by the decline in BET surface area as the bed mass increases. To account for the differences described thus far, the deposited carbon is likely to have regular structural order, with a resulting low surface area, and a lack of catalytic active sites.

In a study of the deposits resulting from the catalytic decomposition of methane over carbon black (another disordered/semi-amorphous carbon), Muradov et al. [39] used X-ray diffraction to investigate the structure of the combined carbon black and deposits. The diffraction patterns revealed columnar ordering consistent with a graphite-like structure (though the observed columnar spacing was slightly further apart than standard graphite). This ordered structure was not present in the diffraction patterns in virgin carbon black, confirming the expectation that the carbon deposited in the cracking of hydrocarbons over catalytic carbonaceous material is structurally ordered, and thus lacks the folds and irregularities that increase surface area and result in high energy active sites.

Overall then, hydrocarbons are adsorbed onto the surface of the activated carbon by the van der Waals forces arising from the folds/pores and the close proximity of multiple carbon atoms. Here, they may interact with high energy active sites and undergo catalytic cracking in the manner described in §6.3.1. Given the nature of the active sites (with free valencies, unpaired electrons, etc.) it is highly likely that in a percentage of these interactions, the hydrocarbon will progress from physisorption to chemisorption, with the creation of a covalent bond between the activated carbon and the hydrocarbon. These bonds may also result from “external” inducement, with an

already adsorbed molecule subject to radical attack, or just a radical itself adsorbing; these could then stabilise through interaction and bonding with the high energy active sites. The end result of such interactions is the creation of an overall more stable molecular structure, but through incorporation into and alteration of the active site, the hydrocarbon reduces or eliminates the active site's ability to catalyse further such reactions.

Even without specific active site deactivation, the accumulation of non-catalytic carbon in the bed will reduce the overall catalytic activity of the bed by reducing the proportion of catalytic material substrate is exposed to (by the end of the 450°C experiment series the bed comprised 25% accumulated mass), though this reduction alone is insufficient to account for the observed reduction in bed activity.

As polymer fragments, some of the hydrocarbons that become bound to the surface of the activated carbon will have long external chains. These chains would still be subject to further reactions, either cracking and separating off, or undergoing radical attack, hydrogen abstraction, and incorporation into the basal activated carbon layer. Over time, the structure of the newly deposited carbon would likely exhibit a tendency towards the structure of graphene due to its highly stable conformation, but in any case the hydrocarbons would be likely to undergo further dehydrogenation and carbonisation. In this way, reacted hydrocarbon deactivates the activated carbon active sites, while "filling in" and/or blocking pores (or at least the micropores responsible for catalytic activity; macropore dimensions are not on the same scale as the hydrocarbon molecules and thus would not present the same van der Waals forces required for adsorption).

This molecular deposition process would occur wherever the hydrocarbon pyrolysis gas is able to physically reach. While small molecule hydrocarbons should be able to perfuse throughout the entire porous structure of the activated carbon, at high temperatures the time scale of the deposition process will be short compared with that of the diffusion process, causing deposition to occur more frequently towards pore mouths, resulting in the deposition distributions previously described in §6.5.5.1, and the more rapid deactivation as pore mouths become closed off.

The formation of the pore/active-site blocking coke may proceed via the same mechanism as that of polyaromatic hydrocarbons (PAHs). These compounds are known to form in the high temperature pyrolysis of polyethylene [283], and were observed in the condensed pyrolysis products formed with activated carbon in this work. PAHs are able to form through the sequential addition of hydrocarbons via both Diels-Alder

and radical-mediated mechanisms [244, 248]. Growth proceeding in this way would mimic the underlying activated carbon graphene structure but without the structural defects, proceding in a piece-wise fashion from single rings into large networks that would blanket the activity of the underlying active sites. Whatever the mechanism, it apparently requires catalytic initiation at the temperatures examined in this work, as the addition of mass to the activated carbon bed declines rapidly in correlation with its decline in catalytic activity. While PAH deposition would be sufficiently regular that the new material would not add micropores or catalytic high energy sites, it is in any case clear that the deposited material does not contain these, or at least if it does they are present in far smaller quantities than in virgin activated carbon, and would become deactivated through the same mechanism as in the original sites, resulting in an overall exponential decline in number.

It is also worth noting that substances that promote acid-based catalysis such as zeolite (and which function with a mechanism similar to the oxygen-based acid active sites discussed in §6.3.1.4) also experience coking when cracking hydrocarbons. Overall this coking is not dissimilar to the process described here, though the underlying mechanisms proposed to account for the coke accumulation (of which there are several owing to ongoing research in this area) proceed along acid/base hydrogen transfer pathways [256, 284–286].

The mechanism for deactivation proposed here, encompassing modification of high energy active sites and addition of ordered carbonaceous matter, accounts for all observations regarding the deactivation of the activated carbon — an increase in mass that reduces as the activated carbon deactivates, the carbonaceous elemental composition of the deposited material, the reduction in surface area/pore volume that accompanies the deactivation — and acts as a logical extension of the argument already advanced for the catalytic activity described in §6.3.1.

### 6.9.1 Carbon Nanofilament Formation via Microwave-Induced Plasma

While the microwave-induced microplasmas discussed in §6.4.2 enhance hydrocarbon cracking, they are also likely to enhance the deactivation of the activated carbon. When Fernendez et al. [144, 287] pyrolysed methane over carbon using microwave heating, a microscopic analysis of the bed showed the growth of carbon nanofibres. Neither the microplasmas nor the nanofibres were observed with conventional electric heating. It

**Figure 6.16:** Carbon filament formation resulting from the creation of microplasmas in the hydrocarbon pyrolysis gas. The formation shown in this image is approximately 2 cm across.

is thought that the plasmification of the pyrolysis gas occurring in these microwave-induced plasma arcs is able to dehydrogenate the hydrocarbon and cause deposition.

While no fibres as such were observed in the SEM images of the activated carbon used in this work, this is because the bed was continuously stirred, resulting in random deposition at distinct sites, rather than the continual growth that could occur with a static bed. Dramatic visual evidence that these nanofibres do occur in the apparatus used throughout this work is presented in figure 6.16. In this case, an undetected arc formed in the waveguide entering the reactor, a space in which pyrolysis gas was able to freely pervade during operation. Over time, the arc induced the deposition of a complex network of carbon fibres. Once initially seeded, the distance between the opposite wall and the conductive tubule growth site was less than any other point on the otherwise parallel waveguide walls, so the arc continued in this location (the lesser distance requiring the least voltage to breach and ionise). The branching nature of the formation results from the fluctuations in the plasma stream as it traverses the constantly varying path of least resistance through the turbulent atmosphere.

Carbon fibres have a very low surface area, and regular structure compared with activated carbon [39, 288], i.e., they are not a source of high energy active sites. Microwave-microplasma induced carbonisation and deposition is thought to contribute to the deactivation of the activated carbon described above, though is certainly not the sole mechanism, given the deactivation observed by other researchers not operating with microwave-mode heating [119, 120].

## 6.10 Summary

The mechanisms outlined in this chapter fundamentally underlie the entire body of work presented in this dissertation. The non-catalytic pathway of HDPE pyrolysis is thought to proceed via a radical-mediated mechanism, these being created with an initial random thermal scission, then going on to react in a chain fashion via intra- and inter-molecular hydrogen transfer and beta-scission. Aromatics are thought to form through Diels-Alder and/or radical-mediated mechanisms, both of which proceed via cyclisation, with aromatisation occurring through subsequent dehydrogenation pathways. These reactions account for almost the entire gamut of species observed in the pyrolysis products produced using the coke bed, though of particular note is the ability of these pathways to account for the alkene, alkadiene, alkane triples that make up so much of these products.

The catalytic pyrolysis of HDPE is thought to derive from high energy active sites on the accessible surface of the carbon, that result from defects, folds, and disorder that alters the structure of the activated carbon away from that of graphene. These sites include unsaturated and free valencies, including unpaired and/or delocalised electrons, which may act to accept, donate, or transfer electrons and/or hydrogen (radicals) between species and the activated carbon bed. The catalytic mechanism may also proceed through acid-catalysis due to oxygen-based functional groups, though evidence for this is mixed.

The generation of microplasmas through microwave irradiation of the activated carbon bed may also contribute to cracking of the HDPE owing to the high temperature of the plasma. This is not a catalytic effect per se, though, and instead arises from the interaction between the microwave heating mode and the physical structure of the activated carbon. The microplasmas were not observed when using the coke bed.

The surface area and pore volume of the activated carbon declines as it processes HDPE and accumulates mass. The loss in surface area, as a proxy for deactivation of the carbon, was modelled with first order kinetics with a good resulting fit. This model was able to explain the temperature dependence of deactivation in terms of exponential temperature sensitivity as described by the Arrhenius equation. This model was then used to calculate the amount of deactivation that would have occurred throughout the course of the batch addition experiments. While some deviation from using a fresh bed every time was noted, overall the catalytic reduction would not have been large, given the quantity of material processed.

Generally the accumulation of mass in the bed correlated well with the reduction in surface area, though at higher temperatures this occurred to a lesser extent initially, but then progressed at a more rapid rate. These results were thought to arise from the increase in reaction rate at high temperatures, such that the hydrocarbon would react and deposit on the surface of the activated carbon before it was able to diffuse very far into pores. As a result, deposition occurred more often at the mouth of pores; initially small molecules could still get through the narrow mouth and access the pore volume inside, accounting for the higher initial measured surface area; however, this was soon followed by the closure of pores and rapid fall-off in measured surface area.

The chemical composition of the deposited material was confirmed to be coke through thermogravimetric analysis coupled with FT-IR, and subsequent elemental analysis using SEM-EDS. The deposited material was indistinguishable from the activated carbon using these techniques. In spite of establishing the deposited mass as carbon, there was still an obvious decline in catalytic activity as it was deposited, indicating that the chemistry/structure of the deposited material was significantly different to that of activated carbon. The observed reduction in surface area suggested that the deposited material exhibited regular structure and did not contain the defects, folds, and irregularities that act as high energy catalytic sites for activated carbon. This theory was in agreement with Muradov et al. [39], who used X-ray diffraction to show graphite-like structure in carbon deposited from catalytic cracking of methane over carbon black.

From these results it was concluded that deposition/deactivation likely proceeded initially from physisorption of hydrocarbon pyrolysis gas through van der Waals forces from pore walls, then proceeded through reaction with the high energy active sites, resulting in the creation of covalent bonding and the integration of hydrocarbon into the base activated carbon structure (where it underwent subsequent dehydrogenation and carbonisation). By incorporation into, and alteration of the active site, this mode of interaction depletes the number of active sites, fills in/blocks pores, and reduces the ability of activated carbon to catalyse further such interactions.

The mechanisms described in this chapter account for the products observed in the pyrolysis of HDPE, both with standard microwave-assisted pyrolysis and when using a catalytic activated carbon bed. By combining theory from the literature with observed changes in chemical and structural properties of the activated carbon as it was used to process HDPE, it was possible to develop a comprehensive mechanistic theory that accounts for both the catalytic properties of the activated carbon, and its

deactivation over time. Having advanced mechanisms to explain the observed data collected throughout this work, this chapter concludes the analysis portion of this dissertation. Nevertheless, the material presented in this body of work raises a number of avenues of potential further study which, along with a broad concluding overview, are presented in the following and final chapter.

# 7

# Project Overview and Further Study

## 7.1 Project Overview

This dissertation began by introducing the fundamental principles of the microwave-assisted pyrolysis of plastics, and presenting the concept of combining the microwave-receptive properties, and relatively unstudied catalytic abilities, of activated carbon for use as a reactor bed in this process, with the intention of producing pyrolysis products with a narrow and useful range of molecular masses. A thorough review of activated carbon, microwave heating, and the wider pyrolysis field established that this avenue of research was both novel, and of sufficient potential to warrant further study.

### 7.1.1 Development of Microwave-Assisted Pyrolysis Equipment

Considerable effort was put into developing safe and reliable apparatus in which to carry out the microwave-assisted pyrolysis of HDPE. An existing reactor that had been used to conduct pyrolysis on liquid hydrocarbons was refurbished for this purpose. A number of improvements to the reactor were made, including the simplification of

the power transmission system — reducing reflected power and eliminating points of failure; the addition of a three-stub capacitive tuner to the transmission pathway to match the impedance of the "load" (the reactor bed) with the magnetron source — thus maximising power transmission; and the design and fabrication of a silicone window and support structure that allowed microwaves to pass through to the reactor, but did not allow damaging pyrolysis gas or heat to return back to the magnetron. A gas-tight method for adding HDPE pellets to the carbon bed when it reached the target temperature was required, and a plunger-like sample injection system was developed for this purpose. The development of suitable apparatus with which to condense produced pyrolysis gases resulted in several iterations based around Liebig condensers that ultimately proved inadequate owing to the pyrolysis products being carried through the condensing apparatus by the constant flow of gas and not settling on the condenser surface. The development of a dry ice condenser through which the pyrolysis gas percolated provided an effective solution to this issue. The entire system was controlled by a computer system based around a PID feedback loop; this was able to vary the power of the magnetron to maintain the reactor at the desired temperature, as well as performing safety monitoring and stopping power to the magnetron in the event that any arcing was detected, a process it performed far more rapidly and effectively than any human controller.

### 7.1.2 Exploratory Experiments with Batch Addition of HDPE

A series of exploratory experiments were conducted pyrolysing HDPE that was added in a single batch to an activated carbon bed over a range of temperatures from 400–600°C. Equivalent control experiments were also conducted using a non-catalytic coke bed. The pyrolysis products produced using the activated carbon bed underwent significantly more cracking than those produced with the non-catalytic coke bed, with the condensed products approximately three times lighter on average (with an average carbon number of 10.0–11.5 vs. 25.0–33.0), indicating that activated carbon could be used as an effective catalyst in this application. The products produced using the coke bed were almost entirely linear aliphatics, while the condensed products produced using the activated carbon bed showed a considerable component of aromatic species (36–45%). The hydrogen that was "freed" through the formation of aromatic species, with lower H/C ratios, resulted in a higher concentration of alkanes in the non-condensable gases.

The range of molecular masses produced when using the activated carbon bed was

much smaller than when the coke bed was used; indeed, the condensed products resulting from the activated carbon bed shared the same mass range as that of the liquid transport fuels petrol and diesel. The aromatic portion of these condensed products consisted of benzene and substituted derivatives (e.g., toluene, ethyl-benzene, and xylene), substantially valuable products in their own right. The non-condensable gases resulting from both beds were relatively similar (aside from the greater alkane proportion in the activated carbon derived gases already mentioned), the species in this fraction being limited by the range of hydrocarbons in the gaseous state at room temperature. These short-chain aliphatics could be used as fuels (e.g., natural gas, LPG) or feedstock for a range of chemical processes including fresh HDPE synthesis (the gases included a high concentration of ethene, the original HDPE monomer). Overall, the entire range of products produced with the activated carbon bed had a high potential economic value, while a large portion of the condensed products produced using the coke bed were longer-chain waxes that would require further cracking before they could be used.

### 7.1.3 Continuous Throughput Pyrolysis of HDPE

Following from the positive results from the batch input study, a second study was conducted to assess the pyrolysis process in greater detail, processing larger quantities of plastic with a continuous throughput of material, a mode any potential commercial plant would be required to operate in for capacity and efficiency reasons. A continuous rotary feeder was designed and built for this purpose which provided a constant flow of plastic pellets into the reactor during operation, while maintaining containment of the pyrolysis gases and microwaves.

Because of the larger quantities of HDPE pyrolysed with the continuous rotary feeder, and as a result of conducting a number of experiments in sequence, it soon became clear that the nature of the pyrolysis products produced with the activated carbon bed was changing over time, with the cracking ability of the bed reducing, and a significant proportion of mass accumulating in the activated carbon bed with each experiment. Both the average molecular mass, and the range of molecular masses of the pyrolysis products increased over time, with a reduction in the proportion of non-condensable gases and an increase in condensed products (themselves heavier). The rate of this catalytic deactivation was highly temperature dependent, occurring very quickly at temperatures of 500°C and over, and much more slowly at and below 450°C. The condensed products produced using the activated carbon bed with the

continuous addition of HDPE initially had an even higher aromatic content (61–85%) than those produced with the batch addition, though this declined over time as the bed processed more HDPE, with a corresponding increase in aliphatic content. Overall, as the activated carbon deactivated, the resulting pyrolysis products came to increasingly resemble those produced using the coke bed.

Aside from the catalytic activity of the activated carbon, the primary influence on the make-up of the pyrolysis products was the temperature at which the pyrolysis was carried out. Increased temperature had the effect of not only increasing the rate of cracking, but also reducing the residence time of the input mass as the pyrolysis products entered the gaseous state and expanded in volume considerably, generating pressure which drove them out of the reactor. The balance of these two factors determined the total amount of cracking that the products underwent: from 450–600°C the overall molecular mass of the combined condensible and non-condensable gases decreased with increasing temperature, implying the increase in cracking rate dominated. Decreasing the temperature below 450°C, the overall average molecular mass decreased again as the time products spent in the hot cracking zone of the reactor increased.

While the economic value of the products produced in the continuous mode was much the same as those produced in the batch mode, as a result of the catalyst deactivation these products changed over time, presenting a potential barrier to producing a saleable product due to the variability of the output. However, at lower temperatures there was an initial period during which the condensed products remained entirely within the liquid transport range: at 450°C this remained the case until the activated carbon had processed approximately three times its mass of HDPE, after which time it came to include less valuable heavier waxes.

The differing modes of HDPE input also affected the pyrolysis products: those produced with the batch input of HDPE underwent less cracking and encompassed a wider range of molecular masses. This was thought to arise from the different rates of sample introduction, the sudden bulk introduction of HDPE in the batch mode resulting in an “explosive” rush of pyrolysis gases being initially produced, and a corresponding large pressure that forced the gases out of the reactor more rapidly; this then declined over time as the mass of material undergoing pyrolysis in the reactor reduced. With the continuous introduction of HDPE, the production of pyrolysis gas quickly settled to a constant rate that was lower than the initial explosive exit rush from the batch case. The shorter and more variable residence time in the batch mode explains the

heavier and more varied products, as well as the differences in chemical composition, with the greater proportion of aromatics in the continuous case arising from the longer time the pyrolysis products spent in the hot zone of the reactor (aromatic formation being time-dependent). The effect of addition mode on reaction rate and residence time was demonstrated with an illustrative mathematical model incorporating the kinetics behind the two input modes.

### 7.1.4 Mechanisms of Pyrolysis, Catalysis, and Deactivation

By combining theory from the literature with the chemical profile of the produced pyrolysis products, reaction mechanisms accounting for the observed species were advanced. Non-catalytic pyrolysis was thought to proceed via a radical-mediated pathway, with initiation occurring by random thermal scission of the polymer backbone, and the resulting highly unstable terminal radicals partially stabilising through intra- and inter-molecular hydrogen transfer. Both of these pathways result in the formation of a more stable intra-molecular radical, while the latter of these also produces an alkane. These intra-molecular radicals stabilise through the process of beta-scission, resulting in the formation of an alkene, and a new terminal radical that initiates a new cycle of hydrogen transfer in a chain reaction. Termination of this reaction cascade occurs through recombination of radicals, or disproportionation (resulting in an alkane and an alkene). The formation of aromatics was thought to occur through Diels-Alder type reactions (where a conjugated alkadiene and alkene react to form a substituted cyclohexene intermediate, which is then dehydrogenated), or more complex radical mediated pathways, where cyclisation and dehydrogenation also occur.

The catalytic activity of the activated carbon was thought to originate from high-energy active sites on the surface of the carbon that are created by defects that skew the atomic carbon structure away from a regular graphene lattice. The resulting folds and pores are responsible for the very high surface area of the carbon, but also create unsaturated and free valencies, including unpaired and/or delocalised electrons, which act to accept, donate, or transfer electrons and/or hydrogen (radicals) between hydrocarbon species and the activated carbon bed. By facilitating these transfers the activated carbon lowers the activation energy for radical-mediated cracking as described above, and other reactions such as the formation of stable aromatic molecules. Oxygen-based active sites may also play a role in the catalytic properties of the carbon through acid/base catalysis.

The physical properties of the activated carbon as it underwent deactivation were

investigated through nitrogen sorption analysis, which revealed a dramatic decline in surface area as mass accumulated in the carbon bed and it deactivated. This decline could be modelled well using first order kinetics, with the temperature dependence fitting the Arrhenius equation, and accounting for the large increase in the rate of deactivation observed at higher temperatures. The bulk of the porosity present in the activated carbon was contributed by pores of <3 nm, approximately twenty times the length of a C-C bond [278], suggesting that an element of shape/size selectivity may have contributed to the narrow range of the hydrocarbons produced with virgin activated carbon.

The composition of the mass deposited in the activated carbon bed was confirmed to be carbon itself through a combination of TGA (with FT-IR of the evolved gases) and SEM-EDS analyses. Deactivation was thought to occur through hydrocarbons forming covalent bonds with the activated carbon bed in a percentage of the interactions with the high-energy active sites, incorporating into the structure and thus deactivating the carbon by "filling in" the pores, and eliminating the sites that mediated the electron/hydrogen transfer. The bonded hydrocarbons would then be dehydrogenated by the abundant radicals in the hydrocarbon gas resulting in an inert carbon layer without the defects from which the activated carbon gained its catalytic ability.

The microwave heating method caused the formation of "microplasmas" in the activated carbon — charge imbalances created by the electromagnetic field that were restricted by the physical boundaries of the carbon particles, and which resulted in a high temperature plasma spark to equalise the induced voltage. It is likely that cracking occurred at a greater rate in these microplasmas, and the observation of the creation of carbon nano-fibres by microwave-induced plasma suggested that these microplasmas also caused rapid dehydrogenation, likely contributing to coke formation and the deactivation of the activated carbon. These microplasmas were not observed in the coke bed, owing to its lack of porous structure, and smaller particle size with corresponding greater electrical continuity.

## 7.2 Further Study

As a study that was primarily exploratory in nature, this work leaves plenty of scope for future work to be carried out to further the understanding of the microwave-assisted pyrolysis process and the use of activated carbon as a catalyst. Indeed, the results

presented in this study suggest a number of potential avenues of exploration, which are presented in the following section.

### 7.2.1 Isolation of Microwave Effects

While microwave-assisted pyrolysis results in different heating profiles and characteristics to conventional heating, as well as additional phenomena in the reactor bed in the form of microwave-induced microplasmas, further research is necessary to definitively attribute any observed differences in pyrolysis products and mechanisms to the microwave-heating mode alone, and controversy remains around whether microwave heating results in non-thermal effects arising from interaction of the electromagnetic field with reactant molecules.

To assess these effects on the pyrolysis of plastics, research could be conducted in a reactor that incorporates both electric and microwave heating mechanisms; with suitable control software it should be possible to ensure that the heating profile for both of these methods is the same. With all else being equal (reactor size, configuration, condensing apparatus, etc.), it would be possible to isolate any differences observed in pyrolysis process and products to the microwave-heating mode itself. Such a reactor would be able to conclusively determine whether or not microwave heating, and the associated microplasma phenomenon, has an impact on any process carried out within it, including the pyrolysis of HDPE, and the deactivation of activated carbon as posited in §6.9.1. If additional benefits were recognised from such a study it might be possible to optimise future reactor and bed configurations to enhance these effects.

### 7.2.2 Other Catalysts

While this study represents the first application of microwave heating to the catalytic degradation of HDPE, it has been limited to one catalyst type. There is a large amount of potential to investigate the decomposition of plastics using other catalysts and microwave heating. It would be particularly interesting to conduct a comparative study using zeolites and conventional FCC catalysts and investigate the products resulting with these catalytic beds. The use of microwave heating in these contexts has the potential to provide efficiency gains, either from non-thermal interactions or simply from the direct application of energy to microwave-receptive catalysts without heating intervening space.

### 7.2.3 Composition of Deposited Carbon Material

While the deposited material that deactivated the activated carbon was identified as a low surface area form of carbon, further study could reveal the structure and form that this deposited material takes, and thus provide additional insight into the deactivation reaction mechanisms.

X-ray crystallography is an analytical technique that could be potentially employed for this purpose, with the ability to identify the presence of regular crystalline graphite-like carbon that is not present in the disordered structure of activated carbon [39]. As an alternative or additional tool, Raman spectroscopy is able to distinguish between different structures of elemental carbon with shift bands identifiable for single crystal graphite at 1580 $cm^{-1}$, imperfect graphite and disordered carbons at 1620 $cm^{-1}$, and other structural carbon imperfections at 1360 $cm^{-1}$ [289, 290]. This technique is also able to provide a quantitative analysis of the relative proportion of these different structural forms.

Using these methods to compare activated carbon deactivated by pyrolysis in a conventionally heated reactor with that carbon deactivated through microwave-assisted pyrolysis could elucidate differences in the deposited material arising from these different heating mechanisms, for example, whether deposition occurred in a different fashion as a result of the activity of microwave-induced microplasmas.

### 7.2.4 Regeneration of Activated Carbon

Given the expense of sourcing activated carbon, and the volume of carbon that would be required to sustain a plastics pyrolysis plant on an industrial scale, the microwave-assisted pyrolysis of plastics using an activated carbon bed with a single use cycle is not likely to be economic. However, deactivation through the pyrolysis of HDPE need not be the final end to the catalyst. Activated carbon can be regenerated, and future work could examine this possibility in detail. Microwave heating has been used to regenerate activated carbon when it has been depleted through the adsorption of pharmaceutical contaminants [291–293], dyes [294–296], and volatile organic compounds [297–299]. However, in these cases the deactivation occurred by adsorption of molecules at low temperatures, and not by the pyrolysis of hydrocarbons at high temperatures where a significant mass of material is deposited and covalently bonded to the carbon surface. Nevertheless, the fact that microwave heating has been successfully used to “activate” carbon in the first place [268, 300–302] suggests that even the covalently bonded

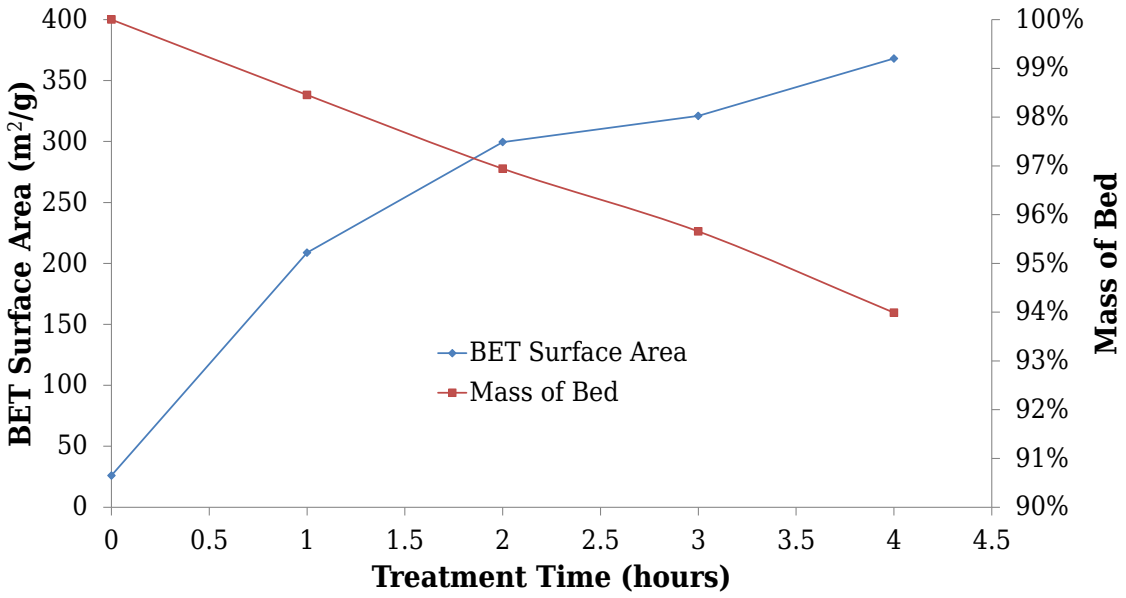


**Figure 7.1:** Activated carbon steam reactivation at 700°C using existing microwave reactor.

deactivated carbon might be reactivated in-situ using the same apparatus with which it was deactivated in the first place.

#### 7.2.4.1 Preliminary Reactivation Data

A preliminary investigation using the existing apparatus and the depleted activated carbon from the 450°C series of continuous addition experiments was carried out, heating the carbon bed to 700°C, and adding water to the bed at a rate of 3.6 mL/min. As seen in figure 7.1, a partial reactivation was achieved, with the activated carbon BET surface area increasing from 26 $m^2$/g to 368 $m^2$/g after four hours of this treatment (compared with around 800 $m^2$/g for virgin activated carbon). The reactivated carbon was able to produce pyrolysis products with the same amount of cracking as the original activated carbon achieved with this surface area. The reasonably large increase in surface area with a relatively small change in bed mass (6% loss, compared with the 25% increase that deactivated the carbon in the first place) suggests that this process may not only be "burning off" deposited material, but actually creating new porous structure.

#### 7.2.4.2 Future Reactivation Work

While this initial study represents an initial proof-of-concept, the reactivation process would need to undergo considerable further development before it became a useful approach to dealing with the deactivation issue. The initial results show incomplete

reactivation, with the rate of increase in surface area declining over time. Furthermore, the process is slow, taking considerable time and energy. In this investigation the reactivation was carried out at 700°C, the maximum safe operating temperature for the reactor; however, this is below the 800–1000°C that the activation process is usually carried out at [275]. It should also be noted that this study was carried out with activated carbon that saw substantial use before any reactivation attempt was made. It may be that the longer the coke remains at high temperature within the reactor, the more “enmeshed” it becomes with the catalyst as it, for example, bonds to multiple atoms in the carbon bed. Further experimentation at higher temperatures, at earlier stages of deactivation, and with different oxidising gases such as $CO_2$, may be able to demonstrate the speed and effectivity improvements necessary to make this a viable process.

If the reactivation could be made efficient and rapid, it could be incorporated into a side-by-side regenerator, where the carbon is continually regenerated in an integrated online facility, as occurs in FCC plants. While the comparison is apt, this would not simply be a reinvention of current FCC, though it would be interesting to examine the possibility of employing activated carbon in place of current catalysts in an FCC plant. As previously argued, activated carbon catalysis proceeds via a different mechanism to current FCC catalysts, and in any case the profile of the products produced using activated carbon in this work differ considerably to those produced using standard FCC catalysts, with a much higher aromatic content of up to 85% (compared with 10–26% typical in FCC plants [223, 303]). Accordingly, a novel process using activated carbon would likely focus on the production of aromatics as an end point. The accumulation of carbon in the bed, with its subsequent activation in the regenerator, would allow for activated carbon to be a secondary output stream of this process. Overall, online reactivation would add considerable complexity and expense to the construction costs of any new plant, and the economic implications of such a development would have to be carefully considered before it was undertaken.

### 7.2.5 Modelling of the Pyrolysis Process

As has been demonstrated in this study, the products resulting from the pyrolysis of plastic are the result of a complex interplay between factors such as mode and rate of mass addition, heat and mass transfer, reactor temperature, reaction rate, and residence time. The parameter space that results from the permutations of these factors is extremely large. However, it should be possible to develop a model of the

pyrolysis process that incorporates the known kinetics and mechanisms of pyrolysis, along with physical heat and mass transfer parameters specific to a reactor, and which would be able to predict the resulting product in a given configuration. A robust model with such a predictive capability would be of enormous use in terms of optimising the production of a desired product, and in the scale-up and design of future pyrolysis systems.

### 7.2.6 Future Reactor/Condensing Systems

While the condensing system used in this study performed reasonably well for the laboratory-scale work conducted here, it presented issues with blockages when high molecular mass products were produced, and in any case would not scale beyond small scale experiments owing to the expense and infeasibility of using dry ice on a larger scale. Two alternatives to the dry ice percolating condenser are presented here, which have the potential to be used in any future microwave-assisted hydrocarbon pyrolysis work.

#### 7.2.6.1 Fractionating Column

Given that one of the issues arising from the pyrolytic breakdown of plastics is the wide range of masses in the produced products, a condensing system with the ability to separate these products into similar fractions by mass would have considerable value. The gold-standard in industry for the separation of hydrocarbons based on molecular mass is the fractionating column. The selective targeting ability of microwave heating should make it possible to combine the fractionating column concept with a microwave reactor, a concept illustrated in figure 7.2. In this scheme, similar microwave generating equipment could be used to that employed in this study (1), with a carbon bed (2) and feeder (3) also operating on the same principle. Pyrolysis would occur in the bed as usual, but rather than having gases leave the reactor and travel into a separate condensing system, the reactor itself could be extended upwards into a fractionating column, with the heat required for operation generated from the microwave-heated carbon bed. Volatile pyrolysis gases would rise upwards, and condensing liquids flow downwards, with condensed substances reaching an equilibrium point on a series of trays (4) spaced vertically throughout the column, from which the products of a particular molecular mass can be tapped. “Bubble caps” on the trays help to ensure good contact between up-flowing vapour and down-flowing liquid. Vapour reaching the top of the column could enter an external condenser (5), where any recovered

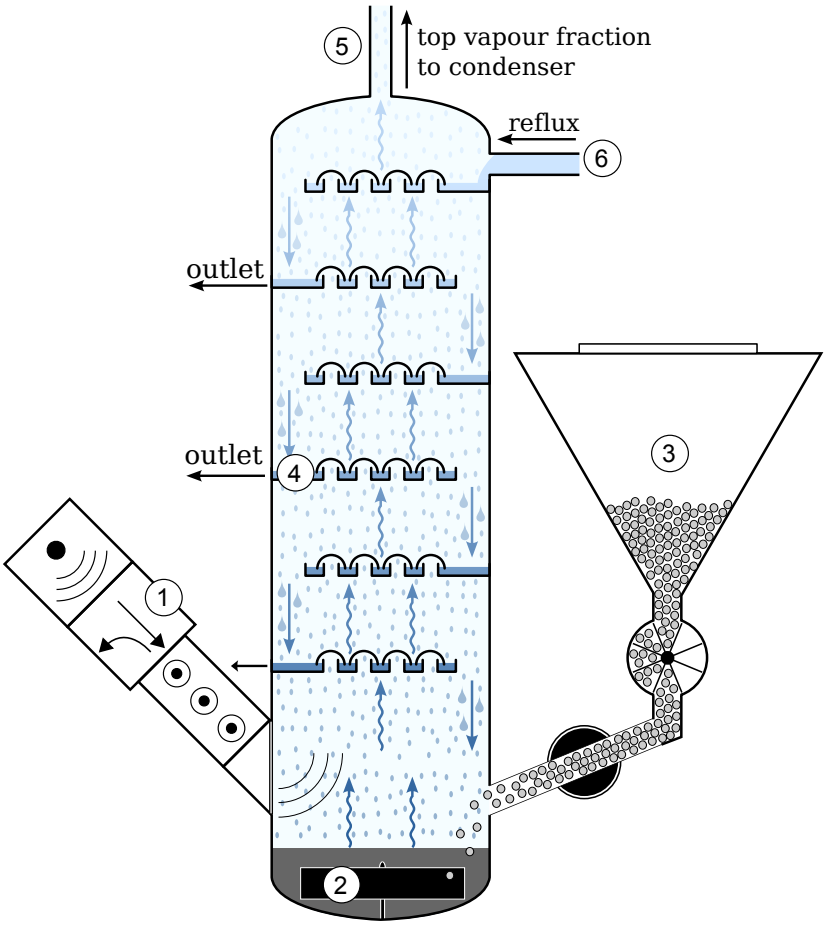


**Figure 7.2:** Schematic of fractionating column reactor. Numbered components are described in the text. Fractionating column graphic modified from [304] under creative-commons licensing.

liquid is refluxed back into the system (6), and the non-condensable gases tapped off. Sufficiently heavy products flow back through the trays to the reactor bed, where they are cracked further before revolatilising and entering the column again.

While such a system does offer a possible solution to the wide range of products produced using microwave-assisted pyrolysis, it is also a significantly more complex and costly design than the simple microwave reactors that have been used to study microwave-assisted pyrolysis in the literature thus far, likely requiring significant scale in order to operate economically. A comprehensive model would need to be developed before commissioning such a scheme, not only of the energy and material inputs and outputs, but also of the economics underlying the process. A capital-intense plant negates one of the advantages of microwave-assisted pyrolysis, with its ability to operate effectively and cheaply on a range of scales.

#### 7.2.6.2 Optimising for Gaseous Hydrocarbon Production

An alternative to the fractionating column reactor presented above is to construct a reactor that is optimised to produce only non-condensable gases, but use the physical properties of these as a separations system (as only the smallest hydrocarbons exist in the gaseous state at room temperature). The mechanics of such an idea could also operate with the reactor integrated into the condensing system. The fundamental principle underlying this concept is for there to be a dramatic temperature gradient between the hot reactor bed and the condensing column. The ability of microwave heating to target only microwave-receptive materials provides a means of achieving this, with input energy dispersed entirely within the carbon bed and a steep fall-off in temperature as distance from the bed increases. By having a simple condenser (effectively just sufficiently high reactor walls), the temperature gradient would be such that liquids and aerosol particulates would fall back into the hot zone of the bed to be re-cracked, and only short-chain gases could leave and be collected.

This method could be employed to obtain a consistent gaseous output stream without catalysis, and indeed would maximise product yield by avoiding the formation of char that is promoted with catalytic cracking. Any char that was produced (which from the results presented in this study would be expected to be inconsequential) would become part of the reactor bed.

A preliminary investigation into the feasibility of this concept showed positive results. Using a small scale quartz reactor with a long vertical glass column that fed into a series of Liebig condensers and a dry ice trap from the top of the column (a small modification of the apparatus described in [150]), resulted in the formation of a clearly distinct “inversion layer” of visible opaque pyrolysis aerosol/gas that did not reach the top of the column. Almost no pyrolysis products were able to be condensed, with the exiting products consisting almost entirely of short-chain hydrocarbons. While this one brief experiment on a small-scale system demonstrates that such a system is potentially viable, further work using similar equipment could develop this promising method fully.

In any case, the system described here compares favourably to other work attempting to achieve the same end; in an attempt to produce light gaseous olefins from HDPE, Artetxe et al. [305] used a conventionally heated conical spouted bed reactor to pyrolyse HDPE, producing long-chain hydrocarbons (waxes at room temperature) that were passed through a cyclone to remove the bed material before entering a second fixed bed HZSM-5 zeolite catalytic reactor that finally resulted in the production of $C_2$–$C_4$ olefins. While an interesting and apparently successful scheme, the equivalent

system proposed here is significantly simpler in operation (with the associated cost and reliability implications), and does not involve the expense of a second catalytic reactor, or the deactivation concerns (as seen in this work) that the use of a catalyst in such a context implies.

### 7.2.7 Contamination and Diversification of Input Streams

As an exploratory study, this work has focused exclusively on the pyrolysis of HDPE as a model plastic for simplicity's sake. This qualification is not limited to this study alone, with HDPE the only plastic in the literature that has been well characterised with microwave-assisted pyrolysis. The development of a microwave-assisted pyrolysis process able to cope with post-consumer waste would necessitate the ability to cope with multiple materials simultaneously, as well as contamination of the sort found in kerb-side collected plastics. There is a large potential to conduct further study in these areas, with the end goal to develop a process sufficiently robust as to produce a high value product from municipal solid waste.

### 7.2.8 Energy Return on Investment

An important consideration in the evaluation of the value of the microwave-assisted pyrolysis process is the amount of energy made available in the final product relative to the energy required to produce the product. The energy return on investment (EROI) is calculated as follows:

$$\text{EROI} = \frac{\text{Energy of product}}{\text{Energy required to produce product}}$$

Values of EROI below one indicate that more energy is consumed in the process than is gained in the final product, while values above one give the multiple of energy gained from the input of one unit. The products of the microwave-assisted pyrolysis of HDPE have a calorific value, i.e., the energy that would be released if they were completely combusted. Future study could determine this by the analysis of a representative sample of the products with a bomb calorimeter. By comparing this to the electrical energy required to operate the magnetron and other apparatus it would be possible to calculate the EROI for the microwave-assisted pyrolysis process as performed in this work.

Based on the work of Lam et al. [152], who conducted the microwave-assisted pyrolysis of waste engine oil with similar apparatus, it is highly likely that the process

described in this work would result in a positive EROI. Lam et al. observed an EROI of up to 8 with their setup, using the methodology similar to that described above; this compares with the EROI of crude oil produced in the USA of 11–18 in the early 2000s (which has likely declined since then) [44]. However, the study carried out by Lam et al. used a prototype reactor, with little attempt made to insulate the reactor and associated fittings from heat loss, and with no attempt made to recover heat energy during the cooling of products in the condensing system (a similar state of affairs was the case with the apparatus used in this study). It is expected that considerable efficiency gains (and a correspondingly higher EROI) would be made in the scale-up of the process, the insulation of the reactor to avoid heat losses, and the recovery of heat from the produced pyrolysis products.

It would also be interesting to conduct calorimetric analyses on the pyrolysis of plastic using microwave heating and catalysts, and investigate how the use of various catalysts is able to change the activation energy of the pyrolysis process, as well as the potential efficiency gains arising from directly heating the catalyst itself.

### 7.2.9 Economic Analysis of the Process

A further important consideration in the evaluation of any future microwave-assisted pyrolysis process for future development is whether or not the process would be economically viable. Ideally, a comprehensive evaluation of all the cost and revenue streams would be undertaken, including: the capital cost of any potential plant, the electrical (and any other) running costs of the process, the cost of the (potentially catalytic) reactor bed and any replacement of this that needs to occur, the cost of any further separation or clean-up of the products required before sale, the market value of the produced products and best route of sale for these, and any potential gate fee that could be collected from disposing of the waste.

While it is not proposed that the apparatus described in this work be directly used to create a commercial venture, the results contained in this study nevertheless provide information that would be valuable if such an undertaking were carried out (e.g., the comparison of batch vs. continuous operation modes, the composition of the various product fractions with activated carbon catalysis and in the non-catalytic mode), and would provide a foundation from which estimates of costs and revenues could based.

## 7.3 Conclusions and Evaluation of Study Objectives

In light of the preceding overview, it is prudent to revisit the objectives of this study set out at the beginning of this dissertation, and assess the progress made towards their fulfilment. The following is a candid evaluation of the work carried out in regard to each of these objectives in turn.

***To develop suitable apparatus to reliably carry out the microwave-assisted pyrolysis of HDPE, and collect the resulting pyrolysis products.***

The inherited reactor described at the beginning of this dissertation possessed numerous issues that prevented it from being used to conduct microwave-assisted pyrolysis of HDPE. The development of the plunger injector and subsequent continuous rotary feeder facilitated the introduction of the HDPE pellets into the reactor, while the high levels of reflected power and arcing were tackled by a systematic approach to identifying and eliminating failure points such as through simplification of the power transmission system, and replacing the quartz window with a redesigned silicone window that integrated the nitrogen gas inlet and water cooling. These changes, combined with a computer-based control system that reacted to failures more rapidly than a human could, dramatically enhanced reliability of the apparatus. After several design iterations, the percolating dry ice condenser maximised collection of the pyrolysis condensate, while the gas sampling system facilitated capture and analysis of the remaining pyrolysis products. The combination of these components saw a functioning microwave-assisted pyrolysis reactor that performed reliably throughout the remainder of the work described in this dissertation.

***To determine whether or not activated carbon is able to act as a catalyst in the microwave-assisted pyrolysis of HDPE.***

The dramatic difference first seen between the products produced using activated carbon and the non-catalytic coke bed conclusively demonstrated that virgin activated carbon is an effective catalyst in the microwave-assisted pyrolysis of HDPE. The resulting pyrolysis products produced in this manner underwent significantly more cracking, resulting in a product containing a much narrower range of hydrocarbons. Unfortunately, activated carbon deactivated relatively rapidly when used as a catalyst for this purpose, with the catalytic activity and resulting effect on produced products declining over time.

***To characterise the products produced by the microwave-assisted pyrolysis of HDPE, and evaluate their potential utility.***

GC/MS analysis proved an effective tool to characterise the products produced from the microwave-assisted pyrolysis of HDPE. With no catalyst, the pyrolysis products comprised almost entirely of linear aliphatics ranging in size from $C_1$–$C_{55}$. Using a virgin activated carbon bed the products ranged from $C_1$–$C_{35}$ across all temperatures studied, though the majority were less than this maximum, with more than 98% of the condensate produced at 450°C in the liquid transport fuel range of $C_5$–$C_{21}$. Indeed, the condensate produced using virgin activated carbon could be used as a transport fuel relatively easily, though the aromatic fraction may have to be separated in order to comply with maximum limits for these compounds in these applications. This aromatic fraction is highly valuable in and of itself, with uses such as solvents, and as precursors for a wide variety of compounds including drugs, lubricants, detergents, plastics (e.g., polystyrene, polycarbonate), and explosives. The condensate produced using the non-catalytic coke bed contained a substantial portion of high molecular weight waxes that would need to be separated out before this fraction could be put to use as a liquid fuel, and which have low value themselves. The non-condensable gases in all cases were short-chain aliphatics which could be used as fuels (e.g., natural gas, LPG) or as feedstock for a range of chemicals (ethene, for example, being the most widely used organic compound in the chemical industry, and is the monomer for HDPE). As the activated carbon deactivated, the profile of the produced products moved toward those produced using the coke bed, with a corresponding reduction in more useful short-chain hydrocarbons and an increase in the less useful waxes.

***To examine the scale-up of the process with a larger capacity and continuous throughput.***

The design and fabrication of the continuous rotary feeder successfully allowed the continuous addition of HDPE with an associated expansion in processing capacity. Through the processing of a larger quantity of HDPE it became clear that the activated carbon deactivated relatively rapidly, presenting a substantial difficulty in the potential scale-up of the process owing to the high cost of replacing the catalyst after its deactivation.

***To understand and characterise the catalytic properties of activated carbon in the context of the pyrolytic breakdown of HDPE.***

The mechanisms presented in chapter 6 are able to account for the species observed in the pyrolysis products in both the catalytic and non-catalytic case. Specifically, activated carbon has a very high surface area that contains high energy active sites that facilitate electron and hydrogen transfer, reducing the activation energy of radical-mediated cracking mechanisms. For example, the reduction in activation energy of aromatic formation allows these more stable hydrocarbons to form, in greater quantities and at a lower temperature. The integration and dehydrogenation of hydrocarbon onto active sites deactivates them and results in the deposition of a non-catalytic low surface area carbon that reduces the effectivity of the catalyst.

***To evaluate the potential of microwave-assisted pyrolysis of HDPE for future commercial development on an industrial scale.***

Microwave-assisted pyrolysis of HDPE using the method as described in this work is not likely to be feasible because of the high cost of the activated carbon, which would need to be frequently replaced. A detailed economic analysis of the process was not conducted owing to the need for a solution to this issue before the prospect of a commercially viable process could be realised. Accordingly, several possibilities were presented that could provide the focus of future work towards this goal, including the reactivation of the activated carbon, either in-situ or in an online regenerator, the incorporation of a fractional separator into the reactor in order to separate the pyrolysis into multiple output streams, and the design of a new reactor built with the intention to exclusively produce short-chain non-condensable gases — this would eliminate the need to separate fractions from one another, and could be designed to be operated with either a catalytic or non-catalytic bed. Given the high aromatic content of the products produced using activated carbon, it is likely that future development of a novel process utilising activated carbon as a catalyst would focus on the production of these compounds.

### 7.3.1 Additional Conclusions

In addition to meeting the objectives laid out at the beginning of this study, several further points worthy of discussion came to light as a result of the intervening work conducted. In general terms, this study contributed to a more complete

characterisation of the products of the microwave-assisted pyrolysis of HDPE, and the reaction parameters under which they were produced. In particular, this study highlighted the importance of residence time in determining the profile of the produced products and the interplay this parameter has with the reaction temperature. This study was also able to provide information on the influence of the mode of sample introduction (i.e., batch or continuous), and how this affects residence time and product composition via reaction kinetics. Characterising the influence of these parameters could help to tailor future processes to target particular products (e.g., enhancing aromatic formation by engineering a longer residence time).

This work also presents the most complete account so far of the use of activated carbon to pyrolyse long-chain hydrocarbons, with the catalytic and deactivation mechanisms married to the carbon's structural and physical properties (e.g., porosity correlating to catalytic ability), with these mechanisms and the product profile (e.g., lack of branched compounds) suggesting a different catalytic mechanism to that of traditional cracking acid catalysts. Aside from its rapid deactivation, which may or may not pose a surmountable issue in future reactor designs, the knowledge of the output products, including the ability to produce a very high proportion of aromatics, even at low reaction temperatures, provides a potential opportunity for future researchers to capitalise on, while the possibilities described in the future work section of this chapter indicate potential paths towards several other avenues of future exploration.

## 7.4 Closing Remarks

As with any doctoral thesis, the ultimate goal of this study was to make a contribution to the total sum of human knowledge. The development of any chemical process necessarily starts out small, and proceeds in incremental steps, each of which introduce new complexities and issues that must be overcome. While the deactivation of activated carbon prevents its use as a catalyst in the pyrolysis of long-chain hydrocarbons, at least in the configuration used in this work, it cannot be argued that this study did not produce valuable knowledge. Not only has this study provided an important contribution to the understanding of the use of activated carbon as a cracking catalyst, using the microwave-assisted pyrolysis of HDPE as an informative case study, but the knowledge from this study has also indicated where the future prospects of activated carbon catalysis may lie. It is hoped that out of the knowledge contained in this study, a future economically beneficial process will be developed that will help to maximise

the utilisation of hydrocarbons such as plastics, and contribute to an improvement in the efficiency with which humanity uses its increasingly scarce and difficult to obtain resources.

# References


[1] Plastics Europe. Plastics — the Facts. An analysis of European plastics production, demand and recovery. Technical report, Association of Plastics Manufacturers, Brussels, 2011.

[2] Plastics Challenge 2020. *Founding Commitments*. http://plastics2020challenge.com, Accessed 22/08/2012, 2010.

[3] Scott G. *Polymers and the Environment*. Royal Society of Chemistry, Cambridge, 1999.

[4] Sorum L., Gronli M.G., and Hustad J.E. Pyrolysis characteristics and kinetics of municipal solid wastes. *Fuel*, 80: 1217–1227, 2001.

[5] Rowat S.C. Incinerator toxic emissions: a brief summary of human health effects with a note on regulatory control. *Medical hypotheses*, 52: 389–396, 1999.

[6] Cormier S.A., Lomnicki S., Backes W., and Dellinger B. Origin and Health Impacts of Emissions of Toxic By-Products and Fine Particles from Combustion and Thermal Treatment of Hazardous Wastes and Materials. *Environmental Health Perspectives*, 114: 810–817, 2006.

[7] Adriano D.C., Page A.L., Elseewi A.A., Chang A.C., and Straughan I. Utilization and Disposal of Fly Ash and Other Coal Residues in Terrestrial Ecosystems: A Review, 1980.

[8] Dry M.E. The Fischer-Tropsch process: 1950-2000. *Catalysis Today*, 71: 227–241, 2002.

[9] Dry M.E. High quality diesel via the Fischer-Tropsch process — a review. *Journal of Chemical Technology & Biotechnology*, 77: 43–50, 2002.

[10] Aguado J., Serrano D.P., and San Miguel G. European Trends in the Feedstock Recycling of Plastic Wastes. *Global NEST Journal*, 9: 12–19, 2007.

[11] Mastral F., Esperanza E., Garcia P., and Juste M. Pyrolysis of high-density polyethylene in a fluidised bed reactor. Influence of the temperature and residence time. *Journal of Analytical and Applied Pyrolysis*, 63: 1–15, 2002.

[12] Domínguez A., Menéndez J.A., Fernández Y., Pis J.J., Nabais J.M.V., Carrott P.J.M., and Carrott M.M.L.R. Conventional and microwave induced pyrolysis of coffee hulls for the production of a hydrogen rich fuel gas. *Journal of Analytical and Applied Pyrolysis*, 79: 128–135, 2007.

[13] Buekens A. and Huang H. Catalytic plastics cracking for recovery of gasoline-range hydrocarbons from municipal plastic wastes. *Resources, Conservation and Recycling*, 23: 163–181, 1998.

[14] Kumar S., Panda A.K., and Singh R. A review on tertiary recycling of high-density polyethylene to fuel. *Resources, Conservation and Recycling*, 55: 893–910, 2011.

[15] Robinson J., Snape C., Kingman S., and Shang H. Thermal desorption and pyrolysis of oil contaminated drill cuttings by microwave heating. *Journal of Analytical and Applied Pyrolysis*, 81: 27–32, 2008.

[16] Jones D.A., Lelyveld T.P., Mavrofidis S.D., Kingman S.W., and Miles N.J. Microwave heating applications in environmental engineering — a review. *Resources, Conservation and Recycling*, 34: 75–90, 2002.

[17] Marken F., Sur U.K., Coles B.A., and Compton R.G. Focused microwaves in electrochemical processes. *Electrochimica Acta*, 51: 2195–2203, 2006.

[18] Zhang X. and Hayward D.O. Applications of microwave dielectric heating in environment-related heterogeneous gas-phase catalytic systems. *Inorganica Chimica Acta*, 359: 3421–3433, 2006.

[19] Miura M., Kaga H., Tanaka S., Takahashi K., and Ando K. Rapid Microwave Pyrolysis of Wood. *Journal of Chemical Engineering of Japan*, 33: 299–302, 2000.

[20] Lei H., Ren S., and Julson J. The Effects of Reaction Temperature and Time and Particle Size of Corn Stover on Microwave Pyrolysis. *Energy & Fuels*, 23: 3254–3261, 2009.

[21] Menéndez J.A., Dominguez A., Inguanzo M., and Pis J.J. Microwave pyrolysis of sewage sludge: analysis of the gas fraction. *Journal of Analytical and Applied Pyrolysis*, 71: 657–667, 2004.

[22] Fernández Y., Arenillas A., Bermúdez J., and Menéndez J. Comparative study of conventional and microwave-assisted pyrolysis, steam and dry reforming of glycerol for syngas production, using a carbonaceous catalyst. *Journal of Analytical and Applied Pyrolysis*, 88: 155–159, 2010.

[23] Udalov E.I., Bolotov V.A., Tanashev Y.Y., Chernousov Y.D., and Parmon V.N. Pyrolysis of liquid hexadecane with selective microwave heating of the catalyst. *Theoretical and Experimental Chemistry*, 46: 370–377, 2011.

[24] Zuo W., Tian Y., and Ren N. The important role of microwave receptors in bio-fuel production by microwave-induced pyrolysis of sewage sludge. *Waste management*, 31: 1321–1326, 2011.

[25] Haque K.E. Microwave energy for mineral treatment processes - a brief review. *International Journal of Mineral Processing*, 57: 1–24, 1999.

[26] Osepchuk J.M. and Fellow L. Microwave Power Applications. *IEEE Transactions on Microwave Theory and Techniques*, 50: 975–985, 2002.

[27] Holland K.M. Process of destructive distillation of organic material, United States Patent 5330623, 1994.

[28] Holland K.M. Apparatus for waste pyrolysis, United States Patent 5387321, 1995.

[29] Ludlow-Palafox C. and Chase H.A. Microwave-Induced Pyrolysis of Plastic Wastes. *Industrial & Engineering Chemistry Research*, 40: 4749–4756, 2001.

[30] Undri A., Rosi L., and Frediani M. *Microwave Pyrolysis of Polymeric Materials*. InTech, 2011.

[31] Anthony E. Fluidized bed combustion of alternative solid fuels; status, successes and problems of the technology. *Progress in Energy and Combustion Science*, 21: 239–268, 1995.

[32] Anthony E.J., Iribarne A.P., Iribarne J.V., Talbot R., Jia L., and Granatstein D.L. Fouling in a 160 MWe FBC boiler firing coal and petroleum coke. *Fuel*, 80: 1009–1014, 2001.

[33] Bryers R.W. Utilization of petroleum coke and petroleum coke/coal blends as a means of steam raising. *Fuel Processing Technology*, 44: 121–141, 1995.

[34] Juntgen H. Activated carbon as catalyst support: A review of new research results. *Fuel*, 65: 1436–1446, 1986.

[35] Aksoylu A., Madalena M., Freitas a., Pereira M.R., and Figueiredo J.L. The effects of different activated carbon supports and support modifications on the properties of Pt/AC catalysts. *Carbon*, 39: 175–185, 2001.

[36] Rodriguez-Reinoso F. The role of carbon materials in heterogeneous catalysis. *Carbon*, 36: 159–175, 1998.

[37] Trimm D.L. *Catalysis, Vol. 4*. The Royal Society of Chemistry, London, U.K., 1981.

[38] Pereira M.F.R., Orfao J.J.M., and Figueiredo J.L. Oxidative dehydrogenation of ethylbenzene on activated carbon catalysts. I. Influence of surface chemical groups. *Applied Catalysis A: General*, 184: 153–160, 1999.

[39] Muradov N., Smith F., and T-Raissi A. Catalytic activity of carbons for methane decomposition reaction. *Catalysis Today*, 102-103: 225–233, 2005.

[40] Key World Energy Statistics. Technical report, International Energy Agency, Paris, 2010.

[41] Klein D. *Organic Chemistry*. John Wiley and Sons, 2001.

[42] Nadim F., Liu S., Hoag G., and Chen J. A comparison of spectrophotometric and gas chromatographic measurements of heavy petroleum products in soil samples. *Water, Air, and Soil Pollution*, 134: 97–109, 2002.

[43] Anderson R. and Kahya D. The cost of petrol and oil: How it breaks down, 2011.

[44] Hall C.A.S., Balogh S., and Murphy D.J. What is the Minimum EROI that a Sustainable Society Must Have? *Energies*, 2: 25–47, 2009.

[45] Cossee P. Ziegler-Natta catalysis I. Mechanism of polymerization of [alpha]-olefins with Ziegler-Natta catalysts. *Journal of Catalysis*, 3: 80, 1964.

[46] Ludlow-Palafox C. *Microwave Induced Pyrolysis of Plastic Wastes*. PhD Thesis, University of Cambridge, 2001.

[47] Gu Xiasheng H.S.K. The Status and Trend of Water Pollution Control Technology in China. *Water International*, 7: 78–80, 1982.

[48] Linkov I. and Bridges T.S. (Eds.). *Climate*. NATO Science for Peace and Security Series C: Environmental Security. Springer Netherlands, Dordrecht, 2011.

[49] Williams A.T. and Simmons S.L. Sources of riverine litter: the river Taff, South Wales, UK. *Water, Air, and Soil Pollution*, 112: 197–216, 1999.

[50] Lodders K. Solar System Abundances and Condensation Temperature of the Elements. *The Astrophysics Journal*, 591: 1220–1247, 2003.

[51] Strock M. *Carbon Allotropes*. http://commons.wikimedia.org/wiki/File:Eight_Allotropes_of_Carbon.png, 2006.

[52] Marsh H. and Rodriguez-Reinoso F. *Activated Carbon*. Elsevier Ltd, Burlington, 2006.

[53] Franklin R.E. The interpretation of diffuse X-ray diagrams of carbon. *Acta Crystallographica*, 3: 107–121, 1950.

[54] Franklin R.E. The structure of graphitic carbons. *Acta Crystallographica*, 4: 253–261, 1951.

[55] Benaddi H., Bandosz T., Jagiello J., Schwarz J., Rouzaud J., Legras D., and Béguin F. Surface functionality and porosity of activated carbons obtained from chemical activation of wood. *Carbon*, 38: 669–674, 2000.

[56] Srinivasakannan C. Production of activated carbon from rubber wood sawdust. *Biomass and Bioenergy*, 27: 89–96, 2004.

[57] Khezami L., Chetouani A., Taouk B., and Capart R. Production and characterisation of activated carbon from wood components in powder: Cellulose, lignin, xylan. *Powder Technology*, 157: 48–56, 2005.

[58] Kirubakaran C.J., Krishnaiah K., and Seshadrit S.K. Experimental Study of the Production of Activated Carbon from Coconut Shells in a Fluidized Bed Reactor. *Industrial & Engineering Chemistry Research*, 30: 2411–2416, 1991.

[59] Gratuito M.K.B., Panyathanmaporn T., Chumnanklang R.a., Sirinuntawittaya N., and Dutta a. Production of activated carbon from coconut shell: optimization using response surface methodology. *Bioresource technology*, 99: 4887–4895, 2008.

[60] Satya Sai P.M., Ahmed J., and Krishnaiah K. Production of Activated Carbon from Coconut Shell Char in a Fluidized Bed Reactor. *Industrial & Engineering Chemistry Research*, 36: 3625–3630, 1997.

[61] Aygun A., Yenisoy-Karakas S., and Duman I. Production of granular activated carbon from fruit stones and nutshells and evaluation of their physical, chemical and adsorption properties. *Microporous and Mesoporous Materials*, 66: 189–195, 2003.

[62] Lafi W.K. Production of activated carbon from acorns and olive seeds. *Biomass and Bioenergy*, 20: 57–62, 2001.

[63] Haimour N.M. and Emeish S. Utilization of date stones for production of activated carbon using phosphoric acid. *Waste management (New York, N.Y.)*, 26: 651–660, 2006.

[64] Kim J.W., Sohn M.H., Kim D.S., Sohn S.M., and Kwon Y.S. Production of granular activated carbon from waste walnut shell and its adsorption characteristics for Cu2+ ion. *Journal of hazardous materials*, 85: 301–315, 2001.

[65] Ahmadpour A. and Do D.D. The preparation of activated carbon from macadamia nutshell by chemical activation. *Carbon*, 35: 1723–1732, 1997.

[66] Teng H. and Lin H.c. Activated carbon production from low ash subbituminous coal with CO2 activation. *AIChE Journal*, 44: 1170–1177, 1998.

[67] Jüntgen H., Knoblauch K., and Harder K. Carbon molecular sieves: production from coal and application in gas separation. *Fuel*, 60: 817–822, 1981.

[68] Lozano-Castello D., Lillo-Ródenas M.A., Cazorla-Amorós D., and Linares-Solano A. Preparation of activated carbons from Spanish anthracite: I. Activation by KOH. *Carbon*, 39: 741–749, 2001.

[69] DiPanfilo R. and Egiebor N. Activated carbon production from synthetic crude coke. *Fuel processing technology*, 46: 157–169, 1996.

[70] Gonzalez J., Gonzalez M., Molina-Sabio M., Rodriguez-Reinoso F., and Sepulveda-Escribano A. Porosity of activated carbons prepared from different lignocellulosic materials. *Carbon*, 338: 1175–1177, 1995.

[71] Rodriguez-Reinoso F. and Molina-Sabio M. Textural and chemical characterization of microporous carbons. *Advances in Colloid and Interface Science*, 76-77: 271–294, 1998.

[72] Caturla F., Molina-Sabio M., and Rodriguez-Reinoso F. Preparation of activated carbon by chemical activation with ZnCl2. *Carbon*, 29: 999–1007, 1991.

[73] Molina-Sabio M. and Rodriguez-Reinoso F. Role of chemical activation in the development of carbon porosity. *Colloids and Surfaces A: Physicochemical and Engineering Aspects*, 241: 15–25, 2004.

[74] Hayashi J., Kazehaya A., Muroyama K., and Watkinson A. Preparation of activated carbon from lignin by chemical activation. *Carbon*, 38: 1873–1878, 2000.

[75] Marsh H., Yan D., O'Grady T., and Wennerberg A. Formation of active carbons from cokes using potassium hydroxide. *Carbon*, 22: 603–611, 1984.

[76] Shih T.C., Wangpaichitr M., and Suffet M. Evaluation of granular activated carbon technology for the removal of methyl tertiary butyl ether (MTBE) from drinking water. *Water research*, 37: 375–385, 2003.

[77] Rengaraj S., Moon S.H., Sivabalan R., Arabindoo B., and Murugesan V. Agricultural solid waste for the removal of organics: adsorption of phenol from water and wastewater by palm seed coat activated carbon. *Waste management (New York, N.Y.)*, 22: 543–548, 2002.

[78] Giusti D., Conway R., and Lawson C. Activated carbon adsorption of petrochemicals. *Journal (Water Pollution Control . . . ,* 46: 947–965, 1974.

[79] Ternes T.a., Meisenheimer M., McDowell D., Sacher F., Brauch H.J., Haist-Gulde B., Preuss G., Wilme U., and Zulei-Seibert N. Removal of pharmaceuticals during drinking water treatment. *Environmental science & technology*, 36: 3855–3863, 2002.

[80] Yoon Y., Westerhoff P., Snyder S.A., and Esparza M. HPLC-fluorescence detection and adsorption of bisphenol A, 17beta-estradiol, and 17alpha-ethynyl estradiol on powdered activated carbon. *Water research*, 37: 3530–3537, 2003.

[81] Snyder S.A., Adham S., Redding A.M., Cannon F.S., DeCarolis J., Oppenheimer J., Wert E.C., and Yoon Y. Role of membranes and activated carbon in the removal of endocrine disruptors and pharmaceuticals. *Desalination*, 202: 156–181, 2007.

[82] Ebie K., Li F., Azuma Y., Yuasa A., and Hagishita T. Pore distribution effect of activated carbon in adsorbing organic micropollutants from natural water. *Water research*, 35: 167–179, 2001.

[83] Pelekani C. and Snoeyink V. Competitive adsorption in natural water: role of activated carbon pore size. *Water Research*, 33: 1209–1219, 1999.

[84] Bjelopavlic M., Newcombe G., and Hayes R. Adsorption of NOM onto Activated Carbon: Effect of Surface Charge, Ionic Strength, and Pore Volume Distribution. *Journal of colloid and interface science*, 210: 271–280, 1999.

[85] Mohan D. and Singh K.P. Single- and multi-component adsorption of cadmium and zinc using activated carbon derived from bagasse-an agricultural waste. *Water research*, 36: 2304–2318, 2002.

[86] Huang C. and Fu P. Treatment of arsenic (V)-containing water by the activated carbon process. *Journal (Water Pollution Control Federation)*, 56: 233–242, 1984.

[87] Kobya M., Demirbas E., Senturk E., and Ince M. Adsorption of heavy metal ions from aqueous solutions by activated carbon prepared from apricot stone. *Bioresource technology*, 96: 1518–21, 2005.

[88] Leggott N.L., Shephard G.S., Stockenström S., Staal E., and van Schatkwyk D.J. The reduction of patulin in apple juice by three different types of activated carbon. *Food additives and contaminants*, 18: 825–9, 2001.

[89] Ahmedna M., Johns M.M., Clarke S.J., Marshall W.E., and Rao R.M. Potential of agricultural by-product-based activated carbons for use in raw sugar decolourisation. *Journal of the Science of Food and Agriculture*, 75: 117–124, 1997.

[90] Ahmedna M., Marshall W., and Rao R. Surface properties of granular activated carbons from agricultural by-products and their effects on raw sugar decolorization. *Bioresource Technology*, 71: 103–112, 2000.

[91] Pandey R., Sanyal P., Chattopadhyay N., and Kaul S. Treatment and reuse of wastes of a vegetable oil refinery. *Resources, Conservation and Recycling*, 37: 101–117, 2003.

[92] Dutta M., Dutta N., and Bhattacharya K. Aqueous phase adsorption of certain beta-lactam antibiotics onto polymeric resins and activated carbon. *Separation and Purification Technology*, 16: 213–224, 1999.

[93] Tamai H., Kakii T., Hirota Y., Kumamoto T., and Yasuda H. Synthesis of Extremely Large Mesoporous Activated Carbon and Its Unique Adsorption for Giant Molecules. *Chemistry of Materials*, 8: 454–462, 1996.

[94] Ruhl M. Recovery of VOCs via adsorption on activated carbon. *Chemical Engineering Progress*, pp. 37–41, 1993.

[95] Gurrath M., Kuretzky T., and Boehm H. Palladium catalysts on activated carbon supports: Influence of reduction temperature, origin of the support and pretreatments of the carbon surface. *Carbon*, 38: 1241–1255, 2000.

[96] Yang Y., Chiang K., and Burke N. Porous carbon-supported catalysts for energy and environmental applications: A short review. *Catalysis Today*, 178: 197–205, 2011.

[97] Prado-Burguete C., Linares-Solano A., Rodríguez-Reinoso F., and de Lecea C.M. The effect of oxygen surface groups of the support on platinum dispersion in Pt/carbon catalysts. *Journal of Catalysis*, 115: 98–106, 1989.

[98] Suh D.J., Park T.J., and Ihm S.K. Characteristics of carbon-supported palladium catalysts for liquid-phase hydrogenation of nitroaromatics. *Industrial & Engineering Chemistry Research*, 31: 1849–1856, 1992.

[99] Auer E., Freund a., Pietsch J., and Tacke T. Carbons as supports for industrial precious metal catalysts. *Applied Catalysis A: General*, 173: 259–271, 1998.

[100] Ma W., Ding Y., and Lin L. Fischer-Tropsch synthesis over activated-carbon-supported cobalt catalysts: Effect of Co loading and promoters on catalyst performance. *Industrial & engineering chemistry . . .* , 43: 2391–2398, 2004.

[101] Ma W., Kugler E.L., Wright J., and Dadyburjor D.B. Mo-Fe catalysts supported on activated carbon for synthesis of liquid fuels by the Fischer-Tropsch process: effect of Mo addition on reducibility, activity, and hydrocarbon. *Energy & Fuels*, 20: 2299–2307, 2006.

[102] Ma W., Kugler E.L., and Dadyburjor D.B. Effect of Properties of Various Activated-Carbon Supports and Supported Fe-Mo-Cu-K Catalysts on Metal Precursor Distribution, Metal Reduction, and Fischer-Tropsch Synthesis. *Energy & Fuels*, 24: 4099–4110, 2010.

[103] Kubickova I., Snare M., Eranen K., Maki-Arvela P., and Murzin D.Y. Hydrocarbons for diesel fuel via decarboxylation of vegetable oils. *Catalysis Today*, 106: 197–200, 2005.

[104] Baroutian S., Aroua M.K., Raman A.A.A., and Sulaiman N.M.N. A packed bed membrane reactor for production of biodiesel using activated carbon supported catalyst. *Bioresource technology*, 102: 1095–1102, 2011.

[105] Dalai A.K., Majumdar a., and Tollefson E.L. Low Temperature Catalytic Oxidation of Hydrogen Sulfide in Sour Produced Wastewater Using Activated Carbon Catalysts. *Environmental Science & Technology*, 33: 2241–2246, 1999.

[106] Wu X., Kercher A.K., Schwartz V., Overbury S.H., and Armstrong T.R. Activated carbons for selective catalytic oxidation of hydrogen sulfide to sulfur. *Carbon*, 43: 1087–1090, 2005.

[107] Richter E. Carbon catalysts for pollution control. *Catalysis Today*, 7: 93–112, 1990.

[108] de Jesús Díaz Velásquez J., Suárez L.M.C., and Figueiredo J.L. Oxidative dehydrogenation of isobutane over activated carbon catalysts. *Applied Catalysis A: General*, 311: 51–57, 2006.

[109] Lisovskii A. and Aharoni C. Carbonaceous deposits as catalysts for oxydehydrogenation of alkylbenzenes. *Catalysis Reviews: Science and Engineering*, 36: 25–74, 1994.

[110] Pereira M., Orfao J., and Figueiredo J. Oxidative dehydrogenation of ethylbenzene on activated carbon catalysts: 2. Kinetic modelling. *Applied Catalysis A: General*, 196: 43–54, 2000.

[111] Pereira M., Orfao J., and Figueiredo J. Oxidative dehydrogenation of ethylbenzene on activated carbon catalysts: 3. Catalyst deactivation. *Applied Catalysis A: General*, 218: 307–318, 2001.

[112] Grunewald G. and Drago R. Oxidative dehydrogenation of ethylbenzene to stykene over carbon-based catalysts. *Journal of Molecular Catalysis*, 58: 227–233, 1990.

[113] Guerrero-Ruiz a. and Rodríguez-Ramos I. Oxydehydrogenation of ethylbenzene to styrene catalyzed by graphites and activated carbons. *Carbon*, 32: 23–29, 1994.

[114] Szymanski G.S. and Rychlicki G. Importance of oxygen surface groups in catalytic dehydration and dehydrogenation of butan-2-ol promoted by carbon catalysts. *Carbon*, 29: 489–498, 1991.

[115] Szymanski G. and Rychlicki G. Catalytic conversion of propan-2-ol on carbon catalysts. *Carbon*, 31: 247–257, 1993.

[116] Szymanski G., Rychlicki G., and Terzyk A. Catalytic conversion of ethanol on carbon catalysts. *Carbon*, 32, 1994.

[117] Muradov N., Smith F., Huang C., and T-Raissi A. Autothermal catalytic pyrolysis of methane as a new route to hydrogen production with reduced CO2 emissions. *Catalysis Today*, 116: 281–288, 2006.

[118] Muradov N.Z. How to produce hydrogen from fossil fuels without CO2 emission. *International Journal of Hydrogen Energy*, 18: 211–215, 1993.

[119] Muradov N.Z. CO2-Free Production of Hydrogen by Catalytic Pyrolysis of Hydrocarbon Fuel. *Energy & Fuels*, 12: 41–48, 1998.

[120] Muradov N. Catalysis of methane decomposition over elemental carbon. *Catalysis Communications*, 2: 89–94, 2001.

[121] Muradov N. Hydrogen via methane decomposition: an application for decarbonization of fossil fuels. *International Journal of Hydrogen Energy*, 26: 1165–1175, 2001.

[122] Jung J., Nam W., Yoon K., and Han G. Hydrogen production by catalytic decomposition of methane over carbon catalysts in a fluidized bed. *Korean Journal of Chemical . . .* , 24: 674–678, 2007.

[123] Petkovic L.M., Ginosar D.M., Rollins H.W., Burch K.C., Deiana C., Silva H.S., Sardella M.F., and Granados D. Activated carbon catalysts for the production of hydrogen via the sulfur-iodine thermochemical water splitting cycle. *International Journal of Hydrogen Energy*, 34: 4057–4064, 2009.

[124] Meredith R. *Engineers' handbook of industrial microwave heating*. The Institution of Electrical Engineers, London, 1998.

[125] Metaxas A. and Meredith R. *Industrial Microwave Heating*. Peter Peregrinus, London, 1993.

[126] Metaxas A. *Foundations of electroheat: a unified approach*. John Wiley and Sons, 1996.

[127] Kaye and Laby. *Tables of Physical & Chemical Constants*. The National Physical Laboratory, Teddington, 2006.

[128] Menéndez J.A., Arenillas A., Fidalgo B., Fernández Y., Zubizarreta L., Calvo E., and Bermúdez J. Microwave heating processes involving carbon materials. *Fuel Processing Technology*, 91: 1–8, 2010.

[129] Atwater J. and Wheeler Jr. R. Microwave permittivity and dielectric relaxation of a high surface area activated carbon. *Applied Physics A: Materials Science & Processing*, 79: 125–129, 2004.

[130] Thostenson E. and Chou T.W. Microwave processing: fundamentals and applications. *Composites Part A: Applied Science and Manufacturing*, 30: 1055–1071, 1999.

[131] Fukushimaa H., Yamanakaa T., and Matsui M. Microwave heating of ceramics and its application to joining. *Journal of Materials Research*, 5: 397–405, 1990.

[132] Marand E., Baker K.R., and Graybeal J.D. Reaction mechanisms of epoxy resins undergoing thermal and microwave cure from in situ measurements of microwave dielectric properties and infrared spectroscopy. *Macromolecules*, 25: 2243–2252, 1992.

[133] Lidström P., Tierney J., Wathey B., and Westman J. Microwave assisted organic synthesis–a review. *Tetrahedron*, 57: 9225–9283, 2001.

[134] Gedye R.N., Smith F.E., and Westaway K.C. The rapid synthesis of organic compounds in microwave ovens. *Canadian Journal of Chemistry*, 66: 17–26, 1988.

[135] Roberts B.A. and Strauss C.R. Toward rapid, "green", predictable microwave-assisted synthesis. *Accounts of chemical research*, 38: 653–661, 2005.

[136] Wei J., Hawley M.C., and Demeuse M.T. Kinetics modeling and time-temperature-transformation diagram of microwave and thermal cure of epoxy resins. *Polymer Engineering and Science*, 35: 461–470, 1995.

[137] Clark D.E. and Sutton W.H. Microwave processing of materials. *Annual Review of Materials Science*, 26: 299–331, 1996.

[138] de la Hoz A., Díaz-Ortiz A., and Moreno A. Microwaves in organic synthesis. Thermal and non-thermal microwave effects. *Chemical Society Reviews*, 34: 164–178, 2005.

[139] Hosseini M., Stiasni N., Barbieri V., and Kappe C.O. Microwave-assisted asymmetric organocatalysis. A probe for nonthermal microwave effects and the concept of simultaneous cooling. *The Journal of organic chemistry*, 72: 1417–24, 2007.

[140] Herrero M.A., Kremsner J.M., and Kappe C.O. Nonthermal microwave effects revisited: on the importance of internal temperature monitoring and agitation in microwave chemistry. *The Journal of organic chemistry*, 73: 36–47, 2008.

[141] Schmink J.R. and Leadbeater N.E. Probing "microwave effects" using Raman spectroscopy. *Organic & biomolecular chemistry*, 7: 3842–6, 2009.

[142] Domínguez A., Fidalgo B., Fernandez Y., Pis J., and Menendez J. Microwave-assisted catalytic decomposition of methane over activated carbon for CO2-free hydrogen production. *International Journal of Hydrogen Energy*, 32: 4792–4799, 2007.

[143] Muradov N.Z. The generation of microwave-induced plasma in granular active carbons under fluidised bed conditions. *Carbon*, 46: 220–228, 2008.

[144] Fernández Y., Fidalgo B., Domínguez A., Arenillas A., and Menéndez J. Carbon nanofilament synthesis by the decomposition of CH4/CO2 under microwave heating. *Carbon*, 45: 1706–1709, 2007.

[145] Jiang S. *Microwave pyrolysis of waste automotive tyres*. CPGS Project Report, University of Cambridge, 2004.

[146] Yatsun a.V., Konovalov P.N., and Konovalov N.P. Gaseous products of microwave pyrolysis of scrap tires. *Solid Fuel Chemistry*, 42: 187–191, 2008.

[147] Lee A. Waving aside tyre incineration. *Engineer*, 292: 12, 2003.

[148] Sharma V., Fortuna F., Mincarini M., Berillo M., and Cornacchia G. Disposal of waste tyres for energy recovery and safe environment. *Applied Energy*, 65: 381–394, 2000.

[149] Lam S.S., Russell A.D., and Chase H.A. Microwave pyrolysis, a novel process for recycling waste automotive engine oil. *Energy*, 35: 2985–2991, 2010.

[150] Lam S.S., Russell A.D., and Chase H.A. Pyrolysis Using Microwave Heating: A Sustainable Process for Recycling Used Car Engine Oil. *Industrial & Engineering Chemistry Research*, 49: 10845–10851, 2010.

[151] Lam S.S. *Microwave-induced Pyrolysis of Waste Automotive Oil*. PhD Thesis, University of Cambridge, 2011.

[152] Lam S.S., Russell A.D., Lee C.L., and Chase H.A. Microwave-heated pyrolysis of waste automotive engine oil: Influence of operation parameters on the yield, composition, and fuel properties of pyrolysis oil. *Fuel*, 92: 327–339, 2012.

[153] Menéndez J.a., Inguanzo M., and Pis J.J. Microwave-induced pyrolysis of sewage sludge. *Water research*, 36: 3261–4, 2002.

[154] Menéndez J.A., Domínguez A., Inguanzo M., and Pis J.J. Microwave-induced drying, pyrolysis and gasification (MWDPG) of sewage sludge: Vitrification of the solid residue. *Journal of Analytical and Applied Pyrolysis*, 74: 406–412, 2005.

[155] Domínguez A., Menéndez J.A., Inguanzo M., and Pís J.J. Production of bio-fuels by high temperature pyrolysis of sewage sludge using conventional and microwave heating. *Bioresource technology*, 97: 1185–93, 2006.

[156] Domínguez A., Menéndez J.A., Inguanzo M., Bernad P.L., and Pis J.J. Gas chromatographic-mass spectrometric study of the oil fractions produced by microwave-assisted pyrolysis of different sewage sludges. *Journal of chromatography. A*, 1012: 193–206, 2003.

[157] Domínguez a., Menéndez J.A., Inguanzo M., and Pis J.J. Investigations into the characteristics of oils produced from microwave pyrolysis of sewage sludge. *Fuel Processing Technology*, 86: 1007–1020, 2005.

[158] Miura M., Kaga H., Sakurai A., Kakuchi T., and Takahashi K. Rapid pyrolysis of wood block by microwave heating. *Journal of Analytical and Applied Pyrolysis*, 71: 187–199, 2004.

[159] Budarin V.L., Zhao Y., Gronnow M.J., Shuttleworth P.S., Breeden S.W., Macquarrie D.J., and Clark J.H. Microwave-mediated pyrolysis of macro-algae. *Green Chemistry*, 13: 2330, 2011.

[160] Huang Y.F., Kuan W.H., Lo S.L., and Lin C.F. Total recovery of resources and energy from rice straw using microwave-induced pyrolysis. *Bioresource technology*, 99: 8252–8258, 2008.

[161] Yagmur E., Ozmak M., and Aktas Z. A novel method for production of activated carbon from waste tea by chemical activation with microwave energy. *Fuel*, 87: 3278–3285, 2008.

[162] Budarin V.L., Clark J.H., Lanigan B.a., Shuttleworth P., Breeden S.W., Wilson A.J., Macquarrie D.J., Milkowski K., Jones J., Bridgeman T., and Ross A. The preparation of high-grade bio-oils through the controlled, low temperature microwave activation of wheat straw. *Bioresource technology*, 100: 6064–6068, 2009.

[163] El Harfi K., Mokhlisse A., Chanâa M.B., and Outzourhit A. Pyrolysis of the Moroccan (Tarfaya) oil shales under microwave irradiation. *Fuel*, 79: 733–742, 2000.

[164] Monsef-Mirzai P. and Ravindran M. The use of microwave heating for the pyrolysis of coal via inorganic receptors of microwave energy. *Fuel*, 71: 716–717, 1992.

[165] Monsef-Mirzai P., Ravindran M., McWhinnie W.R., and Burchill P. Rapid microwave pyrolysis of coal. *Fuel*, 74: 20–27, 1995.

[166] Ma S., Zhao Y., Guo T., and Ma X. Experimental Study on Microwave-Induced NO Decomposition on Activated Carbon Bed. In *2009 Asia-Pacific Power and Energy Engineering Conference*, pp. 1–4. IEEE, 2009.

[167] Fernández Y., Arenillas A., Díez M.A., Pis J.J., and Menéndez J.A. Pyrolysis of glycerol over activated carbons for syngas production. *Journal of Analytical and Applied Pyrolysis*, 84: 145–150, 2009.

[168] Fidalgo B., Fernández Y., Domínguez A., Pis J.J., and Menéndez J. Microwave-assisted pyrolysis of CH4/N2 mixtures over activated carbon. *Journal of Analytical and Applied Pyrolysis*, 82: 162–158, 2008.

[169] Bu Q., Lei H., Ren S., Wang L., Holladay J., Zhang Q., Tang J., and Ruan R. Phenol and phenolics from lignocellulosic biomass by catalytic microwave pyrolysis. *Bioresource technology*, 102: 7004–7, 2011.

[170] Kaminsky W. Thermal recycling of polymers. *Journal of Analytical and Applied Pyrolysis*, 8: 439–448, 1985.

[171] Kaminsky W. Pyrolysis of plastic waste and scrap tyres in a fluid bed reactor. *Resource Recovery and Conservation*, 5: 205–216, 1980.

[172] Williams E.A. and Williams P.T. The pyrolysis of individual plastics and a plastic mixture in a fixed bed reactor. *Journal of Chemical Technology & Biotechnology*, 70: 9–20, 1997.

[173] Williams P.T. and Williams E.A. Fluidised bed pyrolysis of low density polyethylene to produce petrochemical feedstock. *Journal of Analytical and Applied Pyrolysis*, 51: 107–126, 1999.

[174] Conesa J.A., Font R., Marcilla A., and Garcia A.N. Pyrolysis of Polyethylene in a Fluidized Bed Reactor. *Energy & Fuels*, 8: 1238–1246, 1994.

[175] Milne B., Behie L., and Berruti F. Recycling of waste plastics by ultrapyrolysis using an internally circulating fluidized bed reactor. *Journal of Analytical and applied Pyrolysis*, 51: 157–166, 1999.

[176] Aguado R., Olazar M., María J., Gaisán B., and Bilbao J. Wax formation in the pyrolysis of polyolefins in a conical spouted bed reactor. *Energy & fuels*, 16: 1429–1437, 2002.

[177] Mastral F., Esperanza E., Berrueco C., Juste M., and Ceamanos J. Fluidized bed thermal degradation products of HDPE in an inert atmosphere and in air-nitrogen mixtures. *Journal of Analytical and Applied Pyrolysis*, 70: 1–17, 2003.

[178] Mastral J., Berrueco C., Gea M., and Ceamanos J. Catalytic degradation of high density polyethylene over nanocrystalline HZSM-5 zeolite. *Polymer Degradation and Stability*, 91: 3330–3338, 2006.

[179] Berrueco C. and Mastral F. Production of waxes and tars from the continuous pyrolysis of high density polyethylene. Influence of operation variables. *Energy & fuels*, 16: 1148–1153, 2002.

[180] Ludlow-Palafox C. *Enval's Beginnings*. http://www.enval.com/history.php, 2009.

[181] Bockhorn H., Hornung a., Hornung U., and Schawaller D. Kinetic study on the thermal degradation of polypropylene and polyethylene. *Journal of Analytical and Applied Pyrolysis*, 48: 93–109, 1999.

[182] Aguado R., Olazar M., and Gaisán B. Kinetics of polystyrene pyrolysis in a conical spouted bed reactor. *Chemical Engineering . . .* , 92: 91–99, 2003.

[183] Scott D.S., Czernik S.R., Piskorz J., and Radlein D.S.A.G. Fast Pyrolysis of Plastic Wastes. *Energy & Fuels*, 4: 407–411, 1990.

[184] Bockhorn H., Hentschel J., Hornung a., and Hornung U. Environmental engineering: Stepwise pyrolysis of plastic waste. *Chemical Engineering Science*, 54: 3043–3051, 1999.

[185] Kaminsky W. and Franck J. Monomer recovery by pyrolysis of poly (methyl methacrylate) (PMMA). *Journal of Analytical and Applied Pyrolysis*, 19: 311–318, 1991.

[186] Kumar S. and Singh R.K. Recovery of Hydrocarbon Liquids from Waste High Density Polyethylene by Thermal Pyrolysis. *Brazilian Journal of Chemical Engineering*, 28: 659–667, 2011.

[187] Campbell I.M. *Catalysis at Surfaces*. Chapman and Hall, London, 1988.

[188] Sharratt P.N., Lin Y.H., Garforth a.a., and Dwyer J. Investigation of the catalytic pyrolysis of high-density polyethylene over a HZSM-5 catalyst in a laboratory fluidized-bed reactor. *Industrial & Engineering Chemistry Research*, 36: 5118–5124, 1997.

[189] Miskolczi N. and Bartha L. Investigation of hydrocarbon fractions form waste plastic recycling by FTIR, GC, EDXRFS and SEC techniques. *Journal of biochemical and biophysical methods*, 70: 1247–53, 2008.

[190] Seo Y.H., Lee K.H., and Shin D.H. Investigation of catalytic degradation of high-density polyethylene by hydrocarbon group type analysis. *Journal of Analytical and Applied Pyrolysis*, 70: 383–398, 2003.

[191] Bagri R. and Williams P.T. Catalytic pyrolysis of polyethylene. *Journal of Analytical and Applied Pyrolysis*, 63: 29–41, 2002.

[192] Negelein D.L., Lin R., and White R.L. Effects of catalyst acidity and HZSM-5 channel volume on polypropylene cracking. *Journal of Applied Polymer Science*, 37: 341–348, 1998.

[193] Manos G., Garforth A., and Dwyer J. Catalytic Degradation of High-Density Polyethylene over Different Zeolitic Structures. *Industrial & Engineering Chemistry Research*, 39: 1198–1202, 2000.

[194] Garforth A.A., Lin Y.H., Sharratt P.N., and Dwyer J. Production of hydrocarbons by catalytic degradation of high density polyethylene in a laboratory fluidised-bed reactor. *Applied Catalysis A: General*, 169: 331–342, 1998.

[195] Lin Y.H., Yang M.H., Yeh T.F., and Ger M.D. Catalytic degradation of high density polyethylene over mesoporous and microporous catalysts in a fluidised-bed reactor. *Polymer Degradation and Stability*, 86: 121–128, 2004.

[196] Ali S., Garforth A., Harris D., Rawlence D., and Uemichi Y. Polymer waste recycling over "used" catalysts. *Catalysis Today*, 75: 247–255, 2002.

[197] González Y.S., Costa C., Márquez M.C., and Ramos P. Thermal and catalytic degradation of polyethylene wastes in the presence of silica gel, 5A molecular sieve and activated carbon. *Journal of hazardous materials*, 187: 101–112, 2011.

[198] Strouse G., Burns G., Croarkin M., Scroger M., and Guthrie W. Temperature-Electromotive Force Reference Functions and Tables for the Letter-Designated Thermocouple Types Based on the ITS-90. Technical report, National Institute of Standards and Technology, 1993.

[199] King M. *Process Control: A Practical Approach*. Wiley, 2010.

[200] Ziegler J. and Nichols N. Optimum settings for PID controllers. *Transactions of ASME*, 64: 759–768, 1942.

[201] Predel M. and Kaminsky W. Pyrolysis of mixed polyolefins in a fluidised-bed reactor and on a pyro-GC/MS to yield aliphatic waxes. *Polymer Degradation and Stability*, 70: 373–385, 2000.

[202] Kaminsky W. and Zorriqueta I.J. Catalytical and thermal pyrolysis of polyolefins. *Journal of Analytical and Applied Pyrolysis*, 79: 368–374, 2007.

[203] Aboulkas A., El harfi K., and El Bouadili A. Thermal degradation behaviors of polyethylene and polypropylene. Part I: Pyrolysis kinetics and mechanisms. *Energy Conversion and Management*, 51: 1363–1369, 2010.

[204] Arabiourrutia M., Elordi G., Lopez G., Borsella E., Bilbao J., and Olazar M. Characterization of the waxes obtained by the pyrolysis of polyolefin plastics in a conical spouted bed reactor. *Journal of Analytical and Applied Pyrolysis*, 94: 230–237, 2012.

[205] Elordi G., Olazar M., Lopez G., Artetxe M., and Bilbao J. Product Yields and Compositions in the Continuous Pyrolysis of High-Density Polyethylene in a Conical Spouted Bed Reactor. *Industrial & Engineering Chemistry Research*, 50: 6650–6659, 2011.

[206] Cozzani V., Nicolella C., Rovatti M., and Tognotti L. Influence of Gas-Phase Reactions on the Product Yields Obtained in the Pyrolysis of Polyethylene. *Industrial & Engineering Chemistry Research*, 36: 342–348, 1997.

[207] Donaj P.J., Kaminsky W., Buzeto F., and Yang W. Pyrolysis of polyolefins for increasing the yield of monomers' recovery. *Waste management (New York, N.Y.)*, 32: 840–6, 2012.

[208] Hernández M.d.R., García A.N., and Marcilla A. Catalytic flash pyrolysis of HDPE in a fluidized bed reactor for recovery of fuel-like hydrocarbons. *Journal of Analytical and Applied Pyrolysis*, 78: 272–281, 2007.

[209] McCaffrey W., Cooper D., and Kamal M. Tertiary recycling of polyethylene: mechanism of liquid production from polyethylene by thermolysis/reactive distillation. *Polymer Degradation and Stability*, 62: 513–521, 1998.

[210] Blazsó M. Polyaromatization in common synthetic polymers at elevated temperatures. *Journal of Analytical and Applied Pyrolysis*, 25: 25–35, 1993.

[211] Achilias D.S., Roupakias C., Megalokonomos P., Lappas A.A., and Antonakou E.V. Chemical recycling of plastic wastes made from polyethylene (LDPE and HDPE) and polypropylene (PP). *Journal of hazardous materials*, 149: 536–42, 2007.

[212] Al-Salem S. and Lettieri P. Kinetic study of high density polyethylene (HDPE) pyrolysis. *Chemical Engineering Research and Design*, 88: 1599–1606, 2010.

[213] Marcilla A., Beltrán M., and Navarro R. Thermal and catalytic pyrolysis of polyethylene over HZSM5 and HUSY zeolites in a batch reactor under dynamic conditions. *Applied Catalysis B: Environmental*, 86: 78–86, 2009.

[214] Hernández M.d.R., Gómez A., García A.N., Agulló J., and Marcilla A. Effect of the temperature in the nature and extension of the primary and secondary reactions in the thermal and HZSM-5 catalytic pyrolysis of HDPE. *Applied Catalysis A: General*, 317: 183–194, 2007.

[215] Pasel C. and Wanzl W. Experimental investigations on reactor scale-up and optimisation of product quality in pyrolysis of shredder waste. *Fuel Processing Technology*, 80: 47–67, 2003.

[216] Çelikten I., Koca A., and Ali Arslan M. Comparison of performance and emissions of diesel fuel, rapeseed and soybean oil methyl esters injected at different pressures. *Renewable Energy*, 35: 814–820, 2010.

[217] Czernik S. and Bridgwater A.V. Overview of Applications of Biomass Fast Pyrolysis Oil. *Energy & Fuels*, 18: 590–598, 2004.

[218] Graboski M. and McCormick R. Combustion of fat and vegetable oil derived fuels in diesel engines. *Progress in Energy and Combustion*, 24: 125–164, 1998.

[219] Solantausta Y., Nylund N., and Westerholm M. Wood-pyrolysis oil as fuel in a diesel-power plant. *Bioresource Technology*, 46: 177–188, 1993.

[220] ASTM D4814-11b Standard Specification for Automotive Spark-Ignition Engine Fuel. Technical report, ASTM International, 2011.

[221] ASTM D975-11b Standard Specification for Diesel Fuel Oils. Technical report, ASTM International, 2011.

[222] Azev V.S., Emel'yanov V.E., and Turovskii F.V. Automotive Gasolines. Long-Term Requirements for Composition and Properties. *Chemistry and Technology of Fuels and Oils*, 40: 291–297, 2004.

[223] Jones D.S. and Pujado P.R. (Eds.). *Handbook of Petroleum Processing*. Springer Netherlands, Dordrecht, 2006.

[224] Facts and Figures of the Chemical Industry. *Chemical & Engineering News*, 90: 59–60, 2011.

[225] Wampler T. *Applied Pyrolysis Handbook*. CRC Press, Boca Raton, FL, 1st edition, 1995.

[226] Westerhout R.W.J., Waanders J., Kuipers J.A.M., and Swaaij W.P.M.V. Kinetics of the Low-Temperature Pyrolysis of Polyethene, Polypropene, and Polystyrene Modeling, Experimental Determination, and Comparison with Literature Models and Data. *Industrial & Engineering Chemistry Research*, 36: 1955–1964, 1997.

[227] Kim S. and Kim Y.C. Using isothermal kinetic results to estimate the kinetic triplet of the pyrolysis of high density polyethylene. *Journal of Analytical and Applied Pyrolysis*, 73: 117–121, 2005.

[228] Cypres R. Aromatic hydrocarbons formation during coal pyrolysis. *Fuel Processing Technology*, 15: 1–15, 1987.

[229] Rice F.O. The Thermal Decomposition of Organic Compounds from the Standpoint of Free Radicals. I. Saturated Hydrocarbons. *Journal of the American Chemical Society*, 54: 1959–1972, 1931.

[230] Rice F.O., Johnston W., and Evering B. The Thermal Decomposition of Organic Compounds from the Standpoint of Free Radicals. II. Experimental Evidence of the Decomposition of Organic Compounds into Free Radicals. *Journal of the American Chemical Society*, 54: 3529–3543, 1932.

[231] Rice F.O. The Thermal Decomposition of Organic Compounds from the Standpoint of Free Radicals. III. The Calculation of the Products Formed from Paraffin Hydrocarbons. *Journal of the American Chemical Society*, 55: 3035–3040, 1933.

[232] Rice F.O. and Dooley M. The Thermal Decompositon of Organic Compounds from the Standpoint of Free Radicals. IV. The Dehydrogenation of Paraffin Hydrocarbons and the Strength of the C-C Bond. *Journal of the American Chemical Society*, 55: 4245–4247, 1933.

[233] Rice F. and Johnston W. The Thermal Decomposition of Organic Compounds from the Standpoint of Free Radicals. V. The Strength of Bonds in Organic Molecules. *Journal of the American Chemical Society*, 56: 214–219, 1934.

[234] Rice F. and Herzfeld K.F. The Thermal Decomposition of Organic Compounds from the Standpoint of Free Radicals. VI. The Mechanism of Some Chain Reactions. *Journal of the American Chemical Society*, 56: 284–289, 1934.

[235] Kossiakoff A. and Rice F.O. Thermal Decomposition of Hydrocarbons, Resonance Stabilization and Isomerization of Free Radicals. *Journal of the American Chemical Society*, 65: 590–595, 1943.

[236] Simha R. and Wall L.A. Some aspects of depolymerization kinetics. *Journal of Polymer Science*, 6: 39–44, 1951.

[237] Wall L.A., Flynn J.H., and Straus S. Rates of Molecular Vaporization of Linear Alkanes. *Journal of Physical Chemistry*, 74: 3237–3242, 1970.

[238] Roedel M. The Molecular Structure of Polyethylene. I. Chain Branching in Polyethylene during Polymerization. *Journal of the American Chemical Society*, 75: 6110–6112, 1953.

[239] Song C., Lai W.C., and Schobert H.H. Condensed-Phase Pyrolysis of n-Tetradecane at Elevated Pressures for Long Duration. Product Distribution and Reaction Mechanisms. *Industrial & Engineering Chemistry Research*, 33: 534–547, 1994.

[240] van Schooten J. and Evenhuis J.K. Pyrolysis-Hydrogenation-GLC of Polyolefins. *Polymer*, 6: 343–360, 1959.

[241] Wu G., Katsumura Y., Matsuura C., Ishigure K., and Kubo J. Radiation Effect on the Thermal Cracking of n -Hexadecane. 2. A Kinetic Approach to Chain Reaction. *Industrial & Engineering Chemistry Research*, 36: 3498–3504, 1997.

[242] Miller D. Higher Alpha, Omega-Dienes in Paraffin and Olefin Pyrolyzates. *Industrial & Engineering Chemistry Product Research and Development*, 2: 220–223, 1963.

[243] Diels O. and Alder K. Synthesen in der hydroaromatischen Reihe. *Justus Liebig's Annalen der Chemie*, 460: 98–122, 1928.

[244] Crittenden B.D. and Long R. Formation of polycyclic aromatics in rich premixed acetylene and ethylene flames. *Combustion and Flame*, 20: 359–368, 1973.

[245] Cole J.A., Bittner J.D., Longwell J.P., and Howard J.B. Formation Mechanisms of Aromatic Compounds in Aliphatic Flames. *Combustion and Flame*, 56: 51–70, 1984.

[246] Badger G., Buttery R., Kimber R., Lewis G., Moritz A., and Napier I. The Formation of Aromatic Hydrocarbons at High Temperatures. Part I. Introduction. *Journal of the Chemical Society*, pp. 2449–2452, 1958.

[247] Frenklach M., Clary D.W., Gardiner W.C., and Stein S.E. Detailed kinetic modeling of soot formation in shock-tube pyrolysis of acetylene. *Symposium (International) on Combustion*, 20: 887–901, 1985.

[248] Richter H. and Howard J. Formation of polycyclic aromatic hydrocarbons and their growth to soot - a review of chemical reaction pathways. *Progress in Energy and Combustion Science*, 26: 565–608, 2000.

[249] Cejkaa J., ZilkovÃia N., Zonesb S., and BejblovÃia M. Novel Zeolites in Transformation of Aromatic Hydrocarbons. *18th Saudi Japan Symposium*, 1: 1–9, 2008.

[250] Corma A., Fornes V., Garcia H., Marti V., and Miranda M. Acid Zeolites as Electron Acceptors. Use of Thianthrene Radical Cation as a Probe. *Chemistry of Materials*, 7: 2136–2143, 1995.

[251] Sankararaman S., Yoon K., Yabe T., and Kochi J. Control of back electron transfer from charge-transfer ion pairs by zeolite supercages. *Journal of the American Chemisty Society*, 113: 1419–1421, 1991.

[252] Greensfelder B., Voge H., and Good G. Catalytic and Thermal Cracking of Pure Hvdrocarbons. *Industrial and Engineering Chemistry*, 41: 2573–2584, 1949.

[253] Suelves I., Lázaro M., Moliner R., Pinilla J., and Cubero H. Hydrogen production by methane decarbonization: Carbonaceous catalysts. *International Journal of Hydrogen Energy*, 32: 3320–3326, 2007.

[254] Whitmore F.C. Mechanism of the Polymerization of Olefins by Acid Catalysts. *Industrial & Engineering Chemistry*, 26: 94–95, 1934.

[255] Corma A. and Orchilles A.V. Current views on the mechanism of catalytic cracking. *Microporous and Mesoporous Materials*, 35–36: 21–30, 2000.

[256] Cumming K.A. and Wojciechowski B.W. Hydrogen Transfer, Coke Formation, and Catalyst Decay and Their Role in the Chain Mechanism of Catalytic Cracking. *Catalysis Reviews: Science and Engineering*, 38: 101–157, 2006.

[257] Zawadzki J. IR spectroscopy studies of oxygen surface compounds on carbon. *Carbon*, 16: 491–497, 1978.

[258] Ishizaki C. and Marti I. Surface oxide structures on a commercial activated carbon. *Carbon*, 19: 409–412, 1981.

[259] Strelko Jr. V., Malik D.J., and Streat M. Characterisation of the surface of oxidised carbon adsorbents. *Carbon*, 40: 95–104, 2002.

[260] Kolthoff I.M. Properties of Active Charcoal Reactivated in Oxygen at 400A. *Journal of the American Chemical Society*, 54: 4473–4480, 1932.

[261] King A. Studies in chemisorption on charcoal. Part IX. The influence of temperature of activation on the sorption of acids and bases. *Journal of the Chemical Society (Resumed)*, pp. 1489–1491, 1937.

[262] Brunauer S., Emmett P.H., and Teller E. Adsorption of Gases in Multimolecular Layers. *Journal of the American Chemical Society*, 60: 309–319, 1938.

[263] Barrett E., Joyner L., and Halenda P. The Determination of Pore Volume and Area Distributions in Porous Substances. I. Computations from Nitrogen Isotherms. *Journal of the American Chemical Society*, 73: 373–380, 1951.

[264] Sing K.S.W., Everett D.H., Haul R.A.W., Moscou L., Pierotti R.A., Rouquerol J., and Siemieniewska T. Reporting physisorption data for gas/solid systems with special reference to the determination of surface area and porosity (Recommendations 1984). *Pure and Applied Chemistry*, 57: 603–619, 1985.

[265] Rouquerou J., Avnir D., Fairbridge C.W., Everett D.H., Haynes J.H., Pernicone N., Ramsay J.D.F., Sing K.S.W., and Unger K.K. Recommendations for the characterization of porous solids. *Pure and Applied Chemistry*, 66: 1739–1758, 1994.

[266] Rouquerol F., Rouquerol J., and Sing K. *Adsorption by Powders and Porous Solids. Principles, Methodology and Applications*. null. Academic Press, San Diego, 1999.

[267] Marsh H. Adsorption methods to study microporosity in coals and carbons - a critique. *Carbon*, 25: 49–58, 1987.

[268] Menéndez J.A., Menéndez E.M., Garcia A., Parra J.B., and Pis J.J. Thermal treatment of active carbons: A comparison between microwave and electrical heating. *Journal of Microwave Power and Electromagetic Energy*, 34: 137–143, 1999.

[269] Marsh H., Crawford D., O'Grady T., and Wennerberg A. Carbons of high surface area. A study by adsorption and high resolution electron microscopy. *Carbon*, 20: 419–426, 1982.

[270] Gamby J., Taberna P., Simon P., Fauvarque J., and Chesneau M. Studies and characterisations of various activated carbons used for carbon/carbon supercapacitors. *Journal of Power Sources*, 101: 109–116, 2001.

[271] Otowa T., Nojima Y., and Miyazaki T. Development of KOH activated high surface area carbon and its application to drinking water purification. *Carbon*, 35: 1315–1319, 1997.

[272] Evans M.J.B., Halliop E., and Macdonald J.A.F. The production of chemically-activated carbon. *Carbon*, 37: 269–274, 1999.

[273] Kaneko K. Determination of pore size and pore size distribution 1. Adsorbents and catalysts. *Journal of Membrane Science*, 96: 59–89, 1994.

[274] Ismadji S. and Bhatia S.K. Effect of pore-network connectivity on multicomponent adsorption of large molecules. *American Institute of Chemical Engineers Journal*, 49: 65–81, 2003.

[275] Dubinin M. Investigation on the nature of the microporous structure in activated charcoals. *Russian Chemical Bulletin*, 10: 693–698, 1961.

[276] Skalny J., Bodor E.E., and Brunauer S. Investigations of a Complete Pore-Structure Analysis III . Analysis of Carbon Adsorbents. *Journal of Colloid and Interface Science*, 37: 478–483, 1971.

[277] Moreira R., José H., and Rodrigues A. Modification of pore size in activated carbon by polymer deposition and its effects on molecular sieve selectivity. *Carbon*, 39: 2269–2276, 2001.

[278] Margulès L., Demaison J., and Boggs J. The Equilibrium CC Bond Length. *Structural Chemistry*, 11: 145–154, 2000.

[279] Freitas M.M.A. and Figueiredo J.L. Preparation of carbon molecular sieves for gas separations by modification of the pore sizes of activated carbons. *Fuel*, 80: 1–6, 2001.

[280] Foley H.C. Carbogenic molecular sieves: synthesis, properties and applications. *Microporous Materials*, 4: 407–433, 1995.

[281] Gonçalves M., Molina-Sabio M., and Rodriguez-Reinoso F. Modification of activated carbon hydrophobicity by pyrolysis of propene. *Journal of Analytical and Applied Pyrolysis*, 89: 17–21, 2010.

[282] Rouzaud J.N. and Clinard C. Quantitative high-resolution transmission electron microscopy: a promising tool for carbon materials characterization. *Fuel Processing Technology*, 77-78: 229–235, 2002.

[283] Font R., Aracil I., Fullana A., Martin-Gullon I., and Conesa J. Semivolatile compounds in pyrolysis of polyethylene. *Journal of Analytical and Applied Pyrolysis*, 68-69: 599–611, 2003.

[284] Forzatti P. and Lietti L. Catalyst Deactivation. *Catalysis Today*, 52: 165–181, 1999.

[285] Bibby D.M., Howe R.F., and Mclellan G.D. Coke formation in high-silica zeolites. *Applied Catalysis A: General*, 93: 1–34, 1992.

[286] Froment G.F. and Bischoff K.B. Non-steady state behaviour of fixed bed catalytic catalyst fouling. *Chemical Engineering Science*, 16: 189–201, 1961.

[287] Fidalgo B., Fernández Y., Zubizarreta L., Arenillas A., Domínguez A., Pis J., and Menéndez J. Growth of nanofilaments on carbon-based materials from microwave-assisted decomposition of CH4. *Applied Surface Science*, 254: 3553–3557, 2008.

[288] Serrano D., Botas J., and Guil-Lopez R. H2 production from methane pyrolysis over commercial carbon catalysts: Kinetic and deactivation study. *International Journal of Hydrogen Energy*, 34: 4488–4494, 2009.

[289] Johnson C.A. and Thomas K. Applications of Raman microprobe spectroscopy to the characterization carbon deposits on catalysts. *Fuel*, 63: 1073–1080, 1984.

[290] Prasetyo I. and Do D. Pore structure alteration of porous carbon by catalytic coke deposition. *Carbon*, 37: 1909–1918, 1999.

[291] Ania C., Menéndez J., Parra J., and Pis J. Microwave-induced regeneration of activated carbons polluted with phenol. A comparison with conventional thermal regeneration. *Carbon*, 42: 1383–1387, 2004.

[292] Ania C., Parra J., Pevida C., Arenillas a., Rubiera F., and Pis J. Pyrolysis of activated carbons exhausted with organic compounds. *Journal of Analytical and Applied Pyrolysis*, 74: 518–524, 2005.

[293] Ania C., Parra J., Menéndez J., and Pis J. Effect of microwave and conventional regeneration on the microporous and mesoporous network and on the adsorptive capacity of activated carbons. *Microporous and Mesoporous Materials*, 85: 7–15, 2005.

[294] Bo L.L., Wang X.C., and Lu L. Study on the purification and regeneration of activated carbon by microwave and its adsorption capacity for Acid Orange 7. *Xi'an Jianzhu Keji Daxue Xuebao/Journal of Xi'an University of Architecture and Technology*, 40: 413–417, 2008.

[295] Chang S.H., Wang K.S., Liang H.H., Chen H.Y., Li H.C., Peng T.H., Su Y.C., and Chang C.Y. Treatment of Reactive Black 5 by combined electrocoagulation-granular activated carbon adsorption-microwave regeneration process. *Journal of hazardous materials*, 175: 850–7, 2010.

[296] Wang J., Peng X., Luan Z., and Zhao C. Regeneration of carbon nanotubes exhausted with dye reactive red 3BS using microwave irradiation. *Journal of hazardous materials*, 178: 1125–1127, 2010.

[297] Cha C.Y., Wallace S., George A.H., and Rogers S. Microwave Technology for Treatment of Fume Hood Exhaust. *Journal of Environmental Engineering*, 130: 338–348, 2004.

[298] Hashisho Z., Rood M., and Botich L. Microwave-swing adsorption to capture and recover vapors from air streams with activated carbon fiber cloth. *Environmental science & technology*, 39: 6851–6859, 2005.

[299] Kim K.J. and Ahn H.G. A study on adsorption characteristics of benzene over activated carbons coated with insulating materials and desorption by microwave irradiation. *Journal of the Korean Industrial and Engineering Chemistry*, 19: 445–451, 2008.

[300] Norman L.M. and Cha C.Y. Production of Activated Carbon from Coal Chars using Microwave Energy. *Chemical Engineering Communications*, 140: 87–110, 1995.

[301] Guo J. and Lua A.C. Preparation of activated carbons from oil-palm-stone chars by microwave-induced carbon dioxide activation. *Carbon*, 38: 1985–1993, 2000.

[302] Valente Nabais J., Carrott P., Ribeiro Carrott M., and Menéndez J. Preparation and modification of activated carbon fibres by microwave heating. *Carbon*, 42: 1315–1320, 2004.

[303] Lee K.H., Jeon S.G., Kim K.H., Noh N.S., Shin D.H., Park J., Seo Y., Yee J.J., and Kim G.T. Thermal and catalytic degradation of waste high-density polyethylene (HDPE) using spent FCC catalyst. *Korean Journal of Chemical Engineering*, 20: 693–697, 2003.

[304] Padleckas H. *Tray Distillation Tower*. http://commons.wikimedia.org/wiki/File:Tray_Distillation_Tower_EN.svg, 2010.

[305] Artetxe M., Lopez G., Amutio M., Elordi G., Bilbao J., and Olazar M. Light olefins from HDPE cracking in a two-step thermal and catalytic process. *Chemical Engineering Journal*, In Press, 2012.